

Synthesis and Characterization of Mesoporous Silica and Metal Oxide Based Stationary Phase Materials

Von der Fakultät Chemie der Universität Stuttgart
zur Erlangung der Würde eines
Doktors der Naturwissenschaften (Dr. rer. nat.)
genehmigte Abhandlung

Vorgelegt von

Kamalakannan Kailasam

aus Rasipuram (Tamil Nadu), Indien

Hauptberichter:	Prof. Dr. K. Müller
Mitberichter:	Prof. Dr. H. Bertagnolli
Mitprüfer:	Prof. Dr. M. Hunger
Mitprüfer und Prüfungsvorsitzender:	Prof. Dr. T. Schleid
Tag der mündlichen Prüfung:	08 December 2008

Institut für Physikalische Chemie der Universität Stuttgart

2008

**Dedicated to
my dad N. Kailasam and
my mom K. Dhanalakshmi**

Acknowledgment

My sincere thanks go to Prof. Dr. Klaus Müller for giving me the opportunity to pursue my doctoral studies under his guidance. I thank him for his expertise, guidance and intellectual support throughout my research work. My heart felt gratitude to him for his positive feeds, whenever I used to come up with ideas and also open-minded discussions.

I would like to thank the Graduiertenkolleg “Chemie in Interphasen” for providing the fellowship and Deutsche Forschungsgemeinschaft for financial support of this project.

I thank Prof. Dr. Thomas Schleid for taking the chair in the examination board. I also thank Prof. Dr. Helmut Bertagnolli and Prof. Dr. Michael Hunger, co-examiners for my doctoral thesis.

I am grateful to all my co-workers and collaborators during the course of my thesis. My special thanks go to Dr. Silvia Gross, Simone Mascotto, Dr. Antonella Glisenti, Dr. Marta Maria Natile, Dr. Chiara Maccato, Dr. Lidia Armelao and Prof. Dr. Eugenio Tondello from CNR-ISTM, Department of Chemical Sciences, University of Padua, Italy, for providing me with the mixed oxide samples and also for performing XRD, SEM-EDX, XPS, and DRIFT spectroscopic measurements.

I would like to acknowledge Prof. Dr. Helmut Bertagnolli, University of Stuttgart, for the permission to use the Raman spectrometer and also Sankaran Anantharaman for EXAFS measurements. My sincere gratitude goes to Prof. Dr. Emil Roduner and Dr. Herbert Dilger, University of Stuttgart, for allowing me to use the nitrogen physisorption instrument and Dr. Alexander Fels, University of Stuttgart for performing the SEM measurements. I also thank Prof. Dr. Frank Gießelmann and Nadia Kapernaum for their help in SAXS measurements and Prof. Dr. Friedhelm Zabel from University of Stuttgart for permitting me to use the HPLC instrument. My sincere thanks to Prof. Dr. Clemens

Bechinger and Dr. Laurent Helden, University of Stuttgart, for the measurement of Casimir forces on the hydrophobic silica and for the financial support.

I would like to thank Prof. Dr. Ekkehard Lindner, University of Tübingen, for the fruitful discussions and Mrs. Heidrun Lindner for her kind, motherly love and care throughout my doctoral research. I like to acknowledge the professors from University of Tübingen - Prof. Dr. Klaus Albert for the HPLC measurement and Prof. Dr. Hermann A. Mayer for permitting me to synthesize silsesquioxanes and inorganic pincer complexes. I also thank Prof. Dr. Jeremy D. Glennon and Dr. Norma Scully, University College Cork, Ireland, for the synthesis of MCM-41 stationary phases in supercritical medium.

I would be failing in my duty if I forget to thank Mrs. Inge Blankenship for her secretarial assistance and support in bureaucratic formalities. I also thank Dr. Dieter Leicht, Dr. Isabella Waldner and Mrs. Gisela Hoppe for their help in administrative procedures. My thanks to Mrs. Gabi Bräuning, Mrs. Diana Zauser, Mrs. Beatrice Omiecienski and Mrs. Birgit Feucht for their timely help in the laboratory. I would also like to thank Mr. Walter Ottmüller and Mr. Jochen Graf for mechanical workshop support, Mr. Jürgen Hußke for help in electronics and Mr. Werner Hopf for all the glass stuffs.

I want to acknowledge my former colleagues at the University of Stuttgart, Dr. Gokulakrishnan Srinivasan, Dr. Jorge Antonio Villanueva Garibay and Dr. Xiarong Yang for their assistance during my initial days of my research. My heart felt thanks to Fabrizia, Poongodi, Tahira, Tuul, Lida, Christiane, Keisuke and Matthias for their support, comments, suggestions and friendly working atmosphere. I thank Dr. Stefan Jagiella for all the help and support during my research period.

My special thanks goes to all the friends of my school and college, especially, Viji, Selvaraj, Mohan, Vatsan, Baskar, Mani, Prabhu, Elango, Venke, Selina, Sophie, Pragatheeswaran, Shanmugapriyan, Sivanandam, and Riyaz. I also thank the teachers, lecturers, scientists and friends of my Schools, Bishop Heber College, Orchid, CLRI and IGCAR for kindling in me the fire towards research. I am glad to thank Bünsauer Platz

friends – “Büsnau group” for their help and support during my initial days in Stuttgart. My heart felt gratitude to Sony for being always there to help and sincere thanks to Stuttgart friends, Sony, Sudhir, Raja, Sankaran, Sree, Shailesh, Tanu, Suni, Sai and Sandhya.

My heart felt thanks to my mom K. Dhanalakshmi, my dad N. Kailasam and my brother K. Vinoth for their love, encouragement, and their sacrifices. I wouldn't be what I am today without them. I would like to thank my grandma's (Paavai and Pappathi) and uncles Eswaramoorthi and Thiyagarajan, all my special relatives for their great support.

Last but not the least, I thank God Almighty for His blessings throughout the endeavours.

Contents

1 Introduction	1
2 Systems	8
2.1 Solvents	8
2.2 Substrates	10
2.2.1 Mesoporous MCM-41 Silica Spheres	11
2.2.2 Metal Oxides	14
2.2.3 Silica-Zirconia Mixed Oxides	15
2.2.4 Surface Modification of Inorganic Oxides	16
3 Physico-Chemical Techniques	21
3.1 Fourier Transform Infrared Spectroscopy (FTIR)	21
3.1.1 Methylene Stretching Bands	23
3.1.2 Methylene Wagging Bands	25
3.2 Solid-State NMR Spectroscopy (SSNMR)	28
3.2.1 Theory	28
3.2.2 Alkyl Modified Supports and Solid-State NMR Technique	36
3.2.2.1 ²⁹ Si MAS NMR Spectroscopy.....	37
3.2.2.2 ¹³ C MAS NMR Spectroscopy	39
3.3 Small Angle X-Ray Scattering (SAXS)	40
3.4 Nitrogen Physisorption.....	43
3.5 Scanning Electron Microscopy (SEM)	47
4 Experimental Section	50
4.1 Materials and Synthesis.....	50
4.1.1 Chemicals	50
4.1.2 Grafted Silica Gels: Impact of Solvents on C ₃₀ Silica	51
4.1.2.1 Synthesis of C ₃₀ alkyl grafted silica spheres	51
4.1.3 Grafted MCM-41 Silica: Synthesis, Impact of Mono- and Trifunctional C ₁₈ Silanes and Endcapping	51
4.1.3.1 Synthesis of MCM-41 silica spheres.....	51
4.1.3.2 Reaction of silylating agents and HMDS with MCM-41.....	52
4.1.4 Grafted MCM-41 Silica: Synthesis, Impact of Silica Source and Trifunctional C ₁₈ Silane Precursors.....	53
4.1.4.1 Synthesis of MCM-41 silica spheres.....	53

4.1.4.2 Reaction of silylating agents with MCM-41 silica spheres.....	53
4.1.5 Grafted Metal Oxides: Impact of Oxide Supports, Grafting of C ₁₈ Silanes and Grafting Routes	55
4.1.5.1 Reaction with <i>n</i> -Octadecyltrichlorosilanes	55
4.1.5.2 Reaction with <i>n</i> -Octadecyltrihydridosilanes	56
4.1.6 Grafted Mixed Silica-Zirconia Oxides: Impact of Oxide Supports and Grafting of C ₁₈ Silanes	56
4.1.6.1 Preparation of Mixed Oxides	56
4.1.6.2 Preparation of C ₁₈ Alkyl Grafted Mixed Oxides.....	57
4.2 Elemental Analysis.....	58
4.3 Methods.....	59
4.3.1 FTIR Measurements	59
4.3.2 DRIFT Measurements	60
4.3.3 SSNMR Measurements	61
4.3.4 XPS Measurements	61
4.3.5 SAXS Measurements	62
4.3.6 Nitrogen Physisorption Measurements	62
4.3.7 SEM-EDX Measurements.....	62
5 Results and Discussion	63
5.1 Grafted Silica Gels: Impact of Solvents on C ₃₀ Silica	63
5.1.1 Variable Temperature FTIR Spectroscopic Measurements	64
5.1.2 Summary	72
5.2 Grafted MCM-41 Silica: Synthesis, Impact of Mono- and Trifunctional C ₁₈ Silanes and Endcapping	73
5.2.1 Synthesis of MCM-41 Silica Spheres and Grafting with C ₁₈ Chains	73
5.2.2 SAXS Measurements	75
5.2.3 Nitrogen Sorption Isotherm Analysis.....	76
5.2.4 SEM Analysis.....	81
5.2.5 ²⁹ Si MAS NMR Spectroscopy.....	82
5.2.6 ¹³ C MAS NMR Spectroscopy	84
5.2.7 FTIR Spectroscopy.....	86
5.2.8 Summary	88
5.3 Grafted MCM-41 Silica: Synthesis, Impact of Silica Source and Trifunctional C ₁₈ Silane Precursors	89

5.3.1 Synthesis and Characterization of MCM-41 Silica Spheres	89
5.3.2 Preparation of Grafted MCM-41 Silica and Characterization	94
5.3.3 ²⁹ Si MAS NMR Spectroscopy.....	101
5.3.4 ¹³ C MAS NMR Spectroscopy	104
5.3.5 FTIR Spectroscopy.....	108
5.3.6 Summary	110
5.4 Grafted Metal Oxides: Impact of Oxide Supports, Grafting of C ₁₈	
Silanes and Grafting Routes	111
5.4.1 Properties of Metal Oxide Substrates.....	111
5.4.2 DRIFT Measurements for Determination of Surface Properties	111
5.4.3 Cross-linking of Alkylsilanes by FTIR and SSNMR Spectroscopy	114
5.4.4 Conformational Order of C ₁₈ chains by FTIR Spectroscopy	118
5.4.5 Conformational Order of C ₁₈ Chains by Solid-State NMR Spectroscopy	122
5.4.6 Effect of Silylating Agent and Metal Oxide Surface on Surface	
Loading and Conformational Order of C ₁₈ Chains	124
5.4.7 Summary	128
5.5 Grafted Mixed Silica-Zirconia Oxides: Impact of Oxide Supports and	
Grafting of C ₁₈ Silanes	129
5.5.1 Surface characteristics of mixed oxide substrates.....	129
5.5.2 Route for modification of mixed oxides surfaces	129
5.5.3 XPS characterization of mixed oxide substrates	131
5.5.4 Cross-linking of alkylsilanes by SSNMR spectroscopy	132
5.5.5 Conformational order of grafted C ₁₈ chains by SSNMR spectroscopy	135
5.5.6 Conformational order of grafted C ₁₈ chains by FTIR spectroscopy	138
5.5.7 SEM and EDX analysis of C ₁₈ chains grafted on mixed oxides	142
5.5.8 Effect of mixed oxide substrates and silylating agent on chain assembly	
and conformational order	145
5.5.9 Summary	149
6 Summary	151
7 Zusammenfassung.....	155
List of Figures.....	160
List of Tables.....	164
References	165

Chapter 1

1 Introduction

The original form of liquid chromatography is referred to normal phase or adsorption chromatography. Normal phase chromatography makes use of a polar adsorbent such as silica or alumina, and a nonpolar mobile phase. Reversed-phase liquid chromatography (RPLC) on the contrary uses a nonpolar stationary phase and a polar, largely aqueous mobile phase.

RPLC is the most popular analytical technique for separating complex mixtures. The separation is achieved by the interactions of analytes with the stationary phase. The stationary substrate or adsorbent acts as a support for the silylating agents, to be bonded to the surface. The substrate must be rigid and impermeable for the better interaction with the analytes. The mobile phase is the other component in the separation process. Equilibrium is established between the mobile and the stationary phases in the system and these two being the main components of an “interphase” which is generally defined as a system consisting of two well-defined components. In the absence of a mobile phase, the stationary phase is quite heterogeneous. The penetration of the mobile phase into the stationary phase makes the system almost homogeneous. As a result, chemical and physical processes like chromatographic separations take place in an almost homogeneous medium with high selectivity, with analytes still separable from the stationary phase.

In RPLC, the analytes are separated using their hydrophobicity. A solute with more hydrophobic character will be retained on the column longer than the one with lesser hydrophobic nature. Also, polar solutes will interact with the silica surface to cause peak tailing. Water is generally one of the mobile phase components of a binary mixture in RPLC and it does not interact with the hydrophobic stationary phase chains. The most popular mobile phase organic solvents used in RPLC are methanol and acetonitrile and with increasing concentration of these solvents, the retention of the analytes will become lower.

The most important criteria for the chromatographic performance of an adsorbent are particle size, particle porosity, and surface area. Particles should be spherical and the

particle size should be between 3-10 μm with a very small distribution. This greatly enhances the packing of a column and hence the column efficiency.¹ The particle porosity is based on the pore size, shape, and distribution of the adsorbent. The pores of an adsorbent can be modeled with either a cylinder with a small neck that widens, or with parallel slits. The average pore diameters for common adsorbents used in chromatography are between 90-300 \AA . Each adsorbent can exhibit different types of pores depending on the manufacturing processes. The surface area is very important for the chromatographic performance and usually ranges between 100 and 500 m^2/g .

There are numerous types of adsorbents that have been studied over the years. Among them, silica is the most common substrate. Silica gel, SiO_2 , is a partially hydrated and a highly porous form of silica, which is made from the most abundant elements in the earth's crust. Since 1970s, silica gel has been the most widely used support for RPLC. The improvement of the synthetic process for producing very pure starting silica with very controllable particle and pore sizes has enhanced chromatography immensely. In the past few decades, the most promising development for RPLC was the development of microparticles and chemically bonded stable phases. Nevertheless, the chromatographic silica spheres which are commercially available are amorphous and having broad mesopore size distribution.

Since the introduction of the M41S family of ordered mesoporous silica, the activities dealing with the controlled design of porous materials with nanometer scale periodicity have expanded tremendously.^{2,3} Mesoporous materials possess a series of attractive features, such as high surface area, narrow pore size distribution and high adsorption capacities. The control of particle morphology and size of mesoporous silica opens new applications, such as stationary phases in chromatography or as an easy-to-handle form for catalytic purposes.⁴⁻⁸ The large surface area can withstand high mobile phase pressures, which allows the usage of high flow rates and also a decrease length of the chromatographic runs. To exploit the advantage of higher surface area in the separation process, spherical mesoporous silica materials such as MCM-41 were synthesized which has surface area of about 1000 m^2/g .⁹⁻¹¹ However, along with its many advantages, mesoporous silica also has disadvantages that need to be overcome to yield a better solid substrate. These disadvantages include the lack of pH stability due to hydrolysis of the

silica backbone (Si-O-Si) at pH values larger than 8 and smaller than 2 as well as the peak tailing with basic solutes that decrease resolution and peak capacity.

Zirconia (ZrO_2), titania (TiO_2), and alumina (Al_2O_3) are of particular importance for RPLC studies.¹² Zirconia has two large advantages over silica: increased pH stability (0 - 14), and chromatographic separations can be performed at temperatures up to 100 °C.¹³ However, there are other drawbacks which limit its use in chromatography and which are described later.¹⁴ Titania and alumina are also used in some applications in which the former has very good pH stability but less surface area.^{15,16} Recent studies in stationary phase development have lead chromatographers to explore the concept of mixed oxide chromatographic supports and materials for use in liquid chromatography. These include alumina-silica, magnesia-silica, titania-silica, and zirconia-silica.^{17,18} The driving force behind the development of these mixed oxide supports comes from the possibility of attaining a surface with properties that exploit the best attributes of both components in the mixed oxide.

Alkyl-bonded stationary phases for RPLC separations have been developed on the basis of a broad experience and numerous experimental findings by chromatographers. They offer a wide range of chromatographic performance which results from the differences in substrate and stationary phase properties such as, surface area, pore size and pore size distribution, particle size and particle size distribution, porosity and chemical composition,^{12,19,20,21} bonding chemistries (monofunctional, trifunctional solution polymerized and surface polymerized),^{22,23} surface coverage,^{22,23} mobile phase,^{24,25} temperature,^{26,27} solute hydrophobicity and polarity.²⁸⁻³⁰ Formation of these alkyl grafted substrates not only depends on the water content but also on the nature of the silane and temperature. Apart from that, it is also affected by the nature and particle size of the substrate which in turn affects the degree of grafting and ordering of SAMs.

The amount of surface coverage or bonding density is very important to the chromatographer. Bonded phases are prepared by the reaction of the solid substrate with various silylating agents. They can be prepared by covalent attachment of alkyl silanes to a solid support using di- or trichlorosilanes instead of monochlorosilane. There are three types of bonded phases that are generally prepared: brush phase, oligomeric phase, and

bulk phase. All the three types can be made from mono, di, or tri-functional chloro or alkoxy or hydrido silanes.³¹

Meanwhile, the major problem with the RPLC phases was the inability to covalently link the silylating agent to the silanol groups ($8 \mu\text{mol}/\text{m}^2$) on the silica surface. The excess silanols on the surface are referred to as residual silanols and are weakly acidic. These silanols cause peak tailing of basic solutes, which reduces resolution and column efficiency. These silanols are endcapped by using smaller groups (eg., hexamethyldisilazane) for better column performance during the separation process.

In spite of its popularity as a predominant separation technique, the separation mechanism has still not been established unambiguously.^{32,33} This is due to the presence of many parameters that control the molecular recognition in the chromatographic process.^{19,34-39} A profound knowledge of the stationary phase morphology is thus a pre-requisite to understand solute retention mechanisms, and ultimately column selectivity. In order to develop a novel stationary phase for a particular separation, a great number of stationary phases should be synthesized and examined in detail to provide a feedback for developing the strategy for the next synthesis. The systematic characterization of stationary phases is thus very important for the development of more powerful phases with desirable separation performance and optimal exploitation of existing materials.

Physico-Chemical Methods for Evaluating the Stationary Phase Materials

Elemental analysis is one of the basic methods for evaluating the coverage of alkyl chains on the stationary phases.^{40,41} The quantity of carbon and hydrogen can be measured directly by burning the sample in oxygen. The specific surface area of the substrate and carbon analyses are utilized to provide the surface coverage of the resulting alkyl grafted stationary phases in $\mu\text{mol}/\text{m}^2$ or groups/ nm^2 .

Many physico-chemical techniques have been applied for the characterization of the porous structure of oxide-based stationary phase materials. Physical gas adsorption is often the technique of choice to study the pore characteristics of solid materials and the changes therein upon post-synthesis treatment. The technique accurately determines the amount of gas adsorbed on a solid material, which is a direct measure for the porous

properties and structure. Currently available equipment allows carrying out measurements over a wide range of pressure which opens up an opportunity of detailed characterization of surface properties of porous solids.⁴² These in turn are needed to estimate the usefulness of analyzed materials or to monitor the performed modification processes. Nitrogen adsorption-desorption studies provide values for the surface area, total pore volume and pore size distribution (PSD).⁴³⁻⁴⁵ Different probe gases, including N₂, Ar, and CO₂, are used as adsorptives, depending on the nature of the material (adsorbent) and the information required. N₂ adsorption at 77 K and at sub-atmospheric pressures has remained universally pre-eminent and can be used for routine quality control, as well as for investigation of new materials. If applied over a wide range of relative pressures (p/p_0), N₂ adsorption isotherms provide information on size distributions in the micro-, meso- and macroporosity range (approximately 0.5–200 nm).

Small angle X-ray scattering (SAXS) is another technique often used to complement the nanoporous and structural aspects of the materials under investigation.^{46,47} Interference maxima (“Bragg peaks”) are observed in the SAXS measurements which are evaluated in terms of basic concepts of classical crystallography and which provide the corresponding space group. Ordered mesoporous silicas, such as MCM-41 and MCM-48, are fabricated with a liquid crystal template and have channels within the range of 25 to 40 Å. The SAXS pattern provides the hexagonal mesopore arrangement in the MCM-41 silica materials, as also presented in this dissertation.

Knowledge of the microstructural characteristics is important for an understanding of the evolution of the various chromatographic and catalytic supports during preparative procedures and provides useful feedback for modifying the method to obtain materials with the desired properties. SEM measurements reveal the morphological features of the material. It also provides the particle size distribution and diameter of the particles. In this study, SEM studies were done to determine the spherical morphology and dispersity of the parent silica and the MCM-41 silica spheres before and after C₁₈ grafting.

Alkyl-bound stationary phases can be characterized by different techniques to determine the grafting, conformational behavior and mobility of the surface-grafted alkyl chains. They include systematic analysis of the retention behavior for a certain group of solutes,^{28,48-50} various spectroscopic measurements of the stationary phase materials^{22,24-}

^{27,34,35,51-56} and theoretical calculations⁵⁷⁻⁶⁰ of the bonded phase structures. The chain conformation of the stationary phases were primarily studied with the help of chromatographic experiments, which provided essential information about the bonded phase as a function of mobile phase, temperature, solute hydrophobicity and polarity.²⁸⁻³⁰ These studies have demonstrated that the selectivity differences among the columns are not only due to differences in the starting silica material, but also due to differences in the chain density of the alkyl bonded phases. It turned out that the alkyl chain structure and interfacial properties urge the function and utility of these stationary phase materials. It was also demonstrated that the conformational order of the alkyl chain moieties plays an important role in determining the efficiency and selectivity of separations. Such studies, however, provide only indirect evidence about the bonded phase morphology. On the other hand, experimental techniques - such as NMR,^{22,35,53,61-63} FTIR,⁶³⁻⁷¹ Raman,^{24,25,27,56} fluorescence,^{72,73} atomic force microscopy,⁵² ellipsometry⁵² and photo-acoustic spectroscopy^{74,75} - were applied to reveal direct information about the alkyl chain structure, conformation, dynamics of the stationary phase materials.

The application of IR spectroscopy to study alkyl chain conformation is based on the pioneer work by Snyder et al. on *n*-alkanes.⁷⁶ Since this early work, relatively few efforts have been made for characterization of stationary phase materials using FTIR spectroscopy. After the report by Sander et al.⁶¹, Singh et al.²⁶ have used FTIR spectroscopy to study the influence of various parameters of alkyl stationary phases like temperature, alkyl chain length and alkyl chain position more recently. Srinivasan et al. studied the effect of solid supports, pressure, solvents, surface coverage and synthetic routes on various C₁₈ and C₃₀ alkyl modified supports using FTIR spectroscopy.^{63,65,66,68,69,71} Raman spectroscopy provides complementary information about the conformational order of alkyl modified surfaces. Dorsey et al.^{24,27} and Pemberton et al.^{55,56} used Raman spectroscopy to study the influence of temperature, surface coverage, solvents and synthesizing procedure on conformational order of *n*-alkyl modified systems. Even a direct on-column characterization of alkyl stationary phases was carried out by Raman spectroscopy under chromatographic conditions.⁷⁷

Solid-state NMR spectroscopy has significantly advanced the understanding of stationary phase materials by employing ²⁹Si and ¹³C MAS NMR techniques which provide complementary information on chemically modified surfaces.^{22,34,51,52,54} ¹³C NMR

spectroscopy is used to obtain information about the conformation of surface immobilized alkyl ligands. The dynamics of *n*-alkyl modified silica gels was studied by using the cross-polarization time constant, T_{CH} , and 1H or ^{13}C spin-lattice relaxation times.⁷⁸⁻⁸⁰ Pursch et al.⁵⁴ used 2D-WISE NMR to correlate segmental mobility from 1H line-widths with chain conformation from ^{13}C chemical shifts for C_{22} -alkyl modified silica gels. Also, NMR line shape changes were used to study the dynamics of modified silica gel.⁷⁸ The general principle behind this analysis is that the rapid molecular motions average the dipole-dipole interactions, chemical shift anisotropy, and other anisotropic magnetic interactions resulting in some narrowing of the NMR signals. In addition, Pursch et al.⁶² implemented a selective population inversion (SPI) ^{13}C CP/NMR experiment to study the mobility of C_{30} alkyl modified silica gels. 2H NMR spectroscopy on selectively deuterated compounds offers distinct advantages over 1H and ^{13}C NMR methods for probing structure and dynamics in disordered systems.^{53,61,81,82}

In the present work, C_{18} alkyl chains were grafted on inorganic oxide substrates like ordered mesoporous silica (MCM-41), titania, zirconia, hafnia, alumina and silica-zirconia mixed oxide using different octadecyl silylating reagents. The elemental composition was determined by elemental analysis and XPS. Nitrogen sorption studies and SAXS measurements were carried out to determine the porous features of the oxides. ^{29}Si NMR measurements were performed for determining the degree of cross-linking of the silane. ^{13}C CP/MAS NMR and variable temperature FTIR spectroscopic techniques were used to determine the conformational order of C_{18} alkyl modified systems. SEM measurements and EDX analyses provided the morphological features of the solid substrates and information about the distribution of the alkyl chains on the oxides surfaces. Moreover, a comparison was made on the conformational order of the alkyl chains on normal chromatographic silica with the above described systems. In addition, the effect of the mobile phase and temperature on the conformational order of C_{30} alkyl modified silica gel was carried out to elucidate the retention mechanisms for chromatographic separations using FTIR spectroscopy.

Chapter 2

2 Systems

2.1 Solvents

Retention is a function of solvation free energy differences for the analyte molecules in the stationary and mobile phase components. Retention behavior in liquid chromatography is influenced by a variety of physical and chemical properties between the chromatographic system and the analytes of interest. The concept of retention during the separation process is least understood until now which, however, is known to be governed by the intermolecular interactions between the various components in chromatographic columns. In order to elucidate the retention mechanisms for such separations, an understanding of the stationary phase behavior under various separation conditions is essential. The types of interactions include solute-solvent, solvent-stationary phases and solute-stationary phases.

The difficulties in separations by means of selectivity and reproducibility were encountered with traditional C₈ and C₁₈ phases for the separation of structured solutes. C₃₀ alkyl modified silica gels were developed which provide enhanced shape selectivity for structured analytes and improved resolution. This unique column selectivity has been attributed to the increased chain length of the C₃₀ stationary phase in which the larger analytes can interact with stationary phase to a much higher extent. These phases have been applied under highly aqueous mobile phase conditions.⁸³

The role of mobile phase solvents in the separation process is inevitable for the better retention of analytes. The influence of solvent on the bonded ligands has been studied by chromatography,⁸⁴⁻⁸⁶ FTIR,^{55,64,87} NMR,³⁵ fluorescence,⁸⁸ optical transmittance,⁸⁹ and Raman spectroscopy.^{24,25,90,91} These investigations provided information about the alkyl chain structure, conformational order and intermolecular interactions of the alkyl moieties of the stationary phases under solvation. Two models of analyte retention were proposed for the aforementioned types of interactions, namely, the solvophobic and the interphase models.

In the solvophobic model (adsorptive mechanism),⁹²⁻⁹⁴ retention is defined in terms of adsorption. The stationary phase acts as an adsorption site for the analyte molecules. Here, the mobile phase solvates the analyte depending on the adsorption characteristics of the stationary phase, and the solvation behavior of solvents towards the particular analyte. In the interphase model (partitioning mechanism),⁹⁵⁻⁹⁷ the mode of retention is partitioning in which the analyte molecules are fully embedded within the alkyl chains of the stationary phase. The solvent molecules penetrate the alkyl chain region on the silica surface, and interact with the underlying alkyl groups, silica surface, and solvate the analyte molecules. Both models are based on the interaction of analyte molecules and stationary phases during the process of retention. Hence, it is important to study the interactions of solvent molecules and stationary phase to get a better understanding of the retention behavior in these stationary phases. Temperature is also an important factor for the retention in chromatographic separations.³⁷ Hence, the column temperature plays an important role in determining the experimental timing and shape selectivity of structured analytes especially for C₃₀ stationary phases.⁶²

A combined FTIR and solid-state NMR study addressed the conformational order of C₁₈ and C₃₀ alkyl chains.⁶⁶ More recently, the conformational order of the C₁₈ alkyl chains were studied using perdeuterated and protonated solvents by FTIR spectroscopy.⁶⁴ In the present study, we explore the effects of mobile phase and temperature on the conformational order of C₃₀ alkyl modified silica gels for the first time using variable temperature FTIR spectroscopy. The solvents considered here include acetonitrile, methanol, ethanol, 1-propanol, acetone, tetrahydrofuran, carbontetrachloride and *n*-hexane, frequently used in chromatography. The conformational sensitive symmetric and antisymmetric CH₂ stretching regions were analyzed providing information about the conformational order/disorder phenomena of the alkyl chains as a function of temperature and type of the added solvent.

2.2 Substrates

Silica is the most common material used in the early development of column liquid chromatography. It plays a very important role in chromatography through direct and indirect interactions with the analytes. The silica surface consists of three distinct silanol groups, free or isolated, vicinal, and geminal, along with physisorbed water and polymeric siloxane network. Silica has many advantageous properties that include small, spherical particle diameters but with a broad distribution of pore sizes as mentioned in chapter 1. Figure 2.1 shows the scanning electron micrograph of 5 μm silica particles. The total number of reactive silanols on a silica surface is $8 \pm 1 \mu\text{mol}/\text{m}^2$ which can be easily derivatized.¹⁹ Silica directly interacts with the analytes due to residual silanols left on the surface after derivatization. The analytes also interact with a bonded phase that is covalently bound to the silica surface.⁹⁸

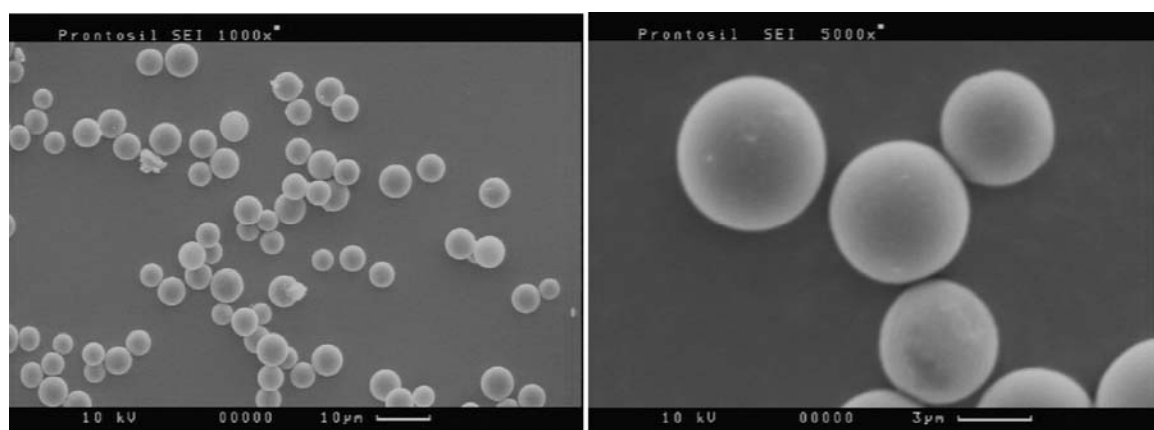


Figure 2.1. SEM micrographs of 5 μm silica spheres at varying degrees of magnification.

Many attempts have been undertaken to overcome the drawbacks of silica-based materials, for instance, by covalently bonding alkyl chains, modification with a polymeric reagent or coating with an inorganic oxide. The use of MCM-41 materials is the other way to enhance the thermodynamic behavior due to an increased solute retention, as well as improved kinetic properties as a result of the solute dispersion on the stationary phase. Another solution to overcome the drawbacks of silica is substitution by an oxide with greater pH stability than silica. Titania, zirconia and alumina could provide an alternative to silica as chromatographic packing materials, giving rise to high mechanical stability,

separation efficiency, and chemical inertness at elevated temperatures and over the entire pH range.¹²

Selective covalent modification of metal oxides and silica are of great interest in research and technology. Such materials have shown to be useful, for instance, as passivating layers and are frequently discussed in various fields of application, including sorption and separation media, wetting and adhesion, pigments, fillers, sensors, biomaterials, catalysis, optical and electronic devices.⁹⁹⁻¹⁰² This section addresses the importance of the mesoporous silica, metal oxide and silica-zirconia mixed oxide based stationary phases in detail.

2.2.1 Mesoporous MCM-41 Silica Spheres

A new concept for the synthesis of open-framework inorganic oxide materials of well-defined geometry was introduced by scientists from Mobil Oil Corporation in 1992.^{2,3} This concept is based on the use of surfactant molecules such as hexadecyltrimethylammonium bromide (CTAB) as structure-directing agent. This guided to the discovery of the so-called M41S family of mesoporous materials. The most important member of the M41S family is MCM-41 which has hexagonal structure with one-dimensional pore structure as shown in Figure 2.2.



MCM-41

Figure 2.2. Structure of MCM-41 material.

The surfactants have amphiphilic nature which allows the silica source to associate into supramolecular structures. This arrangement minimises the unfavourable interaction of the hydrocarbon tails with water, but it introduces a competing unfavourable interaction, the repulsion of the charged head groups. The balance between these competing factors

determines the relative stability of the micelles. Depending on the concentration of the surfactant, different phase structures can be observed, as shown in Figure 2.3.¹⁰³

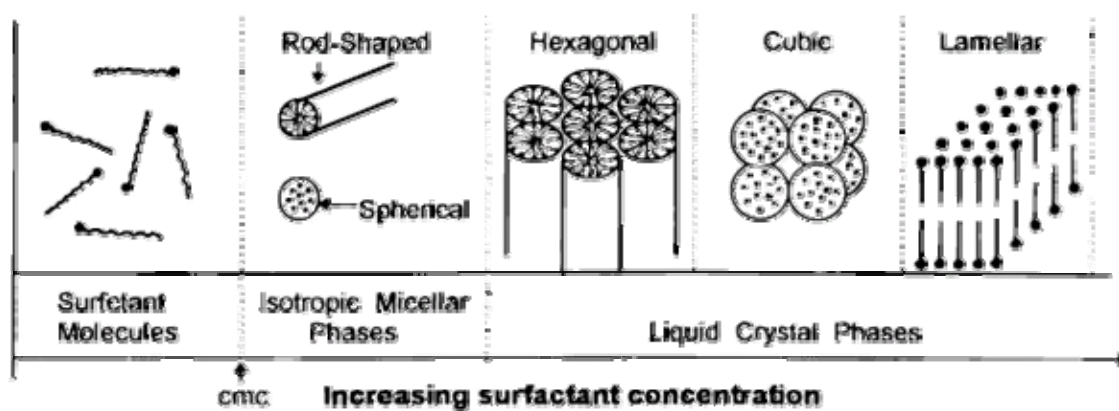


Figure 2.3. Dependence of the phase structure from the concentration of surfactant.

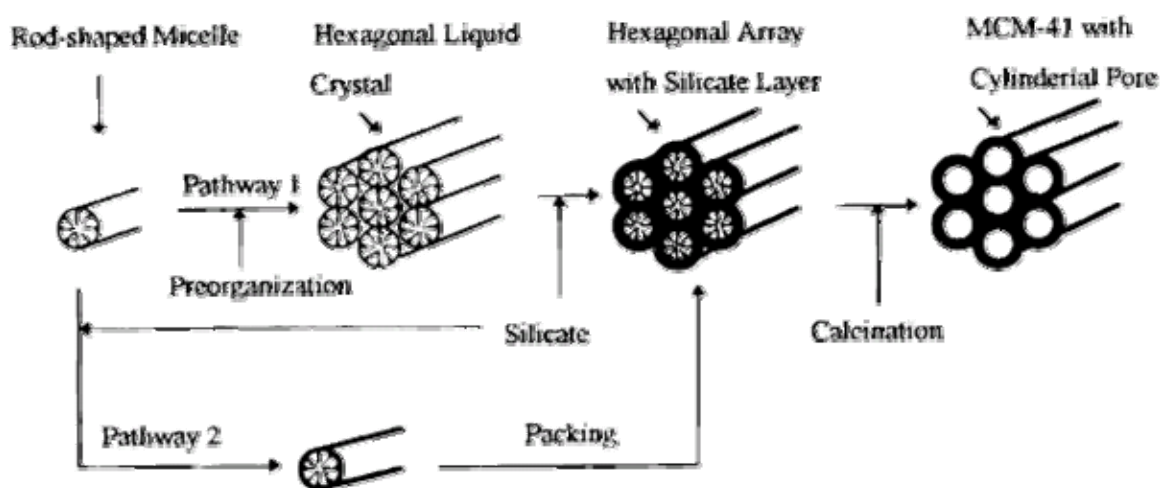


Figure 2.4. Mechanistic pathway of the formation of MCM-41 materials.

The surfactant molecules remain in solution until their concentration has reached the critical micelle concentration (cmc). This concentration is the initial concentration threshold at which monoatomic molecules aggregate to form isotropic micelles. Above this concentration they aggregate as small spherical micelles in order to decrease the system's entropy. These micelles can coalesce to form elongated cylindrical micelles and when the concentration becomes even higher, the formation of liquid crystalline phases occurs (MCM-41, MCM-48, MCM-50).¹⁰⁴ The M41S phases described so far are synthesized via an electrostatic templating procedure based on surfactants with cationic

head groups, and anionic inorganic building units.¹⁰³ The mechanistic pathway leading to the formation of MCM-41 material is shown in Figure 2.4.

By carefully choosing the template molecule, the pore diameter can be adjusted over a wide range. An increase in the pore diameter can be achieved by the addition of an auxiliary organic molecule (mesitylene, *n*-decane etc.) which is trapped inside the core of the micellar assembly. The removal of the template is the last step of the synthesis and can be made by solvent extraction, calcination, oxygen plasma treatment or by supercritical drying.

MCM-41 silicas have been used as stationary phases, catalysis, etc., For instance, in catalysis the control of the particle size represents an important issue for the transfer of catalytic reactions from batch experiments to continuous processes where efficient mass transfer plays a key role.¹⁰⁵ In separation science, the average particle size is found to affect the plate height of the columns and thus their separation efficiency as explained above. In this context, the preparation of mesoporous silica spheres of tunable size is very attractive because they allow a homogeneous filling of the chromatographic columns which in turn should improve the separation performance.^{8,106} The first application of mesoporous materials in chromatography dates back to about a decade.^{6,7,107} So far, MCM-41 silica have been used as stationary phase for conventional HPLC,^{107,108} size-exclusion chromatography¹⁰⁹, capillary gas chromatography,¹¹⁰ chiral HPLC,¹¹¹ and RPLC.⁸ However, there is still a need for further improvement of the basic materials. Although there were many attempts to prepare optimized systems that meet the requirements for HPLC application, quite often only MCM-41 spheres with large particle size-distribution and agglomeration could be obtained.^{6,7,112,113}

Recently, the pseudomorphic synthesis was introduced which represents a new synthetic strategy for MCM-41 preparation with optimized procedures for particle shaping and mesophase self-assembly.⁹ In this method, commercially available preformed silica particles of well-determined shape, size and size-distribution are used as silica source. The term pseudomorphism originates from the field of mineralogy, where a pseudomorph denotes an altered mineral with an outward appearance of another mineral species. In the present context, the pseudomorphic synthesis provides MCM-41 spheres which are pseudomorphs of the parent silica spheres. The key parameter in maintaining the

morphology of the silica particles during the transformation process is to find the optimum synthetic conditions for which the rate of templated silica precipitation is equal to the rate for silica dissolution.

For chromatographic applications, it is advantageous to endcap the reactive silanol groups with suitable organic groups by which a better separation performance can be achieved. Mesoporous spheres with different surface coverages can be prepared by means of suitable silylating agents and after optimizing the reaction conditions. The enhanced hydrophobicity - due to the reduced number of surface silanol groups - plays a key role for both chromatographic⁸ and catalytic applications.¹¹⁴⁻¹¹⁶ Two types of C₁₈ alkyl grafting were carried out on these MCM-41 silica spheres with different silylating agents along with endcapping.

The fundamental understanding of these organic-inorganic hybrid mesoporous materials prepared in both independent studies are very important for their future potential applications. Hence in the present work, several physico-chemical techniques like SAXS, N₂ physisorption, SEM, solid-state NMR and FTIR were employed to determine the mesoporosity, morphology, grafting and organization of alkyl chains on these MCM-41 spheres, respectively.

2.2.2 Metal Oxides

The use of metal oxides like zirconia, titania, and alumina have attracted much attention in chromatography. These metal oxides are expected to provide a more stable column packing and longer column lifetimes, and are potential materials for applications at higher temperatures and extreme pH conditions.^{12,52,117,118}

The nature of surface hydroxyl groups is different in metal oxides, hence silanization is not as easy as with silica gels. In fact, the bonded alkyl chains prepared by silanization of monochlorosilanes, RSi(CH₃)₂X, with zirconia and titania were found to be less stable than their silica-based counterparts, and the stability of the M-O-Si-R unit decreases in the order M = Si > Zr > Ti > Al. The modification of oxides with trifunctional silanes possess multiple bonding with highly ordered and closely packed chains which are very suitable for HPLC applications.¹¹⁹ TGA studies showed that the thermal stabilities of

octadecyl monolayers obtained by grafting of trifunctional silanes on silica, titania, hafnia, and zirconia are very similar.¹²⁰ Fadeev et al. reported on the reaction of organosilicon hydrides, RSiH₃, with titanium and other metal oxides.¹²¹ The reaction of octadecyltrihydrosilane with titania in the presence of ultrasound was studied by Shafi et al.¹²² Ever since, few studies were done on SAMs from organosilicon hydrides supported on metal oxides.¹²⁰⁻¹²² As shown by FTIR, TGA, XPS and wettability studies, SAMs of organosilicon hydrides are in general closely packed and well-ordered.^{120,121}

In the present study, C₁₈ alkyl chains grafted on various metal oxides were prepared by the reaction of *n*-octadecyltrihydrosilanes and *n*-octadecyltrichlorosilanes with titania, zirconia, hafnia, and alumina. The effect of metal oxides, two different silylating agents on the conformational behavior is described along with the corresponding reaction schemes. The conformational order of C₁₈ alkyl modified metal oxides was studied using variable temperature FTIR and solid-state NMR spectroscopy. In addition, pyridine adsorption and DRIFT studies were made to determine the acidic centres (Lewis and Brønsted types) on the ungrafted and grafted metal oxide substrates.

2.2.3 Silica-Zirconia Mixed Oxides

The applicability of zirconia to overcome the drawbacks of silica is somewhat limited due to the presence of Lewis acidic, Brønsted acidic and Brønsted basic sites, which might lead to irreversible adsorption of some analytes. SiO₂-MO₂ (M = Zr, Hf) binary oxides are interesting materials for a wide spectrum of technological applications, comprising catalysis¹²³⁻¹²⁵ and structural materials with enhanced physico-chemical properties (high thermal and chemical stability or fracture toughness).¹²⁶ Such binary systems have been prepared by different routes, for instance, by chemical solution deposition,¹²⁷ and by a conventional sol-gel synthesis starting from the corresponding alkoxides^{128,129} or by using the single-source precursor tris(tert-butoxy)siloxy complexes M[OSi(OtBu)₃]₄ (M= Zr, Hf).¹³⁰ Recently, a new preparation route has been developed which is based on the use of silica and zirconium - based inorganic-organic hybrid materials as composite precursors for the final oxide.¹³¹⁻¹³³

In the present study, mixed oxides prepared by this latter route, i.e. by calcination of silica-based inorganic-organic hybrid materials with embedded zirconium oxocluster Zr₄O₂(OMc)₁₂ were used as supporting materials for alkyl chain functionalization.¹³⁴ The

hybrid materials were prepared starting from methacryloxypropyltrimethoxysilane (MAPTMS = $\text{CH}_2=\text{C}(\text{CH}_3)\text{C}(\text{O})\text{O}(\text{CH}_2)\text{Si}(\text{OCH}_3)_3$) which was copolymerized with the methacrylate-substituted zirconium oxocluster $\text{Zr}_4\text{O}_2(\text{OMc})_{12}$. The hydrolysis and condensation reactions of the silane alkoxy groups form a silica network, whereas by polymerization of the methacrylate moieties of the oxocluster with that of the silane yields a covalent incorporation of the Zr-based building blocks into the silica hybrid backbone. Samples characterized by different $\text{ZrO}_2:\text{SiO}_2$ molar ratios (i.e. $\text{ZrO}_2:\text{SiO}_2$ -1:2.5 and $\text{ZrO}_2:\text{SiO}_2$ -1:10) were prepared and calcined at 600 and 800 °C. Upon calcination, the organic part burns out, leaving a mixed silica-zirconia oxide, as described earlier.¹³¹⁻¹³³ In the present work, C_{18} alkyl chains were attached to the mixed silica-zirconia supports which might provide an opportunity to overcome the aforementioned limitations of pure silica and zirconia.

The prepared alkyl functionalized mixed oxide materials were thoroughly characterized by using different experimental techniques, providing complementary pieces of information on composition, morphology, microstructure, and chain ordering by XPS, SEM, EDX, N_2 physisorption, SSNMR and FTIR, respectively.

2.2.4 Surface Modification of Inorganic Oxides

Organic functionalization of inorganic oxides permits a tuning of surface properties like hydrophilicity, hydrophobicity and surface reactivity.¹³⁵ Usually organosilicon compounds are applied to modify the surface of inorganic materials, as they are very reactive. In this context, mono-, di-, and trifunctional silanes (RSiX_n ; $n = 0-3$; R = alkyl chains of length C_4 , C_8 , C_{12} , C_{18} , C_{22} , C_{30} , etc.; X = chloro or alkoxy groups) have been grafted to the surfaces of various oxide materials. In particular, trifunctional silanes have been frequently used as silylating reagents for surface modification of such oxide substrates which provide closely packed and highly ordered monolayers with enhanced stability.¹³⁶⁻¹³⁸ However, the application of trifunctional silanes may also result in undesired vertical polymerization.¹³⁹ In commercial columns modification is therefore done by means of monofunctional silanes which provide reproducible surface coverages while vertical polymerization is avoided. It should be mentioned that the modification of mono-, di-, or trifunctional silanes on the oxide substrates depends on the targeted applications. Likewise, organosilicon hydrides as grafting agents have several advantages

over other silane coupling agents, since they provide a clean reaction environment. Hence, the uniformity of the alkyl chains on the substrates is improved, closely packed and well-ordered phases may result.^{120,121,140}

Depending on the type of organosilanes used for modification of the surface of inorganic oxides, the resulting reversed-bonded phases are classified into different types as mentioned in the introduction. The first type of bonded phase is the brush-type phase and is prepared using a mono-chlorosilane reagent, and it derives its name due to the similarity to the look of bristles on a brush. Due to the steric hindrance of the large C₈ and C₁₈ dimethylsilanes, the surfaces are not covered fully with alkyl chains, and there are free silanols remaining on the surface even after the modification. It is not clear that the silanol groups are evenly distributed around the silica surface. Mesoporous supports were used in this study which has lower number of silanol groups and are distributed evenly on the surface.¹⁴¹ Hence, these materials can be utilized for uniform functionalization.

The second and third types of stationary phases are called the oligomeric-type phase and the bulk-type phase. The oligomeric phase uses a disubstituted silane reagent, and the bulk phase uses a trisubstituted silane reagent. The oligomeric and bulk-phase stationary phases are used to covalently bond the silane silicon atom to the silica surface with one or more bonds.¹⁴² With these phases, vertical polymerization or horizontal polymerization can occur.

The most common stationary phases used are octadecyldimethyl (C₁₈) phases with silica as the solid support. Generally, the monomeric phases yield very low surface coverage (3-3.5 μmol/m²) whereas maximum surface coverage of 8 μmol/m² can be achieved by using the trifunctional silanes on silica.^{63,138} In this dissertation, the majority of the studies were made using C₁₈ trifunctional silane as the grafting agent.

Monofunctional silane modified stationary phase materials can be obtained by the attachment of alkyl chains through single bonds. When di- or trifunctional silanes are used, two or more bonds per ligands will be formed with the inorganic support along with cross-linking of the neighboring silanes. The resulting bonding situation for mono- and trichloro silane grafted phases is shown in Figure 2.5. The effective bonding in the case of

trimethoxy- and trihydrido-silanes are different with a lower degree of cross-linking when compared to trichlorosilanes, since the formation of HCl as byproduct is faster.

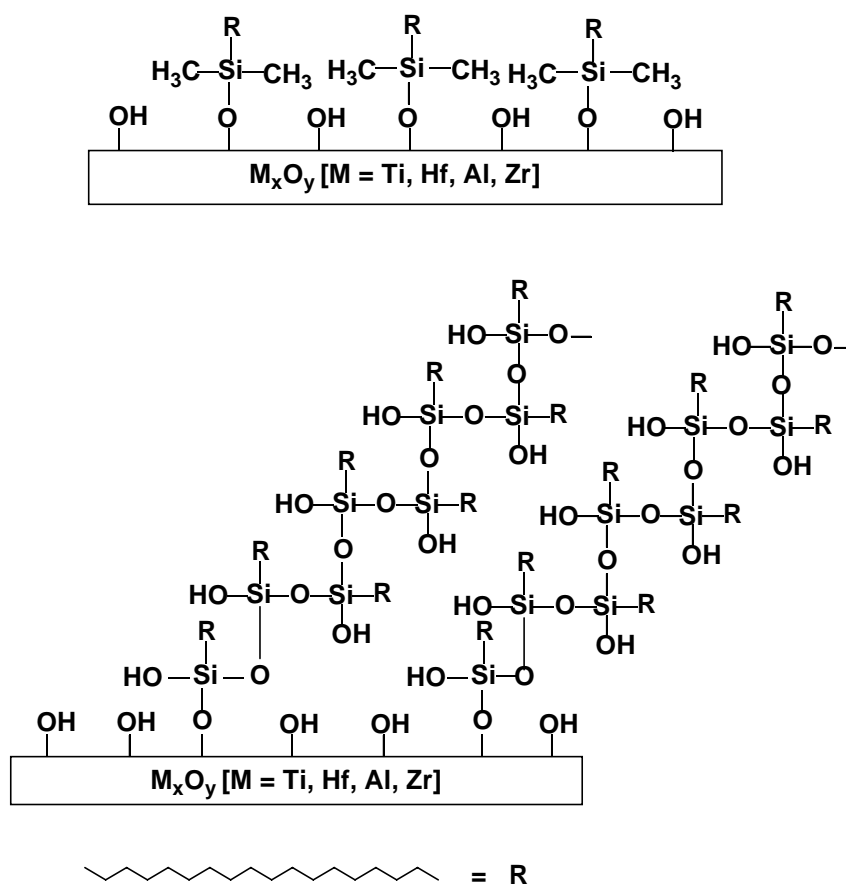


Figure 2.5. Representative structure of the C₁₈ alkyl grafted stationary phases. Top – Phases formed from the monochlorosilane, Bottom – Phases formed from the trichlorosilane.

The procedures used for the polymeric phase synthesis have been described as “solution polymerized” and “surface polymerized” to distinguish the introduction of water for initiating the polymerization (Figure 2.6). For solution polymerization, water is added to slurry of silica containing di- or trichlorosilane. Polymerization occurs in the solution with subsequent deposition onto the silica.^{34,50} Deposition of the silane polymer on the silica surface would result in a surface with some heterogeneity. Most likely, vertical polymerization will occur in this case and the degree of polymerization is due to the amount of water added to the reaction medium.

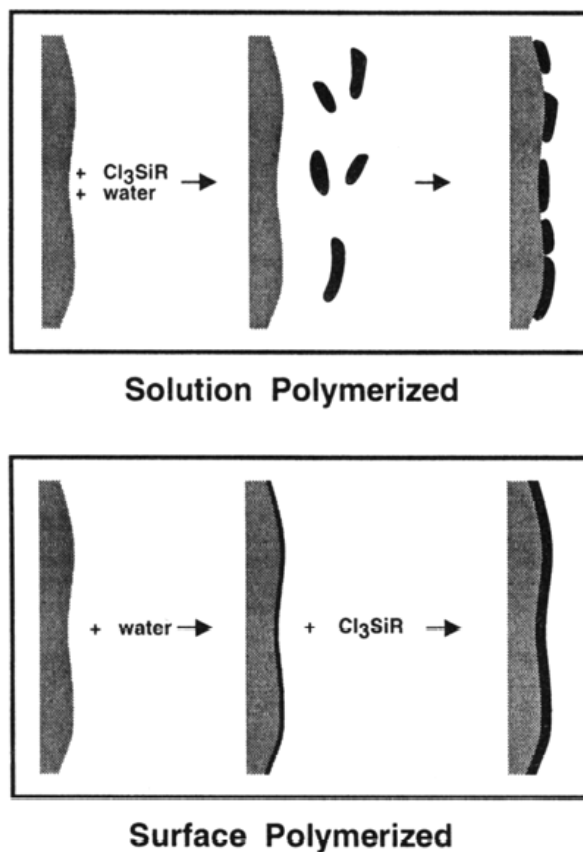


Figure 2.6. Diagram distinguishing two approaches to the synthesis of polymeric stationary phases. Silane polymerization occurs in solution or at the silica surface depending on the order of addition of reagents.

For surface polymerization, water is added to dry silica either through exposure to humid air or by direct addition prior to silanization.^{50,143} Here, monolayer coverage of the water molecules on the silica surface is achieved. Later, wet silica is introduced into a solution containing the silane. The “surface polymerized” procedure is a self-assembled monolayer approach, where higher surface coverage of alkyl chains on the surface and a more regular bonded surface can be reached.^{51,144} These phases are mostly horizontally polymerized and have more alkyl moieties which are bonded to the surface and have the ability to run at the high and low pH extremes.¹⁴⁵ Vertical polymerization also takes place here which actually depends on the amount of water present on the surface and on the type of silylating agent.^{11,146}

After derivatization with alkyl silanes (usually with C₄ to C₃₀ systems), residual silanols remain on the surface.¹⁴⁷ In order to eliminate these silanols, low molecular weight (C₁ to

C₃) alkyl silane reagents are used to endcap the surface. These smaller silanes will react with as many silanols as is allowable by space. Endcapped alkyl modified phases were shown to provide better chromatographic results.^{148,149} The main compound used for endcapping is hexamethyldisilazane (HMDS).¹⁵⁰ In the present study, endcapping was done with HMDS after the grafting of mono- and trifunctional silane on the mesoporous supports. Figure 2.7 provides a schematic drawing of endcapped silica gels after grafting with mono- and tri-functional C₁₈ chains.

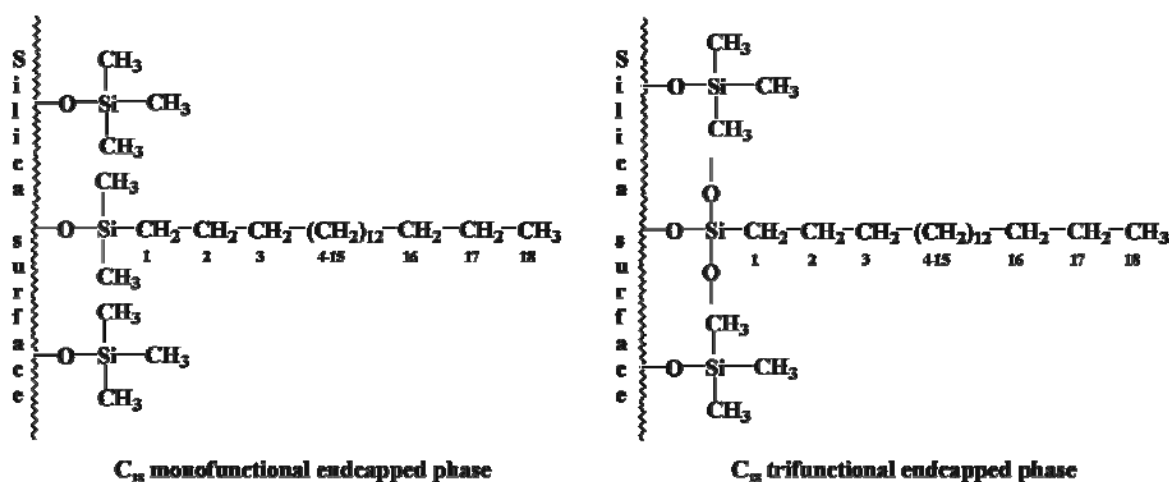


Figure 2.7. Schematic drawing of endcapped silica gels after grafting with mono- and tri-functional C₁₈ chains.

In this dissertation, the inorganic substrates (mesoporous silica, metal oxides and mixed oxides) were functionalized with different octadecyl silylating agents to prepare the stationary phases with different surface coverages. The grafting of these C₁₈ alkyl chains were performed with different reaction procedures which are explained in detail in chapters 4 and 5.

Chapter 3

3 Physico-Chemical Techniques

Covalently bound organic groups on inorganic oxides are used in variety of technological applications. The characterization of physical and chemical properties of chemically modified surfaces is of considerable importance for an improved understanding of interfacial phenomena in various fields, such as catalysis, electrochemistry, and chromatography, etc. Alkylated substrates prepared by the reaction of silanes with porous silica are widely used in liquid chromatography for the separation of polar and nonpolar analytes. Such bonded phase layers have unique properties that differ from the solid and liquid states of matter. By nature of the covalent bond, the degrees of freedom of grafted chains are reduced, and chain motion is intermediate to that of the corresponding alkane melts liquids and crystalline solids. An understanding of the physical nature of the bonded phase is a requisite for a complete description of the analyte retention mechanisms. Properties such as surface coverage and ligand density are routinely calculated from sorbent bulk properties (e.g., substrate surface area and percentage of carbon), but these measurements do not provide any insight into the phase structure at the molecular level. In the past, a variety of techniques were employed to probe the inorganic oxide substrates and their alkyl bound structures.

3.1 Fourier Transform Infrared Spectroscopy (FTIR)

In infrared spectroscopy, radiation is passed through the sample in which radiation is partially absorbed by the sample. The resulting spectrum represents the molecular absorption, creating a molecular fingerprint of the sample which corresponds to the frequencies of vibrations of molecular bonds and chemical environments in which these bonds are present. In this technique, molecules only absorb infrared light at those frequencies where the infrared light affects the dipolar moment of the molecule.

Almost all molecules absorb infrared light (except monatomic and homopolar diatomic molecules), and each type of molecule only absorbs infrared light at certain frequencies. This property provides a unique characteristic for each molecule. It provides a way to identify the molecule type (qualitative analysis) and the amount of this molecule in the

sample (quantitative analysis). Importantly, IR spectroscopy is used for the identification of the functional groups present in the molecules. The major advantage of FTIR spectroscopy is its high sensitivity and relatively easy access to the desired information about the infrared absorption spectrum from the infrared spectral libraries.

FTIR absorption frequencies, band intensities and band shapes have shown to reflect the molecular conformation, configuration and chain packing in polyethylene chains.¹⁵¹ The spectral features of the polyethylene infrared spectra have been used as a base for studying *n*-alkanes and subsequently those of tethered *n*-alkyl chains due to their structural similarities. FTIR spectroscopy probes on a time scale of less than 10^{-10} s and is a versatile tool for examining the chain conformational order in various materials. For instance, it has been proven to be an efficient technique to characterize the conformational features of the chromatographic column materials, i.e. of the tethered long alkyl chains.^{55,63-71}

The degree of alkyl chain conformational order of grafted systems varies substantially from highly ordered (crystalline) to disordered (liquid-like) and are substrate, preparation route and temperature dependent. Alkane chain structure and interfacial properties dictate the function and utility of these materials. In alkane-modified silicas used as stationary phase materials for chromatography, the conformational order of the alkane moieties governs the efficiency and selectivity of the separations.^{50,98,144} The understanding at a molecular level of the alkyl chain conformational order behavior is thus crucial for such materials function in their respective applications.

In a pioneering work, Snyder calculated and tabulated the IR frequencies for an extensive number of vibrations in alkanes, including some that are specific to localized bent structures containing gauche bonds.⁷⁶ Normal mode calculations detail the assignment of various C-H stretching, scissoring, rocking and wagging modes. The observed wavenumbers, intensities and positions of these bands provide quantitative information about various defect structures responsible for disorder in the system. These conformational defects have also been observed in other more complex hydrocarbon assemblies, such as model membranes and biomembranes¹⁵² as well as micellar systems.¹⁵³

In the present dissertation, several vibrational modes have been used to investigate the conformational order of alkyl modified stationary phase materials. Table 3.1 contains the information related to each investigated vibrational mode.

Table 3.1. Conformation-sensitive IR modes used for *n*-alkyl chain conformational analysis.

Vibrational Mode	Wavenumber (cm⁻¹)	Comments
CH ₂ stretching: Symmetric Antisymmetric	2853-2846 2926-2915	Shift to higher frequency indicates more conformational disorder (qualitative)
CH ₂ wagging	1370-1330	Integrated peak intensity provides amount of gauche conformers; kink (gtg' & gtg), double gauche (gg), and end gauche (eg)

3.1.1 Methylene Stretching Bands

The frequency shifts of the band maxima in the CH₂ stretching regions provide information about the conformational order and disorder of the alkyl chains by comparison with the absorption band maxima of *n*-alkanes.¹⁵⁴ For completely disordered “spaghetti-like” structures, the absorption wavenumber of the CH₂ antisymmetric stretching band is close to that of a liquid alkane (2924 cm⁻¹). For well-ordered systems, the absorption maximum is shifted to lower wavenumbers and is close to that of crystalline alkanes (2915 cm⁻¹). A similar shift can be registered for the CH₂ symmetric band. The position of the symmetric and anti-symmetric stretching modes in *n*-alkyl chains grafted on the oxide substrates gives rise to bands from 2853 to 2846 cm⁻¹ and 2926 to 2915 cm⁻¹, respectively.

Figure 3.1 illustrates the FTIR spectra for C₁₈ alkyl chains grafted on titaniumdioxide in the anti-symmetric and symmetric stretching band region between 2950 and 2820 cm⁻¹. They show a shift in the CH₂ stretching band positions towards higher wavenumbers due

to the increasing amounts of methylene groups in gauche conformations under the influence of temperature. In addition, the CH₂ stretching bandwidth can be exploited to study the alkyl chain flexibility of the stationary phase materials. Here, the CH₂ bands are narrower at lower temperatures, reflecting lower alkyl chain flexibility and higher conformational order.⁶³ At higher temperatures, an increase of the CH₂ stretching bandwidth is observed which can be attributed to enhanced alkyl chain flexibility owing to a decrease of conformational order.

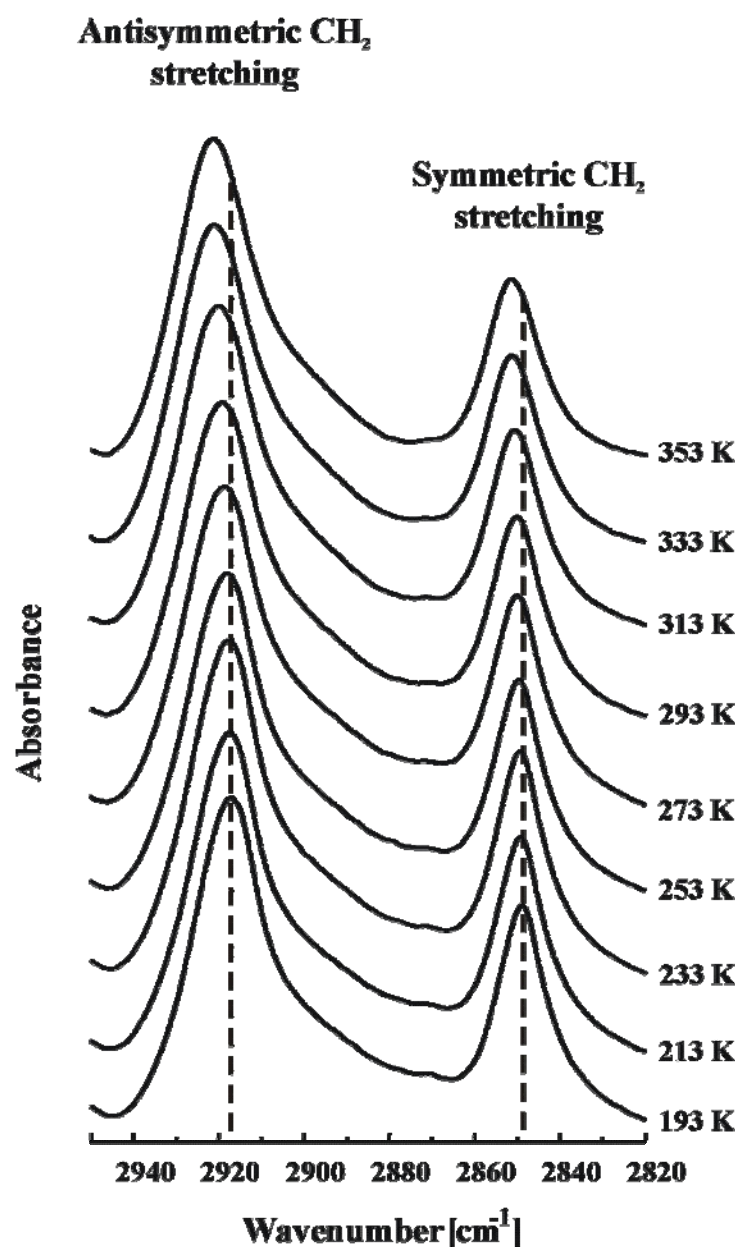


Figure 3.1. Antisymmetric and symmetric CH₂ stretching band spectra for alkyl chains grafted on titaniumdioxide using *n*-octadecyltrichlorosilanes between 193 K and 353 K.

3.1.2 Methylene Wagging Bands

Quantitative information about the presence and amounts of various gauche conformers in the C₁₈ alkyl modified oxide substrates can be obtained by the analysis of the wagging band intensities between 1400 cm⁻¹ and 1330 cm⁻¹.^{76,155} The basis of this conformational study is given by the pioneering work of Synder et al.⁷⁶ who calculated and observed the vibrational frequencies for CH₂ wagging band modes in protonated liquid *n*-alkanes containing specific nonplanar conformers. The conformation dependent wagging modes of interest appear near 1368, 1353, and 1341 cm⁻¹ and arise from kink/gauche-trans-gauche (gtg), double gauche (gg), and end-gauche (eg) sequences, respectively (Figure 3.2). The most intense band in the spectral range from 1300 to 1400 cm⁻¹ is due to the methyl group umbrella deformation mode at 1378 cm⁻¹, which is insensitive to the conformational order and which is used as an internal reference.

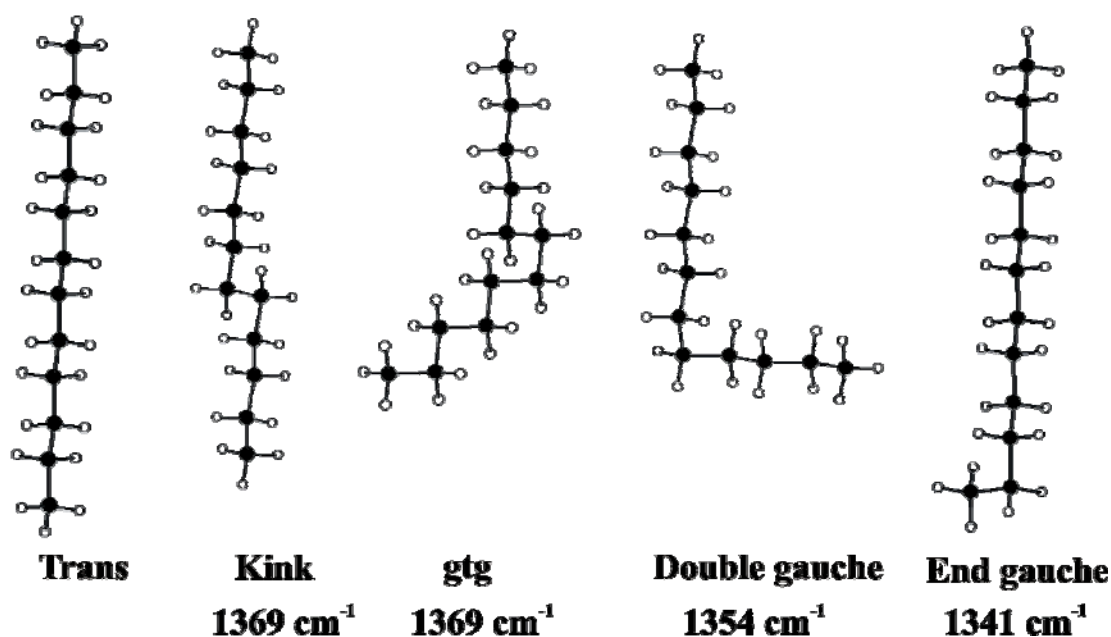


Figure 3.2. Alkyl chain conformations from CH₂ wagging band region. The non-planar conformations give rise to localized mode vibrations, which are observed in FTIR spectra.

In Figure 3.3, a representative experimental FTIR spectrum covering the CH₂ wagging band region between 1330 and 1400 cm⁻¹, recorded at 293 K, is shown along with the theoretical curves from the curve fitting analysis. The intensities of these bands can be used to obtain quantitative information about various “defect” structures within the chains that contribute to the overall disorder of the system. The kink/gtg conformers are taken

together since it is not possible to distinguish them spectroscopically. The kink/gtg sequence provides some disruption in the order of the interior segments of the chain, while the double-gauche sequence creates a severe destruction from the alignment of chains in the all-trans conformation. In contrast, the end- gauche sequence provides the least perturbation to chain order, since it occurs only at the terminal methyl end groups of the chains.

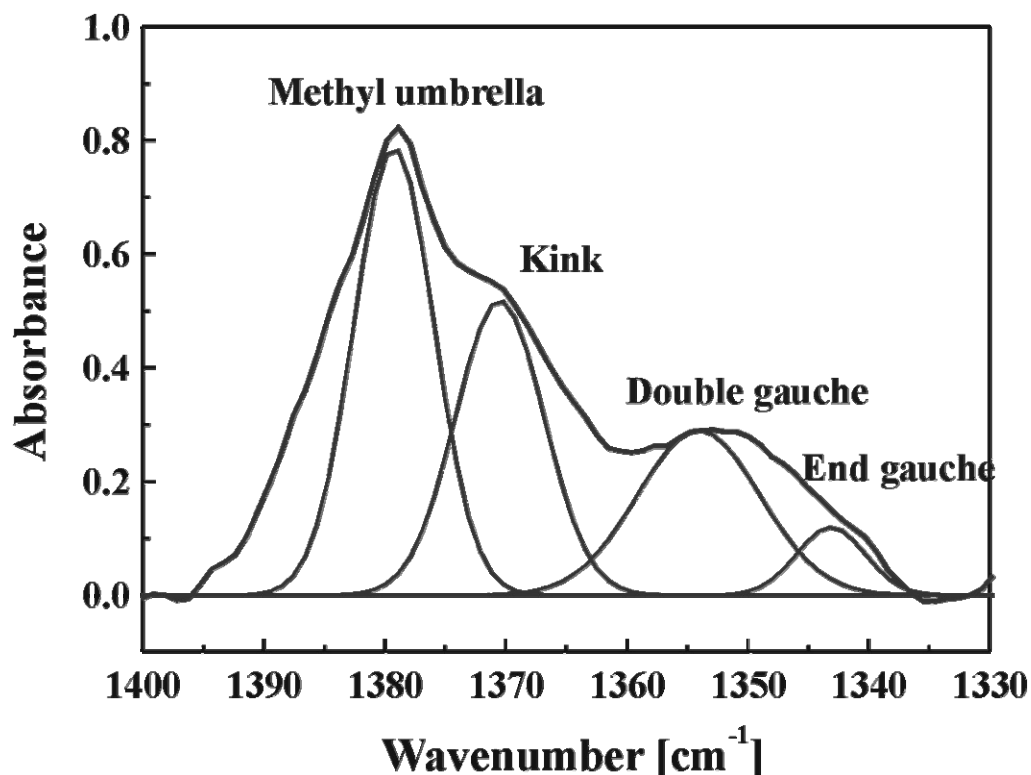


Figure 3.3. Experimental IR spectrum of the CH₂ wagging band region for the C₁₈ alkyl grafted MCM-41 at 293 K. The underlying curves result from a curve fitting analysis.

The specific gauche conformers were calculated based on reference measurements on alkanes and a theoretical approach using the rotational isomeric state (RIS) model given by Flory.¹⁵⁶ The RIS model predicts the fractions and numbers of the three conformations at a given temperature for *n*-alkanes of a given chain length. Calculations have been performed for C₁₄H₃₀ to C₁₈H₃₈ in a temperature range from 273 to 373 K by Senak et al.¹⁵⁵ A cubic polynomial function was fitted to each of the calculated percentages of kink (gtg'/gtg), double-gauche (gg), and end-gauche (eg) conformers as a function of temperature. The calculated percentages, i.e., P_k, P_{gg} and P_{eg}, which are independent of the chain length in accordance with the RIS model, are given as follows:

$$P_k (\%) = -9.092 + 1.249 \times 10^{-2} T - 2.732 \times 10^{-4} T^2 + 2.176 \times 10^{-7} T^3 \quad (3.1)$$

$$P_{gg} (\%) = -7.364 + 8.859 \times 10^{-2} T - 1.388 \times 10^{-4} T^2 + 8.471 \times 10^{-8} T^3 \quad (3.2)$$

$$P_{eg} (\%) = -4.522 + 1.620 \times 10^{-1} T - 3.486 \times 10^{-4} T^2 + 2.855 \times 10^{-7} T^3 \quad (3.3)$$

where T is the temperature in Kelvin and the calculation is valid (for interpolative purposes) in the temperature range between 273 K and 373 K. P_k and P_{gg} include distinct counting of conformers of the type (gg, g'g') or (g'tg, gtg', g'tg' and gtg), respectively, while end-gauche calculations refer to a single state only. The percentage probabilities of these conformers can be converted to their absolute numbers per chain for a particular n -alkane molecule, via the following equations:

$$\text{Number of kink + gtg conformers} = P_k \left\{ \frac{N_{C-C} - 4}{100} \right\} \quad (3.4)$$

$$\text{Number of double-gauche conformers} = P_{gg} \left\{ \frac{N_{C-C} - 3}{100} \right\} \quad (3.5)$$

$$\text{Number of end-gauche conformers} = \left\{ \frac{4P_{eg}/100}{1 + P_{eg}/100} \right\} \quad (3.6)$$

where N_{C-C} , the number of C–C bonds in the n -alkane. The number of end-gauche conformers is chain length independent, since a maximum of two are possible regardless of the chain length.

According to the above model, the band intensities and are determined by curve-fitting analysis of the measured spectrum after baseline corrections. The resultant bands are then normalized to the intensity of the methyl umbrella band.⁷⁶ The amount of specific gauche sequences in the n -alkyl modified system is then calculated using the reference plots of n -alkanes from Neumann-Singh et al.¹⁵⁷ which is based on the RIS model (using Equations 3.1 to 3.6).

The number of conformers per chain was calculated based on the fact that the surface linked alkyl chains contain only one methyl group per chain, in contrast to liquid n -alkanes which contain two methyl groups per chain. The total number of gauche

conformers per chain was obtained by considering the fact that two gauche bonds are necessary to build up one kink or double-gauche sequence and one gauche bond for the end-gauche sequence.

3.2 Solid-State NMR Spectroscopy (SSNMR)

3.2.1 Theory

NMR spectroscopy is a widely employed physical methods, since it provides a powerful tool to investigate the structure and the dynamics of chemical systems. While molecular substances in solution give spectra characterized by sharp peaks, the spectra in the solid state, by contrast, are broad and featureless owing to various internal and external interactions which are described below in detail.

The nuclei with a spin possess a magnetic moment $\vec{\mu}$, which interacts with its surroundings. Generally, these interactions can be divided into two classes that are described by an external and an internal Hamiltonian,^{158,159} i.e.

$$\hat{H} = \hat{H}_{\text{ext}} + \hat{H}_{\text{int}} \quad (3.7)$$

The first term on the right hand side includes the interactions of a spin system with the external static magnetic field \vec{B}_0 (Zeeman interaction, \hat{H}_Z) and the pulsed oscillating radio-frequency (r.f.) fields (\hat{H}_{rf}); the second term includes the interactions of a spin system with internal local fields originating from the chemical shift interaction (\hat{H}_{CS}), direct dipole-dipole interaction (homo-nuclear, \hat{H}_{II} and hetero-nuclear, \hat{H}_{IS}), quadrupole interaction (\hat{H}_{Q}), and indirect J-coupling (\hat{H}_{J}). Thus, Eq. (3.7) can also be expressed as^{158,160}

$$\hat{H} = \hat{H}_Z + \hat{H}_{\text{rf}} + \hat{H}_{\text{CS}} + \hat{H}_{\text{II}} + \hat{H}_{\text{IS}} + \hat{H}_{\text{Q}} + \hat{H}_{\text{J}} \quad (3.8)$$

The external interactions have an identical influence on the whole spin system and contain no structural and dynamic informations about the nucleus of interest which are

conversely included in the internal interactions. All internal Hamiltonian contributions reflect tensoral interactions, which depend on the orientation of the interaction tensor with respect to the external magnetic field direction. In comparison with the external static field, the internal or local interactions are small. Therefore they act only as a first-order perturbation in the high field (secular) limit and produce small shifts and splittings of the Zeeman energy levels which depend on the nature and extent of the couplings and on the number of interacting spins.

The Zeeman interaction

The interaction of the magnetic moment, $\vec{\mu}$, of a nucleus with the static external magnetic field, \vec{B}_0 is called Zeeman interaction and is written as

$$\hat{H}_Z = -\gamma\hbar B_0 \hat{I}_z \quad (3.9)$$

where γ is the gyromagnetic ratio of the nuclear spin \hat{I} , \hbar is the Planck's constant h divided by 2π and \vec{B}_0 , the external magnetic field along the z-direction of the laboratory frame.

Assuming that the Zeeman interaction is the only contribution in the spin Hamiltonian, the magnetic moment of the nucleus experiences a precession around the direction of the magnetic field with the well-known Larmor frequency ω_0 , which is given by

$$\omega_0 = -\gamma B_0 \quad (3.10)$$

For an allowed transition between two states, m and m' ($m' = m \pm 1$), the energy difference is given by

$$\Delta E = \pm\gamma\hbar B_0 \quad (3.11)$$

Eq. (3.11) shows that the energy difference ΔE is directly proportional to the magnitude of the magnetic field. The energy difference between the two states alters along with the variation of the external magnetic field strength. Once the energy of the photon generated

by the radio-frequency irradiation matches the energy difference between the two spin states, absorption of energy by the sample occurs.

When a group of spins is exposed to a magnetic field, the number of spins in the lower energy level, N^+ and the number in the upper energy level, N^- , follow the Boltzmann statistics, as given by

$$\frac{N^-}{N^+} = e^{-\Delta E/kT} \quad (3.12)$$

where k is the Boltzmann's constant, 1.3805×10^{-23} J/Kelvin, and T is the temperature in Kelvin. At room temperature ($N^-/N^+ = 0.99998$), the population difference between the two states is very small. Moreover, the ratio N^-/N^+ decreases with decreasing temperature.

The signal in NMR spectroscopy results from the difference between the energy absorbed by the spins which make a transition from the lower to the higher energy state, and the energy emitted by the spins which simultaneously make a transition from the higher to the lower energy state. The signal is thus proportional to the population difference between the states, as described by Eq. (3.12).

Interaction with the radio-frequency fields

In NMR experiments, the r.f. field is created by the probe coil passing an alternating current at the Larmor frequency, and employed to manipulate the effective Hamiltonian of the spin system. The amplitude of the oscillating r.f. field is substantially smaller than that of the static magnetic field, so \hat{H}_{rf} acts as a perturbation on the spin system, which does not change the energy levels but only induces transitions between them. If an oscillating r.f. magnetic field, $\vec{B}_1 = (B_1, 0, 0)$, is applied along the x-axis perpendicular to the static magnetic field in the laboratory frame, the interaction of a nuclear spin with this field can be expressed by the Hamiltonian

$$\hat{H}_{rf} = -2\gamma\hbar\vec{B}_1 \cos(\omega t + \varphi)\hat{I}_x = -2\gamma\hbar B_1 \cos(\omega t + \varphi)\hat{I}_x \quad (3.13)$$

where ω is the carrier frequency and ϕ is the phase. When the r.f. field oscillates close to the resonance frequency ω_0 , which corresponds to the Zeeman energy splitting, the transition between the spin states will occur.

The introduction of the r.f. pulse complicates the motion of the spin in the magnetic field. On one hand, the spin precesses around the B_0 field with the Larmor frequency, while on the other hand, it nutates due to the action of the r.f. field. In order to facilitate the interpretations, it is useful to introduce the “rotating frame”, which rotates around the z-axis of the applied static magnetic field with frequency ω . The effective Hamiltonian in the rotating frame becomes

$$\hat{H}_{\text{eff}} = -\gamma\hbar(\vec{B}_0 - \vec{B}_f)\hat{I}_z + \gamma\hbar\vec{B}_1\hat{I}_x = (\omega_0 - \omega)\hbar\hat{I}_z - \omega_1\hbar\hat{I}_x \quad (3.14)$$

where $(\omega_0 - \omega)$ is the so-called resonance offset. When $\omega_0 = \omega$, the irradiation is said to be on-resonance.

The Chemical-shift interaction

The chemical shift, or shielding, interaction originates from the effect of B_0 on the electrons around a nucleus. In a magnetic field, the electrons which have a magnetic moment themselves, circulate about the direction of the external magnetic field, B_0 . This circulation induces additional small magnetic fields, which may add to or subtract from the external magnetic field felt by the nucleus. Therefore, the effective magnetic field experienced by the nucleus is altered, as well as its resonance frequency. The chemical shift interaction is an anisotropic interaction, due to the fact that the electronic distribution in the molecules can be thought of as an ellipsoid. The degree to which the electron density affects the resonance frequency of a nucleus depends on the orientation of the electron cloud (and hence the orientation of the molecule) with respect to B_0 . The chemical shift Hamiltonian is expressed by¹⁶¹

$$\hat{H}_{\text{CS}} = \left\{ \sigma_{\text{iso}} + \frac{1}{2} \delta_{\text{CS}} [3 \cos^2 \theta - 1 + \eta_{\text{CS}} \sin^2 \theta \cos(2\phi)] \right\} \hbar\gamma B_0 \hat{I}_z \quad (3.15)$$

here the angles θ and ϕ describe the orientation of the chemical shift tensor with respect to B_0 , while σ_{iso} is the isotropic chemical shift typically in the order of 10^{-6} in ppm.

In a solid sample, the molecular motion narrows the chemical shift tensor by partial averaging, and the resulting powder pattern contains motional and orientation information of the molecules. In solution, the rapid, essentially isotropic motion of the molecule, or molecular segments, averages the shielding tensor to its isotropic value σ_{iso} .

Since the chemical shift is a direct consequence of the electronic structure, the chemical shift tensor can provide information on the structure of the molecules and serve to verify calculations of the electronic structure of molecules. The chemical shift anisotropic interaction contributes significantly to the line broadening of a solid state NMR spectrum, which often obscures the structural information available from the isotropic chemical shifts. This line broadening of the resonances in solid state can be eliminated by spinning the sample at high speed and at a certain angle, the so-called magic angle spinning (see later section).

The direct dipole-dipole interaction

A single nucleus with spin $I = 1/2$ can be placed in the external magnetic field, based on its orientation, either parallel (“spin-up”) or antiparallel (“spin-down”) with respect to the external field. If two dipolar coupled spins i and j within reasonable proximity ($< 10 \text{ \AA}$) are considered, one nuclear spin will experience the magnetic field produced by the other and vice versa. This magnetic field produced by spin j will either add to (“spin-up”) or subtract from (“spin-down”) the external field felt by the spin i , thus the effective magnetic field at the site i changes its resonance frequency. The magnitude of the dipolar-dipolar interaction depends on the spin species, the internuclear distance and the orientation of the internuclear vector with respect to the external magnetic field. Two different cases can be distinguished: homonuclear dipolar coupling between the nuclei of the same type and heteronuclear coupling between different types of nuclei. Dipolar interactions can be eliminated by spinning the sample at the magic angle as described in the following section.

Magic angle spinning (MAS)

Spin interactions can be manipulated by rotating a sample about an axis inclined by an angle θ toward the magnetic field B_0 . If this rotation is at the “magic angle”, the main interactions (i.e. chemical shift, dipolar and first-order quadrupolar interactions) can be removed, narrowing the resonance lines to reveal spectral details. When a sample is spinning at the spinning rate ω_r , all spin interactions are time-dependent and sidebands with the separation ω_r are created. If the spinning rate is much greater than the anisotropic spin interaction, the sidebands are well separated from the central line and become vanishingly small with increasing ω_r .^{162,163}

MAS can either be used on its own, or be combined with other line-narrowing techniques. For instance, it can be used in conjunction with multiple pulse sequences to obtain high resolution NMR spectra, especially for hydrogen and fluorine nuclei in solids, or with cross-polarization and high power heteronuclear decoupling methods to get high resolution spectra for ^{13}C , ^{29}Si and other low abundant nuclei. In case of spin-1/2 nuclei, the line broadening mainly arises from direct dipole-dipole interaction and electron shielding interaction. The effect of MAS on each of them is discussed in the following sections.

Chemical shift and magic angle spinning

Under fast spinning conditions, the molecules rapidly experience all possible orientations, and hence, even a strongly asymmetric electron distribution will appear spherical when viewed on the NMR timescale. The chemical shift Hamiltonian can be divided into an isotropic term and an anisotropic term. For the axially symmetric ellipsoid case, in which $\sigma_{xx} = \sigma_{yy}$, the chemical shift Hamiltonian can be written as

$$\hat{H}_{\text{CS}} = \hbar\omega_0 \hat{I}_z \sigma_{\text{iso}} + \frac{1}{2}(\sigma_z - \sigma_{\text{iso}})(3\cos^2\theta - 1)\hbar\omega_0 \hat{I}_z \quad (3.16)$$

When a solid sample is rotated with angular velocity ω_r about an axis inclined at angle θ_m respect to B_0 and at angle β to the principal axes of the $\tilde{\sigma}$ tensor, the chemical shift Hamiltonian becomes time dependent and is expressed as

$$\hat{H}_{CS} = \hbar\omega_0\hat{I}_z\sigma_{iso} + \frac{1}{2}(\sigma_z - \sigma_{iso})\left[(3\cos^2\theta_m - 1)(3\cos^2\beta - 1) + \xi(t)\right]\hbar\omega_0\hat{I}_z \quad (3.17)$$

Where $\xi(t)$ contains the functions of the Euler angles involved in the coordinate transformation.

The first term (isotropic part) in the right hand side of Eq. (3.17), is invariant under motion; the first term between the square bracket accounts for the averaged anisotropy of the chemical shift tensor which depends on the angle between the spinner axis and the external magnetic field B_0 . When the angle θ_m is 54.7° , the value of the $(3\cos^2\theta_m - 1)$ term in the chemical shift Hamiltonian is zero, the shift anisotropy is removed from the NMR spectrum. If the angle θ_m deviates from the magic angle, a scaled anisotropy is observed. The second term in the square bracket gives rise to sidebands. When the spinning rate is not fast enough to exceed the width of the static line shape, the powder pattern breaks up into relatively narrow lines at the isotropic chemical shift (center band) and sidebands at multiples of ω_r from the center band.

Dipole-dipole interaction and magic angle spinning

In a similar way as shown for the chemical shift Hamiltonian term, the dipolar broadening can be reduced rotating the sample at the magic angle $\theta_m = 54.7^\circ$. Theoretically, provided the MAS rate ω_r is larger than the linewidth resulting from the dipolar interaction, the dipolar broadening may be eliminated. In practice, it is usually not possible to spin faster than the dipolar linewidth. Especially for the case of dominant homonuclear dipolar interactions, and for abundant-spin situations such as ^1H and ^{19}F (at ca. tens of kHz rate), MAS with high frequencies (> 30 kHz) in combination with other line narrowing techniques, such as multiple pulse operation, has to be used to achieve line narrowing. In the situation of dominant heteronuclear dipolar interactions, such as ^{13}C and ^{29}Si NMR spectra, high power heteronuclear decoupling is performed in the experiment.

Cross polarization (CP)

The nuclei with low natural abundance, such as ^{13}C and ^{29}Si , have low spin polarization, hence in NMR experiment their sensitivity is low. In addition, shorter transverse relaxation times and residual anisotropic broadening (homo- and hetero-nuclear dipolar-

dipolar coupling) not completely averaged by rotation reduce not only the resolution but also the S/N ratio in NMR spectra.

In order to enhance the signals from low natural abundance nuclei, a technique called cross polarization (CP)^{158,164} is used (Figure 3.4). The CP technique involves the transfer of polarization from abundant nuclei (usually ^1H nuclei) to a low abundant one such as ^{13}C . The process of CP occurs through the transfer tendency of the magnetization from highly polarized nuclei to nuclei with lower polarizations when they are brought into contact, which is similar to heat flow from a hot object to a cold object when the two objects are in thermal contact. For homonuclear spins, the magnetization can be exchanged through mutual energy-conserving spin flips. For heteronuclear pairs, such as ^{13}C and ^1H , these spin flips are not energy-conserving at high fields. Therefore, the exchange of magnetization must be driven externally by the application of r.f. fields.

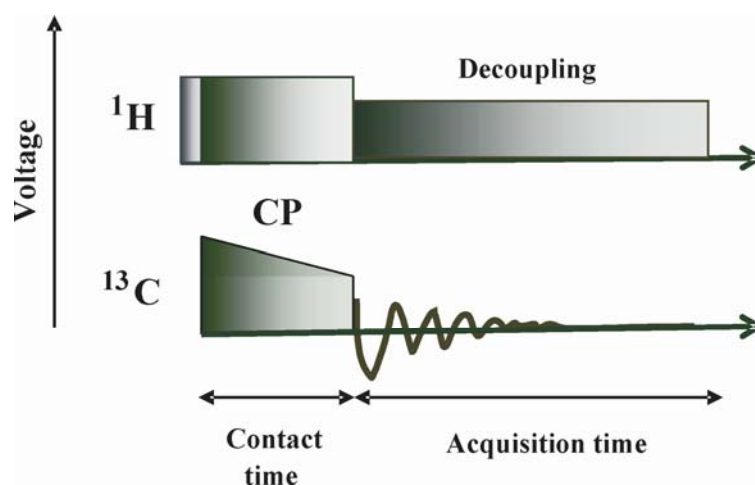


Figure 3.4. Pulse sequence of Cross polarization (CP) technique.

Among the technique for building a dipolar contact between two different spin systems I and S , the Hartmann-Hahn approach is particularly effective. This approach requires the simultaneous application of two continuous r.f. fields, one at the resonance frequency of the spin I and the other at the resonance frequency of the S spin. The effect of any r.f. field is to rotate the magnetization about the axis of the applied field. The rotation rate depends on the frequency and amplitude of the r.f. field. A r.f. field that oscillates at the spin I frequency, for instance 300 MHz, would not have essential effect on S spins with a frequency of 75 MHz and vice versa. By applying two r.f. fields, one tuned to the spin I the other to the spin S , both the I and S spins can be rotated independently around a

particular axis at rates determined by the amplitudes of the two applied fields. When the nutation frequencies of the I and S spins are equal, i.e. the Hartman-Hahn condition, given by¹⁶⁵

$$\gamma_I B_{1(I)} = \gamma_S B_{1(S)} \quad (3.18)$$

is satisfied, an energy-conversing dipolar contact between the two spin systems is created. The maximum enhancement for a CP contact period is γ_I / γ_S . It is through this dipolar contact that the polarization is transferred between the I and S spins.

Thus by employing the CP pulse sequence, the intensity of the signals of the less abundant nuclei can be enhanced and a good signal/noise ratio obtained. The use of CP also shortens tremendously the acquisition time. In this way, excellent spectra of a variety of nuclei in the solid state have been obtained. A careful analysis of these spectra and of the chemical shifts allows to distinguish the different coordinations of an atom. This technique has been extensively employed to study alkyl modified silica and metal oxide based stationary phase materials presented in this dissertation.

3.2.2 Alkyl Modified Supports and Solid-State NMR Technique

SSNMR spectroscopy offers a comprehensive approach to the study of alkyl modified stationary phase materials. With a combination of MAS, CP, and high-power decoupling, SSNMR has rapidly emerged as one of the most important tools in material science. SSNMR measurements of chromatographic materials yield extensive information about the structure of dry bonded phases, in particular for studying the alkyl chain mobility and conformational order of stationary phases.

In the early 1980s, Maciel and Sindorf pioneered the application of solid-state NMR techniques in chromatographic stationary phase materials by examining silica surfaces with ^{29}Si CP/MAS NMR spectroscopy.¹⁶⁶ Later, they explored the structure and mobility of grafted monofunctional C_8 and C_{18} ligands with ^{13}C CP/MAS NMR spectroscopy.⁷⁹ However, it has to be kept in mind that NMR spectra measured by CP/MAS are not quantitative since the efficiency of polarization transfer by CP is highly variable. The signal intensity of different nuclei can only be compared if the contact time maximum and

thus T_{SiH} (cross-relaxation constant) and $T_{1\rho H}$ (proton spin-lattice relaxation time in the rotating frame) values are in the same order. However, ^{29}Si and ^{13}C NMR techniques provide detailed information about the different groups present in substrate and chemically modified surfaces.

3.2.2.1 ^{29}Si MAS NMR Spectroscopy

^{29}Si MAS NMR spectroscopy is employed for the determination of the surface species, amount of alkyl chain grafting and degree of cross-linking of the attached alkylsilanes. Because of the chemical shift dispersion of about 130 ppm for silane and silica gel signals, structural elements can be assigned quite easily by recording ^{29}Si NMR spectra. The different structural elements are illustrated in Figure 3.5.

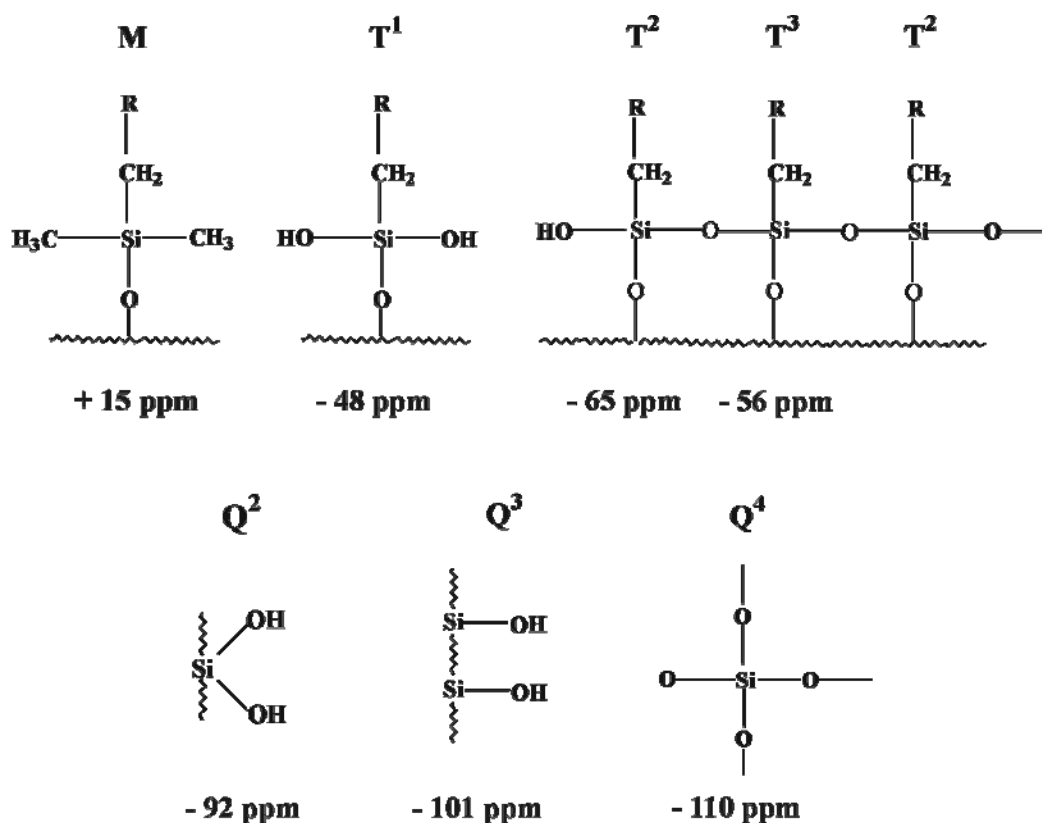


Figure 3.5. Different structural elements of the silicon species present in the C_{18} alkyl grafted silica systems.

The signals from the native silica are Q^2 , Q^3 , Q^4 (Q^n units = $\text{Si}(\text{OSi})_n(\text{OH})_{4-n}$, with $n = 1$ to 4), and are located in the range from -91 to -110 ppm, in which superscripts indicate the number of Si-O-Si bonds.^{26,51,152} In contrast to FTIR spectroscopy, where isolated and

geminal silanols absorb at nearly the same wavenumber, Q^3 units (silanol groups) and Q^2 (geminal silanols groups) can be distinguished by their corresponding chemical shifts at -91 and -100 ppm, respectively. The ^{29}Si NMR signals of the trifunctional silanes ($T^n = \text{RSi}(\text{OSi})_n(\text{OH})_{3-n}$, with $n = 1, 2, 3$) are located in the range from -45 to -70 ppm which refer to tri-functional groups without cross-linking (T^1) at about -48 ppm, with partial (T^2) at about -55 ppm, and with complete cross-linking (T^3) at around -66 ppm.^{26,51,152} In the case of monofunctional silane ($M = \text{R}_3\text{Si}(\text{OSi})$) and the endcapping group ($\text{Si}(\text{CH}_3)_3$), the peak is found at about +14 ppm.⁵¹ The general trend observed from the ^{29}Si NMR signal is the following: the high-field shift of an NMR signal increases as more oxygen neighbors are located about the observed silicon nuclei ($Q > T > M$).

A representative ^{29}Si CP/MAS NMR spectrum of C_{18} alkyl modified MCM-41 silica material of surface coverage $1.65 \mu\text{mol}/\text{m}^2$ is shown in Figure 3.6. The presence of various types of silicon atoms as a result of the silylation step can be ascertained from this spectrum. It reveals the chemistry of surface modification reaction employed in the synthesis of alkyl bonded phases.

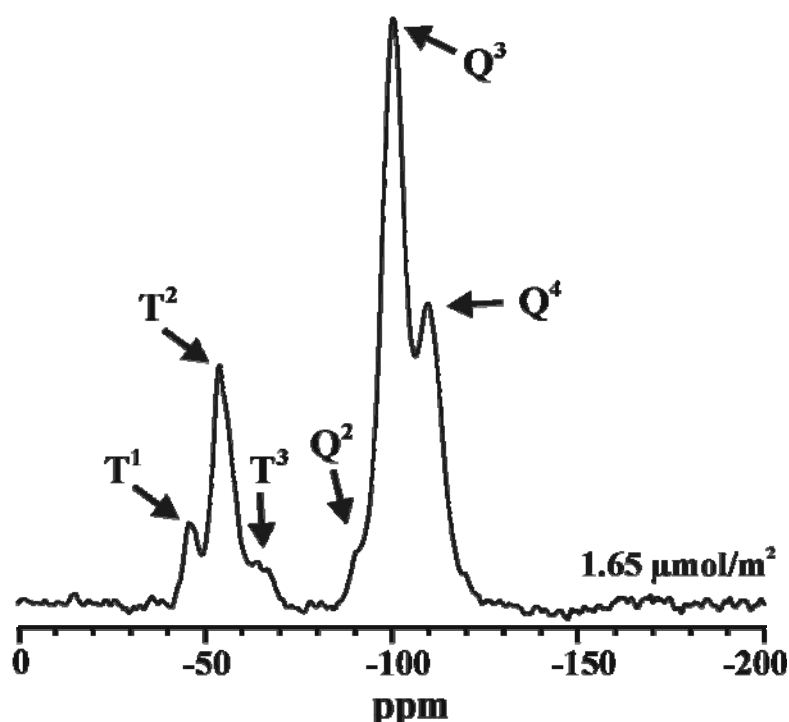


Figure 3.6. ^{29}Si NMR spectrum of the C_{18} alkyl grafted MCM-41 silica sphere with surface coverage of $1.65 \mu\text{mol}/\text{m}^2$.

3.2.2.2 ^{13}C MAS NMR Spectroscopy

^{13}C CP/MAS NMR spectroscopy was used to study the grafted species and to distinguish between regions containing all-trans chains and conformationally disordered chains with gauche bonds. Carbon nuclei offer a wider chemical shift range (220 ppm) than protons (12 ppm) and therefore provide a sensitive indicator of structural changes and the conformational order of immobilized ligands. Figure 3.7 depicts a ^{13}C CP/MAS NMR spectrum of C_{18} alkyl modified alumina.

The signal at around 14 ppm represents the C-18 and C-1 carbons.^{26,167} The peak at around 23 ppm arises from carbons C-2 and C-17 of the alkyl chains. The differences in the alkyl chain conformational order of the C_{18} alkyl chains can be discussed qualitatively by comparing the relative intensity of the ^{13}C NMR resonances from the inner methylene segments C-3 to C-16, attributed to “crystalline-like” trans and “solution-like” trans-gauche conformations.^{52,54,167} The signals at around 30 and 33 ppm are due to chains in the gauche (more mobile part) and in the all-trans conformational state (less mobile part), respectively.

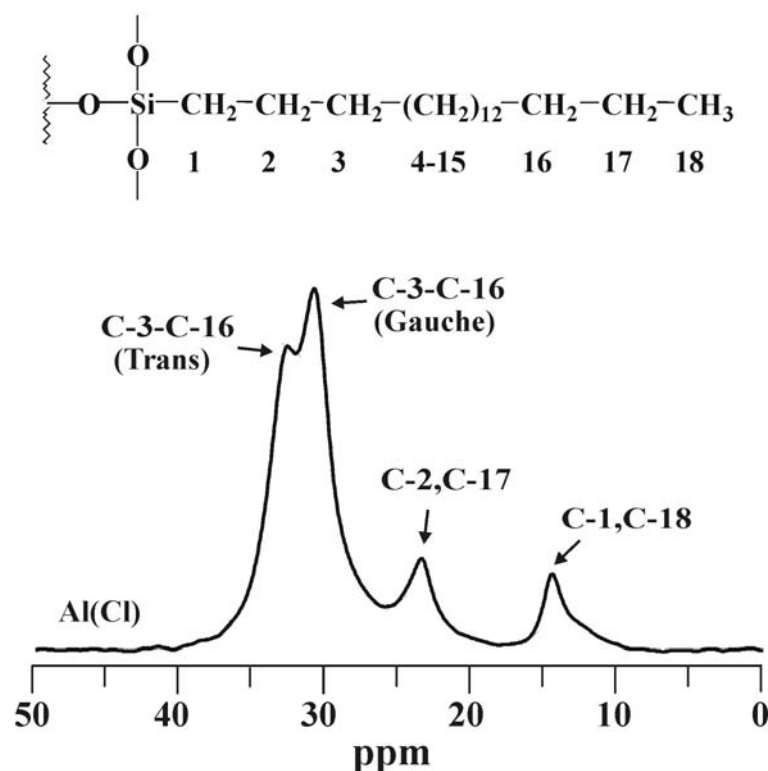


Figure 3.7. ^{13}C CP/MAS NMR spectrum of C_{18} alkyl chains grafted on alumina using *n*-octadecyltrichlorosilane.

The lowfield shift in the ^{13}C CP/MAS NMR spectra of these alkyl modified oxides can be explained through the γ -gauche effect (see Figure 3.8).^{168,169} Thus, the distance between the observed carbon $^{\text{O}}\text{C}$ and its γ -substituent $^{\gamma}\text{C}$ for an alkyl chain segment $^{\text{O}}\text{CH}_2\text{-CH}_2\text{-CH}_2\text{-}^{\gamma}\text{CH}_2$ depends on the conformation of the centre bond. The distance is reduced from 4 to 3 Å when the conformation changes from the trans to the gauche state along with a change of the electron shielding at position $^{\text{O}}\text{C}$, causing an upfield shift in the respective ^{13}C NMR resonance.^{169,170} Changes in alkyl chain conformation that result from changes in surface coverage, alkyl chain length, and temperature thus can be evaluated from the conformational sensitive ^{13}C resonance of the inner methylene units.

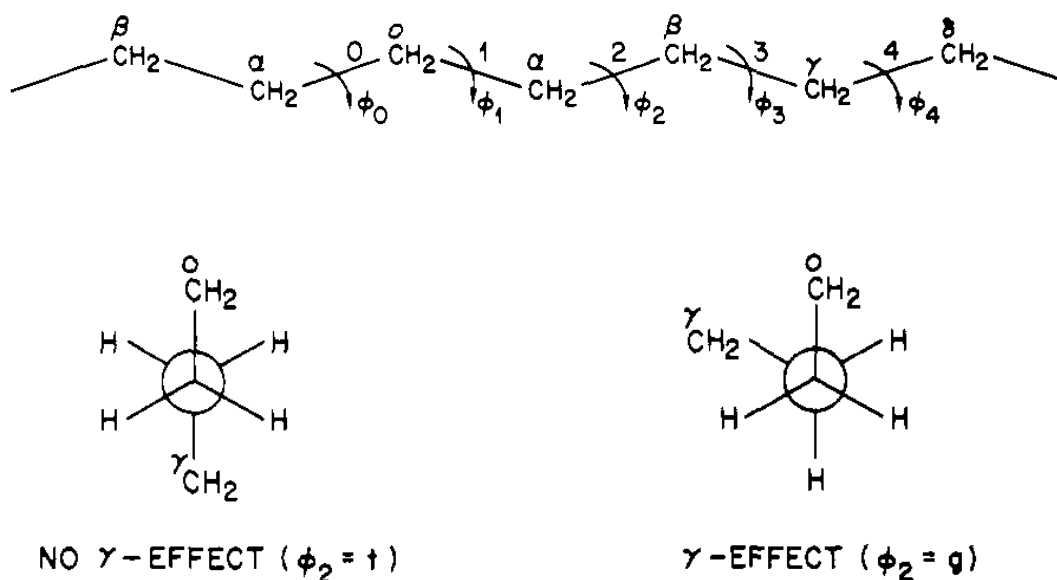


Figure 3.8. Newman projections illustrating the γ -gauche effect.

3.3 Small Angle X-Ray Scattering (SAXS)

Small-angle X-ray scattering (SAXS) is a technique where the elastic scattering of X-rays by a sample which has inhomogeneities in the nanometer range, is recorded at very low angles (typically $0.1\text{-}10^\circ$). SAXS measures spatial correlations in the scattering density, averaged over the time scale of the measurement. Structures with electron density fluctuations on a length scale from several ten nanometers up to the micrometer regime give rise to this scattering.

In a SAXS instrument a monochromatic beam of X-rays is brought to a sample from which some of the X-rays scatter, while most simply go through the sample without interacting with it. The scattered X-rays form a scattering pattern which is then detected at a detector which is typically a 2-dimensional flat X-ray detector situated behind the sample perpendicular to the direction of the primary beam that initially hit the sample. The scattering pattern contains the information on the structure of the sample.

Reliable experimental methods are essential for characterizing tailored pore sizes in a reproducible manner. SAXS measurements typically are concerned even with scattering angles $< 1^\circ$. As dictated by Bragg's Law, the diffraction information about structures with large d -spacings lies in the region. Therefore the SAXS technique is commonly used for probing large length scale structures such as high molecular weight polymers, biological macromolecules (proteins, nucleic acids, etc.), and self-assembled superstructures (e.g. surfactant templated mesoporous materials). In specific, SAXS is used for the determination of the microscale or nanoscale structure of particle systems in terms of such parameters as averaged particle sizes, shapes, distribution, and surface-to-volume ratio.

Mesoporous materials usually have long-range order; however, the pore walls are amorphous. In the absence of such short-range order, they can simply be interpreted as semicrystalline solids. SAXS pattern provide valuable information on a scale of sizes larger than those covered by the more widely applied X-ray diffraction (XRD) at normal angles, and is ideally suited for studying porous structures in the nanometer range.^{10,11,47,171}

Micelle templated silicas exhibit regular hexagonal pattern of cylindrical pores in the case of MCM-41 materials. The unit-cell parameter, a_0 is calculated from the d -spacing as expressed by Bragg's equation (3.19):

$$n\lambda = 2d \cdot \sin\theta \quad (3.19)$$

$$a_0 = d \cdot 2 / \sqrt{3} \quad (3.20)$$

where n , integer determined by the order given; λ , the wavelength of X-rays; d , the spacing between the planes in the atomic lattice; and θ , the angle between the incident ray and the scattering planes.

The wall thickness, t , of the mesoporous materials can be calculated using the unit cell parameter, a_0 , and the pore diameter value obtained from the N_2 sorption measurements and is given in equation (3.21).

$$t = a_0 - D_{pore} \quad (3.21)$$

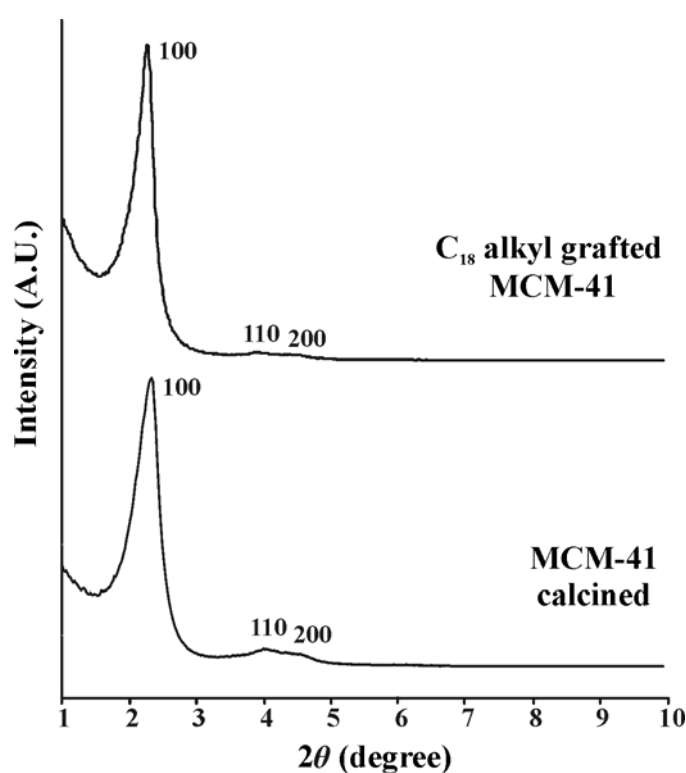


Figure 3.9. SAXS pattern of the calcined MCM-41 silica and C_{18} alkyl grafted MCM-41 silica spheres.

Figure 3.9 shows the SAXS pattern obtained for the calcined MCM-41 silica and C_{18} alkyl grafted materials.¹⁰ Both the materials possess three Bragg reflections at low angles, indexed as (100), (110) and (200), which are consistent with the hexagonal pore arrangement. But the intensity of the higher order reflections in the grafted material was reduced compared to the calcined MCM-41 and their peak broadening was related to a long-range distortion of the hexagonal arrangement of the mesopores. The peak positions

are not altered and it proves that the framework ordering of the mesopores remains intact upon grafting with the organic groups.

3.4 Nitrogen Physisorption

Quantitative evaluation of the pore structure in porous solids is a crucial aspect of the processes involved in the design and application of materials for adsorption and catalysis. The transport and reaction properties of porous solids, e.g., adsorbents and catalyst supports, are determined by their pore morphology, i.e., pore size distribution (PSD) and connectivity of the pore network.⁴³ Conventionally, nitrogen sorption isotherms represent the most widely used methods, often providing the input data for the analysis models for determining pore structure information.^k N₂ adsorption at its normal boiling point is the most popular because of its utility for both micropores and mesopores and because of its convenience and low cost.

For MCM-41, typical sorption measurements follow the type IV isotherm, as illustrated in Figure 3.10, with a high porosity (0.8 cm³/g) and a large surface area of about 800 m²/g.¹¹ At low relative pressures ($p/p_0 < 0.2$), the formation of a monolayer of adsorbed molecules is the prevailing process. At higher pressures ($p/p_0 > 0.2$), the adsorption in mesopores leads to multilayer formation until condensation takes place, giving a sharp increase for the adsorption volume. As the mesopores are filled, the adsorption continues on the external surface. The isotherms are usually reversible for pores smaller than a critical size and exhibit a sharp inflection at $p/p_0 = 0.25-0.45$, depending on the pore size of the material.

The steps in the isotherm (Figure 3.10) qualitatively reflect a narrow and uniform distribution of the pore size, while its height indicates the pore volume. The desorption occurs via evaporation of the adsorbate from mesopores and usually takes place at a pressure lower than that of capillary condensation, resulting in hysteresis. For disordered samples, the step of the isotherm becomes less sharp for the samples with the largest pores, suggesting a widening of the pore size distribution. The hysteresis is, in general, attributed to the different sizes of the pore mouths and pore bodies or to the different adsorption and desorption behaviors in near-cylindrical pores. Materials with uniform pore sizes and shapes exhibit type H1 hysteresis (i.e., parallel adsorption and desorption

branches), whereas those with non-uniform pore sizes and shapes give type H2 hysteresis (e.g., pore blocking, percolation effects, tensile strength, i.e. cavitation effects). In the latter case, condensation takes place in each section at the relative pressure provided by the Kelvin equation, but evaporation from the pore body cannot occur while the pore mouth remains filled. On the other hand, in the former case, the meniscus is cylindrical during condensation and hemispherical during evaporation.

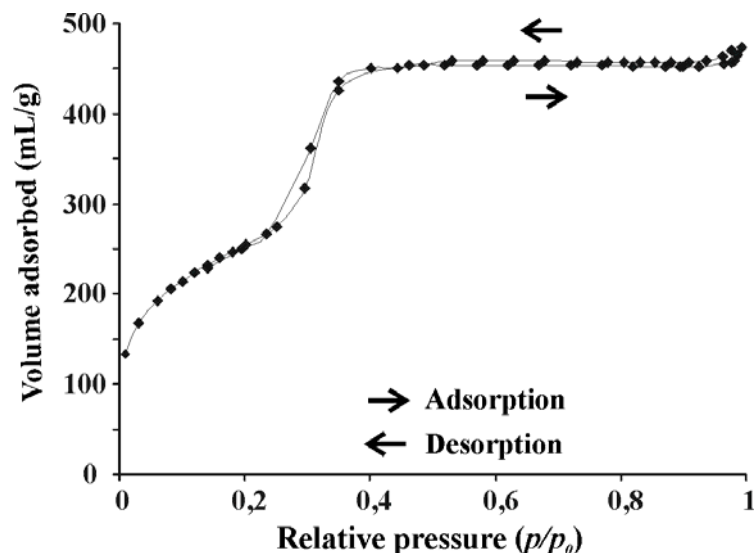


Figure 3.10. Nitrogen sorption isotherm of calcined MCM-41 silica spheres.

Surface Area

The BET method is widely used in surface science for the calculation of surface areas of solids by physical adsorption of gas molecules. The concept of the BET theory is an extension of the Langmuir theory, which is a theory for monolayer molecular adsorption, to multilayer adsorption with the following hypotheses: (a) gas molecules physically adsorb on a solid in layers infinitely; (b) there is no interaction between each adsorption layer; and (c) the Langmuir theory can be applied to each layer. The resulting BET equation¹⁷² is expressed by:

$$\frac{p}{V_a(p - p_0)} = \frac{(C - 1)}{V_m C} \frac{p}{p_0} + \frac{1}{V_m C} \quad (3.22)$$

where p and p_0 are the equilibrium and the saturation pressure of adsorbates at the temperature of adsorption; V_a , the volume of gas adsorbed at pressure p ; and V_m is the

volume of gas required to form a monolayer. C , the BET constant is related to energy of adsorption of the 1st layer.

Equation 3.22 is an adsorption isotherm and can be plotted as a straight line with $p/[V_a(p/p_0)]$ on the y-axis and p/p_0 on the x-axis according to experimental results. This plot is called a BET plot. The linear relationship of this equation is maintained only in the range of $0.05 < p/p_0 < 0.35$. The value of the slope A and the y-intercept I of the line are used to calculate the monolayer adsorbed gas quantity V_m and the BET constant C .

The BET surface area S_{BET} is evaluated by the following equation:

$$S_{BET} = \frac{V_m N s}{V_a} \quad (3.23)$$

where N , Avogadro's number; and s , the adsorption cross section.

In this study, the surface area measurements are based on the BET method on the basis of adsorption data in the range of relative pressures from 0.06 to 0.3 p/p_0 and 0.06 to 0.2 p/p_0 for the normal silica gels and MCM-41 silica spheres, respectively.¹⁷³ BET surface areas were calculated assuming the cross section for nitrogen, $a(N_2) = 13.5 \text{ \AA}^2$.^{174,175}

Pore Volume

The calculation of pore volume is in accordance with the Gurvitsch rule. The amount adsorbed at a relative pressure close to 0.99 represents complete filling of all pores with liquid adsorbate provided that the isotherm shows a course parallel to the relative pressure axis.⁴³ Then V_{tp} is calculated as

$$V_{tp} = X_a V \quad (3.24)$$

where X_a , the amount of adsorbed gas; V , the molar volume of adsorbent gas at the adsorption temperature.

The rule implies that V_{tp} is independent of the type of adsorptive and a close agreement was found in practice in the case of different types of adsorbents.⁴³

Pore Size and Pore Size Distribution (PSD)

Several geometrical and classical methods have been applied to the determination of the mesopore diameter (D_{pore}) of MCM-41. For cylindrical mesopores of uniform shape and width, pore condensation can be described on the basis of the Kelvin equation, i.e., the shift of the gas-liquid phase transition of a confined fluid from bulk coexistence, is expressed in macroscopic quantities like the surface tension γ of the bulk fluid, the densities of the coexistent liquid ρ^l and gas ρ^g ($\Delta\rho = \rho^l - \rho^g$) and the contact angle θ of the liquid meniscus against the pore wall. For cylindrical pores the modified Kelvin equation⁴³ is given by

$$\ln \frac{p}{p_0} = \frac{-2\gamma}{RT\Delta\rho(r_p - t_c)} \cos \theta \quad (3.25)$$

where R , the universal gas constant; r_p , the pore radius and t_c , the thickness of an adsorbed multilayer film, which is formed prior to the pore condensation. The occurrence of pore condensation is expected as long as the contact angle is below 90° . A contact angle of 0° is usually assumed in case of nitrogen adsorption at 77 K.

The Kelvin equation provides a relationship between the pore diameter and the pore condensation pressure, and predicts that pore condensation shifts to a higher relative pressure with increasing pore diameter and temperature. The modified Kelvin equation (eq. 3.25) serves as the basis for many methods applied for mesopore analysis, including the Barrett-Joyner-Halenda method (BJH), which is widely used.

The pore size distribution (PSD) of porous materials is another important characteristic that has received significant attention. Accordingly, several studies have been conducted to determine PSDs of MCM-41 materials using the adsorption of nitrogen. The BJH method for calculating PSD is based on a model of the adsorbent as a collection of cylindrical pores.¹⁷⁶ The theory accounts for capillary condensation in the pores using the classical Kelvin equation, which in turn assumes a hemispherical liquid-vapor meniscus and a well-defined surface tension. The BJH theory also incorporates thinning of the adsorbed layer through the use of a reference isotherm; the Kelvin equation is only applied to the “core” fluid. PSD were calculated from adsorption/desorption branches of

the nitrogen isotherms with the corrected form of the Kelvin equation for capillary condensation in cylindrical pores:⁴⁶

$$r(p/p_0) = 0.416[\log(p_0/p)]^{-1} + t(p/p_0) + 0.3 \quad (3.26)$$

where r , the pore radius and $t(p/p_0)$, the statistical film thickness curve (t-curve) as a function of the relative pressure.

The classical methods based on macroscopic and thermodynamic assumptions for mesopore analysis (methods based on Kelvin equation) cannot describe the sorption and phase behaviour of fluids in narrow mesopores correctly. Another problem is that the mean thicknesses of the presorbed multilayer film for narrow pores of widths < ca. 100 Å does not reflect the real thickness of the preadsorbed film, because curvature effects are not taken into account. It is found that the BJH- and related approaches based on the modified Kelvin equation underestimate the pore size up to 25 % for pores smaller than 100 Å.¹⁷⁷⁻¹⁷⁹

In this dissertation, the pore diameters were calculated from desorption isotherm data by employing the BJH method.^{10,11,67} Thus it would mean that the real pore diameters are about 7 to 9 Å larger than the given values. These corrected values are then in agreement with the literature values from other recent studies on the MCM-41 materials and their subsequent grafting with alkyl chains.^{8,141} In contrast, microscopic method based on Density Functional Theory (DFT) takes into account details of the fluid-fluid interactions and the adsorption potential (which depends on the strength of fluid wall interactions and the pore geometry). Meanwhile, appropriate methods for the pore size analysis based on Non-Local Density Functional Theory (NLDFT) are available for many fluid/substrate systems.^{177,178}

3.5 Scanning Electron Microscopy (SEM)

SEM measurements provide the particle morphology of the material under investigation, their diameter and also the particle size distribution. A Scanning Electron Microscope is a high magnification microscope, which uses a focused scanned electron beam to produce high-resolution images of a specimen. The X-rays emitted are characteristic of the

elements in the top few μm of the sample. After the primary electron beam interacts with the sample, ionized atoms can relax by electron shell-to-shell transitions, which lead to either X-ray emission or Auger electron ejection. Images obtained by SEM provided information on the physical properties of mesoporous silica materials and particulates including particle size, shape, surface morphology, and adherence to surfaces.

The types of signals made by an SEM can include secondary electrons, back scattered electrons, characteristic X-rays and light (cathodoluminescence). These signals come from the beam of electrons striking the surface of the specimen and interacting with the sample at or near its surface. In its primary detection mode, secondary electron imaging, the SEM can produce very high-resolution images of a sample surface, revealing details about 1 to 5 nm in size. Due to the way these images are created, SEM micrographs have a very large depth of focus yielding a characteristic three-dimensional appearance useful for understanding the surface structure of a sample. Characteristic X-rays are the second most common imaging mode for an SEM. X-rays are emitted when the electron beam removes an inner shell electron from the sample, causing a higher energy electron to fill the shell and give off energy. These characteristic X-rays are used to identify the elemental composition of the sample. Back-scattered electrons (BSE) that come from the sample may also be used to form an image. BSE images are often used in analytical SEM along with the spectra made from the characteristic X-rays as clues to the elemental composition of the sample.

For conventional imaging, the SEM requires that specimens be conductive for the electron beam to scan the surface and that the electrons have a path to ground. All samples are generally mounted on some sort of holder. Nonconductive solid specimens are coated with a layer of conductive material. An ultrathin coating of electrically-conducting material such as, gold, gold/palladium alloy, platinum, tungsten or graphite is deposited on the sample either by low vacuum sputter coating or by high vacuum evaporation. This is done to prevent the accumulation of static electric charge on the specimen during electron irradiation. Another reason for coating, even when there is more than enough conductivity, is to improve contrast and resolution, a situation most common when using samples with low atomic number.

In this dissertation, SEM measurements were performed on the amorphous and MCM-41 silica spheres to determine the particle morphology, size and their distribution before and after the pseudomorphic transformation.^{10,11,67} It also provides information regarding the preservation of the MCM-41 silica spheres after the anchoring of the organic groups. Figure 3.11 shows the SEM micrographs of the amorphous and MCM-41 silica spheres and after their modification with organic groups.

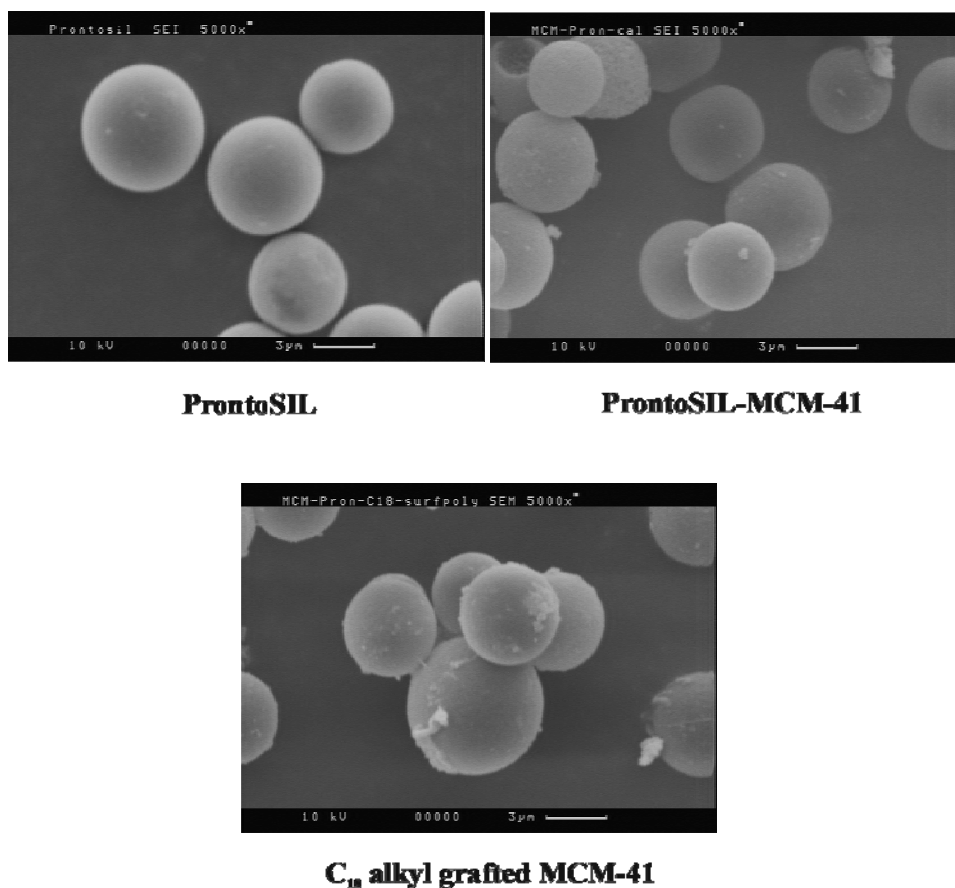


Figure 3.11. SEM micrographs of the amorphous, MCM-41 silica spheres and C₁₈ alkyl grafted MCM-41 silica spheres.

Chapter 4

4 Experimental Section

4.1 Materials and Synthesis

4.1.1 Chemicals

Inorganic oxides

Commercially available silica, ProntoSIL (200-5-Si; 5 μm) and Kromasil (300 Å; 5 μm), were delivered by Bischoff Chromatography (Leonberg, Germany) and Akzo-Nobel (Bohus, Sweden), respectively. Commercially available titania (purity of 99 %), hafnia (98%), and zirconia (99%) were purchased from Aldrich (Sigma-Aldrich Chemie GmbH, Steinheim, Germany). Alumina (99%) was delivered by Fluka (Fluka Chemie AG, Buchs, Germany). Zirconium butoxide was purchased from ABCR, Karlsruhe, Germany.

Functional reagents

n-Octadecyltrichlorosilanes (95%) and *n*-octadecyltrihydrosilanes (98 %) were procured from Aldrich Chemical Company (Steinheim, Germany). *n*-Octadecyltrimethoxysilane (95 %) and *n*-octadecyldimethylmethoxysilane (92 %) were purchased from Fluorochem (Karlsruhe, Germany). The endcapping agent 1,1,1,3,3,3-hexamethyldisilazane (HMDS; 97 %) was obtained from Aldrich (Sigma-Aldrich Chemie, Steinheim, Germany). Methacryloxymethyltriethoxysilane (MAPTMS) and methacrylic acid (99%), purchased from Aldrich, was distilled under reduced pressure. Cetyltrimethylammonium bromide (CTAB) and sodium hydroxide (NaOH) were received from Aldrich Chemical Company (Steinheim, Germany).

Solvents

Reagent grade toluene was distilled two times before use and stored in molecular sieves. Pyridine (spectroscopic grade) was delivered by Sigma-Aldrich and used without further purification. Anhydrous tetrahydrofuran and dibenzoylperoxide were purchased from Aldrich.

4.1.2 Grafted Silica Gels: Impact of Solvents on C₃₀ Silica

4.1.2.1 Synthesis of C₃₀ alkyl grafted silica spheres

Two to three grams of silica gel was preevacuated at 180 °C for 4 h to 5 h. The activated silica gel was suspended in toluene (25 mL) and heated to 80 °C. To this suspension the 2-fold excess (3.2-4.8 mmol) of the *n*-triacontyltrichlorosilane was added. After further addition of a small amount of water (0.5 mL) the solution polymerization reaction started.^{26,50} The reaction mixture was then stirred for 36 h to 48 h under reflux at 120 °C, using a KPG stirrer to avoid breaking of the silica particles. The modified silica gel was filtered (G4 filter) and washed twice with toluene to remove any unreacted *n*-triacontyltrichlorosilane, and then with methanol and petroleum ether (30/50) subsequently to remove toluene. The filtered modified silica gel was dried under vacuum at 60 °C for 4 h to remove all the solvents that were used for washing. After drying the samples were stored in airtight bottles. The calculated surface coverage of the *n*-triacontyl grafted silica was 3.6 μmol/m².

4.1.3 Grafted MCM-41 Silica: Synthesis, Impact of Mono- and Trifunctional C₁₈ Silanes and Endcapping

4.1.3.1 Synthesis of MCM-41 silica spheres

According to the pseudomorphic synthesis, the ProntoSIL silica was stirred in an alkaline solution of cetyltrimethylammonium bromide (CTAB) to produce the MCM-41 type ordered mesoporous spheres.⁹ The reactants, with molar composition SiO₂ : NaOH : CTAB : H₂O = 1 : 0.25 : 0.1 : 20, were slowly mixed under stirring. The reaction mixture was stirred for another 30 min at room temperature. Afterwards, the mixture was transferred to an autoclave and kept at 373 K for 28 h. The as-synthesized MCM-41 material was filtered and dried overnight at 353 K. After heating the sample at a rate of 1 K/min, the surfactant was removed by calcination in air at 823 K for 5 h.

4.1.3.2 Reaction of silylating agents and HMDS with MCM-41

According to the previous reports it was assumed that only 4 $\mu\text{mol}/\text{m}^2$ of the hydroxyl groups are present on the MCM-41 silica surface after calcination at 823 K, while about 8 $\mu\text{mol}/\text{m}^2$ of hydroxyl groups are discussed for normal silica gel surfaces.¹⁸⁰ For grafting of the mesoporous silica, 1 g of the MCM-41 material was preevacuated at 393 K for 4-5 h. The activated MCM-41 was suspended in toluene (20 mL) and heated to 343 K. A two-fold excess (8 μmol of silane per m^2 of calcined MCM-41 silica) of the corresponding *n*-octadecyltrimethoxysilanes (2.9 g) or *n*-octadecyldimethylmethoxysilanes (3.3 g) was added to this suspension. This mixture was placed in a rotavapor for 2 days at 343 K. Afterwards, HMDS (1.2 g, two-fold excess) was added, and the mixture was kept at 343 K for one day. The resulting MCM-41 silica spheres were filtered (G4 filter) and washed with toluene, followed by acetone, ethanol, ethanol/water (1:1, v:v.), water, ethanol, acetone, and pentane. The grafted MCM-41 silica was dried overnight in an oven at 353 K and stored in airtight bottles. The surface modified and endcapped MCM-41 materials are denoted as MF and TF, referring to the samples grafted by means of mono- and trifunctional octadecylsilanes, respectively. The porous features of ungrafted and grafted MCM-41 silica spheres are given in Table 4.1.

Table 4.1. Sample properties of grafted and endcapped MCM-41 silica.

Sample	a_0 (Å)	S_{BET} (m^2/g)	V_{tp} (mL/g)	D_{pore} (Å)		% C
				Primary mesopore	Secondary mesopore	
ProntoSIL	--	170	1.04	246*		--
MCM-Calcined	49	925	0.89	28	36	--
MF	49	494	0.42	24	34	10.32
TF	51	383	0.38	20	32	16.00

a_0 : Unit-cell parameter (from SAXS experiment); S_{BET} : BET surface area (from sorption isotherm)
 V_{tp} : Total pore volume (from sorption isotherm); D_{pore} : Pore diameter (from sorption isotherm)
 *represents parental mesopore diameter

4.1.4 Grafted MCM-41 Silica: Synthesis, Impact of Silica Source and Trifunctional C₁₈ Silane Precursors

4.1.4.1 Synthesis of MCM-41 silica spheres

In the pseudomorphic reaction, the reactants with molar composition SiO₂ : NaOH : surfactant: H₂O = 1 : 0.25 : 0.1 : 20 were slowly mixed under stirring.⁹ ProntoSIL or Kromasil silica, characterized by well-defined spheres, were used as silica source, and the surfactant was cetyltrimethylammonium bromide (CTAB). The reaction mixture was stirred at 400 rpm for 30 min at room temperature, and was then transferred to an autoclave, where it was kept at 373 K for 28 hrs. Afterwards, the as-synthesized MCM-41 material was filtered and dried at 353 K for about 12 hrs. Two procedures were followed to remove the surfactant, namely calcination and solvent extraction. In the former procedure the sample was heated at a rate of 1 K/min to 823 K, and the surfactant was removed in air by keeping the final temperature for 5 hrs. In the solvent extraction the as-received MCM-41 material (1 g) was stirred with acidified ethanol for 24 hrs at 353 K (1.6 mL of 37% HCl in 200 mL ethanol). The textural features of the ProntoSIL and Kromasil silica spheres and of the MCM-41 silica materials, received via the pseudomorphic reaction, are summarized with their sample codes in Table 4.2.

4.1.4.2 Reaction of silylating agents with MCM-41 silica spheres

According to the previous reports it was assumed that only 4 μmol/m² of the hydroxyl groups are present on the MCM-41 silica surface after calcination at 823 K, while about 8 μmol/m² of hydroxyl groups are typically expected for conventional silica gel surfaces.¹⁸⁰ *n*-Octadecylsilyl groups were attached to the calcined and solvent extracted MCM-41 spherical silicas with *n*-octadecyltrihydridosilanes and *n*-octadecyltrimethoxysilanes by direct grafting or surface polymerization.

During *direct grafting*, about 0.5 g of calcined or solvent extracted MCM-41 silica was preevacuated at 393 K for 4 to 5 hours. The activated MCM-41 silica was suspended in toluene (50 mL) and heated to 333 K.

Table 4.2. Textural features of silica and MCM-41 silica spheres.

Sample	Material-conditions	a_0 (Å)	S_{BET} (m ² /g)	V_{tp} (mL/g)	D_{pore} (Å)
Kromasil	Kromasil (silica)	--	90	0.78	350
ProntoSIL	ProntoSIL (silica)	--	170	1.04	236
M1	Kromasil-calcined	49	740	0.74	28
M2 ^a	Kromasil-solvent extracted	54	766	0.87	30
M3	ProntoSIL-calcined	49	780	0.85	28;38 ^b
M4 ^a	ProntoSIL-solvent extracted	57	768	0.93	30;38 ^b

a_0 : unit-cell parameter; S_{BET} : BET surface area; V_{tp} : total pore volume; D_{pore} : pore diameter

^a 2 wt. % carbon found in elemental analysis; ^b Primary and secondary mesopores

In the *surface polymerization approach* about 0.5 g of calcined or solvent extracted MCM-41 silica was preevacuated at 393 K for 4 to 5 h. The resulting dry powders were equilibrated with humid air at room temperature for 7 h which results in a surface coverage with a monolayer of water.^{50,143} These humidified MCM-41 materials were then suspended in toluene (50 mL) and heated to 333 K.

Table 4.3. Octadecyl grafted MCM-41 silica samples used in this work.

Sample	MCM-41 - C ₁₈ alkyl chain grafted silica
<i>n</i>-octadecyltrihydridosilane	
M1H	Kromasil-calcined-direct attachment
M2H	Kromasil-calcined-surface polymerization
<i>n</i>-octadecyltrimethoxysilane	
M3M	ProntoSIL-calcined-direct attachment
M4M	Kromasil-calcined-surface polymerization
M5M	ProntoSIL-solvent extracted-direct attachment
M6M	Kromasil-solvent extracted-surface polymerization

A 4-fold excess (16 μmol of silane per m² of MCM-41 silica surface area) of the corresponding *n*-octadecyltrihydridosilanes or *n*-octadecyltrimethoxysilanes in toluene (30 mL) was added to one of the aforementioned MCM-41 suspensions. This mixture was then placed in a rotavapor for 3 days at 333 K. The resulting MCM-41 silica spheres were filtered (G4 filter) and washed with toluene, acetone, ethanol, ethanol/water (1:1, v:v.), water, ethanol, acetone, and pentane. The grafted MCM-41 silicas were then dried

overnight in an oven at 353 K and stored in airtight bottles. Table 4.3 lists the material codes for the grafted MCM-41 materials prepared in the present work along with respective experimental conditions.

4.1.5 Grafted Metal Oxides: Impact of Oxide Supports, Grafting of C₁₈ Silanes and Grafting Routes

The properties of the metal oxides used in this work are listed in Table 4.4.

Table 4.4. Characteristics of metal oxides.

Metal Oxide	Supplier	Particle size (μm)	S_{BET} (m²/g)	V_{tp} (mL/g)	IEP¹⁸¹
TiO ₂	Aldrich	< 44	8.2 ± 0.2	0.02	2
Al ₂ O ₃	Fluka	120-149	136.8 ± 0.3	0.23	8-9
HfO ₂	Aldrich	-	6.9 ± 0.2	0.05	-
ZrO ₂	Aldrich	< 5	3.8 ± 0.1	0.01	10-11

S_{BET}: BET surface area and V_{tp}: Total pore volume. IEP (Isoelectric point) is an indicator of the pH value for an ionic solid, at which there is no net surface charge in aqueous solution. Higher values denote more basic character, lower values more acidic character.

4.1.5.1 Reaction with *n*-Octadecyltrichlorosilanes

Solution polymerization was employed for the reaction of *n*-octadecyltrichlorosilane and the metal oxides.²⁶ About 1 g metal oxide was preevacuated at 120 °C for 4 to 5 hours. The activated metal oxides were suspended in toluene (20 mL) and heated to 80 °C, and a toluene solution containing 24 μmol of silane per m² metal oxide surface area was added.¹²⁰ This corresponds to a 3-fold excess of the silane with respect to complete monolayer coverage of the surface with *n*-octadecylsilyl groups. After addition of a small amount of water (0.5 mL) the solution polymerization reaction started. The reaction mixture was then stirred for 36 hours under reflux at 120 °C. The modified metal oxide was filtered (G4 filter) and washed with toluene, followed by acetone, ethanol, ethanol/water (1:1, v:v.), water, ethanol, acetone, and pentane. The filtered alkyl modified metal oxide was dried in an oven at 80 °C and stored in airtight bottles.

4.1.5.2 Reaction with *n*-Octadecyltrihydrosilanes

1 g metal oxide was preevacuated at 120 °C for 4 to 5 hours and suspended in 20 mL of toluene. Afterwards a toluene solution containing 24 μmol of *n*-octadecyltrihydrosilane per m² metal oxide surface area was added.¹²⁰ This corresponds to a 3-fold excess of the silane with respect to complete monolayer coverage of the surface with *n*-octadecylsilyl groups. The reaction vessel was then heated to 80 °C for 24 hours. The modified metal oxide was filtered (G4 filter) and washed with toluene, followed by acetone, ethanol, ethanol/water (1:1, v:v.), water, ethanol, acetone, and pentane. The filtered grafted metal oxide was dried in an oven at 80 °C and stored in airtight bottles. Further details of the C₁₈ alkyl modified metal oxides with their sample codes are given in Table 4.5.

Table 4.5. Grafting densities of C₁₈ alkyl chains on metal oxides.

Substrate	Reagent	Samples*	%C	Grafting density ρ [group/nm ²]
TiO ₂	RSiCl ₃	Ti(Cl)	0.91	3.1
Al ₂ O ₃	„	Al(Cl)	10.80	2.6
HfO ₂	„	Hf(Cl)	1.93	8.0
ZrO ₂	„	Zr(Cl)	1.38	10.3
TiO ₂	RSiH ₃	Ti(H)	0.86	2.9
Al ₂ O ₃	„	Al(H)	9.28	2.2
HfO ₂	„	Hf(H)	1.37	5.6
ZrO ₂	„	Zr(H)	0.82	6.1

*Ti(H), Al(H), Hf(H), Zr(H) denote *n*-octadecyltrihydrosilanes grafted to respective oxides and Ti(Cl), Al(Cl), Hf(Cl), Zr(Cl) denote *n*-octadecyltrichlorosilanes grafted to respective oxides.

4.1.6 Grafted Mixed Silica-Zirconia Oxides: Impact of Oxide Supports and Grafting of C₁₈ Silanes

4.1.6.1 Preparation of Mixed Oxides

The investigated materials were prepared as reported elsewhere.¹³³ Four samples were prepared by varying the methacryloxysilane: oxocluster molar ratio and the annealing temperature, as reported in Table 4.6. In this work, samples 1-4 represents mixed oxides;

1H-4H represents humidified mixed oxides; **1F-4F** represents C₁₈ alkyl functionalized mixed oxides.

After polymerization, the zirconium based gels were dried under vacuum at 70° C for 12 h to remove the residual solvent. They were subsequently annealed in air at different temperatures (600 and 800 °C) in a muffle to promote the pyrolysis of the organic components and the conversion to the corresponding binary oxides. The typical annealing procedure consists of a temperature ramp with a heating rate of 5 °C/ min to the target temperature, annealing for 5 h and a temperature decrease to room temperature. Si/Zr atomic percentages determined by XPS, calcination temperature and the textural features of the individual mixed oxides by N₂ physisorption measurements along with the sample codes are reported in Table 4.6. It is found that they are in very good agreement with the nominal values from the precursor solutions.

Table 4.6. Mixed oxide supports used in this work and their textural features.

Mixed Oxide samples ^a	SiO ₂ /ZrO ₂ molar ratio (from XPS)	Calcination temperature (°C)	S _{BET} (m ² /g)	V _{tp} (mL/g)
1	2.5	600	355	0.19
2	10	600	374	0.20
3	2.5	800	185	0.09
4	10	800	138	0.06

a: **1-4** represents mixed oxides. S_{BET}: BET surface area and V_{tp}: Total pore volume.

4.1.6.2 Preparation of C₁₈ Alkyl Grafted Mixed Oxides

About 0.5 g of the hybrid inorganic oxide materials were preevacuated at 150 °C for 4-5 h. The resulting mixed oxide dry powders were equilibrated with humid air at room temperature through a sintered glass frit funnel for 3 hours which results in a surface coverage with a monolayer of water.^{50,143} The humidified oxides were then dispersed in 50 mL of toluene, and a toluene solution containing 24 μmol of silane per m² mixed oxide surface area was added to the slurry. The mixture was stirred, and the temperature was kept at 90 °C. After 17 h, the mixture was refluxed for 45 min and then filtered hot using a G4 filter. The bonded phases were washed with toluene, followed by acetone, ethanol, ethanol/water (1:1, v:v.), water, ethanol, acetone and pentane. After drying the samples

were stored in airtight bottles. The characteristics of C₁₈ grafted mixed oxides are given in Table 4.7.

Table 4.7. Characteristics of C₁₈ alkyl modified mixed oxides.

Samples ^a	%C	Surface Coverage ($\mu\text{mol/ m}^2$)
1F	2.82	0.38
2F	6.46	0.89
3F	3.30	0.87
4F	1.53	0.70

a: **1F-4F** represents C₁₈ alkyl functionalized mixed oxides

4.2 Elemental Analysis

Carbon and hydrogen analyses were performed on a Carlo Erba Strumentazione elemental Analyser 1106 (Italy). The percentage of carbon was utilized for calculating the surface coverage, α_{RP} (in $\mu\text{mol/m}^2$) on the basis of the following equation²⁶

$$\alpha_{RP} = \frac{10^6 P_C}{1200n_C - P_C (M - n_x)} \cdot \frac{1}{S_{BET}} \quad (4.1)$$

The alkyl coverage can also be expressed in terms of grafting density, ρ (in group/nm²) and was calculated using the formula²¹

$$\rho = \frac{6 \cdot 10^5 P_C}{1200n_C - MP_C} \cdot \frac{1}{S_{BET}} \quad (4.2)$$

Here, P_C is the percentage of carbon determined via elemental analysis, n_C is the number of carbon atoms per silane moiety, M is the molar mass of the silane, n_x is the number of reactive groups in the silane ($n_x = 3$ for n -alkyltrichlorosilane), and S_{BET} is the BET surface area of the unmodified support.

4.3 Methods

4.3.1 FTIR Measurements

The samples were measured by means of the KBr pellet technique. The pellets of the alkyl modified systems and KBr (1/10 to 1/15 w/w) of 1 mm thickness were prepared under vacuum using a hydraulic press with a pressure of about 10 kbar. The pellets of the respective samples were placed in a brass cell equipped with an external thermocouple in close vicinity to the sample. The same thermocouple was used for monitoring the actual sample temperature. The brass cell was thermostated in a variable temperature transmission cell (L. O. T. – Oriel GmbH, Langenberg, Germany) equipped with NaCl windows. The temperature was regulated with a temperature control unit which has an accuracy of ± 0.5 °C.

FTIR spectra were recorded with a Nicolet Nexus 470 FTIR spectrometer (Nicolet, Madison/WI, USA) equipped with a DTGS detector, and by purging with N₂ gas. Typically, 256 interferograms covering a spectral range of 4000 to 400 cm⁻¹ at a resolution of 2 cm⁻¹ were collected within a temperature range from 193 to 353 K. The recorded interferograms were apodized with a triangular function and Fourier transformed with two levels of zero filling. The background spectrum was recorded with an empty cell and twice the number of scans as used for the spectra of the modified metal oxide samples, and was automatically subtracted from the subsequent spectra of C₁₈ alkyl modified metal oxides. Data from three independent samples were acquired at all temperatures for all the samples studied, and the FTIR spectra were measured twice for each sample.

The processing and analysis of the spectra for CH₂ stretching band regions were performed with the OMNIC E.S.P.5.1 software (Nicolet, Madison/WI, USA). The wavenumbers of the CH₂ stretching vibrations were calculated from the interpolated zero crossing in the first derivative spectra. The experimental error for the given wavenumbers is ± 0.25 cm⁻¹. Processing and analysis of the spectra in the CH₂ wagging region were performed using Grams 32 software (Galactic, Salem, NH, USA).

CH₂ wagging band analysis was performed by applying a quadratic baseline correction in the spectral region from 1400 cm⁻¹ to 1330 cm⁻¹ and the same baseline points were used

for each spectrum. The experimental spectra were fitted using four vibrational bands where the initial positions were 1378 cm^{-1} (symmetric methyl deformation mode), 1368 cm^{-1} (kink and gauche–trans–gauche sequences), 1354 cm^{-1} (double-gauche sequences), and 1341 cm^{-1} (end–gauche sequences). The band intensities and widths were varied independently during the curve fit analysis. The integrated intensities of the CH_2 wagging bands were normalized with respect to the methyl deformation band. The fraction of specific gauche sequences in the *n*-alkyl modified system was calculated using the reference plots of *n*-alkanes from Neumann-Singh et al.¹⁵⁷ which is based on the rotational isomeric state (RIS) model.^{155,156} The total number of gauche conformers per chain was obtained according to the concept that two gauche bonds are necessary to build up one kink or double–gauche sequence and one gauche bond for the formation of the end–gauche sequence. The estimated coefficient of variation for the various gauche conformers is 10-15%.

4.3.2 DRIFT Measurements

Diffuse Reflectance Infrared Fourier Transform (DRIFT) spectroscopic measurements were performed by Dr. M. M. Natile and Dr. A. Glisenti in University of Padova, Italy. IR spectra were collected with a Bruker Tensor 27 spectrometer, 32 scans were accumulated at a resolution of 4 cm^{-1} , and displayed in Kubelka-Munk units.^{182,183} About 50 mg of the sample were loaded in the sample cup of a low temperature reaction chamber (CHC) installed in the Praying Mantis™ accessory for diffuse reflection spectroscopy (Harrick Scientific Corporation) and fitted with ZnSe windows. The temperature was checked by means of a thermocouple inserted into the sample holder in direct contact with the powder. KBr was used as background for the collection of the IR spectra of the metal oxides at room temperature. Prior to the final measurements, the powder was subject to a dry nitrogen flow to eliminate water traces until a stable IR spectrum was obtained (ca. 2 h). For the chemisorption/DRIFT experiment, the sample was exposed to an argon/pyridine gas stream (flow rate: $75\text{ cm}^3\text{ min}^{-1}$), obtained by flowing argon through a bubbler filled with pyridine. For the DRIFT desorption experiments, the samples were subject to a argon gas flow at the conditions described in the text.

4.3.3 SSNMR Measurements

Solid-state ^{13}C and ^{29}Si NMR spectra were recorded under magic angle spinning (MAS) condition (sample rotation frequency: 5 kHz) at 100.52 MHz and 79.41 MHz, respectively, on a Varian InfinityPlus 400 NMR spectrometer (Varian, Palo Alto, CA, USA), operating at a static magnetic field of 9.4 T and using a 4 mm MAS probe. ^{13}C NMR experiments were done under MAS conditions (sample rotation frequency: 5 kHz) with cross-polarization (CP) excitation using $\pi/2$ pulse widths of 4 μs , contact times of 5 ms, and recycle delays of 5 s. Typical number of scans were 2500. ^{13}C chemical shifts were determined relative to the external standard adamantane. ^{29}Si CP/MAS NMR spectra were recorded using a $\pi/2$ pulse length of 4.5 μs , a contact time of 5 ms, and a recycle delay of 5 s. The spinning speed was 5 kHz, and the typical number of scans was 5000. ^{29}Si chemical shifts were determined relative to external standard Q₈M₈, the trimethylsilylester of octameric silicate.

4.3.4 XPS Measurements

X-ray Photoelectron Spectroscopy (XPS) measurements were carried out by Dr. S. Gross in University of Padova, Italy. The compositions of the powders were investigated by XPS. XPS spectra were run on a Perkin-Elmer Φ 5600ci spectrometer using standard Al- $\text{K}\alpha$ radiation (1486.6 eV) operating at 350 W. The working pressure was $< 5 \cdot 10^{-8}$ Pa. The spectrometer was calibrated by assuming the binding energy (BE) of the Au4f_{7/2} line at 83.9 eV with respect to the Fermi level. The standard deviation for the BE values was 0.15 eV. The reported BE were corrected for the charging effects assigning to the C1s line of carbon with the BE value of 285.0 eV^{184,185} for the non-functionalized samples, whereas after the functionalization they were calibrated by giving to the Si2p peak of silica, with the BE value of 103.6 eV.^{184,185} Survey scans were obtained in the 0-1350 eV range. Detailed scans (58.7 eV pass energy) were recorded for the Zr3p, Zr3d, and Si2p regions. The atomic composition, after a Shirley type background subtraction¹⁸⁶ was evaluated using sensitivity factors supplied by Perkin-Elmer.¹⁸⁵ Charge effects were partially compensated by using a charge neutralizer (flood gun). The assignments of the peaks has been carried out by using the values reported earlier.^{131-133,185,187}

4.3.5 SAXS Measurements

SAXS measurements were performed by Ms. N. Kapernaum in the workgroup of Prof. Dr. F. Gießelmann in University of Stuttgart, Germany. SAXS experiments were performed with a Bruker AXS NanoSTAR system ($\text{Cu}_{K\alpha}$ radiation aligned by Goebel mirrors) equipped with a two-dimensional electronic detector and a temperature controller (MRI Physikalische Geräte, Karlsruhe, Germany).

4.3.6 Nitrogen Physisorption Measurements

Nitrogen adsorption-desorption measurements were performed at 77 K on a Micromeritics ASAP 2010 volumetric adsorption analyzer (Neuss, Germany). For the experiments, 150 mg of ungrafted and C_{18} alkyl grafted MCM-41 were degassed at 393 K for 5 h in the degassing port of the adsorption apparatus. The surface area was estimated using the Brunauer-Emmett-Teller (BET) method and the pore size and their distribution was calculated by Barrett-Joyner-Halenda (BJH) method. The pore volume was determined from the amount of N_2 adsorbed at relative pressure of 0.99.

4.3.7 SEM-EDX Measurements

SEM measurements were performed by Dr. A. Fels in University of Stuttgart, Germany. SEM imaging was performed on a Leica Camscan CS-44 scanning electron microscope. The samples were prepared by placing MCM-41 silica spheres on double-sided carbon adhesive tape mounted on the sample holder. Afterwards, the samples were gold coated (thickness about 20 nm) by cathodic sputtering.

SEM measurements were also carried out by Dr. C. Maccato in University of Padova, Italy. Field Emission-Scanning Electron Microscopy (FE-SEM) and Energy Dispersive X-ray analysis (EDX) were run on a Zeiss SUPRA 40VP equipped with an Oxford INCA x-sight X-ray detector. Morphological analyses were carried out by setting the acceleration voltages at 1.00 kV, while the EDX compositional investigations were obtained by setting the acceleration voltage at 10 kV.

Chapter 5

5 Results and Discussion

5.1 Grafted Silica Gels: Impact of Solvents on C₃₀ Silica

In the present study, the impact of various types of solvents on the conformational order of C₃₀ alkyl modified silica gels (denoted as C₃₀) was examined by variable temperature FTIR spectroscopy. The solvents considered here include acetonitrile, methanol, ethanol, 1-propanol, acetone, tetrahydrofuran, carbontetrachloride and *n*-hexane, frequently used in chromatography and in this whole study, the solvents are denoted by their code as in Table 5.1. These solvents exhibit a wide range of solvent characteristics including polarity, dipole moment, polarizability, shape and size. They were classified according to the solvatochromic parameter π^* introduced by Kamlet et al.¹⁸⁸, which is listed in Table 5.1.

Table 5.1. Solvatochromic parameter, π^* , for the solvents used in the present study.¹⁸⁸

Solvent	Solvent code	π^*
Acetonitrile	ACN	0.75
Acetone	Acetone	0.71
Methanol	MeOH	0.60
Tetrahydrofuran	THF	0.58
Ethanol	EtOH	0.54
<i>n</i> -Hexane	Hexane	0.54
1-Propanol	PrOH	0.52
Carbontetrachloride	CCl ₄	0.28

The π^* scale is an index of solvent polarizability that measures the ability of the solvent to stabilize a dipole by virtue of its dielectric effect. All solvents employed in this work, except for carbontetrachloride, contain carbon-hydrogen bonds. As a result, they also absorb in the CH₂ stretching band region. However, it was found that solvent absorption typically provides a broad background, and can be clearly distinguished from the spectral components due to the C₃₀ alkyl modified silica gels.

5.1.1 Variable Temperature FTIR Spectroscopic Measurements

Variation of the symmetric CH₂ stretching band position of C₃₀ alkyl modified silica gels in the presence of several polar solvents at 293 K is depicted in Figure 5.1. The influence of these solvents on the alkyl chain mobility and their conformational order is clearly visible from the changes of the CH₂ stretching band positions. It is observed that the conformational order successively decreases upon addition of the polar solvents 1-propanol, ethanol, methanol and acetonitrile which is reflected by a shift towards higher wavenumbers, while at the same time the solvatochromic parameter π^* increases. Ducey et al. observed the same trend in C₁₈ alkyl systems for polar solvents like acetonitrile, methanol and water.⁹⁰ They also observed that the conformational order strongly depends on the surface coverage.

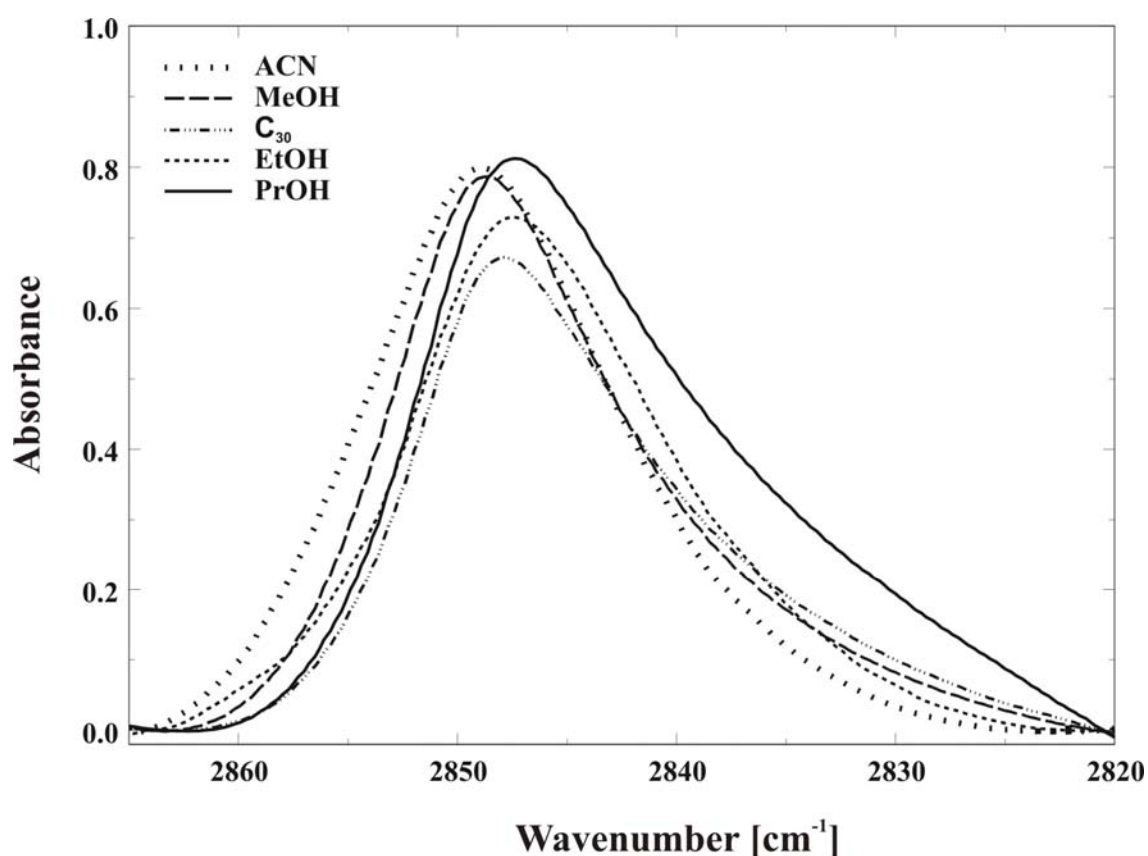


Figure 5.1. Symmetric CH₂ stretching bands of the dry C₃₀ silica gels (C₃₀) and C₃₀ silica in various polar solvents at 293 K.

Figure 5.2 shows the antisymmetric CH₂ stretching band wavenumber as a function of the solvent solvatochromic parameter π^* for C₃₀ alkyl modified silica gels in polar and nonpolar solvents at 293 K. The horizontal dashed line in the figure refers to the value for the dry C₃₀ stationary phase material. Here, for polar solvents like ethanol and 1-propanol, the π^* values are relatively low and the respective antisymmetric CH₂ stretching band maxima are found to be lower than for the dry C₃₀ stationary phase. For the remaining polar and nonpolar solvents, the antisymmetric CH₂ stretching maxima are shifted to higher wavenumbers than those observed for the dry C₃₀ phase. For the polar solvents there is a clear correlation between the solvatochromic parameter π^* and the position of the antisymmetric CH₂ stretching maxima. Moreover, the data points for the two nonpolar solvents are clearly distinguished from those of the polar solvents. For nonpolar solvents a similar correlation might be discussed, although this statement is only based on two data points.

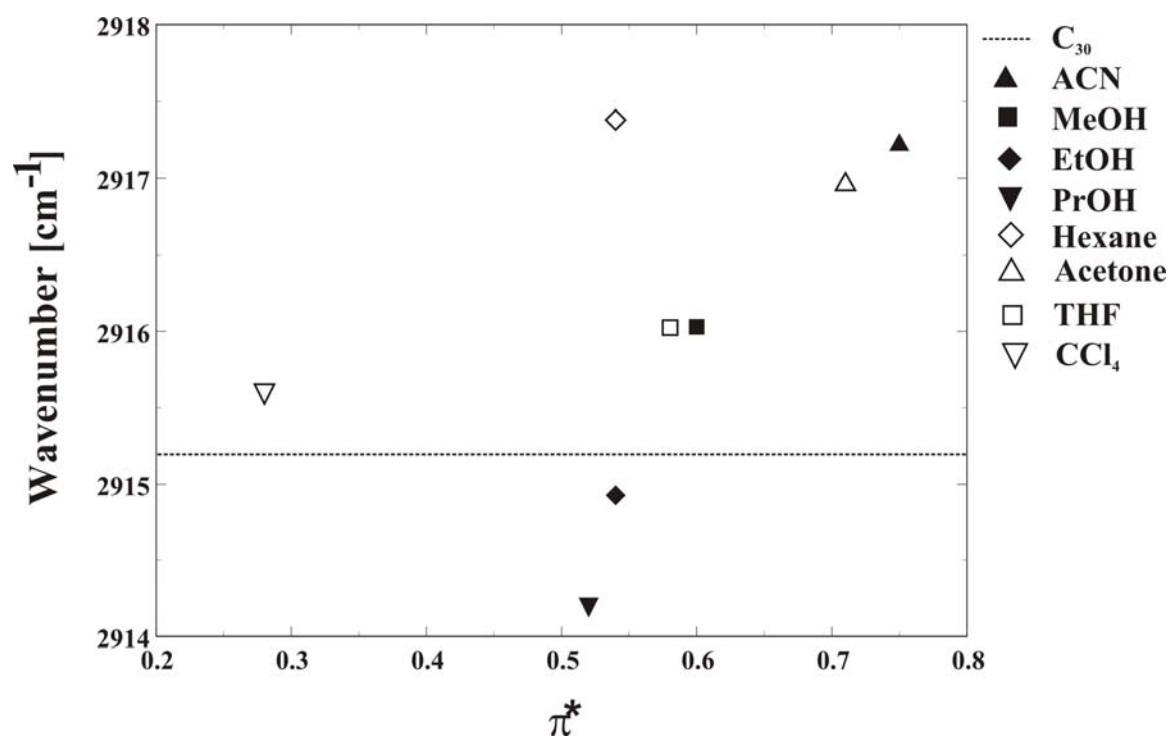


Figure 5.2. Position of antisymmetric CH₂ stretching bands as a function of solvent solvatochromic parameter, π^* , for dry C₃₀ silica gels (C₃₀) at 293 K as indicated by dashed lines (---). C₃₀ phases in various polar and nonpolar solvents at 293 K are indicated by various symbols.

Variable temperature FTIR spectra covering the symmetric and antisymmetric CH₂ stretching band regions for the C₃₀ alkyl modified silica gels in the presence of acetonitrile are depicted in Figure 5.3. It is observed that an increase in sample temperature from 293 to 353 K is accompanied by a higher conformational disorder, as directly reflected by the distinct shift of vibrational band maxima towards higher wavenumbers. At the same time, the IR bandwidths increase due to the higher alkyl chain mobility.

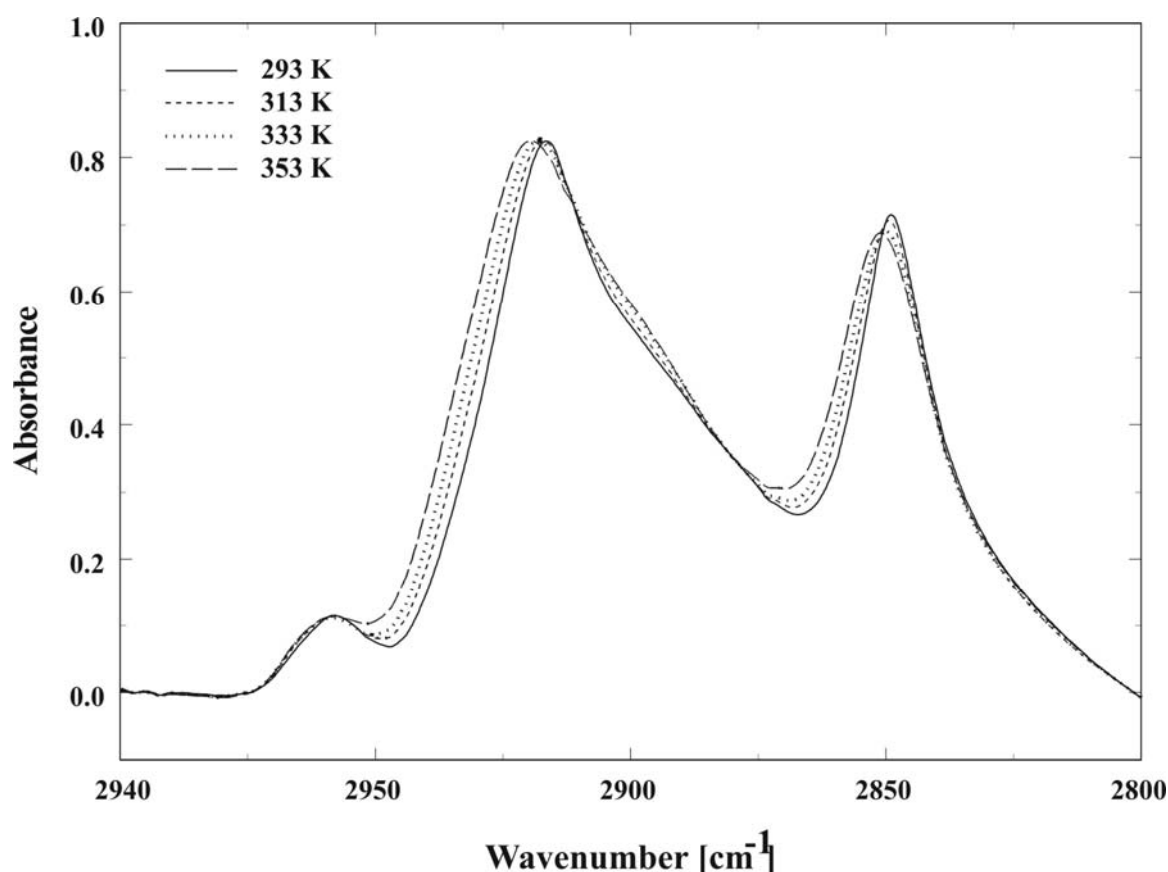


Figure 5.3. Symmetric and antisymmetric CH₂ stretching bands of C₃₀ alkyl modified silica gels at different temperatures in ACN.

The influence of various polar and nonpolar solvents on the symmetric and antisymmetric CH₂ stretching band positions and in turn on the conformational order of the C₃₀ stationary phases is depicted in Figures 5.4 and 5.5. In Figure 5.4 two groups of polar solvents can be distinguished. For acetonitrile and methanol, a higher conformational disorder is observed irrespective of the actual sample temperature if compared with the dry C₃₀ alkyl modified silica gels. At the same time, the addition of ethanol and 1-

propanol results in an increased alkyl chain order which again holds for the whole temperature range covered here.

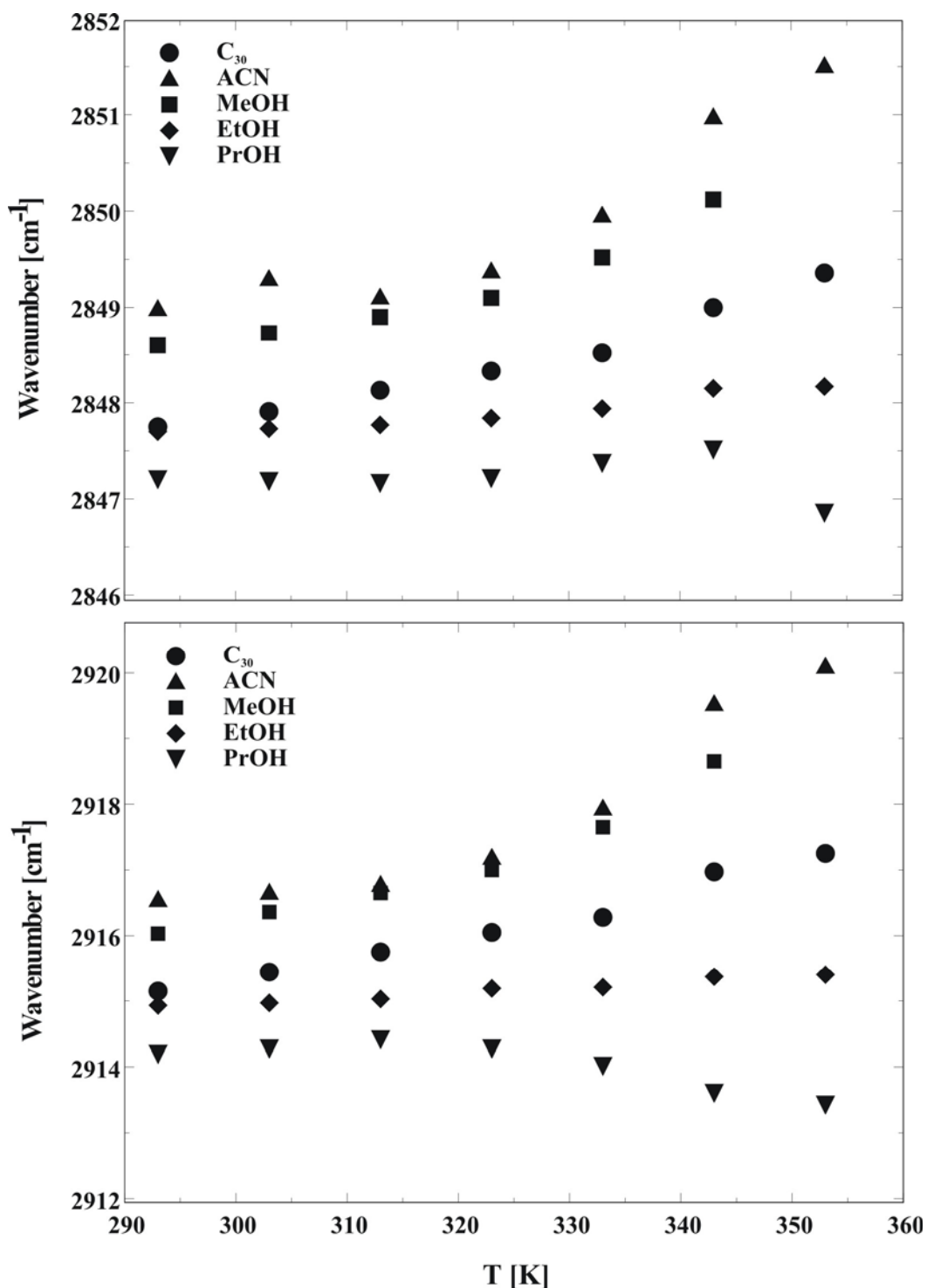


Figure 5.4. Temperature dependence of the CH₂ symmetric stretching (above) and antisymmetric stretching (below) band positions for dry C₃₀ alkyl modified silica gels (C₃₀) and in the presence of various polar solvents.

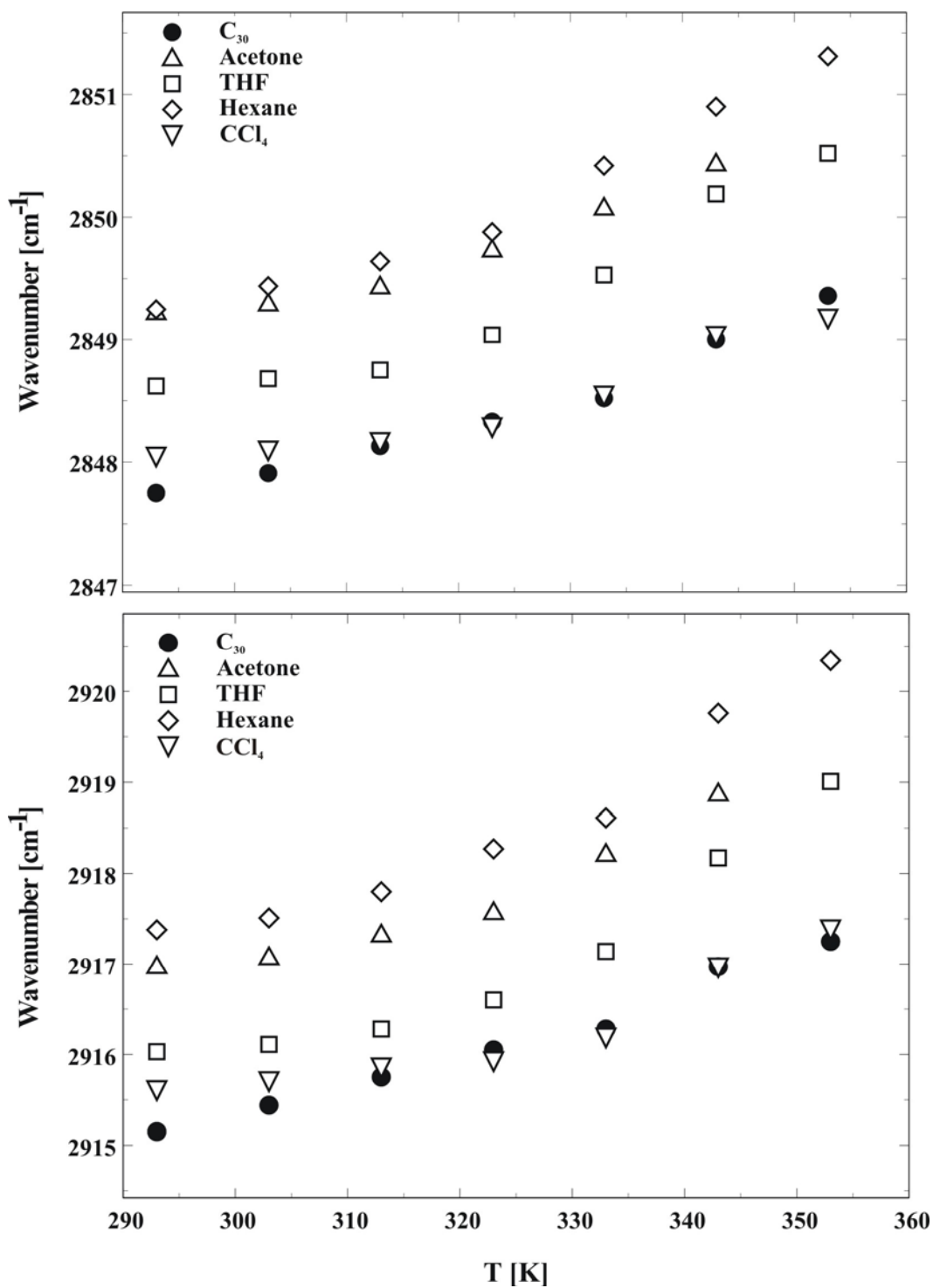


Figure 5.5. Temperature dependence of the CH₂ symmetric stretching (above) and antisymmetric stretching (below) band positions for dry C₃₀ alkyl modified silica gels (C₃₀) and in the presence of polar and nonpolar solvents.

In the presence of methanol and acetonitrile, the conformational order significantly decreases with increase of the sample temperature. These solvent molecules therefore

interact not only with distal methyl groups but also with the underlying methylene groups resulting in higher conformational disorder. The interaction of acetonitrile and methanol with the C₃₀ alkyl chains therefore appears to be partitioning, reflecting pronounced solvent-alkyl chain interactions in these systems. Hence, the alkyl chains are solvated and exhibit a higher mobility in methanol and acetonitrile. Similarly, Zeigler et al. observed an increase in alkyl chain mobility with the addition of acetonitrile on dimethyloctadecylsilyl modified silica using ¹³C NMR line shape and relaxation studies.⁷⁸

In the case of the polar solvents ethanol and 1-propanol, higher conformational order is observed when compared to dry C₃₀ silica gels. For ethanol, the vibrational band maxima of the alkyl chains are slightly shifted towards higher wavenumbers with increase in temperature. This may be due to a moderate penetration of the solvent molecules in the alkyl chain layer. The conformational order increase upon addition of ethanol is less pronounced than in the case of 1-propanol. Here, the solvent molecules are assumed to interact both with the underlying methylene groups and the distal methyl groups. The interaction of ethanol with the C₃₀ alkyl chains therefore appears to be both partitioning and adsorptive, reflecting solvent-alkyl chain and alkyl chain-alkyl chain interactions in this system. In 1-propanol, a distinct higher conformational order of the alkyl chains is registered. Here, the conformational order solely depends on the effect of the solvent, and there is no significant influence of the sample temperature. It is understood that 1-propanol interacts primarily with the distal methyl end of the alkyl chains, and not with the underlying methylene groups. Hence, the adsorptive mechanism operates preserving a higher conformational order even at higher temperatures. This proves that for 1-propanol alkyl chain-alkyl chain interactions dominate the solvent-alkyl chain interactions.

It is therefore concluded that both partitioning and adsorption are observed for C₃₀ alkyl modified systems in the presence of the aforementioned polar solvents. These findings can be understood on the basis of the higher polarity of methanol and acetonitrile which allows them to interact with the surface silanol groups through hydrogen bonding (as they are not endcapped), leading to the higher conformational disorder of alkyl chains as compared to the dry C₃₀ stationary phases. Thus, in methanol and acetonitrile the complete alkyl chains on the silica surface are solvated. As already mentioned, in the case of ethanol and 1-propanol, enhanced ordering of the stationary phase occurs resulting in higher conformational order when compared to that of dry C₃₀ alkyl chains. Here, also the

polarities of these solvents are reduced due to the electron releasing nature (+I effect) of their methyl groups. For 1-propanol and ethanol, the conformational ordering of alkyl chains shows that the chains are only partially solvated. Although ethanol and 1-propanol are more hydrophobic in nature than methanol and acetonitrile, the polarity and relative size may dominate the hydrophobicity during the interactions of polar solvents with C₃₀ alkyl chains. The balancing between the polarity and hydrophobicity decides the conformational order of the C₃₀ alkyl chains in the presence of polar solvents. Thus, the conformational order of the alkyl chains is more pronounced in ethanol and 1-propanol, whereas in acetonitrile and methanol, higher conformational disorder is achieved at different temperatures when compared with the dry C₃₀ stationary phase material. Moreover, it is assumed that the interaction of the 1-propanol solvent molecules with only the distal methyl groups results in a somewhat better packing of the C₃₀ chain ends along with a higher conformational order than for the dry C₃₀ stationary phase, as reflected by the experimental IR stretching data.

All symmetric and antisymmetric CH₂ stretching band positions of the C₃₀ stationary phases in the presence of the polar and nonpolar solvents, given in Figure 5.5, reflect a decrease of alkyl chain conformation with increase of temperature, in agreement with the earlier studies on C₁₈ alkyl systems for nonpolar solvents.^{25,82} Addition of the nonpolar solvent carbontetrachloride leaves the conformational order almost unaltered, while the second nonpolar solvent *n*-hexane induces considerable conformational disorder when compared to the dry C₃₀ stationary phase material.

The conformational disorder in the polar solvents acetonitrile, methanol, acetone and THF and for the nonpolar solvent *n*-hexane is more pronounced than in dry C₃₀ alkyl gels which again suggests that solvation occurs according to the partitioning model. These solvents intercalate and solvate the alkyl chains to some greater extent. A quite similar behavior was reported from former FTIR studies for acetone⁶⁴ and Raman studies for THF and *n*-hexane on C₁₈ alkyl modified systems.²⁵ It was also noted that the alkyl chains behave like in liquid-like state at higher temperatures, while they are more ordered in the solid-like state at lower temperatures, in quite the same way is observed in the present study.²⁵

The high conformational disorder in *n*-hexane might be a result of the stronger hydrophobic interactions between the *n*-hexane molecules and the alkyl groups of C₃₀ stationary phases. Gangoda et al. obtained similar results from ²H NMR investigations.¹⁸⁹ They investigated selectively deuterated dodecyl modified silica gels and observed conformationally highly disordered alkyl chains in the presence of *n*-hexane. However, in a recent FTIR investigation by Srinivasan et al. the C₁₈ alkyl chains were found to be conformationally more ordered in *n*-hexane irrespective of the sample temperature.⁶⁴ These contradictory results can be traced back to the differences for the surface coverages and alkyl chain lengths. It was demonstrated earlier that the surface coverage⁶³ and alkyl chain length²⁶ play important roles for the conformational order of the alkyl chains.

Obviously, in nonpolar solvents, the hydrophobicity plays a major role in inducing the conformational disorder of the C₃₀ alkyl chains. Thus the nonpolar solvents penetrate the alkyl chains to a greater extent and induce more conformational disorder, as evident from the shift in symmetric and antisymmetric absorption bands when compared to the polar solvents.

Finally, we briefly compare the results for the conformational order/disorder behavior of the C₃₀ alkyl chains upon the addition of various polar and nonpolar solvents with the data for nonsolvated C₃₀ stationary phases, i.e. in the dry state. For dry C₃₀ alkyl chains a shift of the vibrational band maxima towards higher wavenumber with increasing temperature is registered (see Figures 5.4 and 5.5), reflecting an increase in alkyl chain mobility and conformational disorder in the same direction. Srinivasan et al. observed similar effects for the conformational order of C₃₀ alkyl systems on silica and other supports using variable temperature FTIR spectroscopy.^{65,66} In addition, variable temperature ¹³C NMR studies on C₃₀ stationary phases have clearly demonstrated the presence of such order/disorder phenomena for the tethered alkyl chains.⁶²

The effect of temperature on the alkyl chain order was described earlier for modified silica with shorter alkyl chains by the Clapeyron relationship in the context of alkyl phase changes.⁵⁶ The phase changes are thought to correspond to simple first-order solid-to-liquid phase transitions. In close analogy, bonded C₃₀ alkyl chains exhibit a higher mobility at elevated temperatures and they are well organized at lower temperatures. However, for the C₃₀ stationary phases the decrease of conformational order is less

pronounced than for systems with shorter alkyl chain lengths which primarily is attributed to stronger alkyl chain-alkyl chain interactions.⁶⁶

5.1.2 Summary

The effect of various polar and nonpolar solvents on the conformational order of the alkyl chains is studied by variable temperature FTIR spectroscopy. In 1-propanol, the solvent molecules only interact with the methyl end groups of the alkyl chains resulting in higher conformational order than in the dry C₃₀ stationary phase, which is in line with an adsorption mechanism for the solvent-stationary phase interactions. In ethanol the interaction with the C₃₀ alkyl chains appears to be both partitioning and adsorptive, as reflected by the changes in conformational order of the underlying methylene groups. For both solvents the conformational order depends on the solvent molecules irrespective of temperature. On the other hand, the conformational disorder increases with increasing temperature in the presence of other solvents, like acetonitrile, methanol, acetone and THF, if compared to dry C₃₀ alkyl systems. These findings are traced back to partitioning of solvent molecules with the underlying methylene groups of alkyl chains. In nonpolar solvents such as n-hexane, the solvent molecules intercalate into the alkyl chain layer at the silica surface and induce more conformational disorder which again is understood by the partitioning model. The conformational disorder at higher temperatures or in the presence of solvents in general also reflects higher chain mobility. Moreover, for the polar solvents, a pronounced correlation is found between the position of the CH₂ stretching band maxima and the solvatochromic parameter π^* . The present investigation demonstrates that the interactions of solvent with alkyl chains not only depend on solvent properties but also on other parameters, such as alkyl chain length, temperature and surface loading.

5.2 Grafted MCM-41 Silica: Synthesis, Impact of Mono- and Trifunctional C₁₈ Silanes and Endcapping

In the following we report on the first preparation of C₁₈ grafted MCM-41 spheres. The materials were obtained via the pseudomorphic synthesis of the MCM-41 particles, followed by grafting with mono- or trifunctional octadecylsilanes and endcapping of the remaining silanol groups. For a comprehensive characterization of the mesoporous materials several experimental techniques were employed. Throughout this work, the surface modified and endcapped MCM-41 materials are denoted as MF and TF, referring to the samples grafted by means of mono- and trifunctional octadecylsilanes, respectively.

5.2.1 Synthesis of MCM-41 Silica Spheres and Grafting with C₁₈ Chains

Spheres of MCM-41 silica were prepared following the pseudomorphic route by using ProntoSIL as silica source. It turned out that the pseudomorphic transformation was not complete since pores of the parent silica are still left, as can be deduced from the nitrogen adsorption/desorption isotherms presented in section 5.2.3.^{9,11,105}

Organic monolayers were grafted on the calcined MCM-41 silica spheres by reaction with *n*-octadecyldimethylmethoxysilane or *n*-octadecyltrimethoxysilane. Afterwards, the remaining silanol groups were endcapped with HMDS to obtain materials with enhanced hydrophobicity which are suitable for reversed-phase chromatographic separations.

Monofunctional silanes can be only grafted to the silica surface by reaction of the methoxy group with a surface silanol group. This method therefore yields only moderate surface coverages since further cross-linking of the silanes is not possible. On the other hand, trifunctional silanes can bind directly to the surface silanol groups and are able to undergo cross-linking reactions with neighboring silane chains. Hence, the latter assemblies typically exhibit a better chain packing with higher surface coverage, good thermal and enhanced chemical stability.¹⁹⁰

The percentage of carbon obtained from the elemental analysis for samples MF and TF are about 10.3 and 16, respectively. The amount of carbon for the present MCM-41 spheres after grafting with mono- and trifunctional octadecylsilane and subsequent

endcapping is very low. For sample MF, grafted with monofunctional octadecylsilane, about 40 % less carbon is found than for sample TF, grafted with trifunctional octadecylsilane. When discussing these data, it should be kept in mind that the given carbon content also comprises the contribution from trimethylsilane attached during the endcapping process. Nevertheless, it appears reasonable that endcapping of the surface silanol groups yields a similar amount of attached trimethylsilane molecules in both samples.

The smaller amount of carbon registered for the MF sample points to a lower degree of C₁₈ coverage upon grafting with the monofunctional silane, most likely as a consequence of the general low reactivity of methoxy silanes and the lower amount of surface silanol groups in MCM-41 materials. In addition, the probability for attachment of a monofunctional methoxy silane is also smaller than for grafting with trifunctional methoxy silanes.

Due to the surface grafting with functionalized octadecylsilane and subsequent HMDS endcapping, absolute numbers for the surface coverage cannot be given. Nevertheless, such values can be estimated and discussed on a qualitative basis. In the case of coverage with only C₁₈ chains, values of about 0.55 and 0.95 $\mu\text{mol}/\text{m}^2$ are obtained for the MF and the TF sample, respectively. With the more realistic assumption that a substantial amount of the available silanol groups were endcapped with HMDS ($\geq 50\%$), as supported by the ²⁹Si and ¹³C NMR data (sections 5.2.5 and 5.2.6), the numbers for C₁₈ surface coverage of the MF and TF samples become even smaller.

Hence, the C₁₈ coverage achieved for the present MCM-41 spheres is substantially lower than the typical values reported for conventional silica based systems. Several reasons can be discussed for these experimental findings: (i) the lower amount of surface silanol groups for calcined MCM-41 materials (only 4 $\mu\text{mol}/\text{m}^2$)¹⁸⁰ than for normal silica surfaces, (ii) the relatively small diameter of about 40 Å of the mesopores (see section 5.2.3) which creates significant difficulties in coating of the interior of the mesopores with C₁₈ chains, and (iii) the octadecyl chains attached near the entrance of the pores which create some hindrance for other molecules to diffuse inside the pores.

It should be mentioned that a low surface coverage in turn affects the alkyl chain conformational order,⁶³ as outlined in sections 5.2.6 and 5.2.7 covering the spectroscopic investigations. In this context, it appears to be very unlikely that on a molecular level higher C₁₈ surface coverages have to be discussed. Rather, a uniform low surface C₁₈ surface coverage appears to be more reasonable. In the case of the TF sample this assumption is supported by the experimental ²⁹Si NMR data, where only a low amount of cross-linked alkylsilane chains is observed. For both the TF and the MF samples only a low degree of conformational alkyl chain order has been derived from the ¹³C NMR and FTIR studies (see below) which strongly supports the presence of isolated C₁₈ chains.

5.2.2 SAXS Measurements

Figure 5.6 shows the SAXS pattern obtained for the calcined MCM-41 silica spheres and the two C₁₈ grafted samples, MF and TF. Calcined MCM-41 silica exhibits three Bragg reflections at low angles, indexed as (100), (110) and (200), which are consistent with the hexagonal pore arrangement of the present mesoporous material.

However, the reflection peaks of the present calcined sample are broader than those reported earlier for highly regular MCM-41 samples,¹⁹¹ resulting in some overlapping of the peaks. Upon grafting of the MCM-41 spheres a further broadening of the reflection peaks is observed.

From earlier studies it is known that such a peak broadening originates from a distortion of the hexagonal symmetry of second- and higher-order neighbor pores around a central pore.¹⁹¹ The broadened reflection peaks in the ungrafted MCM-41 sample thus point to a long-range distortion of the hexagonal arrangement of the mesopores. This observation is in agreement with the data from the nitrogen adsorption/desorption measurements (see next paragraph). Here, a second type of mesopores is found which most probably is randomly distributed, causing the broadening of the SAXS reflection.

The unit cell parameters for the MF and TF samples, reported in Table 4.1, prove that the basic MCM-41 framework remains intact even after alkyl chain grafting. However, the observed decrease of the intensities for the (110) and (200) reflections along with the slightly enhanced peak broadening indicate some further reduction of the long range

order of the MCM-41 framework upon surface grafting, as also observed in other studies on grafted MCM-41 materials.¹⁹²

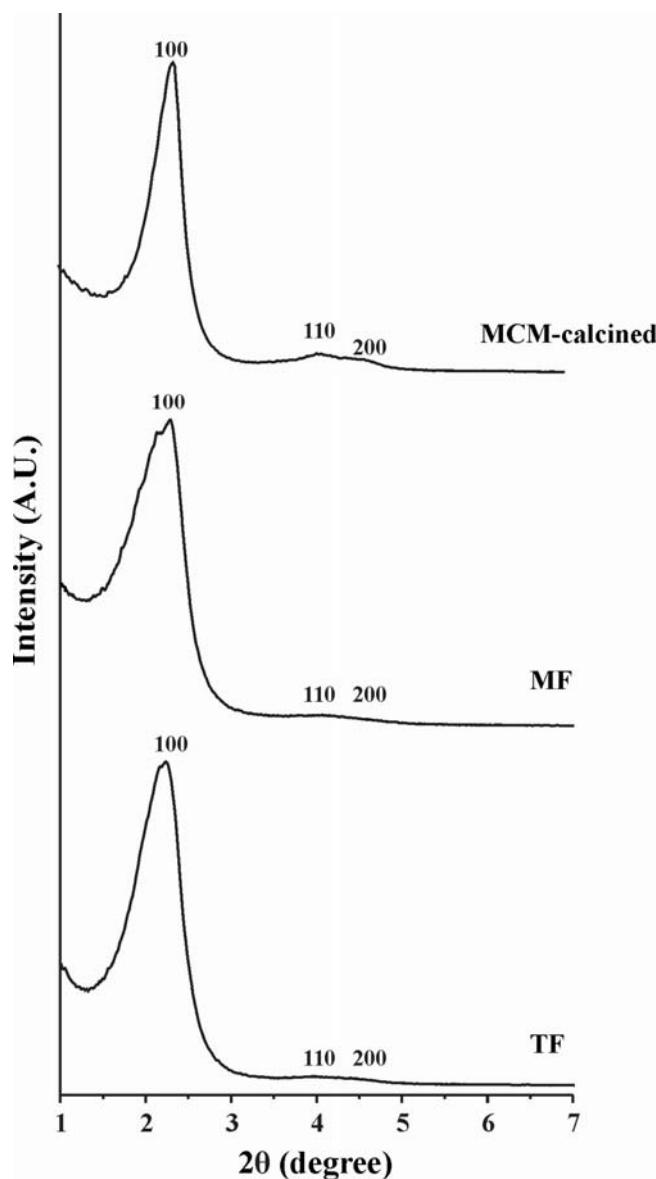


Figure 5.6. SAXS pattern of calcined MCM-41 silica, MF and TF samples.

5.2.3 Nitrogen Sorption Isotherm Analysis

Experimental nitrogen adsorption-desorption isotherms and the derived pore size distribution of the calcined MCM-41 silica spheres, without and after alkyl chain grafting, are shown in Figures 5.7 and 5.8. The textural properties are summarized in Table 4.1. The overall appearance of all BET isotherms is very similar and typical for the group of reversible IV type isotherms. The strong rise of the BET curve for the ungrafted

MCM-41 sample above a relative pressure of $p/p_0 = 0.25$ stems from the capillary condensation in the mesopores and is a characteristic feature for a mesoporous structure.

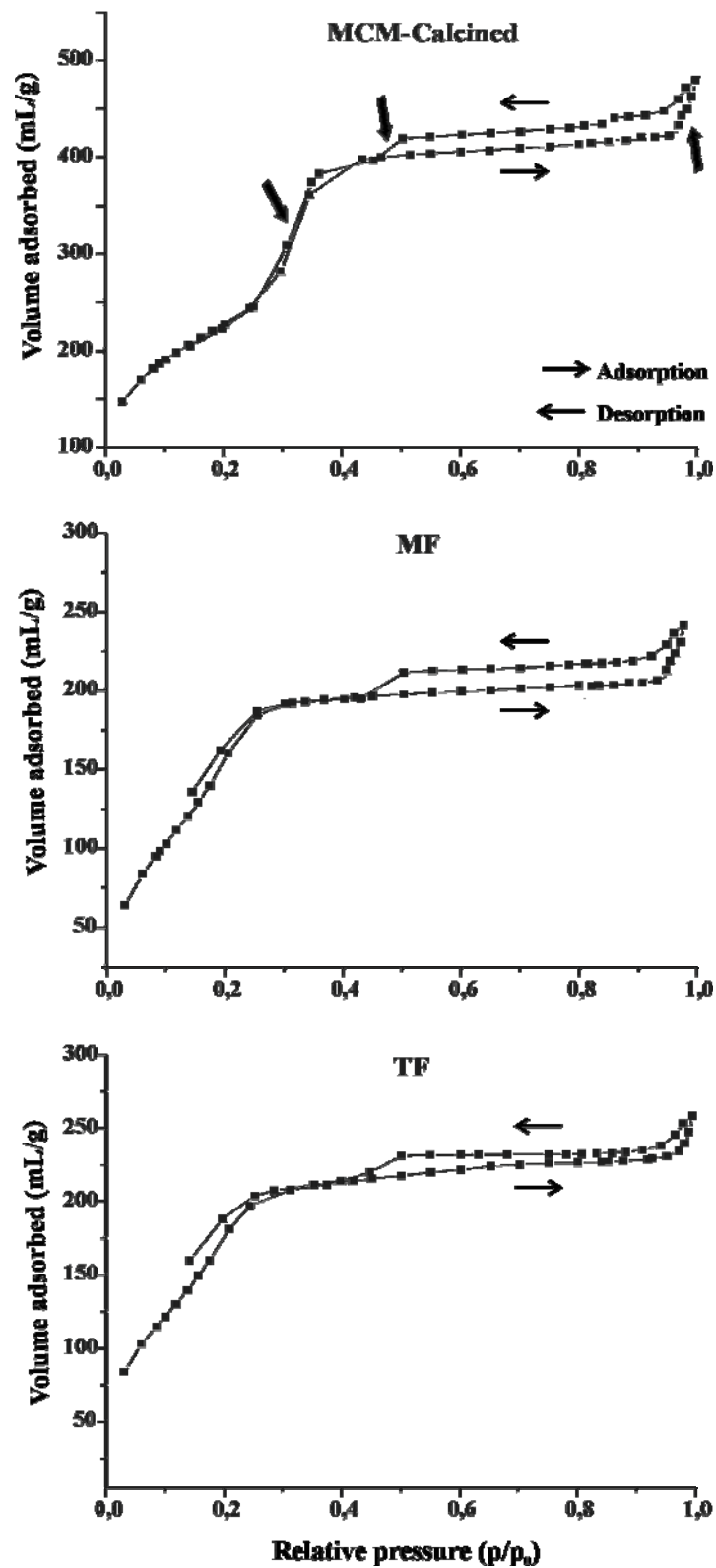


Figure 5.7. Nitrogen sorption isotherm of calcined MCM-41, MF and TF samples.

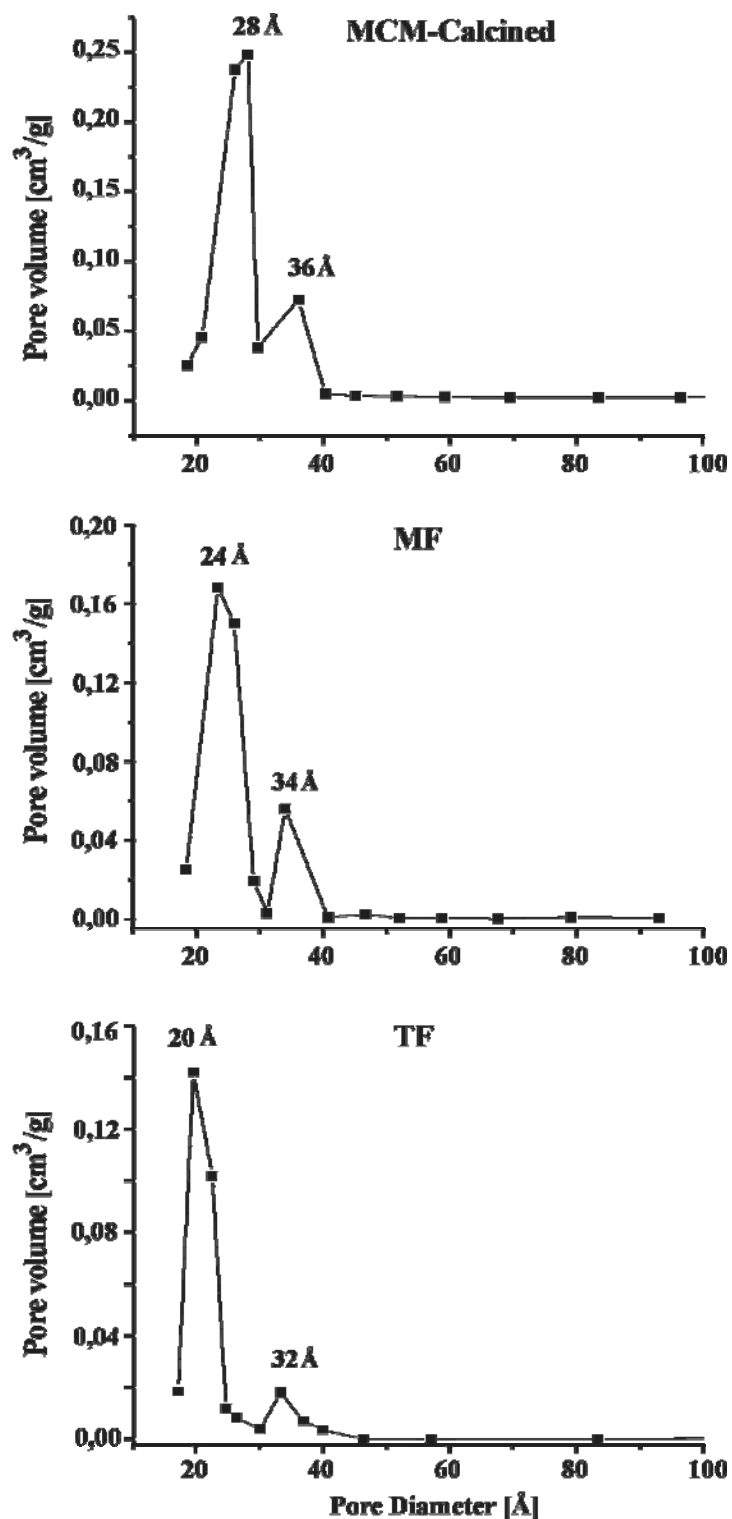


Figure 5.8. BJH pore-size distribution of calcined MCM-41, MF and TF samples.

For the present systems a hysteresis is observed for the nitrogen adsorption/desorption curves between about $p/p_0 = 0.4$ and 1.0 along with an additional step in the desorption curve at about $p/p_0 = 0.45$ (see arrow), which is attributed to the presence of mesopores

with a larger pore diameter. In fact, a similar hysteresis was also reported for other mesoporous samples, prepared via a pseudomorphic transformation.¹⁰⁵ The most likely explanation for this observation is a connection of the larger mesopores to the exterior of the particles by the structured porosity. As a result, desorption of nitrogen condensed in these larger pores is retarded and occurs via a cavitation process.¹⁰⁵ The final rise of the BET isotherms at about $p/p_0 = 0.95$ proves the presence of larger mesopores which remain from the structure of the original silica material employed during the pseudomorphic reaction.

It should be emphasized that grafting of the MCM-41 spheres with octadecylsilane and subsequent endcapping leaves the overall shape of BET curves almost unchanged, i.e., the overall mesoporous structure remains practically unaltered. The major difference is a lowering of the plateau value for the pressure range above $p/p_0 = 0.3$, in agreement with former observations on related materials.¹⁷³ As a direct consequence of the smaller amount of adsorbed nitrogen, the total pore volume and the BET surface area are also significantly reduced after surface modification with octadecylsilane (see Table 4.1), as also found for non-spherical MCM-41 materials.¹⁹³

Alkyl chain grafting is also accompanied by a horizontal shift of the BET curves below $p/p_0 = 0.6$ towards the low pressure region which implies smaller pore diameters, as confirmed by the pore size distribution analysis and which will be further described below. Finally, for the low pressure range ($p/p_0 < 0.3$) again a hysteresis is observed, and the desorption curves for the grafted MCM-41 samples lie above the respective adsorption curves. It is worthwhile to note that similar findings were also reported recently for other MCM-41 spheres which were grafted with shorter alkyl chains than in the present study.^{8,141} These observations might be traced back to the interaction between the nitrogen molecules and the grafted alkyl chains, characterized by a high degree of conformational disorder (see ¹³C and FTIR data below), and some kind of pore blocking effect due to grafting with the long C₁₈ alkyl chains, as will be discussed below.

BJH pore size distribution plots for the MCM-41 samples studied here are given in Figure 5.8. In the ungrafted MCM-41 material two types of mesopores show up, reflecting a primary mesoporosity with a pore diameter of 28 Å and secondary mesoporosity with a pore diameter of 36 Å. In addition, parental silica pores, with a

diameter of 246 Å, are also visible at a relative pressure close to unity (not shown in Figure 5.8; but see arrow in Figure 5.7). Alkyl chain grafting causes a reduction of the pore diameter with values of 24 and 34 Å, and 20 and 32 Å for MCM-41 samples grafted with monofunctional and trifunctional octadecylsilane, respectively.

Earlier it was found that the presence of a secondary mesoporosity depends on the pore volume of the parent silica.⁹ Recently, Galarneau et al. showed that a long reaction time is the method of choice to achieve a uniform mesopore structure.¹⁰⁵ Longer reaction times also promote the complete transformation of the larger mesopores of 246 Å in diameter in the original silica. The actual reaction times and conditions for complete conversion, however, strongly depend on the silica source. In fact, in an ongoing study of our own group also MCM-41 silica spheres with a single type of mesopores and without parental silica pores could be obtained.¹¹

These findings for the BET surface area, total pore volume and pore diameter correlate with the increase in surface coverage (in terms of carbon content) for the present MCM-41 materials after alkyl chain grafting and endcapping, although it should be recalled that the carbon content only provides an integral value for the organic species after grafting and subsequent endcapping.

The reduction in surface area and total pore volume upon surface grafting is traced back to the binding of trimethylsilane in the interior of the pores. The C₁₈ chains appear to be too large to penetrate completely into the pores, and are primarily attached at their entrance, where they provide a steric hindrance for other C₁₈ chains and trimethylsilane molecules. As a result, only a relatively low amount of surface loading can be achieved, since there is limited access to the interior of the mesopores. Likewise, the decrease in pore diameter is in agreement with the relatively low degree of surface coverage.

Jaroniec and co-workers made a detailed study on the grafting of alkyl chains of different length and functionality on the MCM-41 supports with a pore size of about 50 Å.¹⁷³ They showed that the pore diameter reduces gradually with increasing size of the alkyl ligands from C₃ to C₈ chains. In our work the situation is different due to the spatial restrictions imposed by the mesopores on the much longer octadecyl chains.

It is important to note that the given pore diameters were derived with the BJH method which is known to underestimate the pore size up to 25 % for pores with a diameter below about 100 Å.¹⁷⁷⁻¹⁷⁹ For the present data it would mean that the real pore diameters are about 7 to 9 Å larger than the values given in Table 4.1. These corrected values are then in agreement with the literature values from other recent studies on the pseudomorphic preparation of MCM-41 spheres and their subsequent grafting with C₈ chains.^{8,141} At the same time, the corrected pore diameters also prove the expected mesoporous structure for our present materials which is also retained after surface modification with mono- and trifunctional octadecylsilane. The known unit-cell parameter, a_0 , from SAXS measurements, and the corrected pore diameters, can be used to calculate the wall thickness of the various samples. For the primary mesopores, values for the wall thickness are calculated which are close to the ideal values from literature.^{9,105}

5.2.4 SEM Analysis

SEM pictures of the ProntoSIL silica source and the calcined MCM-41 material are shown in Figure 5.9. The obtained pictures clearly demonstrate that the spherical morphology of the silica particles is retained during the pseudomorphic synthesis of the MCM-41 spheres. In addition, there is no evidence for agglomeration of the MCM-41 silica particles. It is also seen that the diameter of the particles and the distribution of the particle size is preserved during the pseudomorphic reaction.

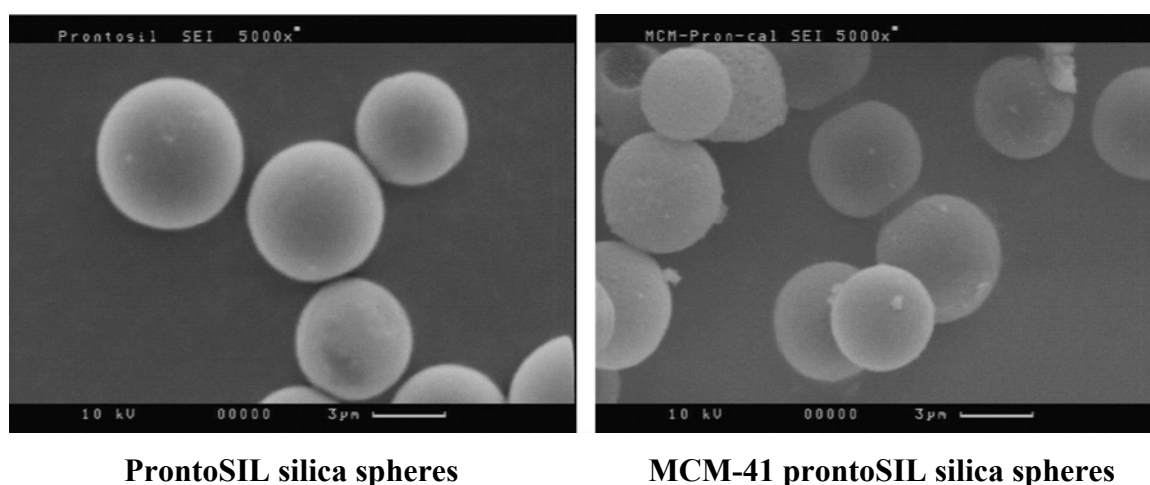


Figure 5.9. SEM micrographs of prontoSIL silica and calcined MCM-41 silica spheres.

Similar pictures were found for the grafted MCM-41 particles (not shown). Hence, both the grafted and ungrafted MCM-41 materials retain the dispersity of the silica spheres which originates from the commercial silica source used for the pseudomorphic transformation.

5.2.5 ^{29}Si MAS NMR Spectroscopy

^{29}Si MAS NMR spectroscopy is employed for the determination of the surface species, amount of alkyl chain grafting and degree of cross-linking of the attached alkylsilanes. The ^{29}Si CP/MAS NMR spectra of the grafted samples, MF and TF, are shown in Figure 5.10. The ^{29}Si chemical shifts of the various species are reported in Table 5.2. The ^{29}Si resonances around -100 and -109 ppm originate from the MCM-41 support, and reflect surface silanol groups (Q^3 units) and Q^4 groups, respectively.^{26,51} The comparison with the ^{29}Si NMR spectrum of the calcined MCM-41 sample prior to grafting (spectrum not shown), with a dominant Q^3 signal as well as Q^2 and Q^4 resonances, reveals a complete loss of the Q^2 signal and a noticeable reduction of the Q^3 peak after surface modification with the alkylsilanes and subsequent endcapping.

Table 5.2. ^{29}Si chemical shift values for grafted MCM-41 silica spheres.

Sample	δ (ppm)					
	Q^4	Q^3	T^3	T^2	T^1	M
MF	-109.0	-101.1	--	--	--	14.5
TF	-108.3	-100.9	-64.5	-56.5	-48.9	15.0

It is obvious that the Q^3 intensity for the present grafted samples is higher than in related systems,¹⁹⁴ which is a consequence of the low surface coverage for the present materials due to the non-accessibility of the silanol groups inside the mesopores. It is thus assumed that the pores are partially blocked after attachment of the C_{18} chains in the vicinity of the pore entrance which in turn prevents the diffusion of smaller trimethyl silyl groups and other C_{18} alkylsilane molecules inside the mesopores.

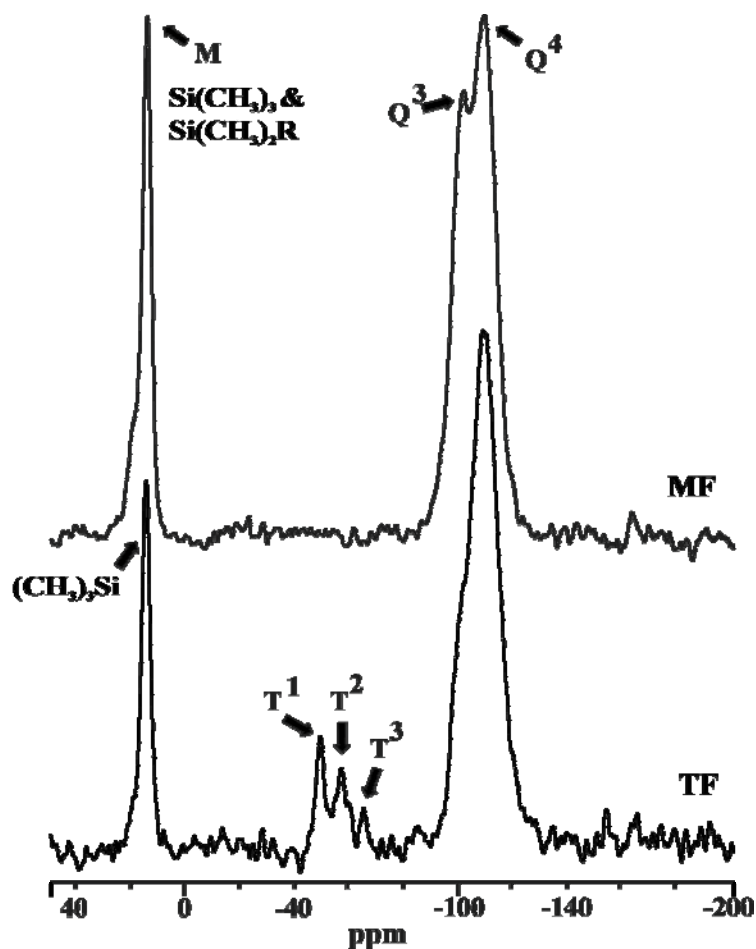


Figure 5.10. ^{29}Si CP/MAS NMR spectra of MF and TF samples at 293 K.

Likewise, the Q^3 intensity for the MF sample is found to be higher than for the TF sample which is consistent with the lower surface coverage (i.e. smaller carbon content, see Table 4.1) registered for the former sample. As mentioned in section 5.2.1, the different surface coverages for the MF and TF samples are most likely a consequence of the general low reactivity of methoxy silanes and the lower probability for monofunctional chains to react with surface silanol groups, which in the present MCM-41 material is about half of that reported for normal silica. Further reasons might be the bulky methyl groups of the monofunctional silane, which provide a sterical hindrance for the binding of HMDS to the silanol groups in the vicinity of an attached alkylsilane chain, and the lack of cross-linking reactions since only a single reactive group is available.

For the MF sample, a further intense peak is found at about 14.5 ppm (M group) which is a superposition of the ^{29}Si resonances due to the attached monofunctional C_{18} chains and the trimethyl silyl groups from the endcapping reaction.⁵¹ Unfortunately, it was not

possible to decompose this NMR signal to extract the relative amount of the two structural components. The same ^{29}Si resonance is also observed for the TF sample which now refers solely to trimethyl silyl groups. Its strong intensity clearly proves that a substantial amount of endcapped silanol groups must be present in the TF sample. This statement even holds when keeping in mind the known intensity distortions due to the application of cross-polarization for ^{29}Si signal enhancement.

In the ^{29}Si CP/MAS NMR spectrum of the TF sample additional T^n group signals between -45 ppm and -70 ppm⁵¹ are identified, which unequivocally prove the attachment and cross-linking of the C_{18} chains on the MCM-41 silica surface, as listed in Table 5.2 (refer sub-chapter 3.2.1). The presence of T^1 and T^2 group signals reflect an incomplete attachment and/or cross-linking of the trifunctional alkylsilane chains. The relative intensity of the T^n signal follows the order $T^1 > T^2 > T^3$ which unequivocally points to a very low degree of C_{18} chain cross-linking along with very flexible octadecyl chains, even by grafting with trifunctional silanes.

5.2.6 ^{13}C MAS NMR Spectroscopy

^{13}C NMR spectroscopy was used to examine the conformational order of the attached alkyl chains and to get further information about the grafting of the MCM-41 silica surface. Figure 5.11 depicts experimental ^{13}C CP/MAS NMR spectra for the two grafted MCM-41 samples, MF and TF and the chemical shift values are given in Table 5.3. The peak around 23 ppm arises from carbons C-2 and C-17 of the alkyl chains. The signal at 32.5 ppm represents carbons C-3 and C-16.

Table 5.3. ^{13}C chemical shift values for grafted MCM-41 silica spheres.

Sample	δ (ppm)						
	OCH_3^*	C-3 & C-16	C-4- C-15	C-2 & C-17	C-1	C-18	$\text{Si}(\text{CH}_3)_3^{**}$
MF	--	32.4	30.1	23.0	17.9	13.4	-0.1
TF	50.3	32.5	30.2	23.0	13.3	11.0	0.5

* OCH_3 : nonreacted methoxy group from trifunctional silane; ** $\text{Si}(\text{CH}_3)_3$: trimethylsilyl group from HMDS

The ^{13}C resonances of carbons C-1 and C-18 typically appear around 13-14 ppm.^{26,167} For samples with high surface coverage the methyl group signal, C-18, sometimes splits up which has been attributed to the presence of methyl groups with different mobilities, as a result of different chain packings, i.e. sample heterogeneity.^{52,65} For the present samples with a low surface coverage such a signal split-up cannot be observed. Hence, the C-1 and C-18 resonate at 13.3 and 11 ppm, while for the MF sample they occur at 17.9 and 13.4 ppm, respectively. The lowfield shift of the former signal for the MCM-41 sample with the monofunctional silane is attributed to the electronic effects from the methyl groups bound to the silicon atom.

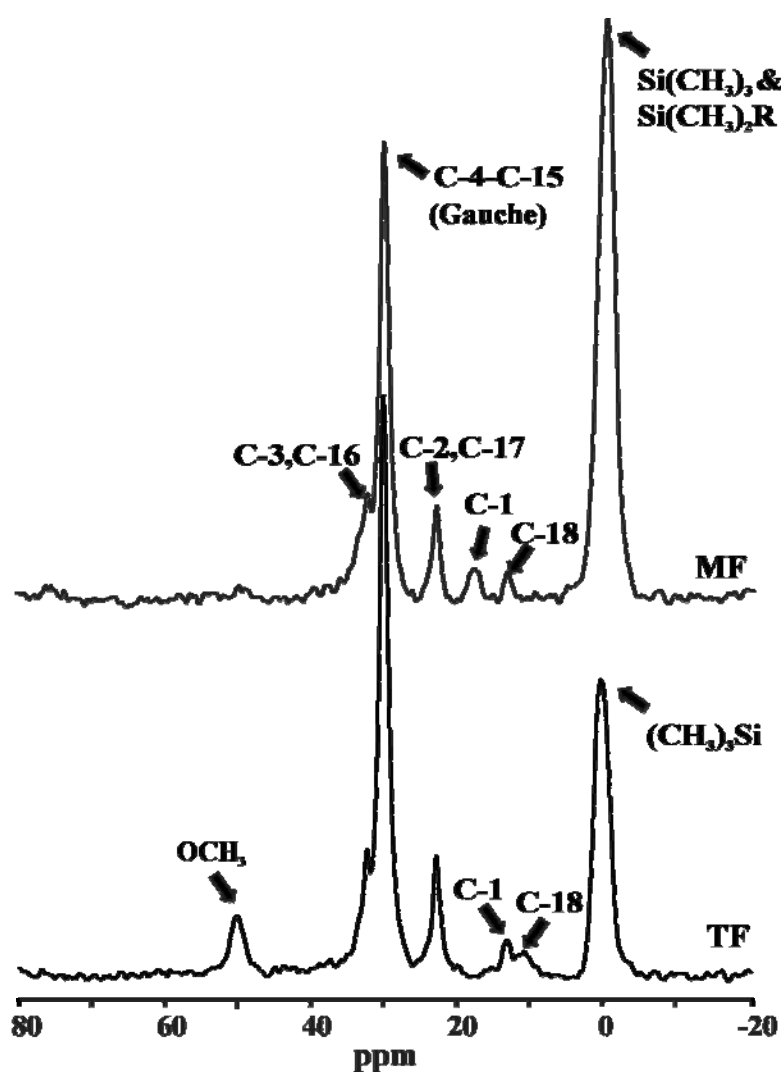


Figure 5.11. ^{13}C CP/MAS NMR spectra of MF and TF samples at 293 K.

The signals at around 30 ppm found in the present work points to C_{18} chains in the gauche state with low conformational chain order (refer sub-chapter 3.2.2). C_{18} chains with a high

degree of chain ordering (trans conformers) are characterized by a ^{13}C resonance at about 32 ppm^{52,167} and obviously do not occur in the present samples. The low conformational order for the present samples points to a large spatial freedom and high chain mobility, in agreement with the low surface coverage discussed above. Such correlations between the alkyl chain conformational disorder and the surface coverage are well known and were discussed earlier during ^{13}C NMR studies on other alkyl chain modified silica materials.^{63,167}

For the TF sample, the additional ^{13}C resonance at around 50 ppm stems from the nonreacted methoxy groups in the trifunctional silane. The presence of nonreacted methoxy groups in the TF sample might be explained by the small amount of accessible surface silanol groups along with a minor probability for closely spaced silanol groups at which all three functional groups of an octadecylsilane molecule can bind. Another explanation might be given by the presence of methoxy groups which were released during the hydrolysis of the trifunctional octadecylsilanes, and which are then chemically bound to the surface silanol groups in a type of endcapping reaction.¹⁹⁵

The trimethyl silyl groups from the endcapping with HMDS resonate at around 0.5 ppm. For the MF sample, this resonance also includes the two methyl groups at the silicon atom of the monofunctional alkyl silane chain. Due to the application of cross-polarization it is again not possible to discuss the ^{13}C NMR signal intensities in a quantitative way. The strong signal intensity of this latter resonance nevertheless points to a substantial amount of trimethyl silyl groups arising from the endcapping reaction, which supports the aforementioned statement about the small octadecyl surface coverage and the resulting general low degree of alkyl chain conformational order, as derived from the ^{13}C NMR spectra and the FTIR data discussed next.

5.2.7 FTIR Spectroscopy

FTIR spectroscopy can be used to probe the structural features of the attached alkyl chains. Figure 5.12 depicts FTIR spectra of TF and MF samples at 293 K covering the region of the CH_2 and CH_3 stretching bands. The peaks at 2963.0 cm^{-1} and 2962.4 cm^{-1} correspond to CH_3 antisymmetric stretching bands arising from the methyl groups in the endcapping reagent and in the alkyl chains (C-18). In the case of the MF sample also two

methyl groups, bound to the silicon atom, contribute which explains the higher relative intensity of the antisymmetric CH₃ stretching band for this sample as compared to the TF sample.

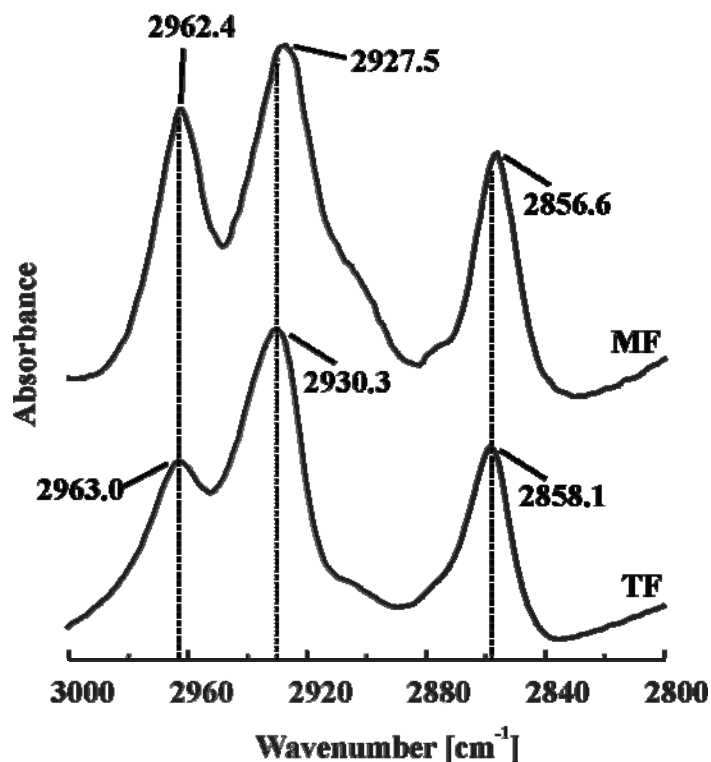


Figure 5.12. Antisymmetric and symmetric CH₂ stretching bands of MF and TF samples at 293 K.

The absorption maxima of the antisymmetric and symmetric CH₂ stretching bands occur at 2930.3 cm⁻¹ and 2858.1 cm⁻¹ for the TF sample, and at 2927.5 cm⁻¹ and 2856.6 cm⁻¹ for the MF sample, respectively, and point to a low conformational chain order, in agreement with the discussed ¹³C NMR resonances of the inner methylene groups (see section 5.2.6). The fact that the stretching band positions in the present samples are shifted to high wavenumbers and lie outside the typical range of normal grafted silica^{26,63,154} indicates a substantial degree of chain disorder and enhanced chain flexibility, as a consequence of the aforementioned very low surface coverage of these MCM-41 samples.

The derived CH₂ stretching band data further imply that the conformational order in the MF sample is higher than in the TF despite the higher carbon content (and thus higher surface coverage) of the latter grafted MCM-41 material. A possible explanation might be

given by the stronger intermolecular interactions of the methyl groups bound to the silicon atom for the MF sample, comprising chain-chain as well as chain-silica surface interactions, and which imposes a higher chain order than for the TF sample. As shown from the ^{29}Si NMR studies for the TF sample also a substantial amount of isolated or partially cross-linked alkyl chains exist. Here, partial cross-linking of the chains might also occur vertical to the silica surface, resulting in loosely packed chains with low conformational order. However, so far there is no final proof for these latter assumptions.

5.2.8 Summary

MCM-41 silica spheres, prepared via pseudomorphic transformation, were surface modified by reaction with mono- or trifunctional octadecylsilane and subsequent endcapping using hexamethyldisilazane. Nitrogen sorption isotherms indicated the presence of three types of pores for both the ungrafted and grafted MCM-41 materials. Apart from the desired primary mesopores, secondary mesopores as well as large parental pores can be distinguished, the latter are a strong indication that the pseudomorphic transformation reaction was not complete. Both the SAXS and N_2 sorption experiments demonstrated that the mesoporosity of the MCM-41 materials is also retained after alkyl chain grafting. In addition, a long-range disorder of the mesoporous structure has been observed. Alkyl chain grafting and chain cross-linking were examined by ^{29}Si and ^{13}C NMR spectroscopy. FTIR and ^{13}C NMR measurements revealed a rather low conformational order of the grafted octadecyl chains in the present MCM-41 materials, most probably due to the general low surface loading found for the present MCM-41 materials. Differences for the alkyl chain conformational order after grafting with mono- and trifunctional alkyl silanes were attributed to variations of the intermolecular interactions for both types of attached alkylsilanes which – due to the very low surface loading - in general possess a substantial degree of spatial freedom. The low surface loading was traced back to (i) the reduced amount of surface silanol groups, (ii) the difficulties caused by the limited pore diameter for attachment of the C_{18} chains in the interior of the MCM-41 pores, and (iii) some steric hindrance by the flexible octadecyl chains near the mesopore entrance which imposes some hindrance on other molecules when diffusing into the mesopores. The same arguments were used for the explanation of the distinct reduction of MCM-41 surface area and total pore volume after surface modification.

5.3 Grafted MCM-41 Silica: Synthesis, Impact of Silica Source and Trifunctional C₁₈ Silane Precursors

In this part we report on the preparation of C₁₈ grafted MCM-41 spheres which were obtained via the pseudomorphic synthesis and subsequent surface modification with trifunctional octadecylsilanes. Different surface loadings were achieved by variation of the preparation conditions. The MCM-41 materials before and after grafting were subject to a comprehensive characterization employing several physico-chemical techniques. Throughout this work, the unmodified and C₁₈ alkyl modified MCM-41 spheres are denoted as **M1-M4** and **M1H-M6M** (refer Tables 4.2 and 4.3), respectively.

5.3.1 Synthesis and Characterization of MCM-41 Silica Spheres

Mesoporous silica spheres were prepared by means of the pseudomorphic route using commercial silica materials, ProntoSIL and Kromasil, as silica source. By choosing the proper reaction conditions, it was possible to prepare silica materials with the same particle characteristics (spherical shape, size and size distribution) as the parent silica material, but with the well-defined mesoporous structure of MCM-41 silica. Moreover, the pseudomorphic transformation is known to provide a homogeneous distribution of the silanol group on the silica surface which can be further exploited, for instance, for uniform surface functionalization or modification.¹⁴¹ The surfactant was removed either by calcination or solvent extraction. As shown by the data from elemental analysis summarized in Table 4.2 (see footnote), 2 wt % carbon are found for the solvent extracted samples (**M2**, **M4**). This finite carbon content stems from ethoxy groups which are attached to the silica surface during surfactant removal, as proven by the ¹³C NMR spectra discussed below.

Representative SEM pictures of the ProntoSIL and Kromasil silica sources and the calcined MCM-41 spheres are shown in Figure 5.13. They clearly demonstrate that the spherical morphology of the silica particles is retained during the pseudomorphic synthesis of the MCM-41 samples. In addition, the average diameter of the particles (approximately 5 μm) and the distribution of the particle size are also preserved. It should be emphasized that there is no evidence for an agglomeration of the received MCM-41 silica spheres. As can be seen, the silica spheres of commercial ProntoSIL or Kromasil

are not completely monodisperse in distribution, and the dispersity of the spheres is also retained during the pseudomorphic transformation.

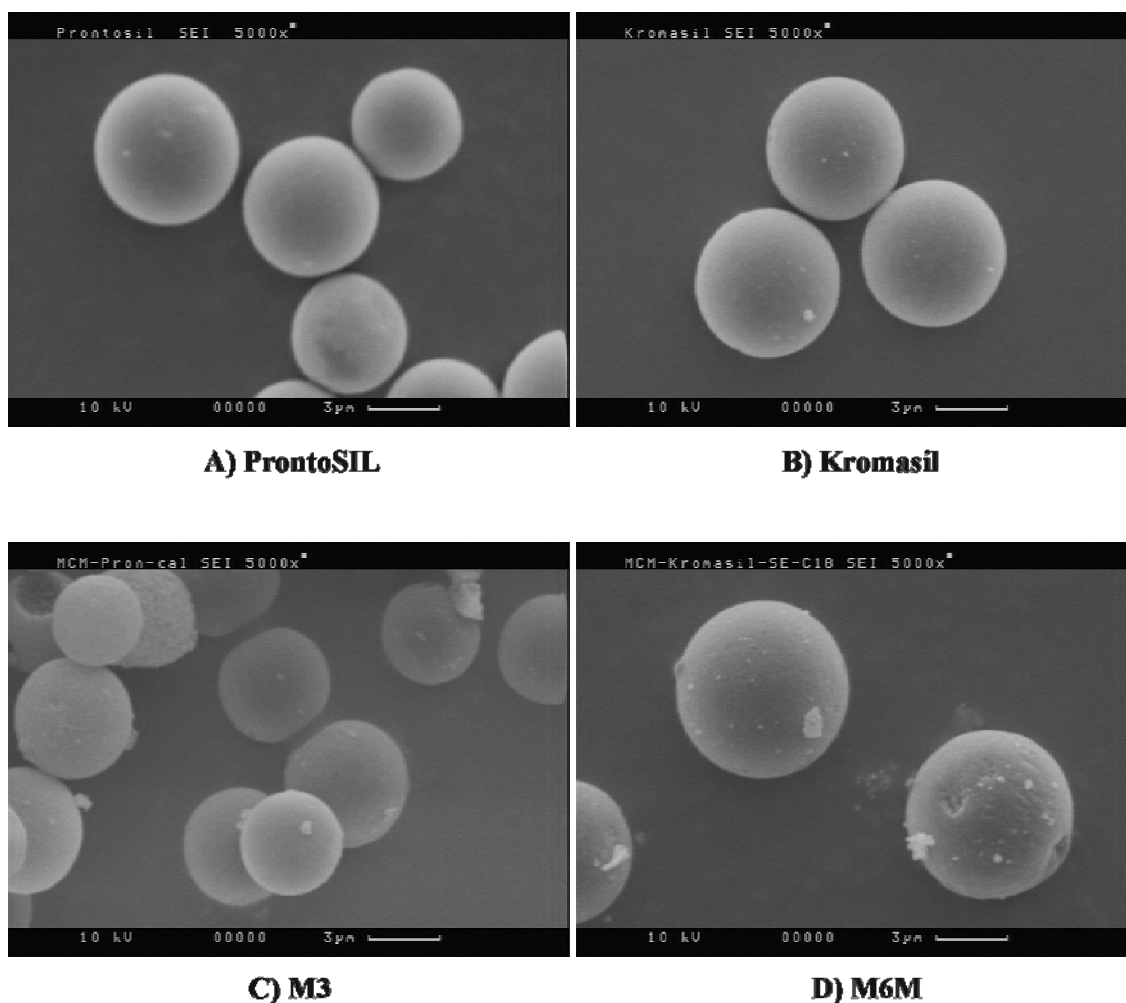


Figure 5.13. SEM micrographs of silica spheres of A) ProntoSIL; B) Kromasil; C) M3; D) M6M.

In Figure 5.14 SAXS patterns of calcined and solvent extracted mesoporous silica spheres are reported. The patterns to the left and to the right refer to samples obtained with ProntoSIL and Kromasil as silica source, respectively. For well-ordered MCM-41 silica four Bragg reflections can be typically observed, indexed as (100), (110), (200) and (210), the latter of which may become rather weak or is even absent in samples with some local disorder.^{178,191} It was also shown that a distortion of the hexagonal symmetry of second- and higher-order neighbouring pores around a central pore is reflected by a broadening of the respective SAXS pattern.¹⁹¹

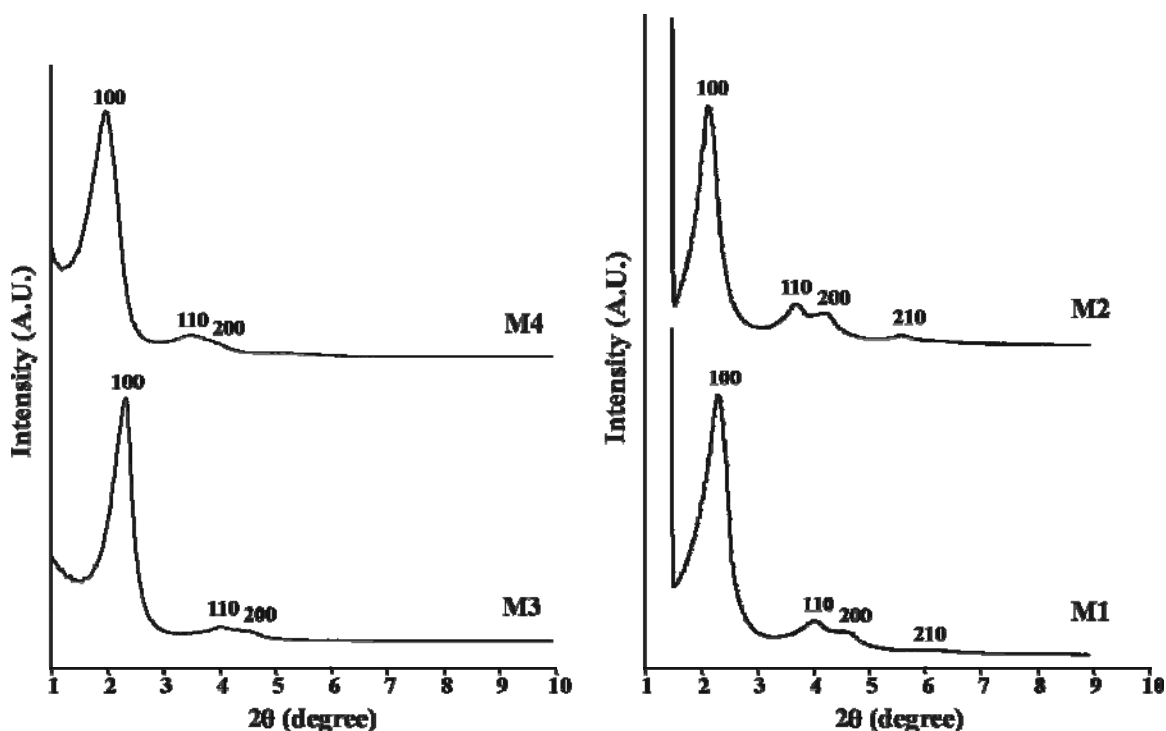


Figure 5.14. SAXS pattern of calcined and solvent extracted MCM-41 silica from ProntoSIL (left) and Kromasil (right).

In fact, for the present MCM-41 samples, **M3** and **M4**, made from ProntoSIL only broadened (100), (110) and (200) reflections are observed with some overlap of the latter two peaks, which implies some long-range distortion of the hexagonal mesopore arrangement.¹⁰ Nevertheless, the SAXS patterns clearly demonstrate that the samples prepared via the pseudomorphic route from the ProntoSIL source are of MCM-41 type. The SAXS patterns of the silica spheres from the Kromasil source (**M1**, **M2**), are shown to the right of Figure 5.14. The (100), (110), (200) and (210) reflections are distinctly narrower than those for the samples obtained from the ProntoSIL source, implying the formation of well-ordered MCM-41 silica spheres with hexagonal pore arrangement.

The shift of the reflection maxima towards higher 2θ values for the calcined MCM-41 samples reflects the fact that the hexagonal pore structure experiences some shrinkage during the calcination process, as also reported earlier for such materials.¹⁹⁶ This can be also seen from the unit-cell parameters, a_0 , calculated from the SAXS pattern, which are listed in Table 4.2.

The mesoporosity of the present samples is further examined by nitrogen sorption experiments. Nitrogen adsorption-desorption isotherms of the available non-grafted MCM-41 samples are shown in Figure 5.15 (left), while Figure 5.15 (right) provides the BJH pore size distribution plots. The textural properties of the ungrafted MCM-41 spheres are summarized in Table 4.2. It is found that all MCM-41 materials of the present study possess isotherms which belong to the reversible IV type.

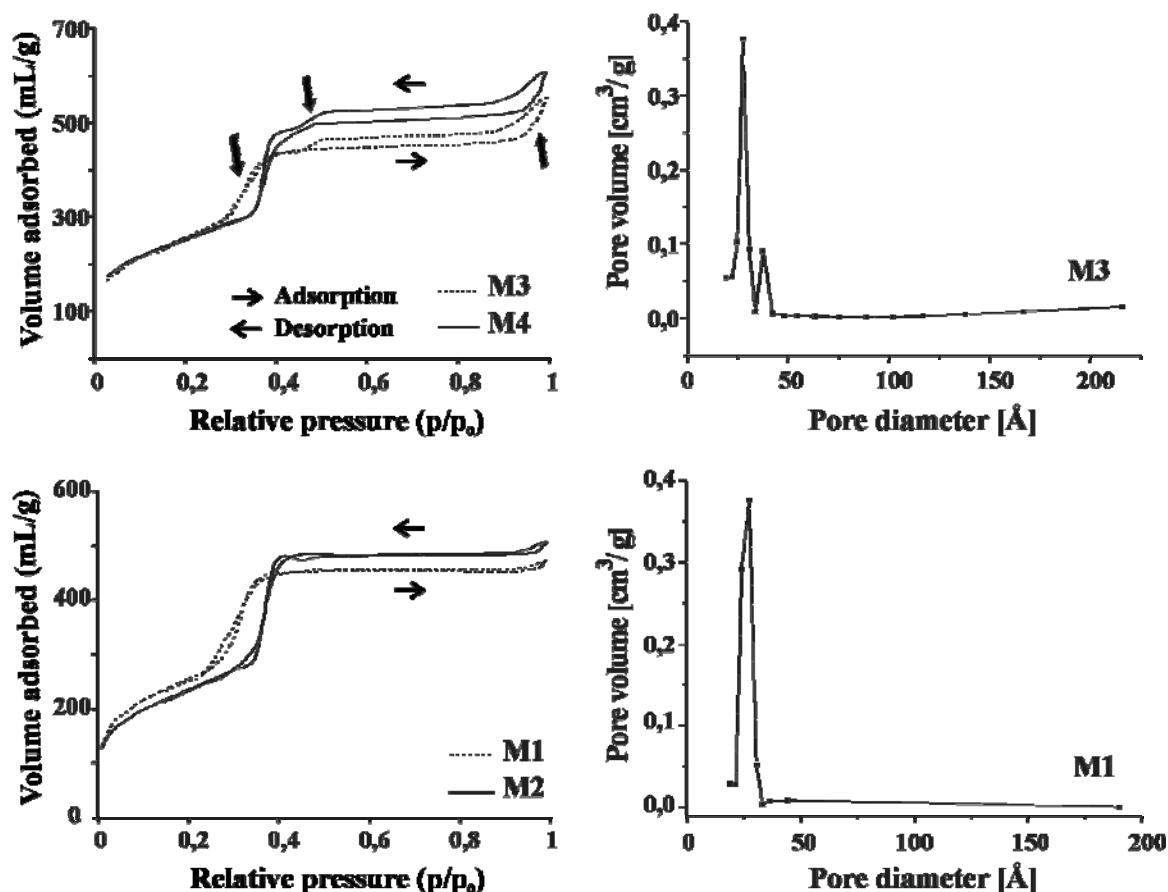


Figure 5.15. BET isotherms and BJH pore-size distribution plots of MCM-41 silica spheres from ProntoSIL (top) and Kromasil (bottom).

The strong rise of the BET curves around a relative pressure of $p/p^0 = 0.32$ and 0.38 for the calcined and solvent extracted samples stems from capillary condensation in the mesopores which is a typical feature of MCM-41 materials. In the sorption curves of the ungrafted MCM-41 samples from the ProntoSIL source, **M3** and **M4**, a hysteresis is found in the pressure range from $p/p^0 = 0.45$ to 1.0 . Similar observations were explained recently by the presence of a secondary mesoporosity where the larger mesopores are connected to the exterior of the particles by the structured porosity. Accordingly,

desorption occurs in these pores via a cavitation process.^{10,105} The respective BJH analysis provides for the calcined MCM-41 material primary mesopores with a diameter of 28 Å and secondary mesopores at a pore diameter of 38 Å, as shown by the BJH pore size distribution plot. Likewise, in the solvent extracted sample, **M4**, the primary and secondary mesopores possess pore diameters of 30 and 38 Å, respectively.

Moreover, parental silica pores of low amount are found to remain for the MCM-41 materials synthesized from the ProntoSIL source, as reflected by the pronounced rise in the isotherms above a relative pressure p/p^0 of 0.95.^{8,10,105} Due to their low fraction and the broad pore size distribution, the parental silica pores provided only a weak and broadened peak at about 236 Å in the respective pore size distribution plots (not shown in Figure 5.15). The MCM-41 samples, **M3** and **M4**, derived from ProntoSIL are thus characterized by a trimodal pore size distribution.

The nitrogen adsorption-desorption isotherms of the calcined and solvent extracted silica samples, **M1** and **M2**, obtained from the Kromasil source, are somewhat different, as they do not exhibit the aforementioned hysteresis between $p/p^0 = 0.45$ and 1.0 due to a secondary mesoporosity. The respective BJH pore size distribution plot in Figure 5.15 shows a single mesopore at a diameter of 28 Å for the calcined MCM-41, while for the solvent extracted sample (see Table 4.2) a pore diameter of 30 Å has been derived. In addition, it can be seen that the final rise in the isotherm at about $p/p^0 = 0.95$ is much less pronounced. The MCM-41 materials, obtained from the pseudomorphic transformation using the Kromasil source, therefore possess a uniform ordered porosity with an insignificant amount of secondary and parental mesopores, in agreement with the higher degree of mesopore order discussed above in connection with the SAXS data.

It should be noted that the given pore diameters are based on the BJH method which underestimates the pore diameter up to about 25 % for pores smaller than 100 Å.¹⁷⁷⁻¹⁷⁹ The real pore diameters are therefore about 7 to 9 Å larger than those given in Table 4.2. After this correction the pore diameters are very close to the values reported from other studies on the pseudomorphic preparation of MCM-41 spheres.^{8,141} Likewise, the wall thicknesses, calculated from the unit cell-parameter, a_0 , and the corrected D_{pore} values, are in agreement with other published data for such MCM-41 silica materials.^{9,105}

As shown above, the presence of a secondary mesoporosity depends on the actual silica source used during the pseudomorphic transformation, despite otherwise identical reaction conditions. Likewise, it was found that the pore volume of the parent silica also plays an important role.⁹ From a recent investigation it was concluded that prolonged reaction times are a good way to achieve MCM-41 silica spheres with uniform porosity. The optimum conditions (duration, temperature, etc.) for complete pseudomorphic transformation, however, were also found to strongly depend on the silica source.¹⁰⁵ Multimodal pore size distributions are of great interest for materials used in separation science since they significantly enhance mass transfer of the products to adsorption sites.¹⁹⁷

5.3.2 Preparation of Grafted MCM-41 Silica and Characterization

After removing the surfactant by calcination or solvent extraction, the MCM-41 spheres were surface modified by reaction with *n*-octadecyltrihydridosilane or *n*-octadecyltrimethoxysilane through direct grafting or surface polymerization (via humidification), as listed in Table 4.3. As already mentioned for the ungrafted MCM-41 samples, obtained from solvent extraction, ethoxy groups are bound to the surface silanol groups. This finite carbon content was taken into account for the calculation of the respective surface coverages.

Variation of the grafting conditions generally results in different degrees of surface coverage along with changes of the surface hydrophobicity, which is an important parameter for the selectivity in reversed-phase chromatographic separations and in catalysis. Surface modification of mesoporous silica materials is of particular interest, since – as demonstrated recently – grafted mesoporous silica spheres possess substantially improved mechanical stability.¹⁴¹ A higher surface coverage in general implies that the assemblies exhibit a better chain packing due to stronger van der Waals interactions as well as better thermal and chemical stability.¹⁹⁰

Materials **M1H** and **M2H** were synthesized by using *n*-octadecyltrihydridosilane as silylating agent. Surface modification using *n*-octadecyltrihydridosilane is advantageous over other silane coupling agents since it provides a cleaner reaction medium in which water or hydrogen are by-products. C₁₈ chains were grafted directly on the calcined

MCM-41 silica (sample **M1H**) or by the humidification of the calcined MCM-41 silica and subsequent grafting with *n*-octadecyltrihydrosilane (sample **M2H**). The achieved surface coverage of sample **M1H** was found to be higher than for sample **M2H** (see Table 5.4).

Table 5.4. Textural features of octadecyl grafted MCM-41 silica spheres.

Sample	a_0 (Å)	S_{BET} (m ² /g)	V_{tp} (mL/g)	D_{pore} (Å)	Wt. % C	Surface coverage (μmol/m ²)
M1H	49	621	0.52	25	7.84	0.40
M2H	49	592	0.44	27	9.77	0.52
M3M	49	527	0.34	22;35 ^a	13.78	0.78
M4M	49	343	0.23	24	15.83	0.94
M5M	54	412	0.39	23;38 ^a	14.27	0.79
M6M	54	240	0.17	24	23.86	1.65

a_0 : unit-cell parameter; S_{BET} : BET surface area; V_{tp} : total pore volume; D_{pore} : pore diameter

^a Primary and secondary mesopores (see text)

n-Octadecyltrimethoxysilane was used to prepare the samples **M3M**, **M4M**, **M5M** and **M6M**. Sample **M3M** was prepared by grafting the C₁₈ chains directly, and **M4M** was prepared by surface polymerization, i. e. humidification of the calcined MCM-41 silica spheres. The latter sample showed again higher surface coverage. The same holds for samples **M5M** and **M6M** which were prepared by grafting the C₁₈ chains directly and after humidification of the solvent extracted MCM-41 silica spheres, respectively.

Surface modification of the MCM-41 particles with *n*-octadecyltrimethoxysilane generally yields a higher surface coverage than by grafting with *n*-octadecyltrihydrosilane which is a consequence of the higher reactivity of the methoxy groups in the former silane. This difference in reactivity is confirmed by the ²⁹Si NMR spectra, further discussed below, which after grafting with *n*-octadecyltrihydrosilane exhibit T_H signals with intact Si-H bonds, while after reaction with *n*-octadecyltrimethoxysilane only Si-OH bonds apart from Si-OSi bonds remain. The main drawback of the reaction with *n*-octadecyltrimethoxysilane is the production of alcohol as byproduct which may adsorb or react with the substrate to form methoxy-derivatized surfaces (see also discussion of ¹³C NMR data).¹⁹⁵

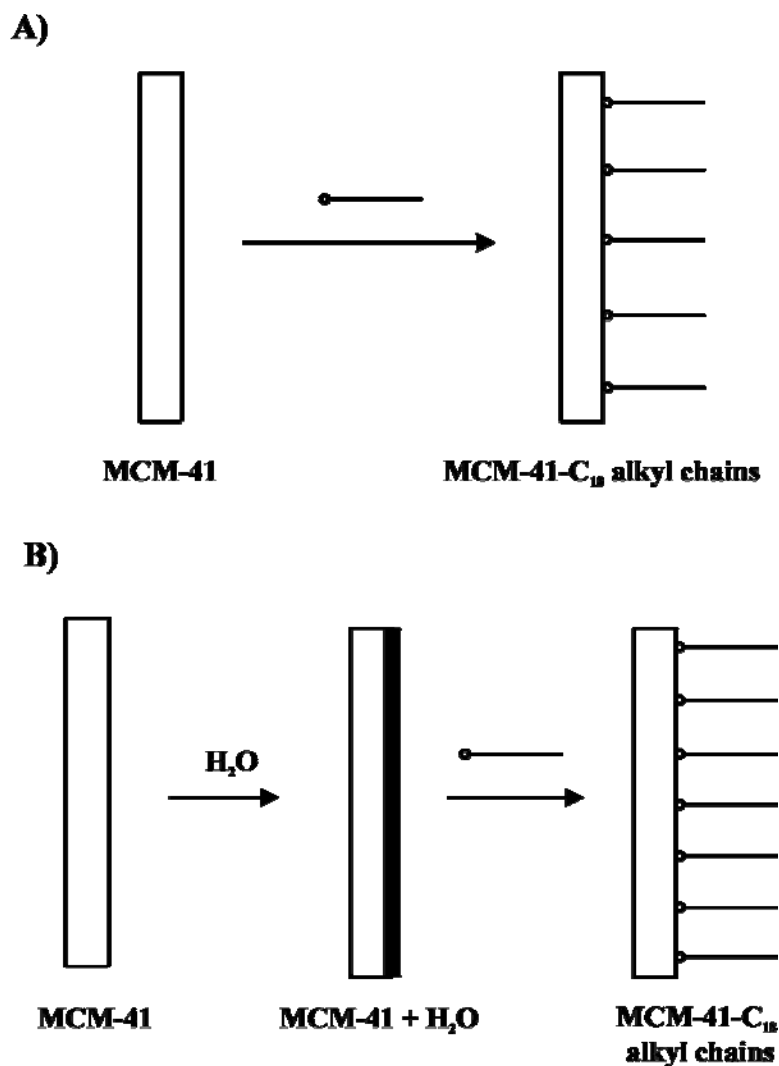


Figure 5.16. Schematic representation of direct grafting (A) and the surface polymerization approach (B). Please note that cross-linking of the silane molecules is not indicated.

Silica grafting employing the surface polymerization approach is known to result in higher grafting densities,²² since the adsorbed surface water promotes enhanced binding to the surface and induces cross-linking through polymerization of neighbouring molecules (see Figure 5.16). In the case of direct grafting, the grafting density depends only on the available surface silanol groups resulting in a lower surface coverage than via the surface polymerization method. Our results for the grafted MCM-41 spheres are in full agreement with these earlier observations, and the highest surface coverage was thus achieved for the samples made via surface polymerization (samples **M2H**, **M4M**, **M5M** and **M6M**, see Table 5.4).

For the present samples the achieved surface coverage is lower when compared to conventional grafted silica gels.¹⁹⁸ This is a consequence of the lesser amount of surface silanol groups especially for the calcined MCM-41 materials, and also of the relatively small diameter of the mesopores which create difficulties in coating the interior of the mesopores. In addition, some kind of pore blocking at the entrance of the mesopores by the relatively long C₁₈ chains may occur which prevents other chains to diffuse inside the pores. This may furthermore lead to cross-linking of alkyl chains at the entrance of the mesopores along with a high local grafting density. This assumption would also explain the observation of a high alkyl chain ordering (see discussion of ¹³C NMR and IR data) despite the relatively low overall surface coverage of the present samples.

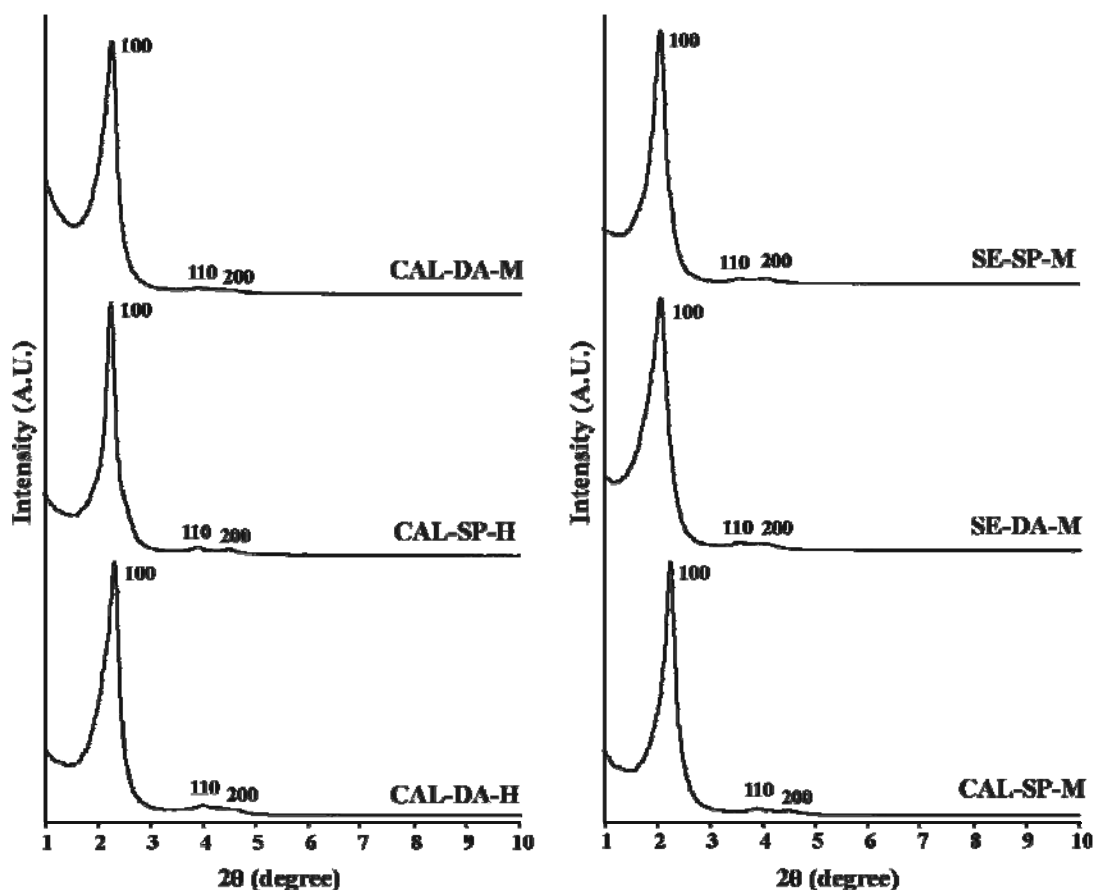


Figure 5.17. SAXS pattern of C₁₈ grafted MCM-41 silica spheres.

The SEM pictures given in Figure 5.13 for the samples after surface grafting clearly demonstrate that the spherical morphology, the particle size and size distribution are maintained. The SAXS pattern of the C₁₈ grafted MCM-41 silica spheres are shown in Figure 5.17. Three Bragg reflections, (100), (110) and (200), can be identified, where the

latter two are broadened when compared to the ungrafted materials. Moreover, the (210) reflection, which was clearly visible in the ungrafted material, is missing. Both findings are in complete agreement with other reports on grafting of mesoporous silica,¹⁹² and can be related to some distortion of the periodicity upon surface coverage with the alkyl chains. However, the peak positions along with the unit cell parameters are not altered (see Tables 4.2 and 5.4). It proves that the framework ordering of the mesopores remains intact upon grafting with C₁₈ chains, in agreement with the observations for other surface modified MCM-41 materials.^{10,199}

The general appearance of the nitrogen isotherms of the grafted MCM-41 samples (see Figure 5.18) remains the same as described earlier for the ungrafted materials. It demonstrates that the mesoporous structure is preserved upon surface grafting. The main difference is the lowering of the plateau values for all grafted samples which correlates with the surface coverage, in agreement with former observations for both spherical and non-spherical MCM-41 materials.^{8,141,173} Accordingly, surface grafting results in a pronounced reduction of the surface area and the total pore volume, as can be deduced from the values listed in Tables 4.2 and 5.4.

After surface grafting of the MCM-41 spheres, the first bend in the isotherm is somewhat shifted towards lower pressure which reflects a slight reduction in pore diameter (see Table 5.4). Moreover, below $p/p^0 \sim 0.3$ a low-pressure hysteresis is observed for all grafted samples, i.e. the desorption curve lies above the adsorption curve. Earlier studies on alkyl grafted samples revealed a similar hysteresis behaviour which has been attributed to the interactions between the nitrogen molecules and the conformationally disordered aliphatic chains as well as to some pore blocking effect due to grafting with the long C₁₈ chains.^{8,10,141} In addition, the desorption curve for sample **M6M** lies somewhat above the adsorption curve over the whole pressure range, which so far cannot be explained satisfactorily.

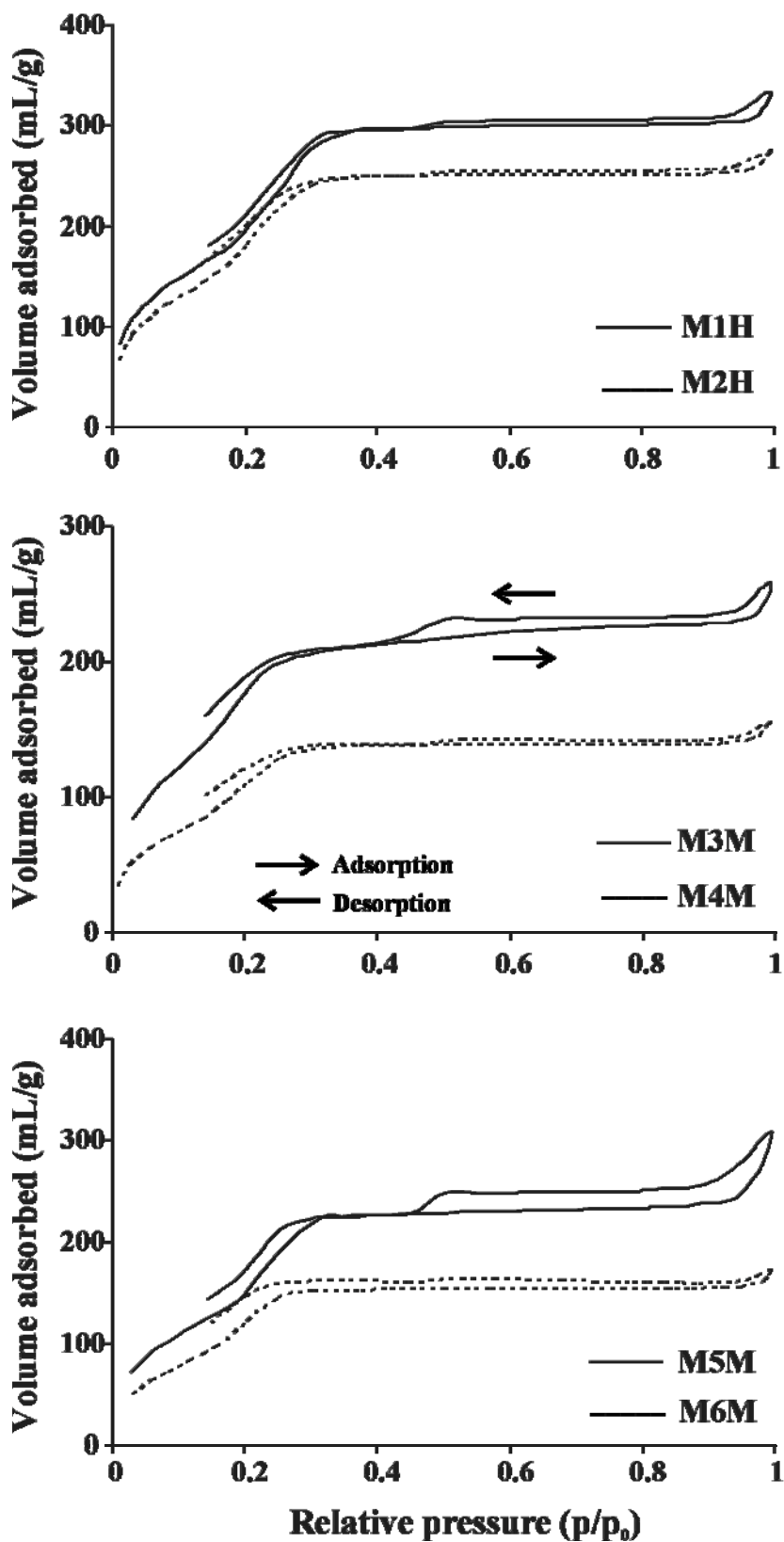


Figure 5.18. BET isotherms of C_{18} grafted MCM-41 silica spheres prepared using *n*-octadecyltrihydrosilane (top), and *n*-octadecyltrimethoxysilane (middle and bottom).

Grafting of the present mesoporous silica with C₁₈ chains is different from the situation in former studies where shorter alkyl chains have been used.^{173,194} Since the C₁₈ ligand possesses a cross-sectional area and a length for the all-trans conformation of about 20 Å² and 23 Å, respectively, it cannot easily diffuse deeply into the mesopores with 38 Å in diameter (corrected pore diameter, see former discussion). Rather, the octadecyl chains are mainly grafted near the entrance of the primary mesopores. In the case of the MCM-41 materials, obtained with the ProntoSIL silica source, the alkyl chains most probably are also grafted into the larger mesopores (from parent silica) and into the secondary mesopores.

Detailed studies about alkyl chain grafting on MCM-41 and FSM-type mesoporous supports with 50 and 36 Å pore size were published only recently.^{173,194} They showed that the pore diameter reduces gradually with increase in alkyl chain length from C₃ to C₈. Surprisingly, in the present study the derived pore sizes are only slightly reduced after surface grafting (see also above remarks on “corrected” pore diameters in connection with discussion of the nitrogen isotherms for the ungrafted materials). At the same time, a pronounced reduction of the surface area and the total pore volume is observed, as already mentioned above (see Tables 4.2 and 5.4).

The different behaviour for the surface area and the total pore volume on the one side and the pore diameter on the other side is surprising, but is a general observation for MCM-41 samples grafted with longer alkyl chains.^{10,194} One explanation might be given by the low surface coverage and the weak interactions between the alkyl chains and the nitrogen molecules. That is, at small p/p^0 values nitrogen adsorption is practically unaffected by the low alkyl chain concentration on the surface, and the nitrogen molecules primarily interact with the silica surface. This process might be further promoted by the alkyl chain mobility and conformational disorder. As a consequence, the first slope of the adsorption curves for the grafted samples almost follows that of the ungrafted samples. However, a much more detailed study of the nitrogen sorption behaviour for these materials would be necessary to get a definite and satisfactory explanation of all experimental results from the nitrogen sorption experiments.

5.3.3 ^{29}Si MAS NMR Spectroscopy

^{29}Si NMR spectroscopy is a suitable technique for the examination of the surface species, grafting and degree of cross-linking of the alkyl silanes. ^{29}Si CP/MAS NMR spectra of the grafted MCM-41 silica spheres are shown in Figures 5.19 and 5.20. For comparison, the spectrum of the calcined MCM-41 material is also given. The ^{29}Si chemical shifts of the various species are reported in Table 5.5. It should be emphasized that a quantitative analysis of these spectra is not possible, since the spectra were recorded with cross-polarization for signal-to-noise ratio enhancement and reduction of the total experimental time. Cross polarization, however, alters the signal intensities, and they can therefore not be used to derive the amount of the underlying molecular species. Nevertheless, ^{29}Si CP/MAS spectra can be discussed on a qualitative basis, for instance, for a comparison of the spectral alterations in samples of similar constitution.

Table 5.5. ^{29}Si chemical shifts for octadecyl grafted MCM-41 silica.

Sample	^{29}Si chemical shift (ppm)					
	Q^4	Q^3	Q^2	T_H^3	T_H^2	T_H^1
M1H	-108.1	-100.8	-91.5	-53.2	-30.5	-16.2
M2H	-108.0	-100.2	-91.5	-53.5	-30.8	-17.0
	Q^4	Q^3	Q^2	T^3	T^2	T^1
M3M	-108.0	-100.5	-92.1	-65.3	-55.1	-47.2
M4M	-108.8	-100.6	-91.8	-	-54.5	-46.9
M5M	-109.8	-100.6	-90.1	-	-54.3	-47.6
M6M	-110.0	-100.7	-90.7	-64.5	-54.1	-46.1

As a general trend one finds that surface modification with C_{18} chains is accompanied by a lowering of the intensities for the Q^2 and Q^3 units relative to the intensity of the Q^4 units (also when compared to the calcined samples), since the former ones are used for alkyl chain attachment.^{26,152} At the same time, T_H^n and T^n units are formed, depending whether octadecyltrihydrosilane or octadecyltrimethoxysilane is employed during the grafting process.

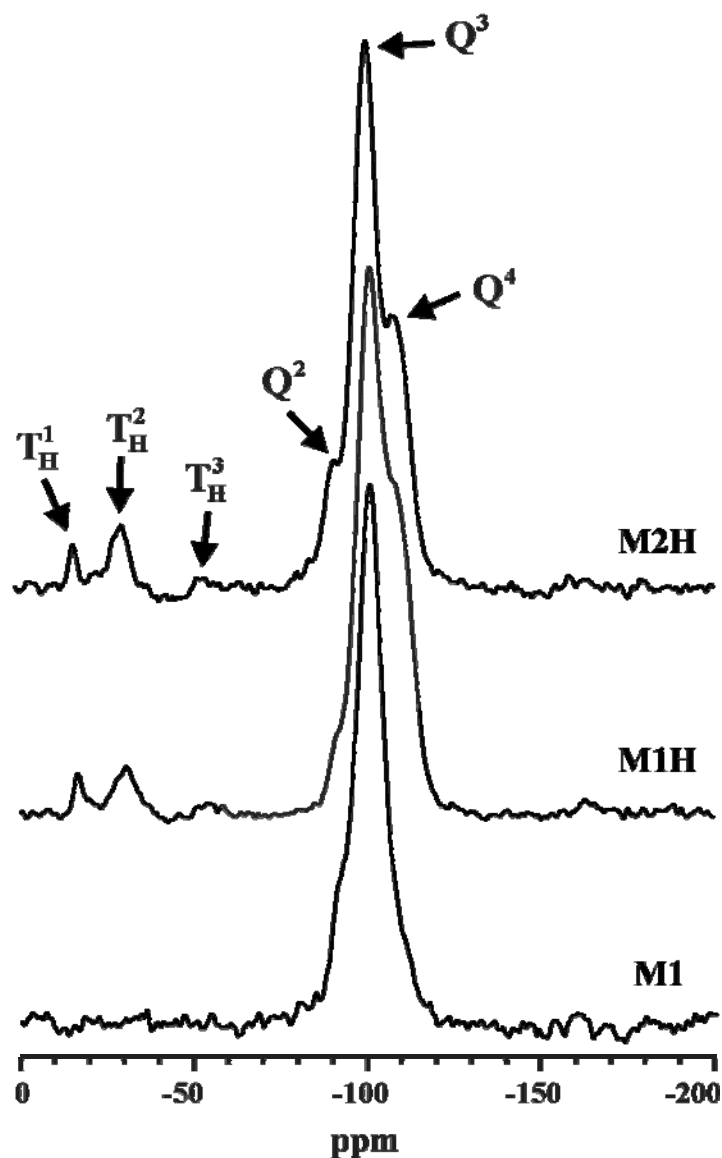


Figure 5.19. ^{29}Si NMR spectra of the ungrafted (**M1**) and grafted MCM-41 silica spheres with *n*-octadecyltrihydrosilane.

^{29}Si NMR spectra of the samples grafted with octadecyltrihydrosilane (samples **M1H** and **M2H**) are given in Figure 5.19. Here, $T_{\text{H}}^1, T_{\text{H}}^2$ signals for partial and T_{H}^3 units for complete cross-linking (with $T_{\text{H}}^n = (\text{OSi})_n(\text{H})_{3-n}$, $n = 1, 2, 3$) at -17, -30 ppm and -53 ppm, respectively,²⁰⁰ can be separated. The T_{H}^2 signal exhibits the highest relative intensity in both samples. The presence of T_{H}^1 and T_{H}^2 signals reflects incomplete hydrolysis of the hydrido groups, in agreement with the ^{13}C NMR data, discussed below. Moreover, the relative intensity of the T_{H}^n resonances follows the order $T_{\text{H}}^2 > T_{\text{H}}^1 > T_{\text{H}}^3$ which indicates only partial cross-linking of the grafted C_{18} chains. It is seen that the relative overall

intensity of the T_H^n signals correlates with the amount of surface coverage, i.e. a higher surface coverage is accompanied by a higher overall intensity for the T_H^n resonances.

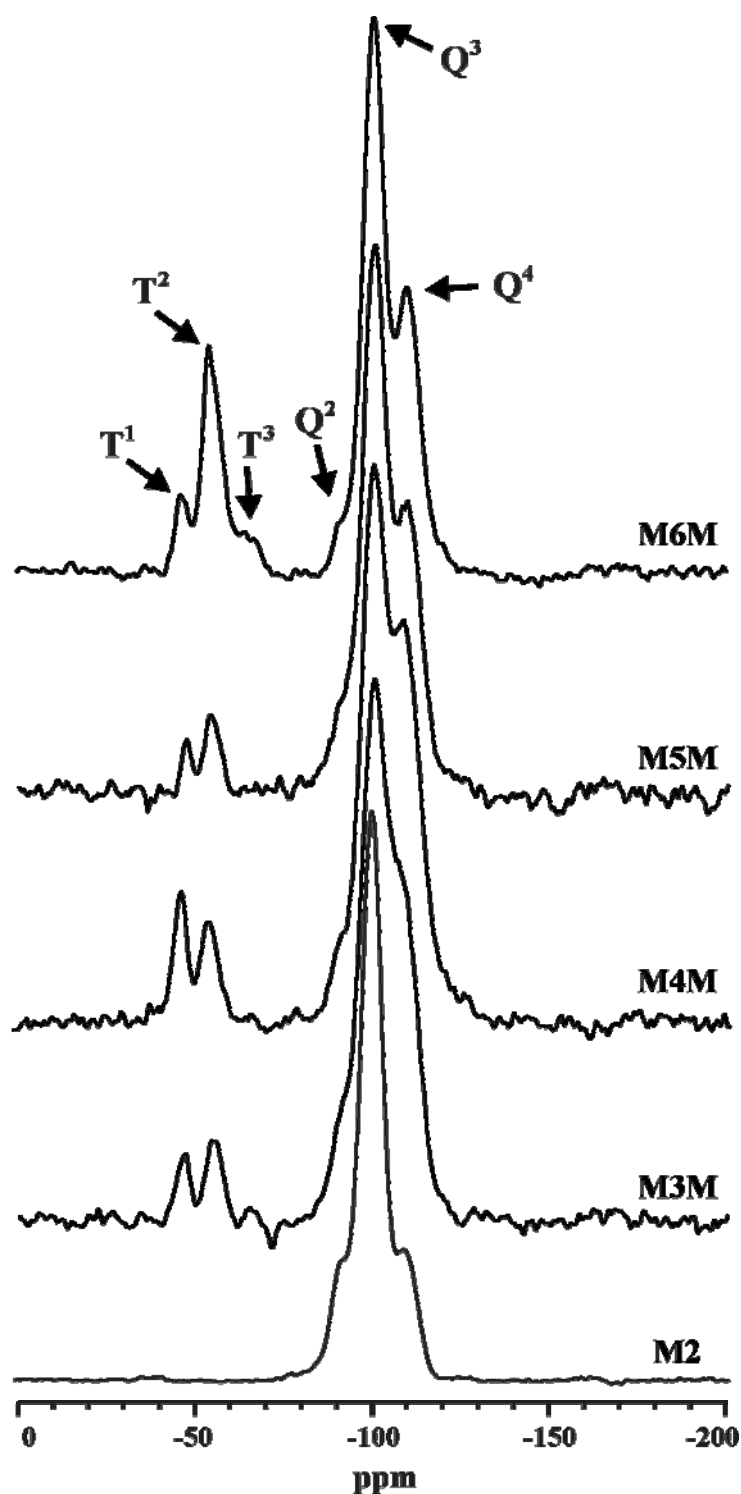


Figure 5.20. ^{29}Si NMR spectra of the ungrafted (M2) and grafted MCM-41 silica spheres with *n*-octadecyltrimethoxysilane.

The ^{29}Si CP/MAS NMR spectra of *n*-octadecyltrimethoxysilane grafted MCM-41 materials, given in Figure 5.20, show the same general features.⁵¹ The main difference is that now T^n instead of T_H^n signals are involved, as listed in Table 5.5. As before, the intensities of the T^1 and T^2 signals are higher than the intensity of the T^3 group signal which reflects incomplete cross-linking, and the overall intensity of the T^n group signals correlates with the surface coverage.

Larger amounts of Q^2 and Q^3 units and a lesser amount of Q^4 groups are present in the samples derived from the solvent extracted MCM-41 materials (samples **M5M** and **M6M**). These findings can be attributed to a higher surface silanol group concentration as compared to the calcined materials. This effect is even more pronounced in the sample grafted via surface polymerization (sample **M6M**) which can be traced back to the increase of surface hydroxyl groups as a consequence of the humidification prior to surface grafting.

5.3.4 ^{13}C MAS NMR Spectroscopy

^{13}C NMR spectroscopy was used to study the conformational order of the grafted alkyl chains and to acquire more information regarding the alkyl attachment. Figure 5.21 depicts ^{13}C CP/MAS NMR spectra of the MCM-41 samples grafted with *n*-octadecyltrihydrosilane (samples **M1H** and **M2H**). The ^{13}C chemical shift values are reported in Table 5.6. The peak at about 23 ppm can be attributed to carbons C-2 and C-17 of the octadecyl chains. The signal at 32.5 ppm arises from carbons C-3 and C-16. Carbons C-4 to C-15 resonate at around 30 ppm which points to a low conformational order of the alkyl chains in these samples.^{52,167}

The ^{13}C resonances of carbons C-1 and C-18 typically appear around 13-14 ppm.^{26,167} For samples **M1H** and **M2H** a signal at 13 ppm and a broad spectral component between 13 and 16.5 ppm can be distinguished. The former signal can be attributed to carbon C-18. The broad component is attributed to carbon C-1 which reflects a mixed bonding situation near this carbon position. That is, in agreement with the former discussion of the ^{29}Si NMR data, for these samples both partially and complete cross-linking occurs, each of which slightly changes the ^{13}C resonance position for carbon C-1.

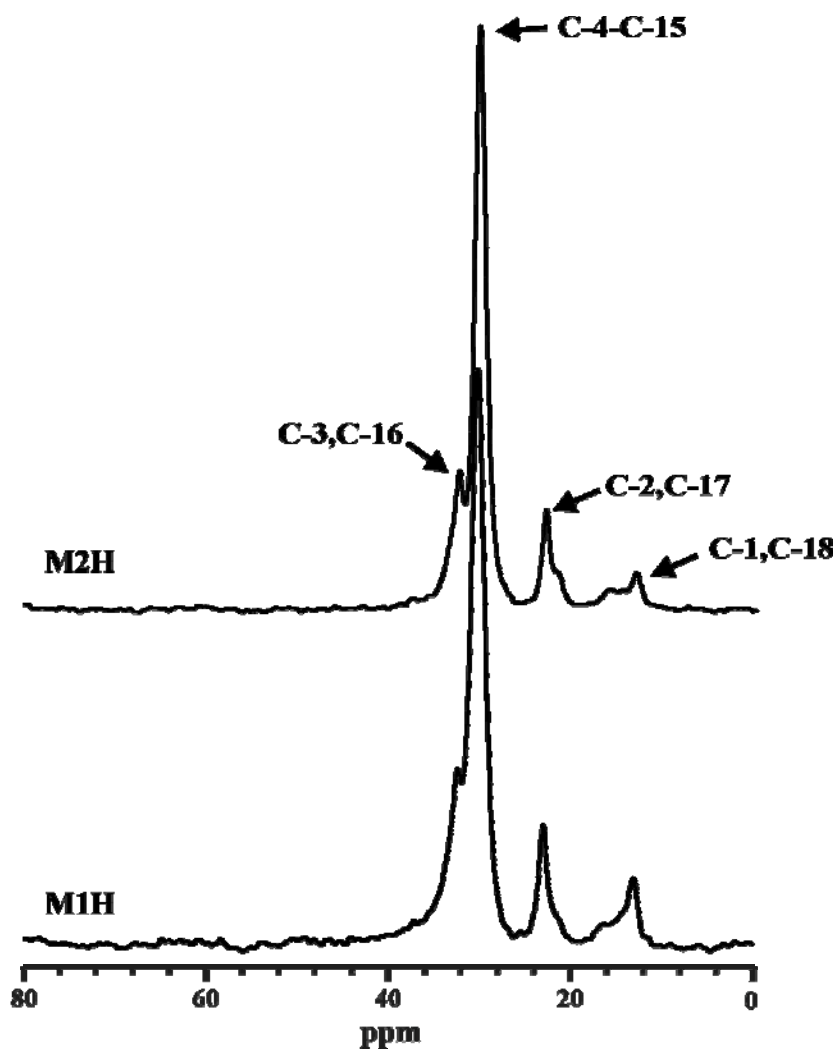


Figure 5.21. ^{13}C NMR spectra of MCM-41 silica spheres grafted with *n*-octadecyltrihydrosilane.

Table 5.6. ^{13}C chemical shifts for octadecyl grafted MCM-41 silica.

Sample	^{13}C chemical shift (ppm)				
	C-4 – C-15	C-3 & C-16	C-2 & C-17	C-1 & C-18	OCH ₃
M1H	30.1	32.4	23.0	13.0	
M2H	30.2	32.4	22.9	13.0	
M3M	30.3	32.5	23.0	13.2	50.8
M4M	30.4	32.6	23.1	13.3	50.6
M5M ^a	30.5	32.6	23.2	13.4	50.3
M6M ^a	30.5	33.2;32.5 ^b	23.2	13.4	-

^a Signals at 60 and 18 ppm for methylene and methyl groups of the attached ethoxy molecules (see text).

^b Signal at 32.5 ppm originate from C-4–C15 methylene units corresponding to trans conformer (see text).

The ^{13}C CP/MAS NMR spectra of the MCM-41 samples grafted with *n*-octadecyltrimethoxysilane is shown in Figure 5.22.

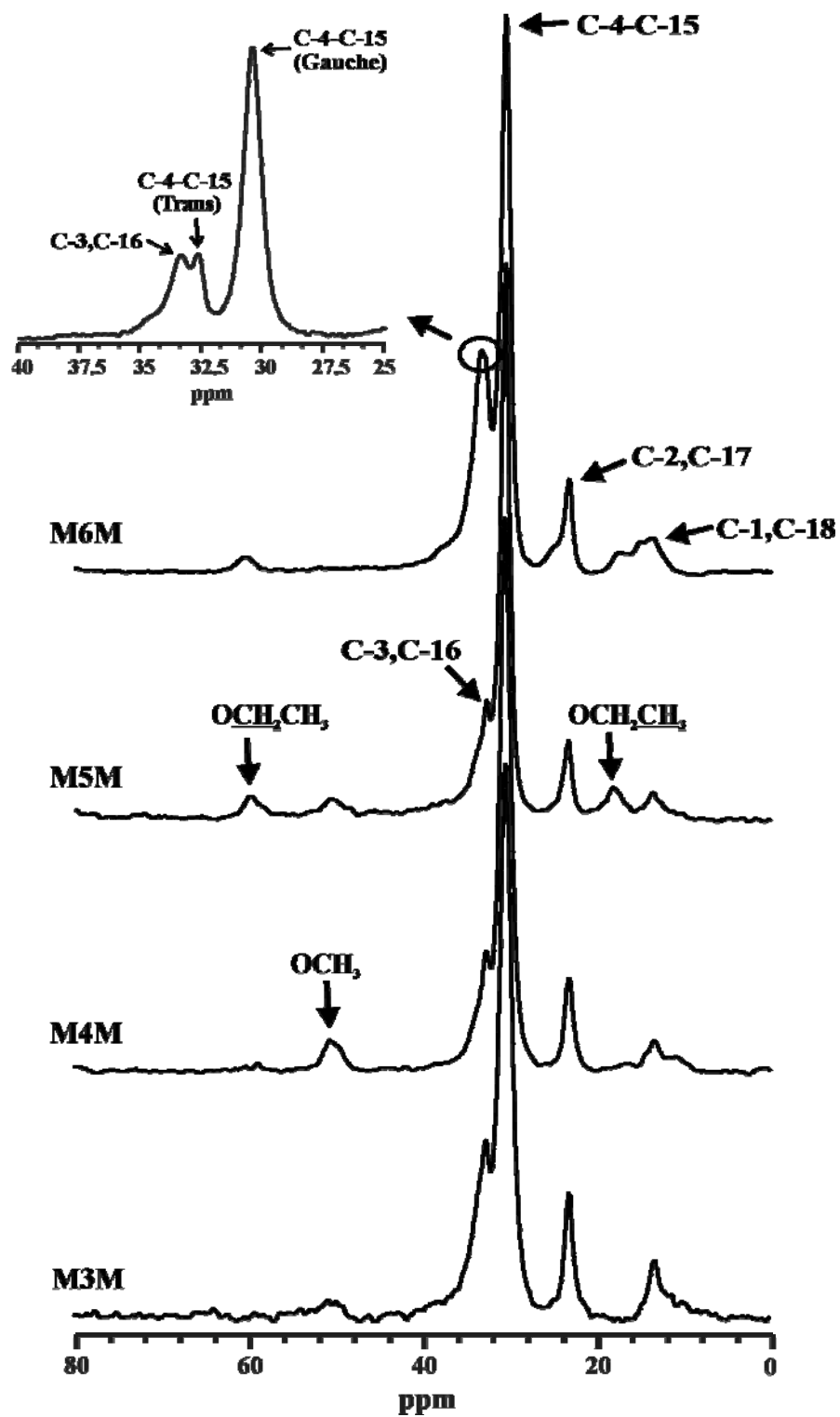


Figure 5.22. ^{13}C NMR spectra of MCM-41 silica spheres grafted with *n*-octadecyltrimethoxysilane.

In general very similar and the same signal positions can be distinguished that of MCM-41 silica spheres grafted with *n*-octadecyltrihydrosilane. In some samples an additional resonance at about 50 ppm can be observed which most probably stems from methoxy groups from the silylating agent, which are chemically bound to the surface silanol groups in a type of endcapping reaction.^{10,190} Another possibility are nonreacted methoxy groups in the attached silanes which, however, seem to be less likely.

For the samples **M5M** and **M6M**, derived from the solvent extracted MCM-41 materials, a ¹³C resonance at 60 ppm is registered which can be assigned to methylene groups of surface-bound ethoxy units originating from the solvent extraction process,⁶³ also visible in the aforementioned finite carbon amount of 2 wt % in the ungrafted material. Accordingly, in both samples an additional signal at 18 ppm (see Figure 5.21) can be identified and attributed to the methyl carbons of the ethoxy units.

Carbons C-4 to C-15 of the attached octadecyl chains are again visible by a resonance around 30 ppm reflecting alkyl chains in a conformationally disordered (*gauche*) state, while the ¹³C signal at around 33 ppm arises from carbons C-3 and C-16. For sample **M6M**, with the highest surface coverage, the signal around splits up into two resonances at 32.5 and 33.2 ppm. The latter signal stems from the C-3 and C-16 signals, while the former one has been attributed to carbons C-4 to C-15 in a more ordered *trans* conformational state (high conformational order, higher rigidity).^{22,51,167} Hence, sample SE-SP-M with the highest surface coverage must possess regions with alkyl chains that are closely packed and well ordered. For all other samples with lower surface coverage only loosely packed alkyl chains occur along with alkyl chains with low conformational order. Similar correlations between the alkyl chain conformational disorder and the surface coverage were reported, for instance, for C₁₈ chains grafted on normal silica supports.^{63,167}

The discussed differences in surface coverage and alkyl chain conformational order are directly related to the employed method for surface modification and the nature of the MCM-41 material. The trifunctional silanes employed in this work may cross-link (depending on the water content on the surface) to yield a higher density for the attached chains along with higher conformational order when compared to mono- and difunctional silanes. Likewise, the calcined MCM-41 samples possess a lower concentration of surface

silanol groups, and the grafting efficiency is thus lower, resulting in disordered alkyl chains. For solvent extracted MCM-41 supports, the silanol group density is higher, and surface grafting is much easier which provides denser packed and higher ordered chains. When surface polymerization is applied,^{50,143} a monolayer of water is formed on the surface leading to a higher degree of grafting, increase of chain cross-linking, denser packed chains along with higher alkyl chain conformational order, as found in the ¹³C NMR experiments as well as by the FTIR investigations, as will be discussed next.

5.3.5 FTIR Spectroscopy

For the examination of the conformational properties of grafted alkyl chains several conformation-sensitive vibrational bands can be exploited.^{76,201,202} Among these, the symmetric (2853-2846 cm⁻¹) and antisymmetric CH₂ stretching bands (2926-2915 cm⁻¹) are the most intense signals and in the majority of cases are easily accessible (refer sub-chapter 3.1.1). Their positions directly provide qualitative information about the conformational order in the aliphatic chains.¹⁵⁴

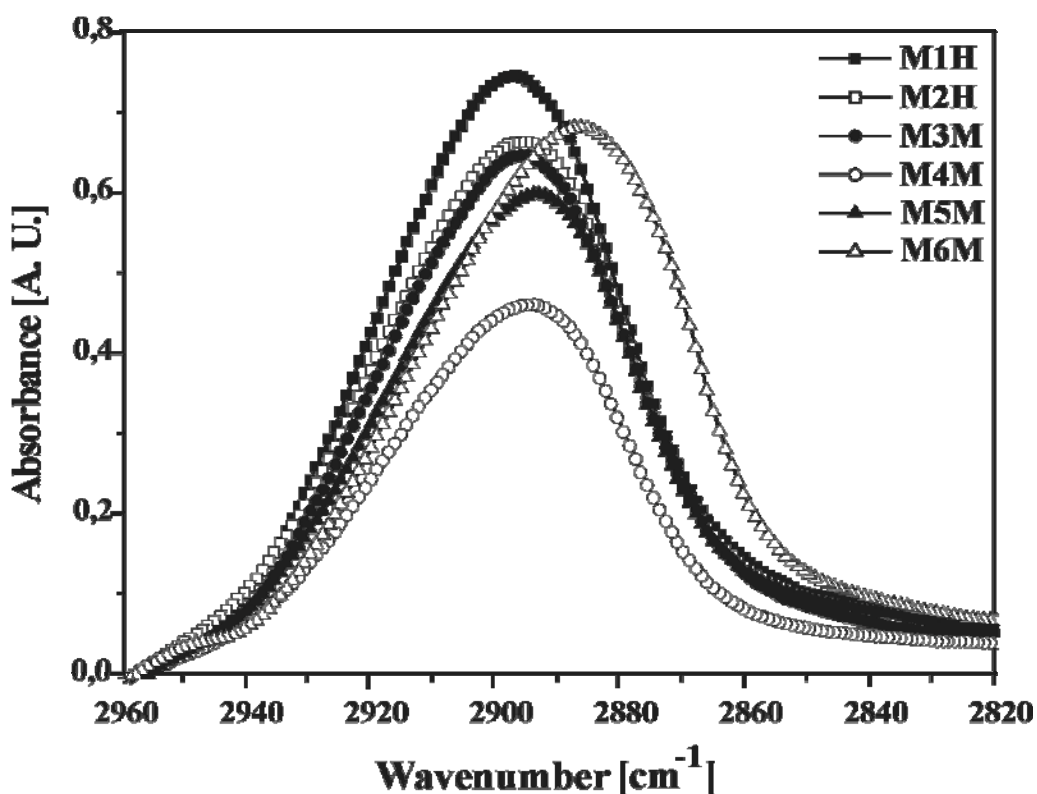


Figure 5.23. Antisymmetric CH₂ stretching bands of MCM-41 silica spheres at 293 K, grafted with *n*-octadecyltrihydrosilane and *n*-octadecyltrimethoxysilane.

The variation of the antisymmetric CH₂ stretching band positions of the C₁₈ alkyl chains grafted on the MCM-41 silica spheres for the various samples of this work is shown in Figure 5.23. A closer inspection shows that the CH₂ stretching band positions are shifted towards lower wavenumbers upon increase of the surface coverage, pointing to higher conformational order in agreement with the aforementioned ¹³C NMR data. The highest conformational order is found for the samples grafted via surface polymerization, which also exhibit the highest surface coverages. In general, the band positions are found to lie at higher wavenumbers than those reported for grafted normal silica gels,^{26,63} which is attributed to the lower surface coverage of the present samples.

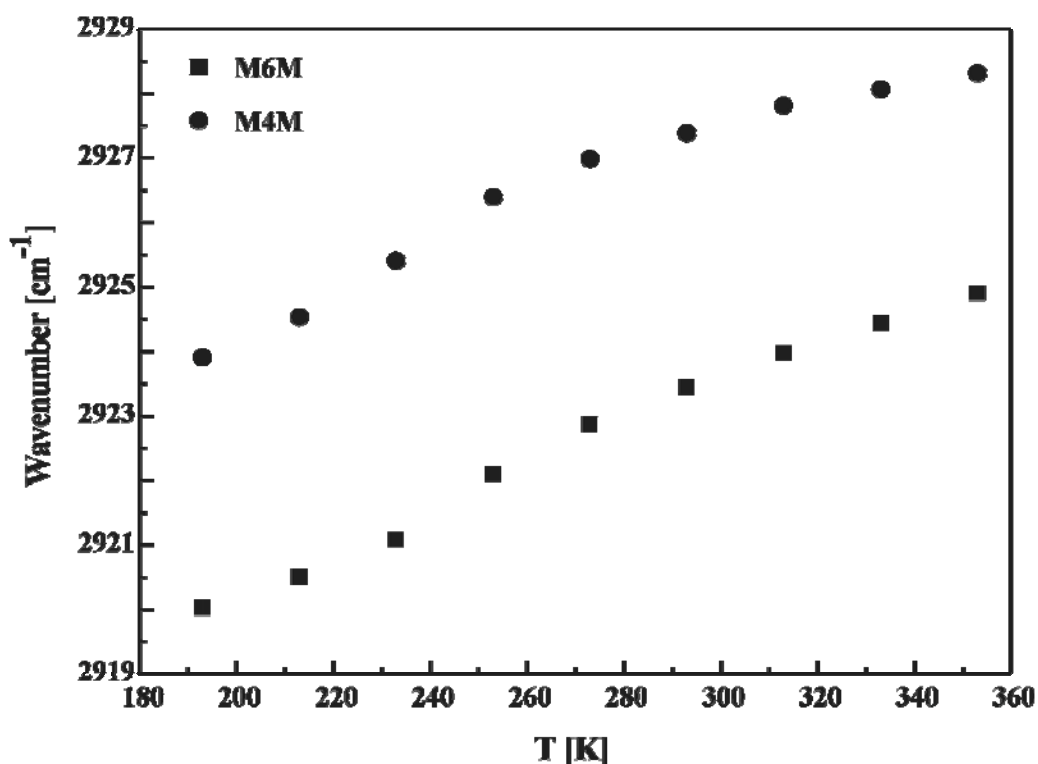


Figure 5.24. Temperature dependence of the antisymmetric CH₂ stretching band positions for samples M4M and M6M.

Variable temperature IR measurements between 193 and 353 K were carried out for samples M4M and M6M with the highest surface coverage. It is seen that the antisymmetric CH₂ stretching band positions, given in Figure 5.24, of both samples are shifted towards larger wavenumbers upon sample heating which reflects increasing conformational disorder. The overall variation with temperature is found to be almost identical for both samples. These results are in agreement with similar variable

temperature FTIR studies on other alkyl modified silica gels, where normal silica supports have been applied.^{26,63,65}

5.3.6 Summary

MCM-41 silica spheres were synthesized via the pseudomorphic route using two commercial silica sources (ProntoSIL and Kromasil). The resulting MCM-41 spheres were grafted with trifunctional octadecyl silanes from which materials with different surface coverages could be obtained. SAXS and nitrogen sorption isotherms of the ungrafted and grafted MCM-41 spheres, prepared from ProntoSIL silica, showed a trimodal pore size distribution, whereas the MCM-41 spheres from Kromasil silica are highly ordered with practically uniform mesopores.

C₁₈ alkyl chain grafting and chain cross-linking were examined by ²⁹Si and ¹³C NMR spectroscopy. FTIR and ¹³C NMR measurements revealed that the alkyl chains grafted by using *n*-octadecyltrimethoxysilanes are conformationally more ordered when compared to the materials obtained from modification with *n*-octadecyltrihydrosilanes, which correlates with the higher surface coverage of the former ones. The combination of solvent extraction for the MCM-41 preparation and surface polymerization for surface modification is found to result in higher surface coverage along with a higher degree of conformational order of the alkyl chains. Nevertheless, for the present samples only a relatively low surface coverage and low conformational order of the attached alkyl chains is achieved. These findings might be traced back to the relatively small diameter of the mesopores and pore blocking effects due to the usage of relatively long octadecyl chains.

5.4 Grafted Metal Oxides: Impact of Oxide Supports, Grafting of C₁₈ Silanes and Grafting Routes

In the present study, C₁₈ alkyl chains were attached to titania, zirconia, hafnia, and alumina using *n*-octadecyltrihydridosilanes and *n*-octadecyltrichlorosilanes. Throughout this work, the surface modified metal oxides are referred by their sample codes. Where Ti(H), Al(H), Hf(H), Zr(H) denote *n*-octadecyltrihydridosilanes grafted to respective oxides and Ti(Cl), Al(Cl), Hf(Cl), Zr(Cl) denote *n*-octadecyltrichlorosilanes grafted to respective oxides as in Table 4.5 (Ti-titania, Al-Alumina, Hf-Hafnia, and Zr-zirconia). These alkyl grafted metal oxides were characterized by several experimental techniques.

5.4.1 Properties of Metal Oxide Substrates

The relevant characteristics of the commercial metal oxide substrates used in the present work are summarized in Table 4.4. Nitrogen sorption studies were performed which provided the BET surface areas, pore volumes and micropore areas. It is seen that the surface areas, S_{BET}, of titania, zirconia and hafnia are significantly smaller than the typical surface area of silica which is in the order of 100-300 m²/g. The same holds for the total pore volume, V_{tp}, with values between 0.01 and 0.05 mL/g for the present metal oxide substrates which have to be compared with 0.6-1.0 mL/g for silica. Alumina is found to have values which lie between these limiting positions.

These data imply that the titania, zirconia and hafnia supports possess relatively flat and smooth surfaces, while silica – and to some extent also alumina – exhibit an uneven surface with large mesopores.

5.4.2 DRIFT Measurements for Determination of Surface Properties

The surface acidity of metal oxides depends on the cation radius, its charge and the local atomic arrangement. The acid-base properties of oxides are characterized by their “isoelectronic points” (IEP),¹⁸¹ as given in Table 4.4. The isoelectronic point is an indicator of the pH value for an ionic solid, at which there is no net surface charge in aqueous solution. Surfaces with high IEP values possess more basic character and surfaces with low IEP values show more acidic character. IEP values do not give the

absolute values for the basicity or acidity of the surface, but express their relative strengths.²⁰³

To ascertain the presence of Lewis and Brønsted acidic sites on the oxide surfaces, which might be responsible for the differences in surface loading (heterogeneity or homogeneity of coverage) and in turn for the alkyl chain conformational order, the interaction with pyridine was studied by means of DRIFT spectroscopy both on the untreated as well as grafted titania and hafnia.

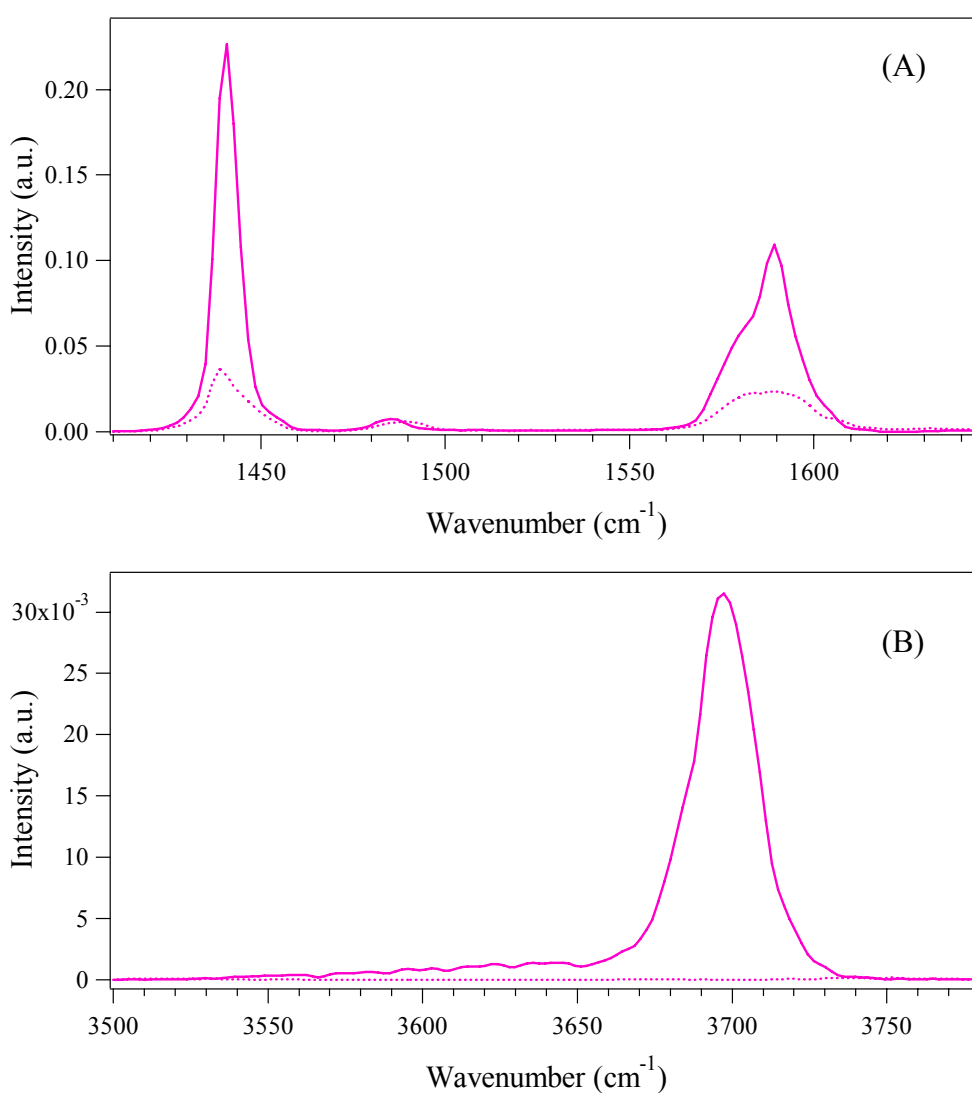


Figure 5.25. DRIFT spectra obtained after the exposure of bare TiO₂ (—) and Ti(Cl) (.....) particles to the pyridine+Ar mixture at RT. (A) Spectral region from 1410 to 1645 cm⁻¹; (B) Spectral region from 3500 to 3780 cm⁻¹.

DRIFT spectra, obtained after exposure of the samples TiO₂ and Ti(Cl) to a pyridine/argon mixture at room temperature, are shown in Figure 5.25. Table 5.7 summarizes the relevant ring stretching vibrational modes (8a, 8b, 19a and 19b) of liquid and adsorbed pyridine.²⁰⁴⁻²⁰⁶ The spectral region of the ring stretching modes mainly reveals the presence of liquid-like pyridine and pyridine H-bound to the surface hydroxyl groups. This is pointed out by the position and shape of the vibrational modes at 1441, 1485, 1579, and 1589 cm⁻¹. The comparison of the two spectra implies that the amount of pyridine interacting with surface hydroxyl groups is significantly higher for the ungrafted TiO₂ sample. A weak shoulder above 1600 cm⁻¹ may suggest the existence of weak Lewis acidic sites. The presence of a significant amount of Brønsted acidic sites is ruled out owing to the absence of spectral components at about 1537 and 1490 cm⁻¹ (see Table 5.7). The peak at 3697 cm⁻¹ for TiO₂ in Figure 5.25B points to pyridine molecules which interact with hydroxyl groups bound to titanium.^{207,208}

Table 5.7. FTIR data of vibrational bands (cm⁻¹) of liquid and adsorbed pyridine (vs = very strong; s = strong; m = medium; w = weak; v = variable) for comparison of the DRIFT measurements carried out in this study.²⁰⁴⁻²⁰⁶

	Liquid and/or physisorbed Py ²⁰⁴	H-bound Py ^{205,206}	Lewis-bound Py ^{205,206}	Brønsted-bound Py ^{205,206}
8a	1583 vs	1580-1600 s	1600-1633s	~1640
8b	1572 m		~1580 v	1608
19a	1482	1485-1490 w	1488-1503 v	1535-1540 s
19b	1432-1441	1440-1447 vs	1447-1460 v	1485-1500 vs

The DRIFT spectra, shown in Figure 5.26, were recorded after exposure of the TiO₂ and Ti(Cl) samples to a pyridine/argon mixture at room temperature, and successively to an argon stream for different periods of time. It is seen that for both samples the argon stream causes a strong decrease of the signal components due to liquid-like and H-bound pyridine along with fast desorption of these species, whereas the small signal component arising from pyridine interacting with Lewis acidic sites only slowly decreases. Similar data are available for the HfO₂ and Hf(Cl) samples (data not shown). Again, only a small signal contribution due to Lewis acidic sites was detectable (above 1600 cm⁻¹) which was even weaker than the aforementioned signal of the titania samples, given in Figure 5.25.

In summary, these data imply that Brønsted and Lewis sites are of minor importance for the present titania and hafnia samples.

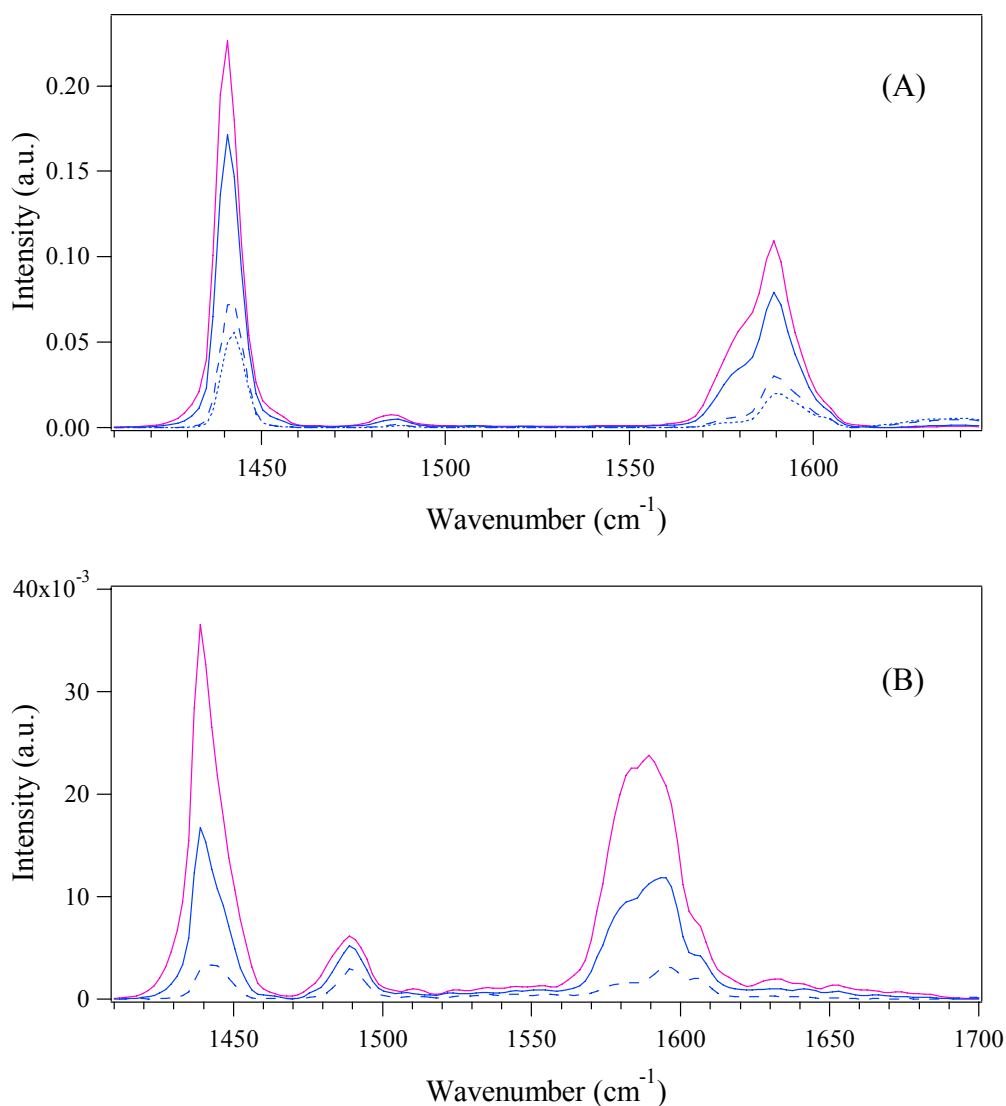


Figure 5.26. DRIFT spectra obtained at RT after exposure of the bare TiO₂ (A) and TiCl₄ (B) to pyridine+Ar mixture for 5 min (—) and successively to Ar for 1 min (—), 8 min (---) and 15 min, only for TiO₂ particles (.....). Spectral region from 1410 to 1700 cm⁻¹.

5.4.3 Cross-linking of Alkylsilanes by FTIR and SSNMR Spectroscopy

Figure 5.27 depicts FTIR spectra of *n*-octadecyltrihydrosilane and of C₁₈ modified hafnia from reaction with *n*-octadecyltrihydrosilane. Cross-linking of the alkylsilanes can be verified by the broad vibrational band at about 1070 to 1170 cm⁻¹ which reflects

the formation of Si-O bonds.¹³⁹ For the C₁₈ alkyl modified samples IR bands around 2150 cm⁻¹ are absent, indicating the complete hydrolysis of the Si-H groups to form Si-O bonds, i. e. Si-OH, Si-O-Si and Si-O-M units (M = metal). In pure liquid *n*-octadecyltrihydrosilane, the antisymmetric and symmetric CH₂ stretching band positions occur at 2923.5 and 2853.1 cm⁻¹, respectively. After attachment of the alkyl chains on the metal oxide surface these signals are shifted to 2921.4 and 2850.7 cm⁻¹ which are close to the positions reported for crystalline alkanes in the all-trans conformational state.¹⁵⁴ This confirms that after grafting on the metal oxide surface, the alkyl chains possess a higher conformational order than in liquid *n*-octadecyltrihydrosilane.

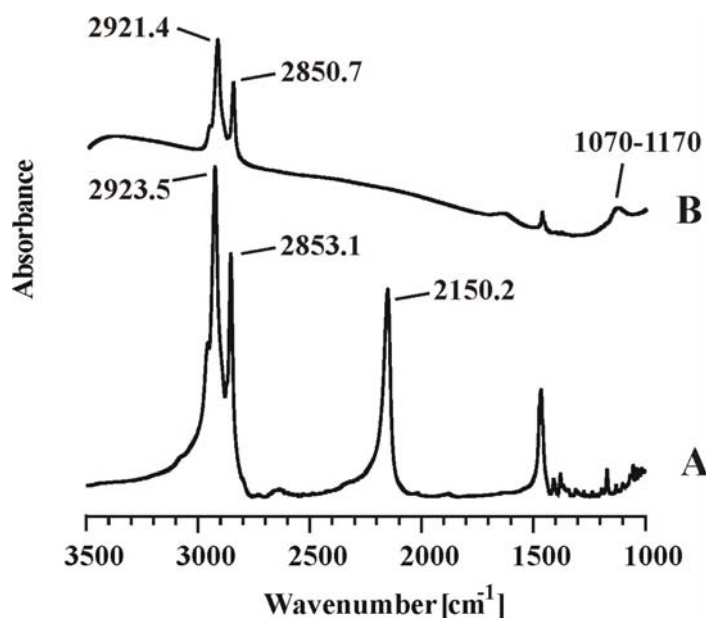


Figure 5.27. IR spectra for liquid *n*-octadecyltrihydrosilane (A) and *n*-octadecyltrihydrosilane grafted on hafnia (B) measured at 293 K.

The degree of cross-linking of the silanes during the modification step was qualitatively checked by ²⁹Si CP/MAS spectroscopy. Figure 5.28 shows ²⁹Si CP/MAS NMR spectra of different metal oxide substrates after grafting with *n*-octadecyltrichlorosilane and *n*-octadecyltrihydrosilane. ²⁹Si NMR signals of the trifunctional silanes (Tⁿ = RSi(OSi)_n(OH)_{3-n}, with n = 1, 2, 3) are located in the range between -40 ppm and -70 ppm.⁵¹ They refer to T¹ and T² groups with partial and T³ groups with complete cross-linking at approximately -42 ppm, -56 ppm, and -66 ppm, respectively. T² and T³ groups reflect Si-O-Si units which are formed by vertical polymerization of the silanes, as

discussed above (see Figure 5.29). A better signal-to-noise (S/N) ratio is observed for the ^{29}Si NMR spectra of Al(Cl) and Al(H) which reflects the higher surface loading (i.e. carbon content) and the resulting larger amount of Si nuclei (see Table 4.5). Al(H) shows a peak at around -35 ppm which corresponds to D_H^2 groups ($\text{D}_\text{H}^2 = \text{RSi}(\text{OSi})_2\text{H}$). Smaller signal intensities are observed in the ^{29}Si NMR spectra for the Hf(Cl) and Zr(Cl) samples which are a consequence of their lower surface coverages (see Table 4.5). The signal-to-noise ratio of the ^{29}Si NMR spectra for the other samples, Ti(Cl), Ti(H), Zr(H), and Hf(H), was too poor, and an unequivocal peak assignment was therefore impossible.

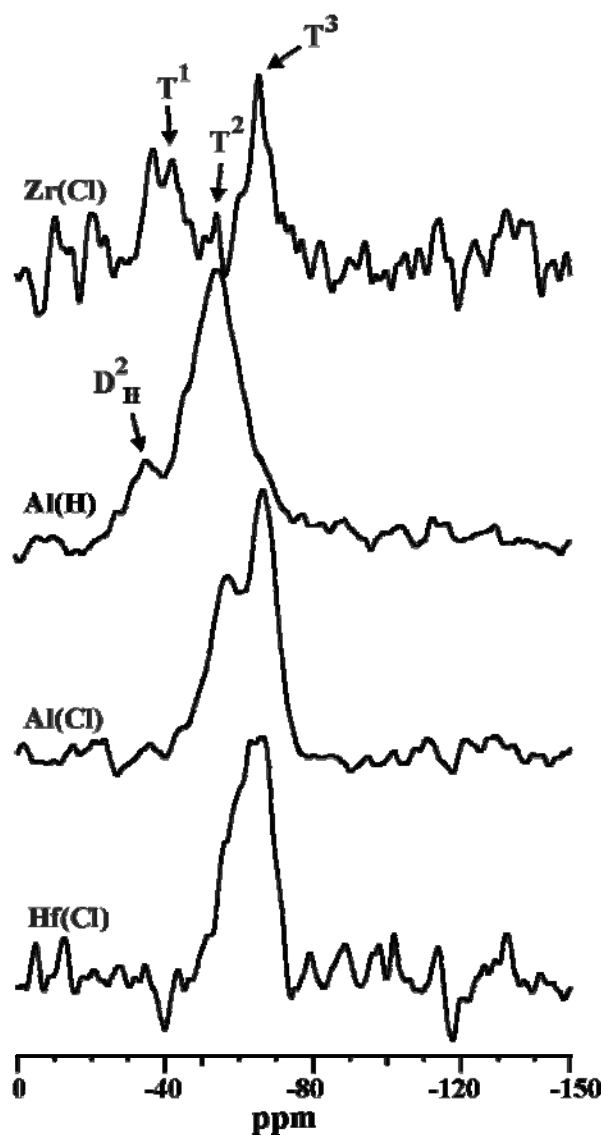
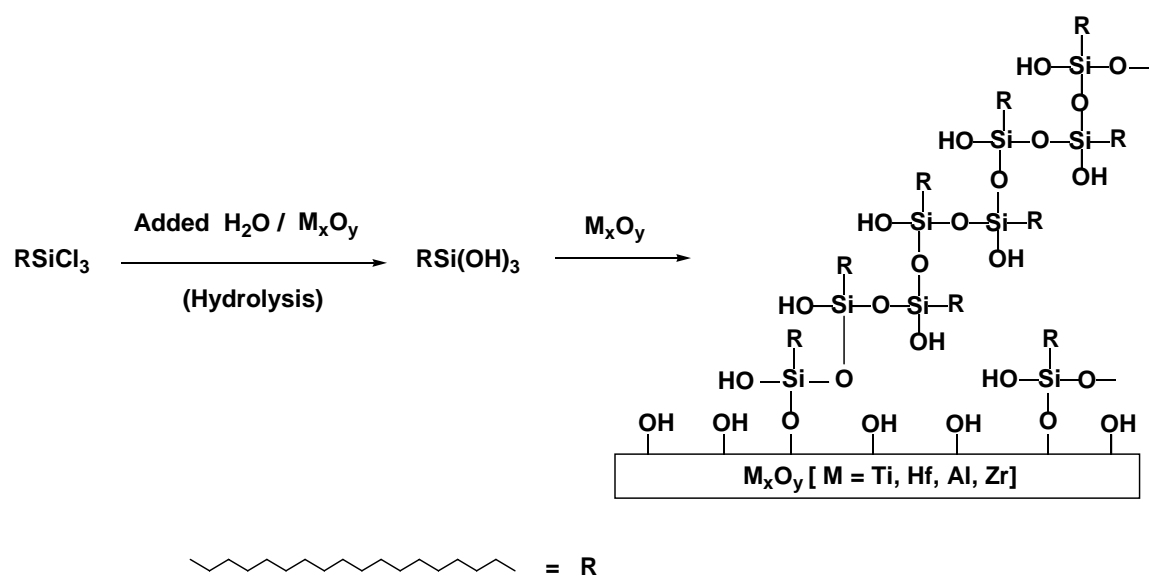


Figure 5.28. ^{29}Si CP/MAS NMR spectra of metal oxide substrates grafted with *n*-octadecyltrichlorosilane (Cl) and *n*-octadecyltrihydrosilane (H).

(A)



(B)

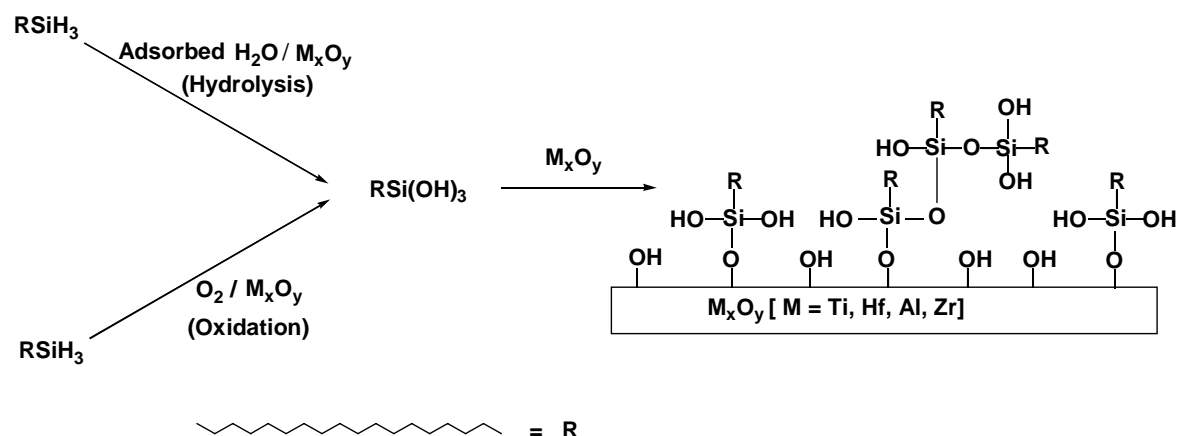


Figure 5.29. Reaction of *n*-octadecyltrichlorosilane (A) and *n*-octadecyltrihydrosilane (B) with metal oxides (based on grafting density).

It is difficult to provide an absolute proof for the formation of M-O-Si bonds from the present ^{29}Si NMR spectra, since the observed signals are too broad and rather featureless. Obviously, the local environment around the Si atoms is too heterogeneous to distinguish between well-separated resonances from Si-O-Si and Si-O-M segments. These findings are in line with an earlier work by Fadeev and coworkers, who were confronted with the same problems.²⁰⁹ Likewise, in a ^{29}Si NMR study on mixed silica/zirconia samples, recently performed in our group, it was again impossible to distinguish between Si-O-Si and Si-O-Zr units, despite the large amount of the latter ones.²¹⁰ A definitive proof for M-O-Si bond formation might be possible, for instance, by ^{17}O NMR experiments which, however, would require the use of (expensive) ^{17}O enriched samples.

5.4.4 Conformational Order of C₁₈ chains by FTIR Spectroscopy

The positions of the band maxima in the symmetric (2853-2846 cm⁻¹) and antisymmetric CH₂ stretching band regions (2926-2915 cm⁻¹) provide information about the conformational order of the alkyl chains and defect structures in the alkyl chain region.¹⁵⁴ For completely disordered “spaghetti-like” structures, the absorption wavenumber of the antisymmetric CH₂ stretching band is close to that of a liquid alkane (2924 cm⁻¹). For well-ordered systems, the absorption maximum is shifted to lower wavenumbers, i.e. to a limiting value of 2915 cm⁻¹ reported for crystalline alkanes. A similar shift can be registered for the symmetric CH₂ stretching band regions.

Variable temperature FTIR spectra for titania grafted with *n*-octadecyltrihydrosilanes, Ti(H), in the temperature range between 193 K and 353 K are depicted in Figure 5.30. The influence of temperature on the alkyl chain mobility and on their conformational order is clearly visible from the changes of the CH₂ stretching band positions. For instance, the antisymmetric CH₂ stretching band maximum varies between 2917.2 cm⁻¹ at 193 K and 2922.2 cm⁻¹ at 353 K. The overall change in the antisymmetric CH₂ stretching band position is thus about 5 cm⁻¹ for the temperature interval examined here. In a recent study of C₃₀ alkyl modified titania,⁶⁵ the antisymmetric CH₂ stretching band position varied between 2913.4 cm⁻¹ at 193 K and 2915.4 cm⁻¹ at 353 K, with an overall change of only 2 cm⁻¹ for the same temperature range. Such differences in alkyl chain conformational order along with its alteration are very important, since they have a great impact on the separation of solutes in chromatography.⁵² The comparison of the present experimental FTIR spectra with the available literature also points to larger IR bandwidths for the present samples with C₁₈ chains which is attributed to their higher mobility as compared to the longer C₃₀ chains.⁶⁵

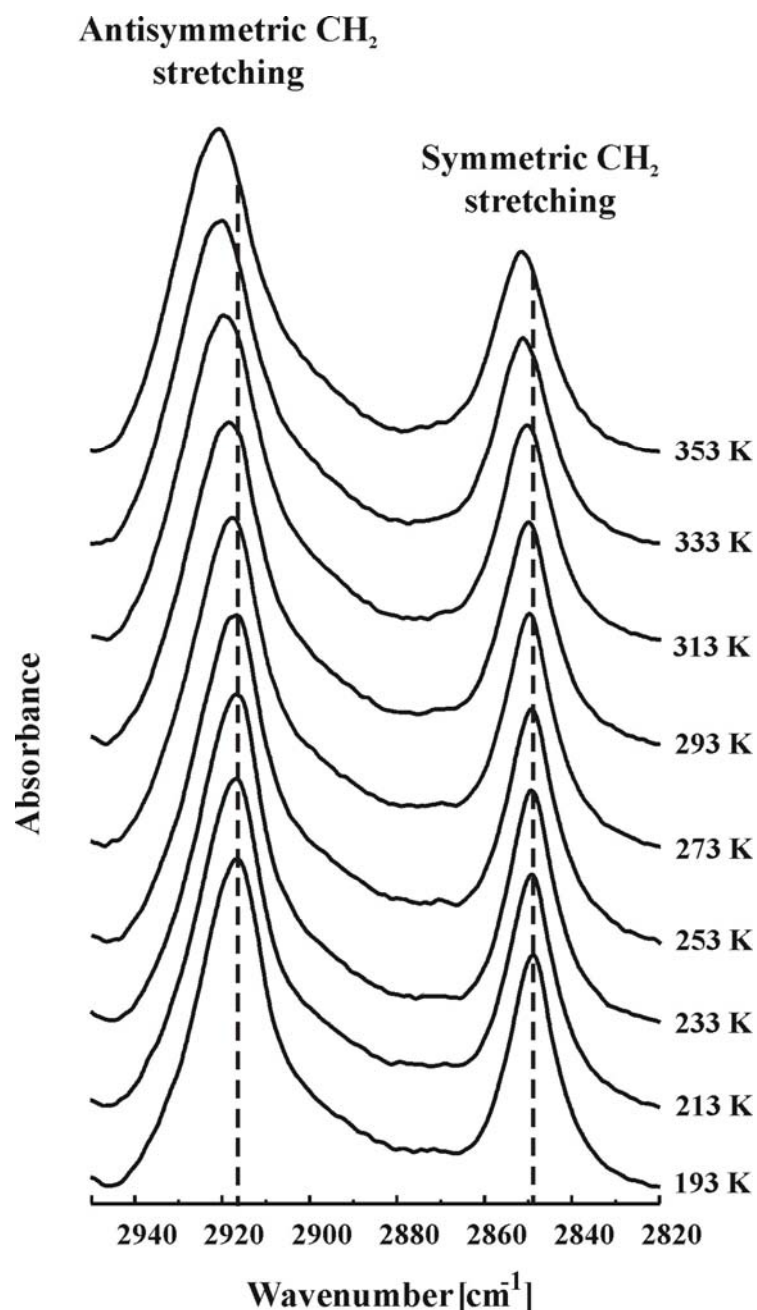


Figure 5.30. Antisymmetric and symmetric CH₂ stretching band spectra between 193 K and 353 K for titaniumdioxide modified with *n*-octadecyltrihydridosilanes, Ti(H).

The influence of temperature on the antisymmetric and symmetric CH₂ stretching band positions for the oxides modified with *n*-octadecyltrichlorosilane is depicted in Figure 5.31. The pronounced shift of the stretching band position towards higher wavenumbers, observed for all samples, clearly proves an increase in conformational disorder with increasing temperature. At lower temperatures ($T < 293$ K) the conformational order of the alkyl modified oxides follows the sequence $\text{Al(Cl)} \sim \text{Hf(Cl)} \sim \text{Ti(Cl)} > \text{Zr(Cl)}$. At

higher temperatures ($T \geq 293$ K) the C_{18} chains on titania are more ordered than those on hafnia and alumina, while the grafted chains on zirconia exhibit the lowest conformational order, following the sequence $Ti(Cl) > Hf(Cl) > Al(Cl) > Zr(Cl)$.

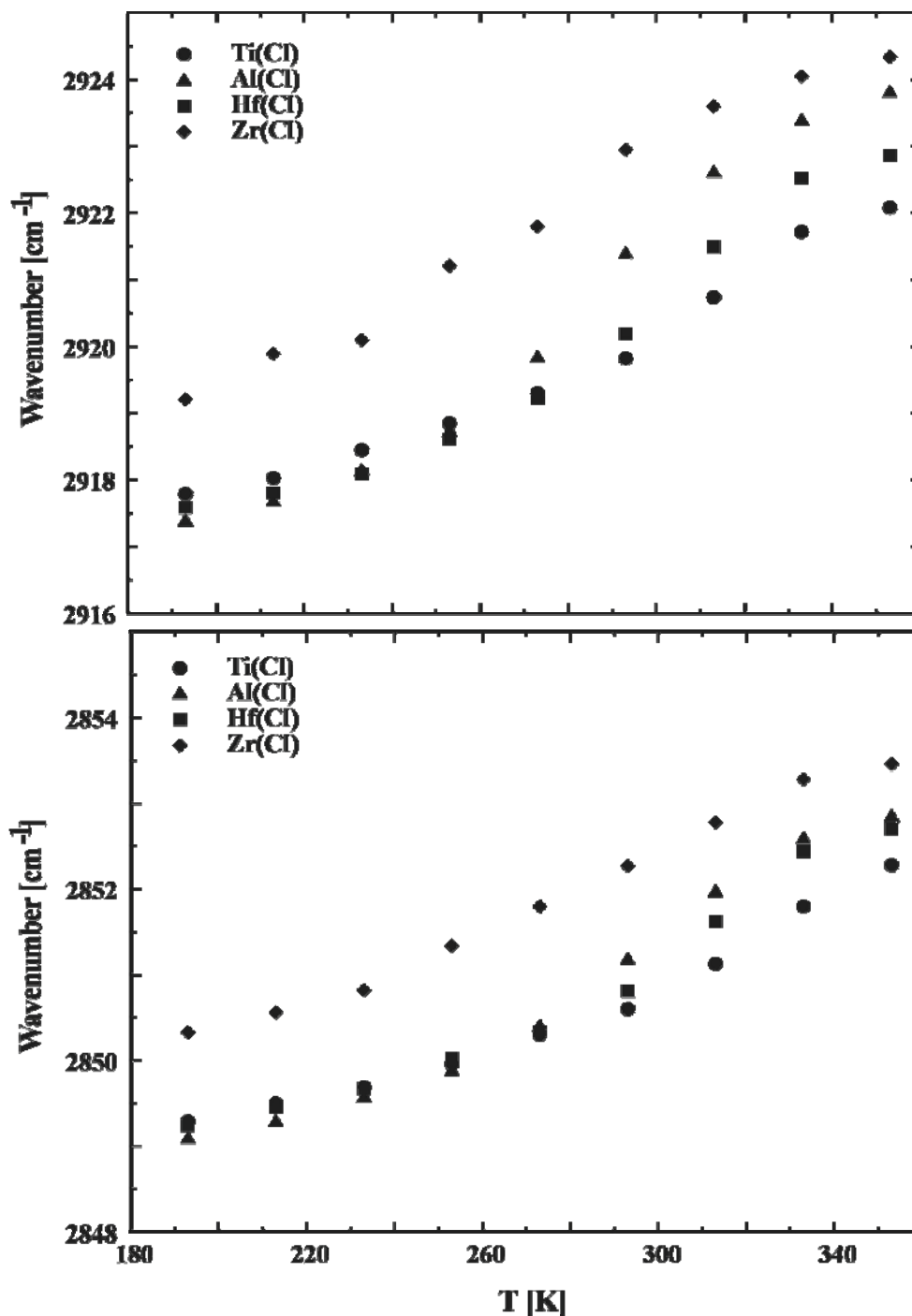


Figure 5.31. Temperature dependence of the antisymmetric (above) and symmetric (below) CH_2 stretching band positions for alkyl chains grafted on four different metal oxide substrates using *n*-octadecyltrichlorosilanes.

Variable temperature FTIR investigations were reported for C₃₀ chains grafted on zirconia using *n*-octadecyltrichlorosilanes.⁶⁵ In that work for the CH₂ antisymmetric stretching band position a value of 2917.7 cm⁻¹ was found at room temperature, which is about 5 cm⁻¹ smaller than the value of 2923 cm⁻¹ for the present systems. Obviously, C₃₀ modified systems are conformationally more ordered than the corresponding inorganic supports with attached C₁₈ chains. The same trend is also found for C₁₈ and C₃₀ chains grafted on silica substrates.⁶⁶

Figure 5.32 depicts the temperature dependence of the antisymmetric and symmetric CH₂ stretching band positions for the metal oxide substrates after reaction with *n*-octadecyltrihydrosilane. In summary, the C₁₈ chains on titania are conformationally more ordered than on the other metal oxides, which holds for the entire temperature range covered here. At lower temperatures, the conformational order follows the sequence Ti(H) > Hf(H) > Al(H) > Zr(H), while at higher temperatures the sequence is given by Ti(H) > Hf(H) > Zr(H) ~ Al(H). It is seen that – apart from the titania support – attachment by means of *n*-octadecyltrihydrosilane yields conformationally more disordered chains than from reaction with *n*-octadecyltrichlorosilane, which is a direct consequence of the differences in grafting density. Similar results were reported by Srinivasan et al.⁶³ who studied the conformational disorder of alkyl chains bound to silica. Fadeev et al. studied C₁₈ SAMs from reaction of *n*-octadecyltrihydrosilane with titania, hafnia, and alumina.¹²⁰ Their FTIR data showed at room temperature absorption band maxima that are shifted towards lower wavenumbers than those of the present study, which can be related to differences in the grafting densities.

The CH₂ wagging band region offers a possibility to derive quantitative information about the amount of various gauche conformers in alkyl chain containing systems (e. g. alkanes, phospholipids, surface modified systems).⁷⁶ This possibility was, however, not available in the present study, since there is an overlap between a relatively strong peak at 1384 cm⁻¹, arising from the metal oxides, and the symmetric methyl deformation band, the latter of which is essential for the analysis of the wagging band region.

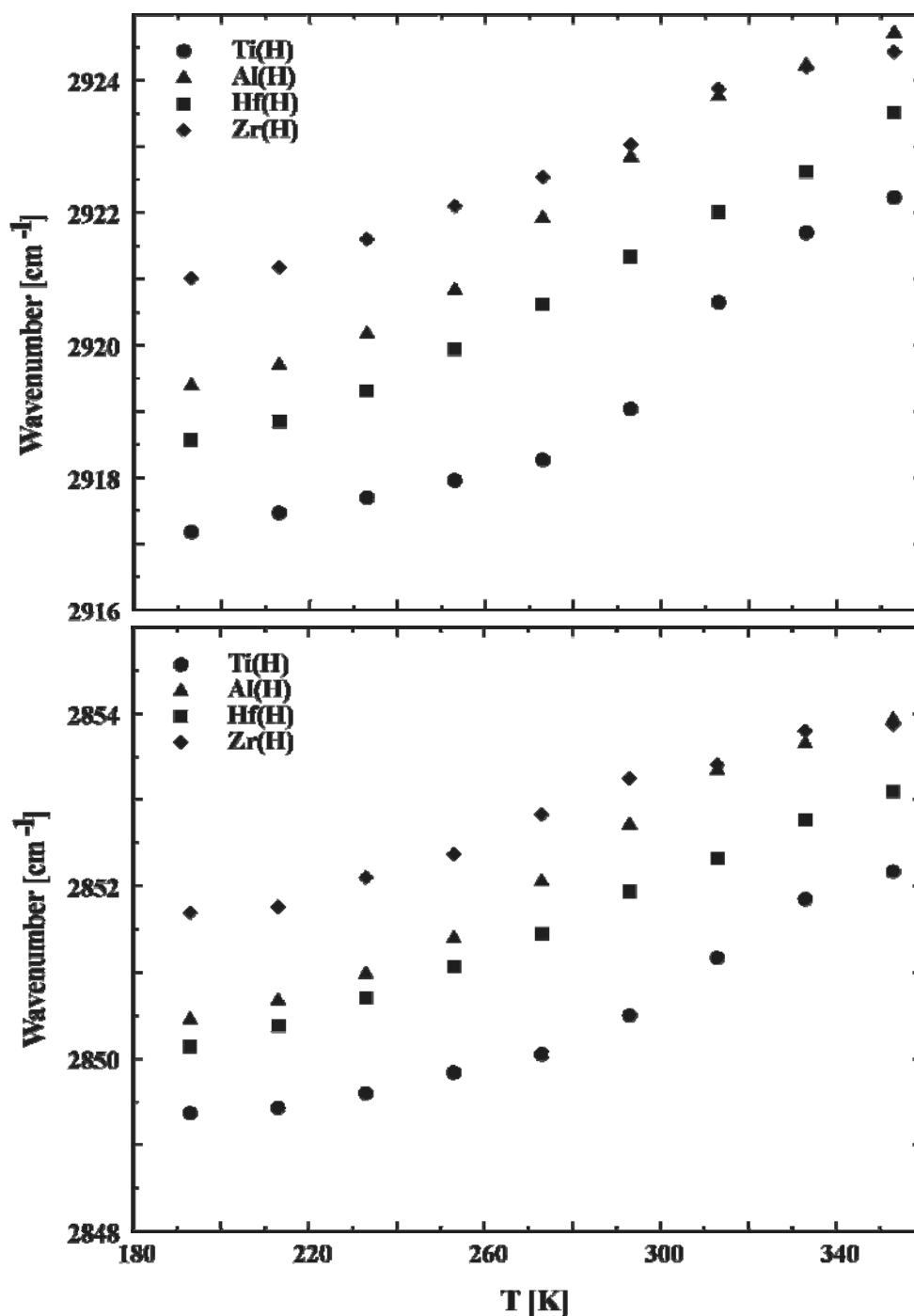


Figure 5.32. Temperature dependence of the antisymmetric (above) and symmetric (below) CH₂ stretching band positions for alkyl chains grafted on four different metal oxide substrates using *n*-octadecyltrihydrosilanes.

5.4.5 Conformational Order of C₁₈ Chains by Solid-State NMR Spectroscopy

¹³C CP/MAS NMR spectroscopy was used to distinguish between regions containing all-trans chains and regions with conformationally disordered chains, containing gauche

bonds. Figure 5.33 depicts ^{13}C CP/MAS NMR spectra of alkyl chains grafted on four metal oxide substrates.

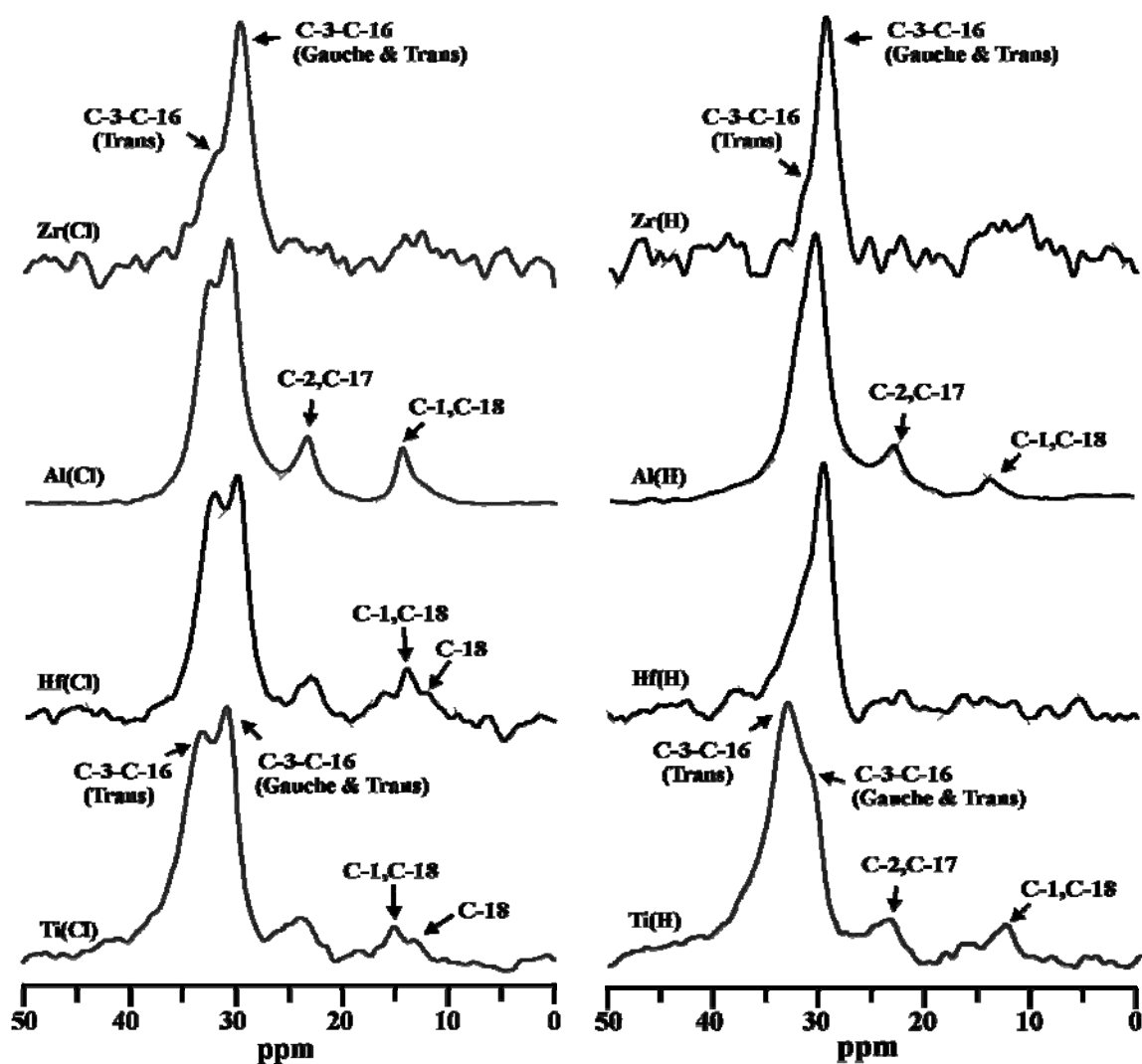


Figure 5.33. ^{13}C CP/MAS NMR spectra of alkyl chains grafted on four different metal oxide substrates using *n*-octadecyltrichlorosilanes and *n*-octadecyltrihydrosilanes.

The signal at around 14 ppm represents the C-18 and C-1 carbons. The peak at around 23 ppm arises from carbons C-2 and C-17 of the alkyl chains. Differences in the alkyl chain conformational order of the present C_{18} modified metal oxides can be discussed on the basis of the ^{13}C NMR resonances from the inner methylene segments C-3 to C-16 at around 32 and 30 ppm, attributed to trans (less mobile or “crystalline-like”) and trans-gauche (mobile or “solution-like”) conformations,^{52,54,167} where the lowfield shift of the former resonance can be explained by the γ -gauche effect.^{168,169} In fact, during former solid-state ^{13}C NMR investigations on silica samples grafted with alkyl chains of different

lengths (C_{18} , C_{22} , C_{30} , C_{34}) and variable amount, it was possible to distinguish between both resonances and the related conformational states.^{52,54,63,167}

For the present samples, obtained from surface modification with *n*-octadecyltrichlorosilane, Ti(Cl), Hf(Cl), Al(Cl), and Zr(Cl), again both resonances for the inner methylene segments could be observed. Based on the relative intensity of the trans-peak at around 32 ppm, samples Hf(Cl) and Ti(Cl) possess the highest alkyl chain order, and the conformational order follows the sequence Hf(Cl) ~ Ti(Cl) > Al(Cl) > Zr(Cl). In the case of samples Ti(H), Hf(H), Al(H), and Zr(H), obtained from surface modification with *n*-octadecyltrihydrosilane, sample Ti(H) displays the highest degree of conformational order which for these sample follows the sequence Ti(H) > Hf(H) > Al(H) > Zr(H). Summing up, the ^{13}C NMR results imply a lower chain conformational order for samples Hf(H), Al(H), Zr(H) and Zr(Cl) than for the other grafted substrates, which is attributed to a larger spatial freedom and hence higher mobility of the alkyl chains in these systems.

5.4.6 Effect of Silylating Agent and Metal Oxide Surface on Surface Loading and Conformational Order of C_{18} Chains

Self-assembly of alkyl chains on oxide substrates requires hydrolysis of the *n*-octadecyltrichlorosilane and *n*-octadecyltrihydrosilane moieties.^{211,212} The resulting trisilanols are then stabilized by hydrogen bonds with surface hydroxyl groups and neighboring silane molecules, until covalent bonds are formed.

In the present work, the solution polymerization route is used for surface modification with *n*-octadecyltrichlorosilane, where after addition of water polycondensation takes place to form octadecyltrisilanol. This intermediate is very reactive and yields highly cross-linked siloxane structures which grow vertically to the metal oxide surface (“perpendicular polymerization”), as schematically depicted in Figure 5.29A.^{139,213} Hence, these assemblies exhibit a better chain packing with higher grafting density,²¹⁴ alkyl chains in an almost all-trans conformation along with a good thermal and chemical stability.^{190,215} The main drawback of this reaction is the production of HCl as byproduct which might be adsorbed or even react with the substrate.

A second set of surface modified samples was obtained by using *n*-octadecyltrihydrosilane. This reagent is advantageous over other silane coupling agents, since the reaction medium only provides water and hydrogen as byproducts. Therefore, only small amounts of water and oxygen are available which are adsorbed on the metal oxide surface during exposure to the atmosphere. The formed trisilanols primarily react with surface hydroxyl groups. Since only a small number of trisilanol molecules is present, vertical polymerization is largely avoided (see Figure 5.29B), cross-linking is less pronounced than in the former route, and only a moderate grafting density can be achieved.^{120,209}

The amount and type of hydroxyl groups varies, depending on the surface nature of the metal oxide particles (surface area, roughness, porosity, etc.). For instance, at least 12 different types of hydroxyl groups are discussed for titania from which two types appear to be important for surface reactions,²¹⁶ while for alumina five types of surface hydroxyl groups are considered.²¹⁷ Zirconia exhibits a higher concentration of hydroxyl groups (about 20 $\mu\text{mol}/\text{m}^2$) on the surface.²¹⁸ Hence, the maximum number of titratable protons on titania is 2.79 $\mu\text{mol}/\text{m}^2$ which is less than that observed for zirconia with a value of 8 $\mu\text{mol}/\text{m}^2$.^{219,220} However, as for the hafnia support, the number of surface hydroxyl groups is so far unknown. Furthermore, hydroxyl groups with different acidic and basic properties (Lewis and Brønsted types) occur resulting in some surface heterogeneity.

The comparison of surface coverage values, given in Table 4.5, implies some correlation between these data and the number of available hydroxyl groups. That is, the zirconia substrate with highest amount of hydroxyl groups yields the highest amount of surface coverage, while metal oxides with less surface hydroxyl groups are accompanied by a lower surface coverage. It is interesting to note that this trend and the sequence for the surface loading are independent of the alkylsilane used for surface modification. The achieved surface loading is generally higher after reaction with *n*-octadecyltrichlorosilane than with *n*-octadecyltrihydrosilane, which indicates an enhanced reactivity for the former silylating reagent, in good agreement with earlier reports.¹¹

The DRIFT studies performed on the titania and hafnia samples did not provide conclusive information about the surface heterogeneity (in terms of Lewis and Brønsted acidic sites) which may affect the self-assembly of the silanols, the surface coverage

process, and in the turn the alkyl chain packing and the chain conformational order. Hence, from the present DRIFT investigations only some signal components from Lewis acidic sites are detectable which were much too weak to explain any difference in surface loading or chain conformational order, as found during the NMR and FTIR studies. For the same reasons it was also not possible to draw any meaningful connections between the strength of acidic sites on the metal oxide surface, as also expressed by the IEP values (see Table 4.4), which express the surface acidity and basicity by a global parameter, and the self-assembly process.

Consistent data for the conformational order of the surface-bound octadecyl chains were derived from FTIR as well as ^{13}C NMR spectroscopy, via examination of the CH_2 stretching bands and through analysis of the signal positions for the inner methylene group signals, respectively. As outlined earlier, both spectroscopic methods provide a qualitative measure for the alkyl chain conformational order. For the metal oxides grafted with *n*-octadecyltrichlorosilane or *n*-octadecyltrihydrosilane, the degree of conformational order was found to follow the sequences $\text{Ti}(\text{Cl}) > \text{Hf}(\text{Cl}) > \text{Al}(\text{Cl}) > \text{Zr}(\text{Cl})$ and $\text{Ti}(\text{H}) > \text{Hf}(\text{H}) > \text{Al}(\text{H}) > \text{Zr}(\text{H})$.

It is interesting to note that for the hafnia, alumina and zirconia supports the conformational order after grafting with *n*-octadecyltrichlorosilane is higher than for modification with *n*-octadecyltrihydrosilane which can be directly related to the differences in surface coverage. However, for both titania samples almost the same conformational order is observed.

SAMs supported on titania by reaction with *n*-octadecyltrichlorosilane and *n*-octadecyltrihydrosilane were studied earlier by Fadeev et al.²²¹ The reported room temperature FTIR spectra indicate a somewhat higher conformational order than in the present work which stems from the higher grafting density achieved in the former work.

In a former ^{13}C NMR and FTIR study on C_{30} grafted titania and hafnia a similar trend for the alkyl chain conformational order was found, i.e. for the titania support the chain order was substantially higher than for the zirconia support, despite the almost identical surface coverages.^{52,65} It should be emphasized that for the present metal oxides the surface coverage and the C_{18} conformational order follow opposite trends, i.e. the lowest grafting

density is accompanied by the highest conformational order. At present, we cannot provide a final and definite explanation, along with some experimental evidence, for these findings. On the basis of the earlier work on silica supports it is, however, very likely that the surface grafting is heterogeneous, i.e. island structures with a higher density of alkyl chains are formed, and that this tendency varies with the metal oxide support. For the samples obtained by the reaction with *n*-octadecyltrichlorosilane - using the solution polymerization approach - the island formation might be even accompanied by the aforementioned “vertical polymerization” due to the high reactivity and self assembly of the alkylsilanols.

In this context it should be mentioned that a former FTIR study on C₃₀ SAMs on titania also revealed island formation of the grafted alkyl chains, despite the fact that those SAMs were prepared via surface polymerization.⁶⁵ Similar observations were made during C₁₈ grafting of mixed oxide substrates by surface polymerization.¹⁴⁶ Both studies imply that the actual preparation route (i.e. surface or solution polymerization) is less important than the nature of the metal oxide surface.

The further comparison of the CH₂ stretching band data for the present C₁₈ modified metal oxides and the earlier studied C₃₀ modified titania and zirconia supports⁶⁵ implies that the alkyl chain conformational order in the C₃₀ systems is higher, and its temperature variation is much less pronounced than for the present C₁₈ modified materials. Both findings can be understood by the stronger van der Waals interactions for the longer C₃₀ chains,²²² which imposes spatial constraints for the chain motions along with an increase of the chain conformational order.

The most striking result concerns the substantially higher conformational order of the C₁₈ chains of all present modified metal oxides if compared with the results from studies of C₁₈ chains grafted on silica, and despite their lower grafting densities. An explanation can be given by the differences in porosity, as characterized by the surface area and the pore volume. For silica the typical values are 100-300 m²/g and 0.6-1.0 mL/g, respectively, which are much larger than the values of the metal oxide supports of the present work (see Table 4.4). Accordingly, the metal oxide surfaces can be considered to be rather flat and even with lower porosity, while for silica a rather uneven and rough surface with higher mesoporosity is expected. At the even surfaces of the metal oxides the grafted chains are subject to more spatial constraints which results in a higher alkyl chain

conformational order. The situation is different for the irregular surface in silica, where the chains possess much more spatial freedom and thus a higher degree of conformational disorder. Although the alumina support exhibits porosity data which point to an irregular surface, the respective data for the alkyl chain conformational order are very similar to those of the other metal oxides. This experimental result is so far not completely understood. An explanation might be found in the higher tendency for island formation for the alumina support which obscures the tendency for a less dense packing expected on the basis of the porous alumina surface.

5.4.7 Summary

Octadecyl chains grafted on titania, zirconia, hafnia, and alumina by means of *n*-octadecyltrihydrosilane and *n*-octadecyltrichlorosilane were characterized by variable temperature FTIR and solid-state NMR spectroscopic techniques. FTIR and ^{29}Si CP/MAS measurements revealed cross-linking of the silanes through vertical polymerization during metal oxide surface grafting. In the ^{13}C CP/MAS NMR spectra regions with all-trans chains and regions with conformationally disordered chains, containing gauche bonds, can be distinguished. FTIR studies provided information about the conformational order of the alkyl chains through the analysis of the CH_2 stretching data. The conformational disorder of the C_{18} alkyl chains increases with increasing temperature for all metal oxide substrates. Grafting with *n*-octadecyltrichlorosilane shows a higher degree of conformational order than grafting with *n*-octadecyltrihydrosilane.

The derived results on conformational order and surface loading are discussed on the basis of the available amount of surface hydroxyl groups, porosity of the metal oxide support, the reactivity of the silylating reagents and the reaction scheme used during the grafting step. Differences in the conformational order for the different metal oxide supports are traced back to the presence of island structures for the grafted alkyl chains. The substantial higher alkyl conformational order of the present C_{18} modified samples as compared to C_{18} modified silica is attributed to the higher porosity of the silica supports along with a larger spatial freedom of the attached alkyl chains.

5.5 Grafted Mixed Silica-Zirconia Oxides: Impact of Oxide Supports and Grafting of C₁₈ Silanes

In the following we report on the characterization of four samples consisting of SiO₂/ZrO₂ supports whose surfaces were modified by chemical attachment of C₁₈ alkyl chains. In the whole work, samples **1-4** represents mixed oxides; **1H-4H** represents humidified mixed oxides; **1F-4F** represents C₁₈ alkyl functionalized mixed oxides.

5.5.1 Surface characteristics of mixed oxide substrates

The characterization of the surface properties of the mixed oxides was carried out in order to determine the surface area and pore volume of these oxides. The isotherms follow type I isotherms typical of microporous material.¹⁹³ The samples **1** and **2** prepared by calcination at 600 °C has higher surface area and pore volume when compared to samples calcined at 800 °C, **3** and **4** (Table 4.6). Thus with increase in annealing temperature, the porous features are decreasing regardless of the amount of zirconium present. This is likely due to a partial “collapse” of the microporous structure induced by the higher temperature annealing, as previously reported.¹³³ Samples **2** and **4** with higher silica content have a higher microporous volume while the samples with lower silica content **1** and **3** have a negligible microporous area and volume.

5.5.2 Route for modification of mixed oxides surfaces

The most frequent routes used to obtain higher alkyl surface coverage for chemical modification of silica gels and related oxides are the solution and surface polymerization techniques, which have been extensively reviewed in various articles.^{26,50,66,143,144} Silica grafting employing the surface polymerization approach is known to result in higher grafting densities, since the adsorbed surface water promotes enhanced binding to the surface and induces cross-linking through polymerization of neighboring molecules.^{11,143} The amount of hydroxyl groups (of both silica and zirconia) gets reduced due to the condensation with neighboring hydroxyl groups at calcination temperatures (600 and 800 °C) and the remaining groups are randomly distributed on the surface of these mixed oxides. Hence, by employing the surface polymerization technique for the reaction with *n*-octadecyltrichlorosilane, more surface coverage can be obtained.

The as-received mixed oxides were carefully equilibrated with humid air to increase the amount of hydroxyl groups and adsorbed water prior to surface modification. ^{29}Si NMR measurements confirmed the increase in the amount of silanol groups (Q^3 group, $\text{Q}^3 = \text{Si}(\text{OSi})_3(\text{OH})$)^{22,51} on the surface of these silica-zirconia mixed oxides (Table 5.8). It should be noted that the values reported here only represent the silanol groups on the silica surface. The zirconia which constitutes these mixed oxides also has hydroxyl groups on the surface and increase in their amount after humidification was unknown (discussed in detail in section 5.5.4 and 5.5.8). Hence it should be accounted that apart from the increase of silanol groups on the surface; there also should be an increase in hydroxyl groups on the zirconium sites of these silica-zirconia mixed oxides.

Table 5.8. ^{29}Si single pulse NMR chemical shift values after fitting the experimental spectra for mixed oxides, after humidification and their grafting with C_{18} alkyl chains.

Samples	Q^2			Q^3			Q^4		
	δ (ppm)	FWHM (Hz)	I (%)	δ (ppm)	FWHM (Hz)	I (%)	δ (ppm)	FWHM (Hz)	I (%)
1	-91	290	1	-99	772	27	-108	1036	72
1H	-91	374	1	-100	889	37	-108	990	62
1F	-91	204	1	-100	577	18	-109	1064	81
2	-	-	-	-101	561	6	-110	1148	94
2H	-91	218	1	-100	596	14	-109	1033	85
2F	-	-	-	-101	484	12	-109	966	88
3	-	-	-	-100	536	3	-109	1322	97
3H	-92	229	1	-100	532	5	-109	1304	94
3F	-93	331	1	-99	501	5	-108	1280	94
4	-	-	-	-101	219	-	-109	1200	100
4H	-	-	-	-101	282	1	-109	1233	99
4F	-	-	-	-100	279	1	-109	1178	99

δ : chemical shift value; Fwhm: full width at half maximum; I: relative intensity.

The compositional and morphological characteristics of the C_{18} alkyl modified mixed oxides are summarized in Tables 4.7 and 5.9. Despite the aforementioned pretreatment, the surface coverages of the modified samples are rather low as compared to the values typically reported for modified silica gels.^{26,65,66} This might be explained by the fact that due to the high calcination temperatures (600 or 800 °C) used for the present silica/zirconia hybrid materials, much lesser amount of hydroxyl groups are present on

the surface of the mixed oxides. A similar reduction in hydroxyl groups was also observed on the silica surface at the calcination temperature ($> 550\text{ }^{\circ}\text{C}$) in the earlier studies.^{10,180} The aforementioned pre-conditioning of the oxide surfaces was therefore not sufficient to provide a considerable increase of the amount of surface hydroxyl groups on both silica and zirconia.

Table 5.9. Atomic percentages determined by XPS, before and after functionalization of mixed oxides with C₁₈ alkyl chains.

Samples	%Zr	%Si	%O	%C
1	5.7	16.6	69.3	8.4
1F	2.6	13.3	36.5	47.6
2	1.5	17.6	57.3	23.6
2F	0.5	10.4	27.3	61.8
3	4.1	15.5	51.4	29.0
3F	2.5	13.5	35.0	49.0
4	0.8	12.0	49.4	37.8
4F	0.5	10.6	26.5	62.4

5.5.3 XPS characterization of mixed oxide substrates

The composition of the samples before and after alkyl chain grafting was determined by XPS. XPS analysis showed that the obtained Si/Zr molar ratios (see Table 5.9) are in good agreement with the nominal values derived from the starting solutions. The determined carbon content showed a considerable increase after surface modification which can be directly attributed to the alkyl chains grafted on the surface of mixed oxides. The residual carbon content in the as-prepared mixed oxides was attributed to atmosphere contamination.

Figure 5.34 depicts survey spectra of sample **3** before (a) and after (b) functionalization of the mixed oxides (**3F**), acquired by using the same experimental parameters. In both spectra the peaks of all species of interest (Si, Zr, O, C) are clearly visible. After functionalization, a considerable increase of the carbon peak intensity and a corresponding decrease of the silicon and zirconium peak intensities can be observed. It should be pointed out that XPS is a surface sensitive technique, and the changes in the relative intensities, which are also confirmed by the values of the atomic percentages

reported in Table 5.9, are a consequence of the carbon enrichment at the surface after the grafting of the alkyl chains.

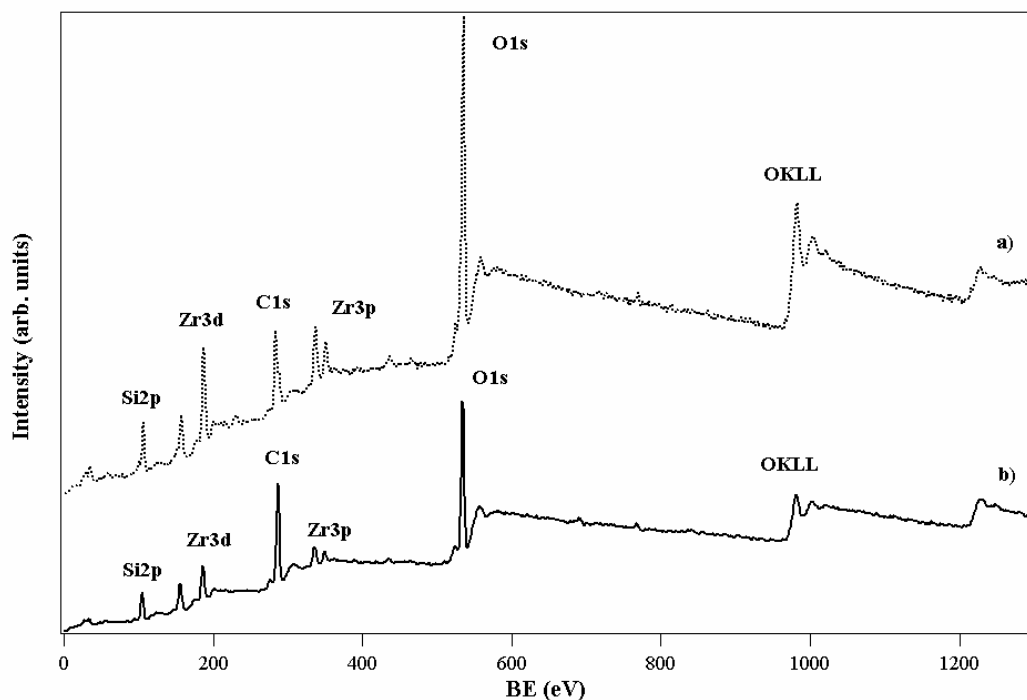


Figure 5.34. XPS survey spectra of sample **3** before (a) and after (b) the functionalization (**3F**).

XPS also provides information about the chemical state of the species. As far as silicon is concerned, the binding energy (BE) values occur between 103.5 and 103.7 eV which is typical for silicon in silicon dioxide.^{185,187} Similarly, the values of the Zr3d region are consistent with those reported for zirconium dioxide.^{131-133,185,187,210} In the analyzed peaks, no shoulder or broadening could be observed, which would be expected in the presence of species with different chemical environment.

5.5.4 Cross-linking of alkylsilanes by SSNMR spectroscopy

²⁹Si NMR spectroscopy is suitable for determining the nature of surface species of the modified mixed oxides as well as the degree of cross-linking of the silane after alkyl chain grafting. Figure 5.35 shows ²⁹Si CP/MAS NMR spectra of the present alkyl modified mixed oxides. The broad intense peak observed in ²⁹Si NMR spectra indicates the presence of surface silanol species, Q¹, Q² and Q³ units, and polymerized bulk Q⁴

groups ($Q^n = \text{Si}(\text{OSi})_n(\text{OH})_{4-n}$, with $n = 1, 2, 3$ and 4) around $-84, -91, -100,$ and -109 ppm, respectively (Table 5.10).^{22,51,53,66}

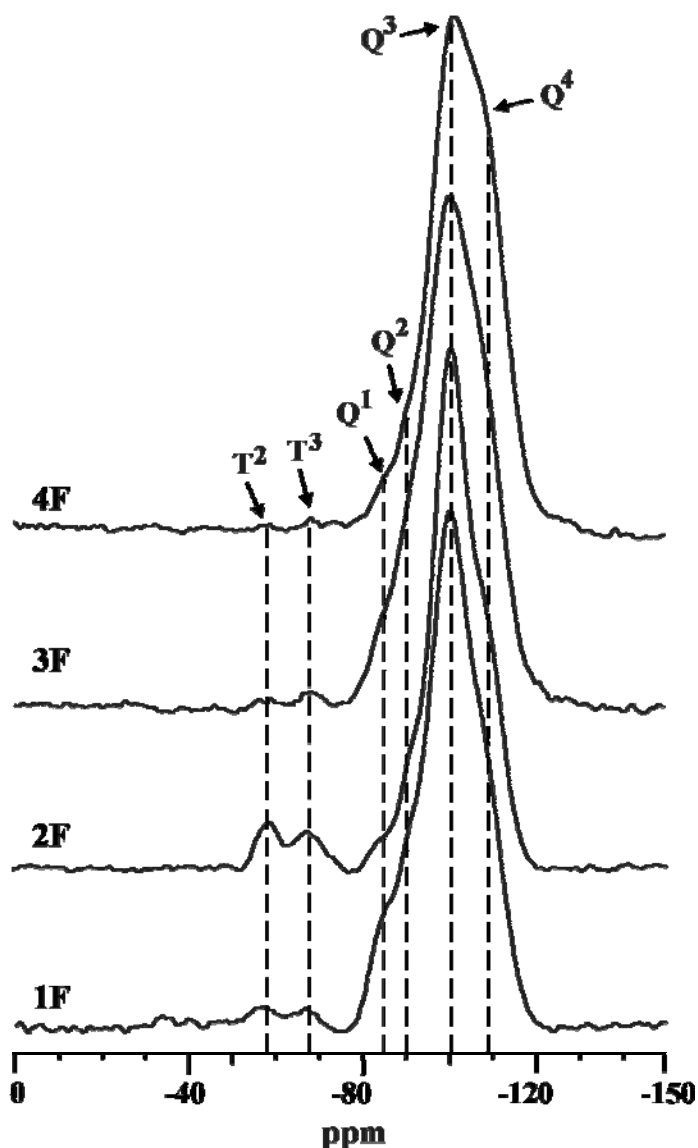


Figure 5.35. ^{29}Si CP/MAS NMR spectra of C_{18} alkyl grafted silica-zirconia mixed oxides using *n*-octadecyltrichlorosilane.

^{29}Si single-pulse NMR spectra were also recorded under MAS conditions for bare mixed oxides, humidified oxides and C_{18} alkyl modified mixed oxides to determine the amount of silanol groups present on the silica surface and to compare the amount before and after functionalization reactions. The spectra generally consist of three spectral components, Q^2 , Q^3 , and polymerized bulk Q^4 groups. Quantitative information about the sample

composition is achieved by Gaussian-Lorentzian spectral deconvolution and the best fit results are summarized in Table 5.8.

Table 5.10. ^{29}Si chemical shifts for C_{18} chains grafted on silica-zirconia mixed oxides.

Sample	^{29}Si chemical shift (ppm)					
	Q^4	Q^3	Q^2	Q^1	T^3	T^2
1F	-109.0	-100.2	-91.9	-85.2	-67.1	-57.0
2F	-108.7	-100.5	-91.4	-83.7	-67.4	-58.4
3F	-109.2	-100.5	-91.9	-84.3	-68.0	-57.0
4F	-108.3	-101.7	-90.5	-85.0	-68.4	-58.2

The given data demonstrates that mixed oxide samples calcined at 600 °C (**1** and **2**) have a higher amount of silanol groups when compared to the samples calcined at 800 °C (**3** and **4**). At higher temperatures, the condensation of silanol groups is very high which is reflected in the higher amount of Q^4 groups for the samples calcined at 800 °C. The trend observed in these mixed oxide samples during the whole grafting process is described here: after the humidification of the bare mixed oxides, there is an increase in the amount of Q^3 groups on the surface of the mixed oxides. This is due to the breaking of some siloxane bonds due to the physisorbed water to form silanol groups. Similar effect can also be observed in the formation of zirconia hydroxyl groups on the surface but due to the broad ^{29}Si spectra, it was not able to distinguish the signal. Another reason to be mentioned is the formation of new hydroxyl group because of hydrogen bonding of adsorbed water with the existing hydroxyl groups on the surface with the zirconia and silica bulk oxide polymeric structure. After grafting with C_{18} alkyl chains, the mixed oxide calcined at 600 °C shows a reduction in the amount of silanol groups whereas this was not observed in the case of samples calcined at 800 °C, as described in detail in section 5.5.8.

Apart from Si-O-H and Si-O-Si units, also Si-O-Zr segments should be present in these materials. However, it is difficult to provide an absolute proof for the formation of Si-O-Zr units from the present ^{29}Si NMR spectra, since the observed signals are too broad and featureless. Obviously, the local environment around the Si atoms is too heterogeneous to distinguish between well-separated resonances from the Si-O-Si and Si-O-Zr segments, as

similar to an earlier work.²⁰⁹ Likewise, a similar ²⁹Si NMR study on mixed silica/zirconia samples in our group again shows the impossibility to distinguish between Si-O-Si and Si-O-Zr units due to the large line widths of the ²⁹Si resonances, despite the expected large amount of Si-O-Zr segments.^{71,210} A definitive proof for M-O-Si bond formation might be possible, for instance, by ¹⁷O NMR experiments which, however, require expensive ¹⁷O enrichment.

²⁹Si NMR signals of the attached and cross-linked trifunctional silanes are denoted by the Tⁿ signals (Tⁿ = RSi(OSi)_n(OH)_{3-n}, where n = 2 and 3).^{22,26,51,66} Here, T³ signals around -67 to -68 ppm with complete and T² signals around -57 to -58 ppm with partial cross-linking can be distinguished in the present mixed oxides (see Table 5.10). For alkyl modified silica, the resonances for T³ and T² groups are usually observed around -65 and -56 ppm, respectively.^{22,26,51,66} The observed upfield shift of the T² and T³ resonances for the present samples may reflect averaged values due to bond formation with both the silane and zirconia hydroxyl groups, which, however, cannot be further spectroscopically separated. As mentioned earlier, ¹⁷O NMR studies might be very helpful to determine the grafting of C₁₈ chains on the zirconia hydroxyl groups.

The amount of cross-linking increases with increase in surface coverage of the chemically modified samples. Therefore, a spectrum with a better signal-to-noise ratio was obtained due to efficient cross-linking for sample **2F**. The ²⁹Si NMR spectra of samples **1F**, **3F** and **4F** are characterized by weaker signal intensities reflecting the rather lower cross-linking of the chains and hence the efficiency of cross polarization is reduced in these samples.

5.5.5 Conformational order of grafted C₁₈ chains by SSNMR spectroscopy

¹³C NMR spectroscopy yields information about the conformation and mobility of surface-immobilized alkyl ligands. It distinguishes between the regions containing all-trans chains and regions with conformationally disordered chains containing gauche bonds.^{22,51} Figure 5.36 depicts ¹³C CP/MAS NMR spectra of alkyl chains grafted on four different mixed oxide substrates using *n*-octadecyltrichlorosilanes. The corresponding chemical shifts for the various carbon resonances are given in Table 5.11. The C-1 and C-18 resonances for the present samples are found between 15 and 16.4 ppm. For all samples, these resonances appear to be broadened, characterized by low-field or high-

field shoulders. These experimental observations might imply some heterogeneity in alkyl chain arrangement on the surface, i.e. the presence of methyl groups with different molecular mobility because of a different chain packing, as also described earlier for chemically modified silica materials.^{52,63}

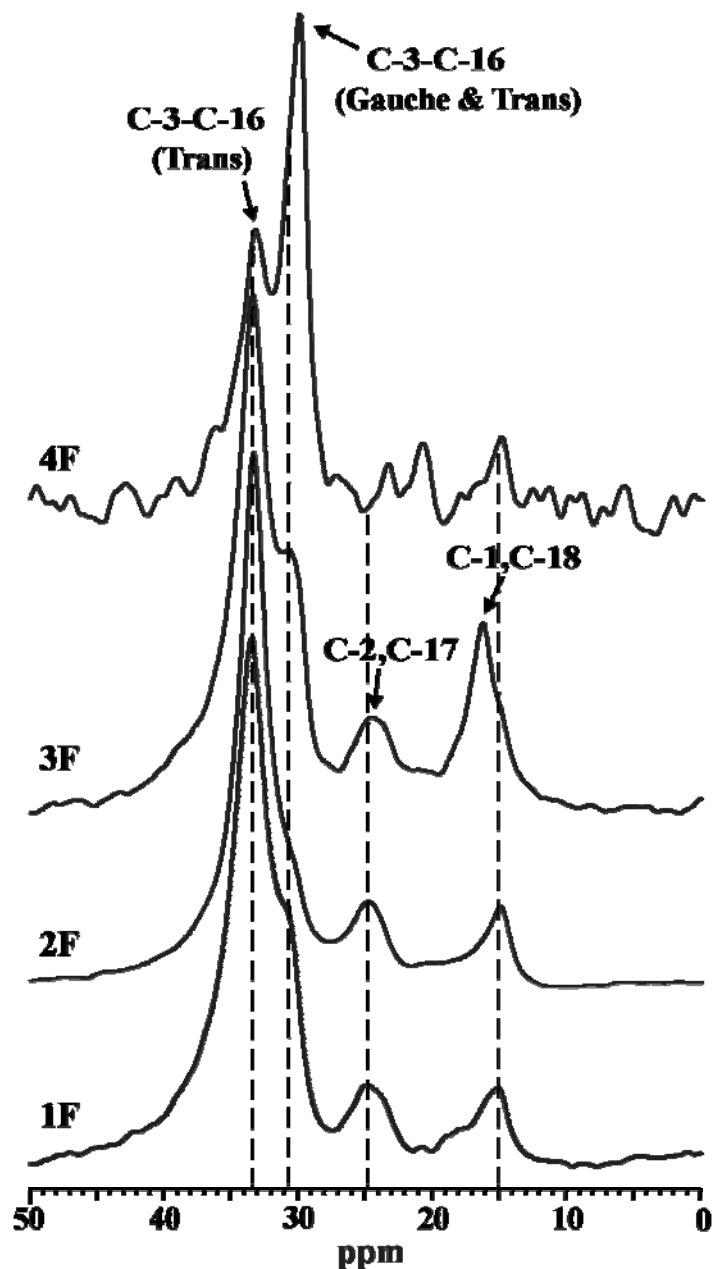


Figure 5.36. ^{13}C CP/MAS NMR spectra of C_{18} alkyl grafted silica-zirconia mixed oxides using *n*-octadecyltrichlorosilane.

Table 5.11. ^{13}C chemical shifts for C_{18} chains grafted on silica-zirconia mixed oxides.

Sample	^{13}C chemical shift (ppm)			
	C-3–C-16 (Trans)	C-3-C-16 (Gauche)	C-2 & C-17	C-1 & C-18
1F	33.5	30.7	24.9	15.1
2F	33.5	30.5	24.8	15.0
3F	33.4	30.7	24.6	16.4
4F	33.2	29.9	a	15.0

a: C-2 and C-17 give signal at 23.3 and 20.7 ppm

When compared with earlier studies on samples with alkyl chains grafted on silica and other metal oxides with a typical value of about 14 ppm,^{26,167} the ^{13}C chemical shifts of the C-1 and C-18 carbon atoms in the present samples were shifted to low-field which can be explained on the basis of the γ -gauche effect.^{168,169} Accordingly, alkyl chains exhibit a higher conformational order than for related systems with pure silica or metal oxide supports. For samples **1F**, **2F**, and **3F** the peak within 24-25 ppm is due to carbon atoms C-2 and C-17 of the alkyl chains which has to be compared to the values for carbon atoms C-17 in *n*-alkanes of 22.6 and 25 ppm in the liquid state with conformationally disordered chains and in the crystalline state with all-trans chains, respectively.²²³ Hence, the C-17 signals for samples **1F**, **2F**, and **3F** again imply high alkyl chain conformational order. In the case of sample **4F**, the signal-to-noise ratio was too poor to extract the resonances for carbon atoms C-2 and C-17.

The above results for the conformational order in the chain next to the chain ends (carbon atoms C-17 and C18) and close to the solid surface (C-1 and C-2) are in complete agreement with the findings for the methylene groups C-3 to C-16 of the C_{18} chains, as discussed next. Here, typically two resonances around 33 ppm and 30 ppm, reflecting “crystalline-like” trans and “solution-like” trans-gauche conformations, respectively, are distinguished.^{54,126,167} The same resonances are also observed for the present samples, as shown by Figure 5.36 and Table 5.11. However, the relative intensities of both resonances for the inner methylene segments strongly vary with the actual sample. The strongest relative intensity of the “trans” peak is thus found for sample **2F**, followed by samples **1F** and **3F**, while sample **4F** behaves differently, as the “trans” peak is even smaller than the “gauche” peak, reflecting the sample with the lowest conformational

order. Especially, sample **2F** shows the maximum peak intensity at 33.5 ppm with the maximum peak intensity and discussed in detail in section 5.5.7.

5.5.6 Conformational order of grafted C₁₈ chains by FTIR spectroscopy

Independent information about conformational properties of the alkyl chains tethered to the mixed silica/zirconia supports can be achieved by variable temperature FTIR spectroscopy by analysis of conformational vibrational bands^{26,63,65,66} - the CH₂ stretching and wagging modes - as will be presented next. Here, the shifts of the band maxima in the symmetric (2853-2846 cm⁻¹) and antisymmetric CH₂ stretching band regions (2926-2915 cm⁻¹) provide qualitative information about the alkyl chain conformational order by comparison with the absorption maxima in pure *n*-alkanes.¹⁵⁴ For completely disordered structures, the absorption wavenumber of the antisymmetric CH₂ stretching band is close to that of liquid *n*-alkanes (2924 cm⁻¹). For well-ordered systems, the absorption maximum is shifted to lower wavenumbers where the limit of 2915 cm⁻¹ is given by crystalline alkanes which exist in an all-trans conformational state. A similar shift can be registered for the symmetric CH₂ stretching band regions.

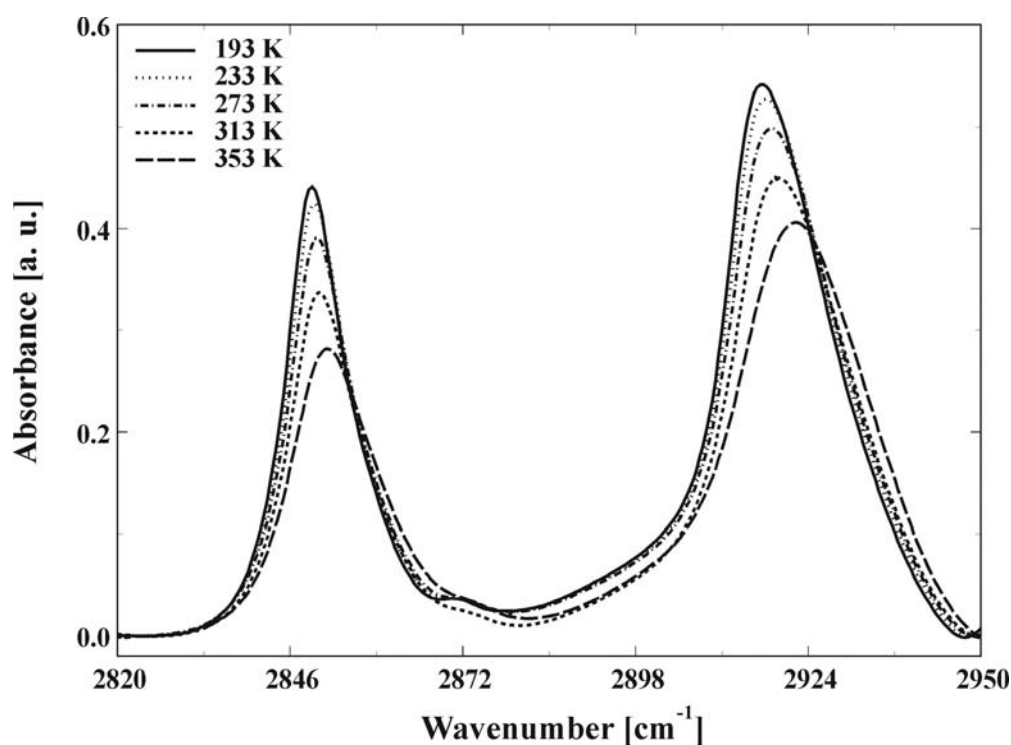


Figure 5.37. Temperature dependence of the symmetric and antisymmetric CH₂ stretching band spectra of sample **2F**.

Representative variable temperature FTIR spectra of sample **2F**, covering the stretching band region of the tethered C₁₈ chains, are shown in Figure 5.37. Similar spectra are observed for the other samples of the present work. It is evident that the band positions of the CH₂ stretching bands are shifted towards higher wavenumbers with increasing temperature in covered range between 193 and 353 K, implying enhanced conformational disorder in the same direction. At the same time, the bandwidths of both stretching bands increase upon temperature rise, which can be understood by higher alkyl chain mobility, as also observed earlier.⁶⁵

Figure 5.38 depicts the temperature dependence of the antisymmetric CH₂ stretching band positions for samples **1F-4F**. Samples **1F** and **2F** (Figure 5.38 top), annealed at 600 °C, exhibit a pronounced shift of the absorption bands towards higher wavenumbers with increasing temperature, implying increasing conformational disorder in the same direction. Similar variable temperature data for the CH₂ stretching bands were also reported earlier for other systems.^{26,65} It can be further stated that the alkyl chain conformational order in sample **2F** with the lower zirconia content is higher than in sample **1F**. Similar plots for the temperature dependences of the antisymmetric CH₂ stretching band positions were observed in samples **3F** and **4F** (Figure 5.38 bottom), which were obtained by calcination at 800 °C, with increasing conformational order upon rise in temperature. However, the dependence of the conformational order on the zirconia content is now reversed. Hence, sample **3F** with the higher zirconia content now exhibits a higher conformational order than sample **4F** with the higher silica content.

Quantitative information about the presence and amounts of various gauche conformers in the C₁₈ SAMs can be obtained by the analysis of the wagging band intensities between 1400 and 1330 cm⁻¹.^{76,155,157} The conformation dependent wagging modes of interest appear near 1368, 1353, and 1341 cm⁻¹ and arise from kink/gauche-trans-gauche (gtg), double gauche, and end-gauche sequences, respectively. The most intense band in the spectral range from 1300 to 1400 cm⁻¹ is due to the methyl group umbrella deformation mode at 1378 cm⁻¹, which is insensitive to the conformational order and which is used as an internal reference (see experimental section). Bands attributed to specific gauche defect sequences are obtained through deconvolution of the spectra in this spectral range

using the three conformational sensitive wagging band and the methyl group umbrella deformation band, as described elsewhere.^{26,144,155-157}

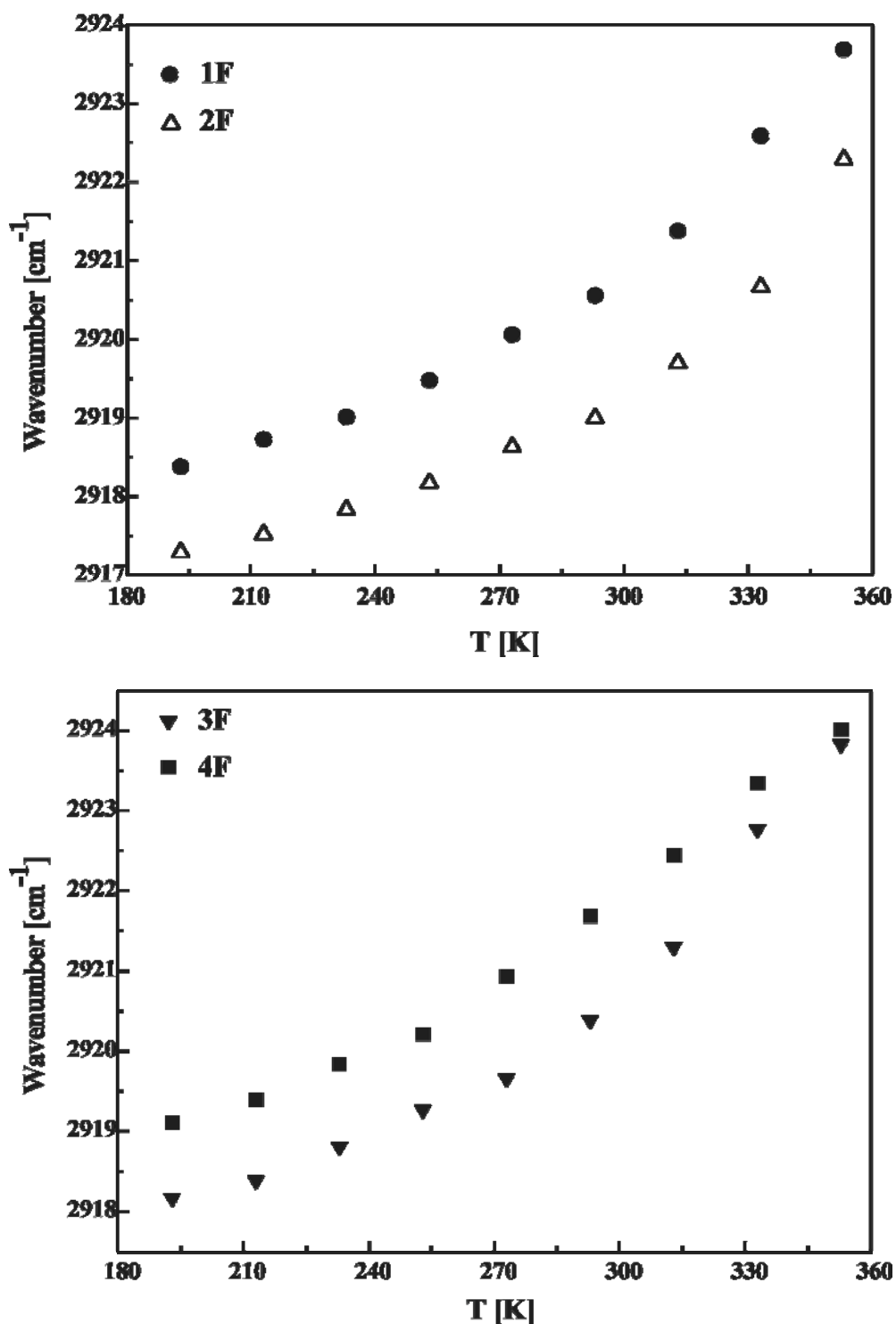


Figure 5.38. Temperature dependence of the antisymmetric CH₂ stretching band positions of samples 1F-4F.

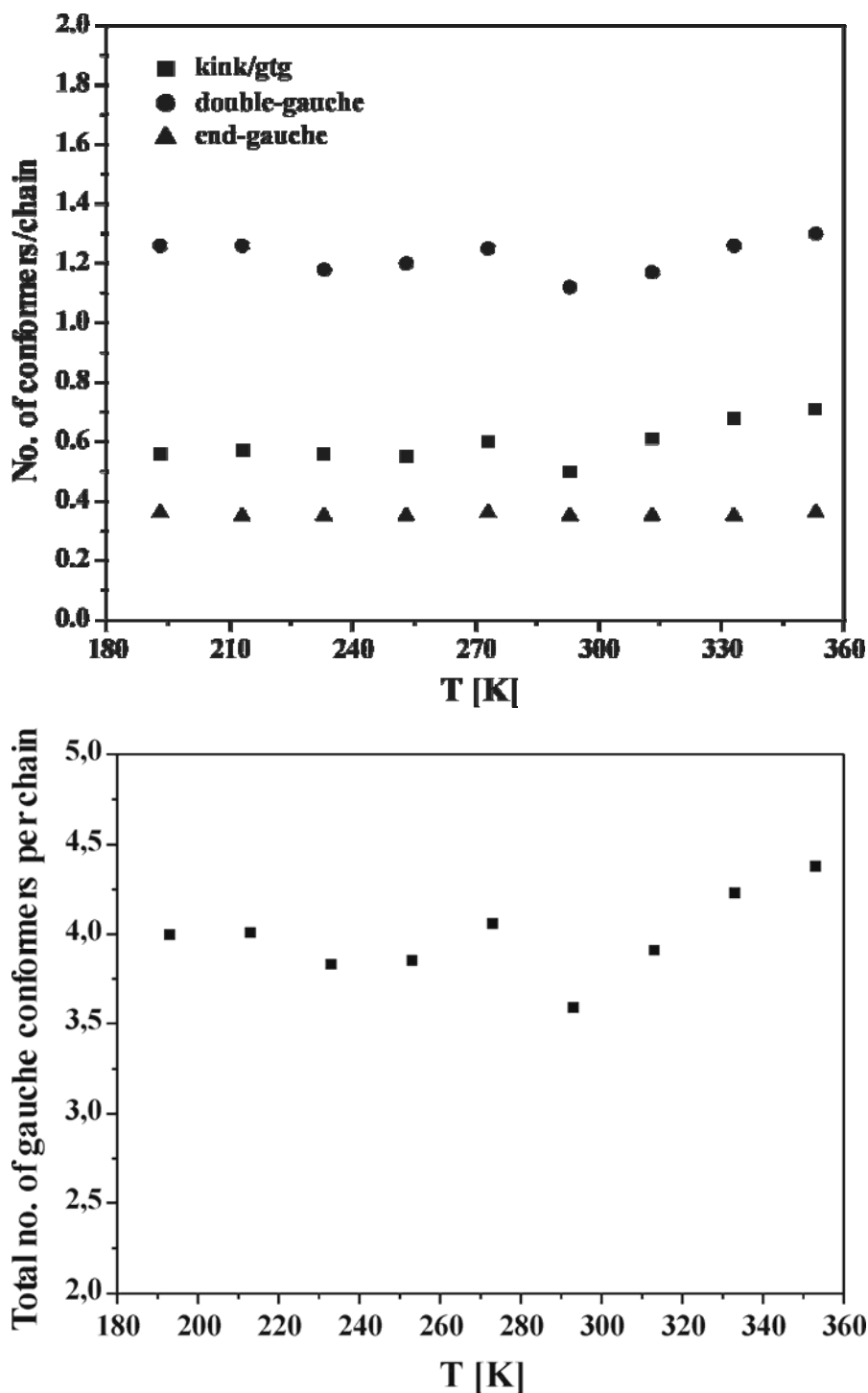


Figure 5.39. Number of kink/gtg, double-gauche, and end-gauche conformers per chain (top); Total number of gauche isomers per chain as a function of temperature (bottom) for sample **2F** from 193 K to 353 K.

The experimental FTIR spectra of sample **2F** for the whole temperature range are contrasted to its theoretical counterpart from the curve fitting analysis. The results obtained from the curve fitting analysis of the CH₂ wagging bands in terms of the

amounts of the kink/gtg, double gauche and end gauche conformers are summarized in Figure 5.39 (top). The number of end-gauche conformers per chain (0.35) remains almost unaffected by the sample temperature examined^{26,63} and the RIS model¹⁵⁶ developed for liquid *n*-alkanes, which predicts that the fraction of end-gauche conformers is independent of alkyl chain length and temperature, and is lower than the fraction of double-gauche and kink/gtg conformers. The trend for the increasing or decreasing of kink/gtg and double-gauche conformers are also independent with rising temperature. For instance, the number of kink/gtg conformers and double-gauche conformers per chain are in the range of 0.47 to 0.70 and 1.1 to 1.3 at temperatures between 193 and 333 K, respectively.

The total number of gauche conformers per chain is presented in Figure 5.39 (bottom). There is no clear trend in the amount of gauche conformers with increasing temperature and at both the lower and higher temperature extremes which indicates that the chains are highly mobile. In our earlier studies on C₁₈ alkyl modified silica gels, the amount of gauche conformers is very low and it increases with increasing temperature. In the present case, the number of gauche conformers is higher and it might be due to the presence of lower number of grafted alkyl chains on the surface in comparison to other systems studied earlier.^{26,63,65,66,224-226} Moreover, at room temperature it is surprising to note that the alkyl motions are more restricted. It should be noted that for samples **1F**, **3F** and **4F** the signal-to-noise ratio in the wagging band region was not resolved, and a similar wagging band analysis was therefore not possible.

5.5.7 SEM and EDX analysis of C₁₈ chains grafted on mixed oxides

SEM micrographs pertaining to samples **1F** and **3F** are shown in Figure 5.40. They show a compact substrate with some corrugated features. The former is associated with the mixed oxide phase while the latter is attributed to regions with the tethered C₁₈ chains. These observations are confirmed by the EDX analysis carried out for the same samples. The SEM micrographs reveal that the analyzed powders contain two different phases, the SiO₂-ZrO₂ mixed oxide phase, and sponge-like structures ascribable to the regions with grafted C₁₈ chains. A compact morphology analogous to the one of the present mixed oxide phase was recently observed in other (non-grafted) mixed oxide materials synthesised with the same synthetic route.¹³³ The peculiar sponge-like features were

found in all the alkyl grafted systems with small differences regarding the sponge distributions on the oxide supports. Actually, these sponge-like structures are further characterized by (i) a spot spreading on the oxide matrix, and (ii) a high porosity with respect to the supporting material.

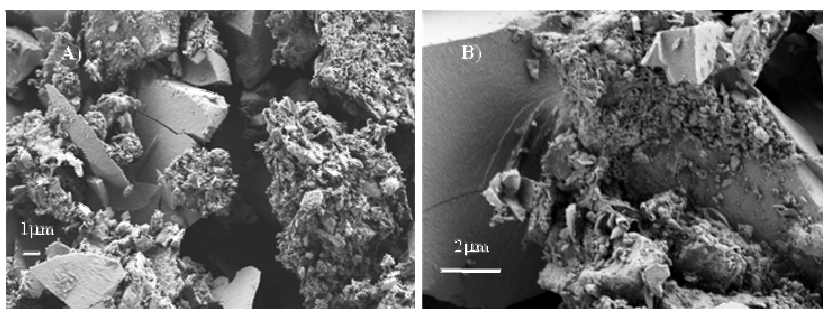


Figure 5.40. SEM micrographs pertaining to samples **1F** and **3F**.

EDX maps pertaining to samples **2F** and **4F** are presented in Figures 5.41 and 5.42 for a particular area in which Zr, Si, O and C analyses were made. They reveal a homogeneous distribution of zirconium in the bulk silica network, in tune with the XPS data, for both samples. On the other hand, carbon is not uniformly distributed and they are densely populated in some areas. It is further seen that sample **2F** contains larger areas of carbon than sample **4F**. This finding is consistent with the respective surface coverages for these samples (see Table 4.7).

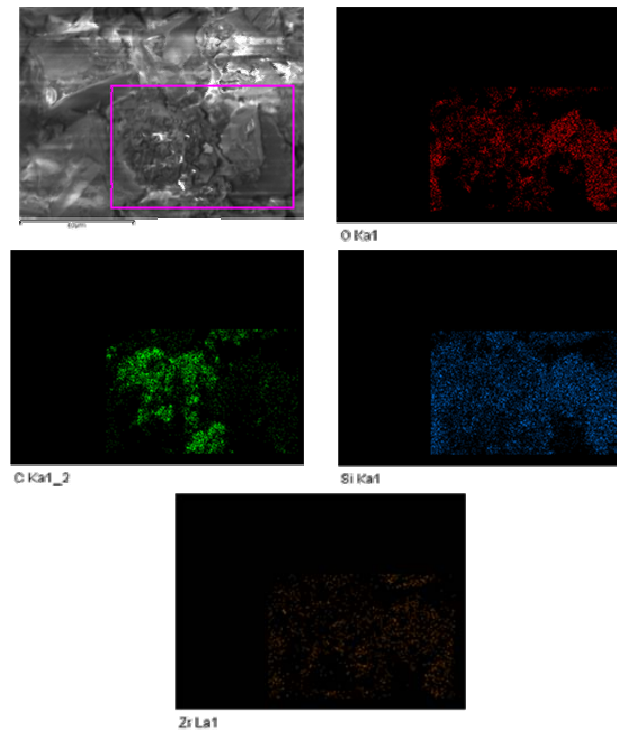


Figure 5.41. EDX maps carried out at an acceleration voltage of 10kV and relative to a restricted area of sample **2F**.

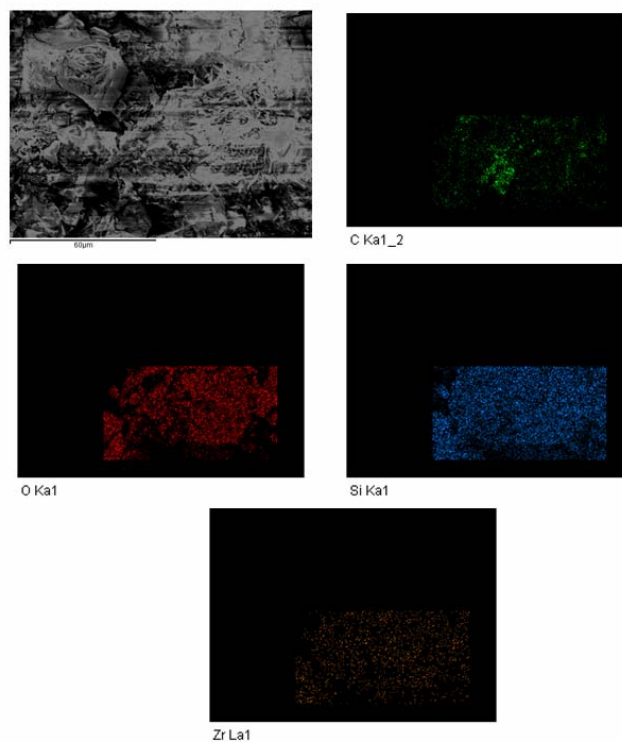


Figure 5.42. EDX maps carried out at an acceleration voltage of 10kV and relative to a restricted area of sample **4F**.

5.5.8 Effect of mixed oxide substrates and silylating agent on chain assembly and conformational order

Alkyl chain packing and conformational order are known to affect the enhanced shape selectivity for geometrical isomers in chromatographic separations^{26,50,63} and their applications in electronics,²²⁷ biological interfaces²²⁸ and catalysis.²²⁹ In the present work, alkyl chain conformational order was studied by variable temperature FTIR spectroscopy and ¹³C NMR spectroscopy at room temperature which provided consistent results. Upon inspection the ¹³C NMR spectra and the CH₂ stretching band positions at room temperature, it is found that the alkyl chain conformational order follows the sequence **2F** > **1F** ~ **3F** > **4F**.

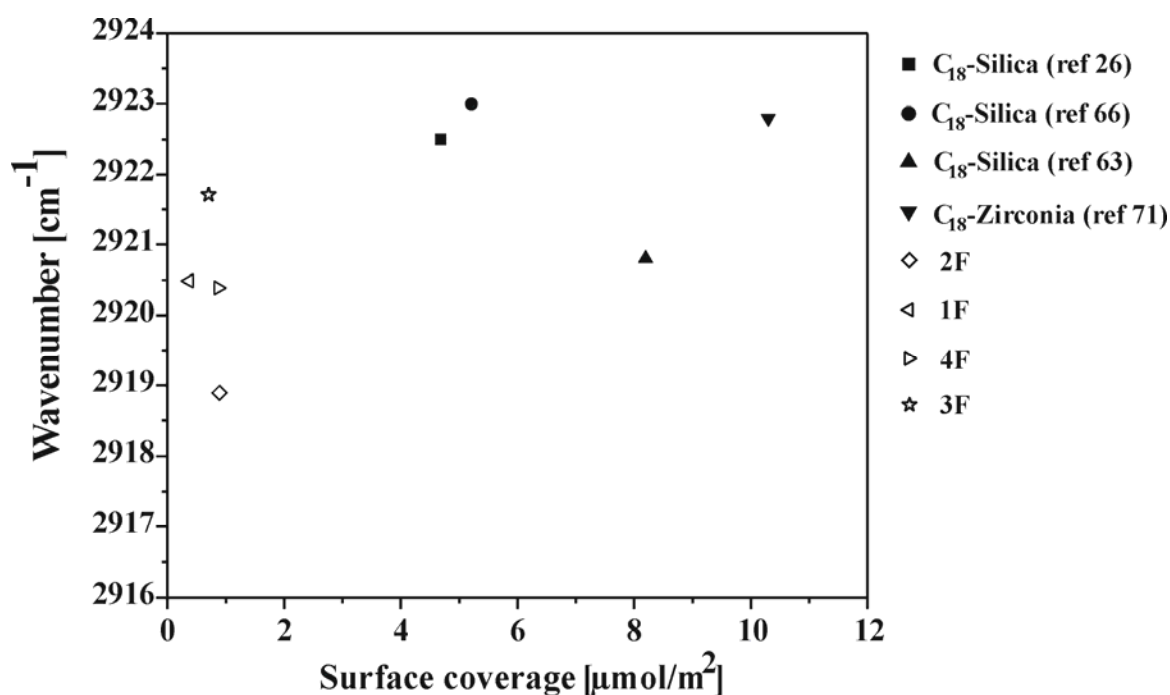


Figure 5.43. The antisymmetric CH₂ stretching band positions of C₁₈ and C₃₀ alkyl chains on silica and zirconia compared with C₁₈ alkyl chains on silica-zirconia mixed oxides at 293 K as a function of surface coverage.

Table 5.12 and Figure 5.43 provide further information regarding the surface coverage, solid substrates, alkyl chain length and conformational order, expressed by the CH₂ antisymmetric stretching band position at 293 K, by comparison with representative

literature data.^{11,26,63,65,71} It is seen that there exists no simple relationship between surface coverage and alkyl conformational order. However, pure silica and zirconia based C₁₈ SAMs generally show higher conformational disorder than the present mixed oxide C₁₈ SAMs, irrespective of the higher surface coverages of the former ones.^{26,63,71} The C₁₈ mixed oxide SAMs are even conformationally more ordered than the C₃₀ silica SAMs.⁶⁵ It should be noted that for a high grafting density the alkyl motions are spatially constrained as a consequence of increased van der Waals interactions resulting in higher conformational order.²²²

Table 5.12. Details of the various C₁₈ alkyl grafted substrates from the present and previous studies.

Type of substrate	Reference	Preparation route (polymerization)	Surface coverage (μmol/m ²)
Silica	26	Solution	4.68
Silica	66	Surface	5.21
Silica	63	Surface	8.20
Zirconia	71	Solution	10.3
1F	Present work	Surface	0.38
2F	“	Surface	0.89
3F	“	Surface	0.87
4F	“	Surface	0.70

A comparison of the observations in this study, for instance, with the results from solid-state ¹³C NMR studies on C₃₀ polymeric silica phases⁶² reveals that in those cases less trans conformers exist than for sample **2F**. These systems are even comparable to all-trans chains in C₁₈ alkanethiol on gold²²⁶ and C₁₈ phosphonic systems on zirconated silica.²²⁵

It is very striking that the present mixed oxides show an unusual high alkyl chain conformational order despite the much lower surface coverage than for the other alkyl grafted systems, given in Figure 5.43. Thus for the present systems, the surface coverage follows the order **2F** > **3F** > **4F** > **1F** which is not consistent with the derived sequences for the conformational order as discussed above. Hence, there are other factors such as different amounts of surface hydroxyl groups due to different calcination temperatures,

surface properties, etc., affect the alkyl chain conformational order and are discussed below in detail. Similar trend was observed earlier for the alkyl modified metal oxide SAMs in which the surface coverage and conformational order does not correlate with each other and it was found that the porous features of the metal oxides play a certain role for this behavior.⁷¹

Similar to the earlier observation on metal oxide SAMs,⁷¹ the higher conformational order of the alkyl chains on these mixed oxides inspite of lower surface coverage is due to the presence of microporous structure in these oxides. The cross-sectional area of the C₁₈ chain molecules is about 20 to 22 Å² and the length of the chain is about 23 Å. The alkyl chains assemble at the outer surface and at the pore entrance of these oxides along with cross-linking of neighboring silanes resulting in a closely-packed alkyl arrangement which give rise to higher conformational order as deduced from ¹³C NMR and FTIR data. The C₁₈ ligands are unable to diffuse into the available micropores. While in the case of silica gels, the available surface area and pore volume of silica is about (100-300 m²/g, 0.6-1.0 mL/g) and hence the alkyl chains does not have a closer arrangement on the surface, leading to lower conformational order unless other methods are employed to attain the higher surface coverage.

The difference in amounts of hydroxyl groups on the silica and zirconia on the mixed oxide surface is another reason for the difference in surface coverage on these modified samples. Table 5.8 shows that for samples with the higher silica content (**2** and **4**) irrespective of the annealed temperature, lower amount of silanol groups were present and it implies that there was a higher degree of condensation in these samples. After the humidification of all these mixed oxides **1-4**, an increase in the amount of the silanol groups was observed. This indicates that there should be also an increase in the amount of zirconia hydroxyl groups. Consequently after the grafting, the amount of silanol groups (Q³ groups) was reduced due to the grafting of alkyl chains on the surface especially for 600 °C calcined samples (**1** and **2**). Earlier studies on heat treated silica estimated that approximately half the silanol groups are removed at 550 °C, but most of the remaining hydroxyl groups are still in the neighbourhood of another hydroxyl group.²³⁰ Since these groups are not isolated, hydrogen bonding of a water molecule to the surface hydroxyl group is possible which generates more hydroxyl groups and results in higher surface coverage.

Sample **2F** has a higher surface coverage and conformational order when compared to sample **1F** inspite of having lower silanol groups. This shows that higher amount of zirconia hydroxyl groups are present **2F** which are very stable at 600 °C. Another important reason for this behavior is due to the higher amount of micropores, which leaves more outer surface for the dense and closer-packing of the alkyl chains (see Tables 4.6 and 4.7).

For samples **3** and **4**, due to calcination at higher temperature (800 °C), a very low amount of silanol groups was present and the surface modification occurs on the zirconia hydroxyl groups present (Table 5.8).¹³³ It should be noted that the surface polymerization also play a major role for the obtained surface coverage for these modified samples (**1F-4F**) as mentioned in section 5.5.2. It also explains the fact that the zirconia hydroxyl groups are very stable even at higher temperatures. As expected, the samples **3F** and **4F** contains lower amount of surface coverage with respect to samples **1F** and **2F**. This can be easily evident from the EDX maps of the samples **4F** (Figure 5.42) when compared to sample **2F** (Figure 5.41). Sample **4F** have lower surface coverage to sample **3F**, since the amount of silanol groups was lower in sample **4**, as discussed above. The effect of calcination at higher temperature (800 °C) can be understood on the basis of an early study on the silica surface, in which there is only isolated silanol groups on the surface when calcined beyond 750 °C.²³¹ If this fact is applied to the present study, only isolated silanol groups will be present at 800 °C and it would limit the hydrogen bond formation with the neighboring hydroxyl group which results in fewer number of alkyl chains. Hence the sample **4F** contains lesser carbon content than sample **2F** as seen from the EDX maps.

Still it is very surprising to observe the surface coverage values for samples **3F** and **4F** are higher with lower amount of hydroxyl groups and the values are closer to sample **2F**. This can be explained by the presence of lower values of surface area and pore volume of the samples **3** and **4**, which are calcined at 800 °C when compared to samples **1** and **2**. This leaves a smooth surface which is responsible for the closer packing of alkyl chains in samples **3F** and **4F**. The reason behind the higher conformational order of sample **1F** inspite of its lower surface coverage is not clear. It may be due to the presence of considerable amount of micropores to that of the latter samples and closer proximity of

hydroxyl groups in which the alkyl chains are closely packed resulting in higher conformational order.

The reason ascribable to the opposite trend observed for the increase in conformational order for the high silica content samples at 600 and 800 °C substrates are quite clear. It is due to the presence of higher microporosity of sample **2** which leads to closer packing of alkyl chains as evident from the EDX pictures of sample **2F** showing higher carbon density in several portions of the sample area (Figure 5.41) when compared to sample **4F** (Figure 5.42).

However, the role of heterogeneous surface of zirconia in these mixed oxides cannot be ruled out and there is no strong evidence to prove their role on the assembly of alkyl chains except the low field shift of for carbons C-1 and C-18 as discussed in section 5.5.5. In addition, pyridine adsorption followed by DRIFT measurements were made to ascertain the nature of the surface of these mixed oxide substrates.²³² It was found that there were several acidic sites present on these mixed oxides. But how far they played the role during the alkyl modification remains to be investigated for the better understanding with the insitu studies of the grafting process.

Thus the degree of condensation of the hydroxyl groups on the silica and zirconia surface during the evolution of these mixed oxides, the presence of microporous structure at different molar ratios of these oxides, surface polymerization approaches collectively play a major role in the achieved higher surface coverage of the alkyl chains and in turn higher conformational order of the immobilized alkyl chains. From this study, it is learnt that alkyl modification of these mixed oxides with decrease or increase in zirconia and silica amount, calcination temperature, different modifying methods to increase the degree of hydrophilicity-to-hydrophobicity which will find many applications especially in catalysis, separation media, sensors, etc.

5.5.9 Summary

C₁₈ alkyl chains were grafted on various silica-zirconia mixed oxide supports using *n*-octadecyltrichlorosilanes and characterized by means of XPS, FTIR, solid-state NMR, SEM and EDX techniques. ²⁹Si single-pulse MAS NMR measurements provided the

information that different amount of silanol and zirconia hydroxyl groups on the surface before and after the surface modification. ^{29}Si CP/MAS measurements revealed the degree of cross-linking of silanes after the modification step. ^{13}C CP/MAS NMR studies distinguish among the regions containing all-trans chains and the regions with conformationally disordered chains, containing gauche bonds. FTIR study shows that the conformational disorder of the C_{18} alkyl chains increases with increasing temperature on all the grafted mixed oxide substrates. The conformational order information from FTIR and ^{13}C CP/MAS NMR spectroscopic techniques is pretty much comparable. CH_2 wagging band analysis provides the amount of various gauche conformers present at wider temperature range but not in complete agreement with the CH_2 stretching data.

Surface polymerization technique provided in general the more surface coverage of alkyl chains on these mixed oxide systems. The annealed temperature for the preparation of the mixed oxides and the presence of different amounts of the individual oxide systems determines the surface properties (porosity, amount of hydroxyl groups and acidity-basicity) and in turn the alkyl chain assembly on these systems. An unusual high conformational order is observed for the grafted C_{18} alkyl chains irrespective of the lower surface coverage than for the other alkyl grafted systems. The unmodified mixed oxide samples were shown to have the microporous structure, in which the alkyl chains grafted on the external surface providing a dense and closer-packing of alkyl chains on the surface with higher conformational order. EDX analysis of the grafted samples shows the effect of annealed temperature on the coverage of alkyl chains on these hybrid mixed oxides. The present study provides the way to prepare oxides in different proportions and with different coverage of alkyl moieties, which paves the way for using these inorganic-organic hybrid systems for emerging applications of SAMs in various fields.

Chapter 6

6 Summary

Silica gels are successfully used as stationary phase for separations in adsorption chromatography as they are very stable at high pressure, and they yield reproducible separation efficiencies. However, unmodified silica spheres are amorphous, and have low surface area and broad pore size distribution. They also have certain limitations, such as adsorptivity towards basic analytes due to interactions with the silanol groups as well as lack of pH stability. In this dissertation, mesoporous MCM-41 silica spheres with high surface area and narrow pore size distribution were synthesized and characterized using various techniques. Likewise, detailed studies of alkyl grafted metal oxides and mixed oxides are presented. These latter systems provide an alternative to silica based stationary phase materials since, as they exhibit high mechanical stability, separation efficiency and chemical inertness at elevated temperatures and over the entire pH range.

The development of covalently bonded alkyl stationary phases is one of the most important advances in the field of chromatography that lead to the growth of reversed-phase high-performance liquid chromatography (RP-HPLC) as a widely used separation technique. In this dissertation, conventional amorphous and ordered MCM-41 silica, metal oxides (titania, hafnia, alumina, and zirconia) and silica-zirconia mixed oxides were grafted with octadecyl chains, using different silylating agents and employing various preparation routes. Several physico-chemical techniques were employed to determine the mesoporosity, morphology, grafting and organization of alkyl chains on these inorganic oxide substrates. From small angle X-ray scattering experiments and nitrogen sorption isotherms the pore size, pore volume and surface area were derived. Scanning electron microscopy measurements provided the morphological features of the particles. The elemental composition was determined by elemental and XPS analysis.

Solid-state ^{29}Si NMR spectroscopy was employed to probe the grafting and degree of cross-linking of the alkyl chains on these substrates. Recent studies have cleared that the conformation features, chain dynamics and their concomitant effects on retention and selectivity depend on various factors such as alkyl chain lengths, surface coverage, supporting material, temperature and pressure, etc. The conformational order, chain

length and chain packing of the *n*-alkyl chains are known to play a dominant role in determining the separation performance of the chromatographic phases. Therefore, Fourier transform infrared spectroscopy – through analysis of the symmetric and antisymmetric CH₂ stretching bands – was used to get information about the conformational order of the alkyl chains. In addition, solid-state ¹³C NMR spectroscopy provided independent information about the conformation and mobility of the surface-attached alkyl ligands and other organic components.

In the first part, the effect of the mobile phase and temperature on the conformational order of C₃₀ alkyl modified silica gel was investigated using FTIR spectroscopy at variable temperatures. Polar solvents showed both enhanced conformational order and disorder of the alkyl chains – irrespective of temperature – when compared to dry C₃₀ alkyl modified silica gels, while nonpolar solvents in general give rise to enhanced conformational disorder in the alkyl chain region. Both partition and adsorption models were considered to play an important role for the solvent-alkyl chain interactions which in turn determines the conformational order of the alkyl chains and thus the chromatographic properties of these phases.

In the next part, mesoporous MCM-41 silica spheres were obtained by using commercial Kromasil and ProntoSIL silica spheres via the pseudomorphic synthesis. SAXS and nitrogen sorption isotherms of MCM-41 spheres prepared from ProntoSIL silica showed a trimodal pore size distribution, whereas the MCM-41 spheres from Kromasil silica were highly ordered with practically uniform mesopores. The resulting MCM-41 spheres were grafted with three different silylating agents, mono- and trifunctional octadecylsilanes and subsequent endcapping using hexamethyldisilazane. Grafting was successfully done with either direct route or by surface polymerization. The mesoporosity of the MCM-41 spheres was retained after alkyl grafting in all the samples. In addition, a long-range disorder of the mesoporous structure and distinct reduction of surface area and pore volume has been observed.

Alkyl chain grafting and chain cross-linking on these MCM-41 spheres were examined by ²⁹Si and ¹³C NMR spectroscopy. FTIR and ¹³C NMR measurements revealed a rather low conformational order of the grafted octadecyl chains containing gauche bonds. C₁₈ alkyl chains grafted by using *n*-octadecyltrimethoxysilanes were conformationally more

ordered when compared to the materials obtained from modification with *n*-octadecyltrihydrosilanes, which correlated with the higher surface coverage of the former ones. The combination of solvent extraction for the MCM-41 preparation and surface polymerization for surface modification was found to result in higher surface coverage along with a higher degree of conformational order of the alkyl chains. Nevertheless, for the present samples only a relatively low surface coverage and low conformational order of the attached alkyl chains was achieved when compared to alkyl modified amorphous silica gels. These findings were traced back to the relatively lower number of silanol groups, small diameter of the mesopores and pore blocking effects due to the usage of relatively long octadecyl chains.

Furthermore, owing to certain limitations of the silica gels, C₁₈ alkyl grafted metal oxides were prepared from oxides like titania, zirconia, hafnia, and alumina using two types of silylating reagents, *n*-octadecyltrihydrosilanes and *n*-octadecyltrichlorosilanes. The cross-linking of the silanes during the surface modification through vertical polymerization was revealed through FTIR and ²⁹Si CP/MAS measurements. In the ¹³C CP/MAS NMR spectra regions with all-trans chains and regions with conformationally disordered chains, containing gauche bonds, could be distinguished. FTIR studies provided information about the conformational order of the alkyl chains through the analysis of the CH₂ stretching data, and the order decreased with increasing temperature for all the grafted samples. Grafting with *n*-octadecyltrichlorosilane showed a higher degree of conformational order than grafting with *n*-octadecyltrihydrosilane.

The derived results on conformational order and surface coverage on metal oxides were discussed on the basis of the available amount of surface hydroxyl groups, porosity of the metal oxide support, the reactivity of the silylating reagents and the reaction scheme used during the grafting step. The conformational order of the C₁₈ alkyl chains grafted on metal oxides was higher than in silica based systems, and was attributed to the lower porosity of the metal oxide supports along with a closer and dense packing of alkyl chains. Differences in the conformational order for the different metal oxide supports were traced back to the presence of island structures for the grafted alkyl chains.

In the final part, silica–zirconia mixed oxide substrates were prepared and grafted with C₁₈ alkyl chains using *n*-octadecyltrichlorosilane. The surface properties and Si/Zr molar

ratios were determined by nitrogen physisorption and XPS, respectively. ^{29}Si MAS NMR measurements revealed the degree of cross-linking of the silanes. From ^{13}C CP/MAS NMR and FTIR spectroscopy information about the conformation and mobility of the surface-immobilized alkyl chains was obtained. SEM and EDX measurements provided the morphological features of the solid substrates and information about the elemental distribution of the alkyl grafted mixed oxide surfaces. The annealing temperature for the preparation of the mixed oxides and the presence of different amounts of the individual oxide systems determined the surface properties (amount of hydroxyl groups and porosity), and in turn the alkyl chain assembly on these systems. An unusual high conformational order was observed for the grafted C_{18} alkyl chains irrespective of the lower surface coverage than for the other alkyl grafted systems. The unmodified mixed oxide samples were shown to have a microporous structure, in which the alkyl chains grafted on the external surface are densely packed resulting in higher conformational order.

In summary, it was demonstrated that the various inorganic supports like ordered mesoporous silica, metal oxides and mixed oxides can be used as alternative solid supports for the functionalization of the alkyl chains in alternative to the amorphous silica gels. Various physico-chemical techniques, like SAXS, nitrogen physisorption, SEM-EDX, XPS, FTIR and solid-state NMR, have shown to be powerful tools for the examination of these stationary phase materials. On the basis of the present investigations it can be stated that the surface properties (amount of hydroxyl groups and micro- and mesoporosity) of the inorganic substrates, type of silylating agents, and surface modification schemes play important roles in determining the surface grafting, conformational order and mobility of the alkyl chains in these stationary phase materials, which in turn determine their chromatographic and catalytic performance. An understanding of these materials on a molecular level in the presence of solvents, analytes and pressure under real chromatographic or catalytic conditions is necessary for the utilization of these materials for further applications.

Chapter 7

7 Zusammenfassung

Silikagele spielen eine wichtige Rolle als stationäre Trägerphasen in der Adsorptionschromatographie. Sie weisen in der Regel eine sehr gute Stabilität, auch unter erhöhtem Druck, auf und zeichnen sich durch eine gute Reproduzierbarkeit der erzielten Trennwirkung aus. Konventionelle, unbehandelte Silikagelpartikel sind amorph, besitzen eine geringe Oberfläche und zeigen eine breite Verteilung der Partikeldurchmesser. Es sind jedoch auch verschiedene Einschränkungen beim Einsatz dieser Materialien bekannt, wie beispielsweise bei der Verwendung basischer Analyte (wegen der Wechselwirkungen mit der Oberflächen-Hydroxylgruppen) oder bei Arbeiten unter extremen pH-Werten.

Im Rahmen dieser Dissertation wurden mesoporöse MCM-41-Silikagelkugeln, die sich durch eine große Oberfläche und durch geringe Porengrößenverteilung auszeichnen, hergestellt und umfassend charakterisiert. Ein weiterer Abschnitt der Arbeit widmete sich alkyloxy-modifizierten Metalloxiden und Mischoxiden, die sich durch eine erhöhte mechanische Stabilität, bessere Trennwirkung und verbesserte chemische Stabilität bei erhöhten Temperaturen auszeichnen, was auch den Einsatz über einen großen pH-Bereich einschließt.

Die Entwicklung von Stationärphasen mit an der Oberfläche kovalent gebundenen Alkylketten eröffnete das Gebiet der Umkehrphasen-HPLC (RP-HPLC), welches heutzutage ein weitverbreitetes und sehr effizientes Trennverfahren darstellt. Im Rahmen dieser Arbeit wurden MCM-41 Materialien, Metalloxide (Zirkondioxid, Hafniumdioxid, Aluminiumoxid und Titandioxid) und Mischoxide, bestehend aus Siliziumdioxid und Zirkoniumdioxid, unter chemischer Anbindung von Octadecylsilanen oberflächenmodifiziert, wobei verschiedene Silylierungsreagenzien und Präparationstechniken zum Einsatz kamen. Verschiedene physikalisch-chemische Messmethoden lieferten Aussagen über die Porosität, Morphologie sowie über Anbindung und Organisation der Alkylketten auf den verschiedenen anorganischen Substraten. Mittels Röntgenkleinwinkelstreuung und Stickstoffsorptions-Experimenten wurden Porengröße, Porenvolumen und Teilchenoberfläche bestimmt. Rasterelektronenmikroskopische Untersuchungen lieferten Aussagen über die

morphologische Beschaffenheit der Proben, während die Probenzusammensetzung aus der chemischen Elementanalyse und XPS-Messungen ermittelt wurden.

Festkörper ^{29}Si NMR-Messungen dienten primär der Bestimmung der Oberflächenanbindung der Alkylketten sowie der Quernetzung der Ketten während der chemischen Anbindung. Aus früheren Untersuchungen war bekannt, dass die Alkylkettenkonformation und -dynamik von verschiedenen molekularen Parametern, wie Alkylkettenlänge, Oberflächenbeladung, Art des verwendeten anorganischen Trägers, Temperatur, Druck, etc. abhängen. Ferner war festgestellt worden, dass die Konformationsordnung, Kettenlänge und Kettenpackung einen wichtigen Einfluss auf das makroskopische Verhalten (d.h. Trennwirkung) dieser Trennphasen haben. Deshalb wurden im Rahmen dieser Arbeit IR-spektroskopische Verfahren zur Bestimmung der Konformationsordnung eingesetzt. Unabhängige Aussagen zur Alkylkettendynamik und -konformationsordnung waren zudem aus ^{13}C NMR-Messungen zugänglich.

Im ersten Abschnitt der Arbeit ging es um den Einfluss der mobilen Phase (d.h. Lösungsmittel) und der Temperatur auf das Konformationsverhalten von C_{30} -modifizierten Silikagelen, wobei im Wesentlichen temperaturabhängige FTIR-Messungen durchgeführt wurden. Polare Lösungsmittel zeigten - im Vergleich zu den trockenen Silikagelen - sowohl erhöhte als auch erniedrigte Konformationsordnungen der gebundenen Alkylketten, während unpolare Lösungsmittel generell zu einer Erniedrigung der Alkylkettenkonformation führten. Es zeigte sich, dass verschiedene Modellansätze („Verteilungsmodell“, „Adsorptionsmodell“) bei der Beschreibung der Lösungsmittel-Alkylketten-Wechselwirkungen herangezogen werden müssen. Es ist offensichtlich, dass diese Wechselwirkungen für das Konformationsverhalten der gebundenen Alkylketten in diesen Trägermaterialien verantwortlich sind und damit letztlich deren chromatographischen Trenneigenschaften bedingen.

Im zweiten Abschnitt der Arbeit wurden mesoporöse MCM-41-Kugeln über eine pseudomorphe Synthese, unter Verwendung von kommerziellen Silikagel-Kugeln (Kromasil und ProntoSIL), hergestellt. Aus den Röntgenkleinwinkel- und Stickstoffadsorptions-Messungen an den aus ProntoSIL hergestellten Proben ließ sich eine trimodale Porengrößenverteilung nachweisen, während sich bei Verwendung von Kromasil als Silikagelquelle MCM-41 Materialien mit hoch geordneten und einheitlichen

Poren erzielen ließen. Die MCM-41-Kugeln wurden mit mono- bzw. trifunktionalen Octadecylsilanen und anschließend mit Hexadecylsilazan oberflächenbehandelt, wobei zwei unterschiedliche Präparationstechniken verwendet wurden. Es zeigte sich, dass der mesoporöse Charakter der Proben auch nach der Oberflächenbehandlung erhalten bleibt. Allerdings steigt die „langreichweitige“ Unordnung und die Oberfläche bzw. das Porenvolumen nimmt ab.

Die Alkylkettenanbindung und Quervernetzung an der MCM-41-Oberfläche wurden mittels ^{13}C und ^{29}Si NMR-Spektroskopie bestimmt. FTIR und ^{13}C NMR-Messungen zeigten eine relative geringe Konformationsordnung der gebundenen Octadecylketten. Bei Verwendung des Silylierungsmittels *n*-Octadecyltrimethoxysilan wurden besser geordnete Ketten vorgefunden als bei der Herstellung mit *n*-Octadecyltrihydridosilan, was letztlich mit den unterschiedlichen Oberflächenbeladung in Beziehung gebracht werden kann. Die höchste Oberflächenbeladung und demzufolge die größte Konformationsordnung der Octadecylketten fand man bei der MCM-41-Materialien, die durch Lösungsmittlextraktion hergestellt und mit anschließender Oberflächenpolymerisation beladen wurden. Die im Vergleich zu normalen Silikagelen geringere Oberflächenbeladung wurde auf die geringere Anzahl von Silanolgruppen, den kleineren Porendurchmesser und der damit verbundenen Blockierung der Poren für die relativ langen Octadecylketten zurückgeführt.

Ein weiterer Abschnitt der Arbeit widmete sich der Untersuchung von mit Octadecylketten beladenen Metalloxiden (Titandioxid, Zirkondioxid, Hafniumdioxid und Aluminiumoxid), wobei zur Herstellung zwei Silylierungsreagenzien - *n*-Octadecyltrihydridosilan und *n*-Octadecyltrichlorsilan - verwendet wurden. Die Anbindung der Ketten an die Metalloxidoberfläche und das Ausmaß an Quervernetzung senkrecht zur Oberfläche wurde mittels FTIR und ^{29}Si NMR-Messungen untersucht. Aus den ^{13}C NMR-Spektren konnten Bereiche mit hoch geordneten all-trans-Ketten und Bereiche mit ungeordneten Alkylketten mit hohem gauche-Anteil nachgewiesen werden. Mittels FTIR-Messungen konnte eine zunehmende konformative Unordnung der Alkylketten mit zunehmender Temperatur nachgewiesen werden. Nach der Oberflächenbehandlung mit *n*-Octadecyltrichlorsilan wurde durchweg eine höhere Konformationsordnung der Ketten gefunden als bei den Metalloxidproben, die unter Verwendung von *n*-Octadecyltrihydridosilan hergestellt wurden.

Diese Ergebnisse für die oberflächenbehandelten Metalloxide hängen mit der Zahl der zur Verfügung stehenden Hydroxylgruppen, der Porosität der anorganischen Trägermaterialien, der Reaktivität der Silylierungsreagenzien und dem Herstellungsverfahren zusammen. Generell zeigte sich bei den hier untersuchten modifizierten Metalloxiden eine gegenüber konventionellen Silikagelen erhöhte Alkylkettenkonformationsordnung, was mit der geringeren Porosität der Metalloxide und der dichteren Packung der Alkylketten zusammenhängt. Zusätzliche Variationen in der Alkylkettenkonformationsordnung wurden mit dem Auftreten von Inselstrukturen für die oberflächengebundenen Alkylketten in Zusammenhang gebracht.

Im letzten Abschnitt der Arbeit wurden Mischoxide mit unterschiedlichem Anteil an Siliziumdioxid und Zirkondioxid mit Octadecylketten beladen und untersucht. Die Oberflächeneigenschaften und das Si/Zr-Verhältnis der Materialien wurden mittels Stickstoffsorptions- und XPS-Messungen bestimmt, während ^{29}Si NMR-Spektren den Vernetzungsgrad der gebundenen Silane lieferten. Das Konformationsverhalten der gebundenen Alkylketten wurde aus ^{13}C NMR- und FTIR-Messungen ermittelt. Die morphologischen Eigenschaften der Substrate und der Elementverteilung auf der Oberfläche wurden mittels SEM- und EDX-Verfahren bestimmt. Es zeigte sich, dass die Auslagerungstemperatur bei der Herstellung der Mischoxide die Oberflächeneigenschaften der Proben (Zahl der Hydroxylgruppen, Porosität) bestimmt, was direkte Auswirkungen auf die Anordnung der Alkylketten auf der Oberfläche hat. Allgemein beobachtete man eine außergewöhnlich hohe Konformationsordnung der Ketten bei vergleichsweise geringer Oberflächenbeladung. Die Mischoxide sind mikroporös, d.h. die Octadecylketten können praktisch nicht in die Poren eindringen. Demzufolge sind die gebundenen Alkylketten an der noch zugänglichen Oberfläche relativ dicht gepackt, was die hohe Alkylkettenkonformation erklärt.

Zusammenfassend lässt sich feststellen, dass die hier untersuchten Materialien – mesoporöse Silikagele, Metalloxide, Mischoxide - grundsätzlich eine Alternative für die heute eingesetzten chromatographischen Trägermaterialien darstellen. Ebenfalls sind die hier eingesetzten experimentellen Messtechniken, wie Kleinwinkelstreuung, Stickstoffsorption, SEM, EDX, XPS, FTIR- und Festkörper-NMR-Spektroskopie, geeignete Verfahren zur Charakterisierung solcher Stationärphasen. Die hier

durchgeführten Untersuchungen zeigten, dass die Oberflächeneigenschaften (Zahl der Hydroxylgruppen, Porosität) der anorganischen Substrate, das Silylierungsreagenz sowie das Herstellungsverfahren zur Oberflächenmodifizierung in entscheidender Weise die Oberflächenbeladung, die Konformationsordnung und die Mobilität der gebundenen Alkylketten bei diesen Stationärphasen bedingen, was sich wiederum auf die chromatographischen Eigenschaften auswirkt. Eine genaue Kenntnis der molekularen Eigenschaften dieser Materialien unter realistischen Bedingungen, d.h. in Gegenwart von Lösungsmittel, Analyten und unter Druck, ist Grundvoraussetzung für eine zielgerichtete Modifikation der Materialeigenschaften im Zusammenhang mit zukünftigen, spezifischen Anwendungen im Bereich der Chromatographie oder auch der Katalyse.

List of Figures

Figure 2.1. SEM micrographs of 5 μm silica spheres at varying degrees of magnification.....	14
Figure 2.2. Structure of MCM-41 material.....	15
Figure 2.3. Dependence of the phase structure from the concentration of surfactant.....	16
Figure 2.4. Mechanistic pathway of the formation of MCM-41 materials.....	16
Figure 2.5. Representative structure of the C_{18} alkyl grafted stationary phases. Top – Phases formed from the monochlorosilane, Bottom – Phases formed from the trichlorosilane.....	22
Figure 2.6. Diagram distinguishing two approaches to the synthesis of polymeric stationary phases. Silane polymerization occurs in solution or at the silica surface depending on the order of addition of reagents.....	24
Figure 2.7. Schematic drawing of endcapped silica gels after grafting with mono- and tri-functional C_{18} chains.....	25
Figure 3.1. Antisymmetric and symmetric CH_2 stretching band spectra for alkyl chains grafted on titaniumdioxide using <i>n</i> -octadecyltrichlorosilanes between 193 K and 353 K.....	28
Figure 3.2. Alkyl chain conformations from CH_2 wagging band region. The non-planar conformations give rise to localized mode vibrations, which are observed in FTIR spectra.....	29
Figure 3.3. Experimental IR spectrum of the CH_2 wagging band region for the C_{18} alkyl grafted MCM-41 at 293 K. The underlying curves result from a curve fitting analysis.....	30
Figure 3.4. Pulse sequence of Cross polarization (CP) technique.....	39
Figure 3.5. Different structural elements of the silicon species present in the C_{18} alkyl grafted silica systems.....	41
Figure 3.6. ^{29}Si NMR spectrum of the C_{18} alkyl grafted MCM-41 silica sphere with surface coverage of $1.65 \mu\text{mol}/\text{m}^2$	42
Figure 3.7. ^{13}C CP/MAS NMR spectrum of C_{18} alkyl chains grafted on alumina using <i>n</i> -octadecyltrichlorosilane.....	43
Figure 3.8. Newman projections illustrating the γ -gauche effect.....	44
Figure 3.9. SAXS pattern of the calcined MCM-41 silica and C_{18} alkyl grafted MCM-41 silica spheres.....	46

Figure 3.10. Nitrogen sorption isotherm of calcined MCM-41 silica spheres.....	48
Figure 3.11. SEM micrographs of the amorphous, MCM-41 silica spheres and C ₁₈ alkyl grafted MCM-41 silica spheres.....	53
Figure 5.1. Symmetric CH ₂ stretching bands of the dry C ₃₀ silica gels (C ₃₀) and C ₃₀ silica in various polar solvents at 293 K.....	68
Figure 5.2. Position of antisymmetric CH ₂ stretching bands as a function of solvent solvatochromic parameter, π^* , for dry C ₃₀ silica gels (C ₃₀) at 293 K as indicated by dashed lines (---). C ₃₀ phases in various polar and nonpolar solvents at 293 K are indicated by various symbols.....	69
Figure 5.3. Symmetric and antisymmetric CH ₂ stretching bands of C ₃₀ alkyl modified silica gels at different temperatures in ACN.....	70
Figure 5.4. Temperature dependence of the CH ₂ symmetric stretching (above) and antisymmetric stretching (below) band positions for dry C ₃₀ alkyl modified silica gels (C ₃₀) and in the presence of various polar solvents.....	71
Figure 5.5. Temperature dependence of the CH ₂ symmetric stretching (above) and antisymmetric stretching (below) band positions for dry C ₃₀ alkyl modified silica gels (C ₃₀) and in the presence of polar and nonpolar solvents.....	72
Figure 5.6. SAXS pattern of calcined MCM-41 silica, MF and TF samples.....	80
Figure 5.7. Nitrogen sorption isotherm of calcined MCM-41, MF and TF samples.....	81
Figure 5.8. BJH pore-size distribution of calcined MCM-41, MF and TF samples.....	82
Figure 5.9. SEM micrographs of prontoSIL silica and calcined MCM-41 silica spheres.....	85
Figure 5.10. ²⁹ Si CP/MAS NMR spectra of MF and TF samples at 293 K.....	87
Figure 5.11. ¹³ C CP/MAS NMR spectra of MF and TF samples at 293 K.....	89
Figure 5.12. Antisymmetric and symmetric CH ₂ stretching bands of MF and TF samples at 293 K.....	91
Figure 5.13. SEM micrographs of silica spheres of A) ProntoSIL; B) Kromasil; C) M3; D) M6M.....	94
Figure 5.14. SAXS pattern of calcined and solvent extracted MCM-41 silica from ProntoSIL (left) and Kromasil (right).....	95
Figure 5.15. BET isotherms and BJH pore-size distribution plots of MCM-41 silica spheres from ProntoSIL (top) and Kromasil (bottom).....	96

Figure 5.16. Schematic representation of direct grafting (A) and the surface polymerization approach (B). Please note that cross-linking of the silane molecules is not indicated.....	100
Figure 5.17. SAXS pattern of C ₁₈ grafted MCM-41 silica spheres.....	101
Figure 5.18. BET isotherms of C ₁₈ grafted MCM-41 silica spheres prepared using <i>n</i> -octadecyltrihydridosilane (top), and <i>n</i> -octadecyltrimethoxysilane (middle and bottom).....	103
Figure 5.19. ²⁹ Si NMR spectra of the ungrafted (M1) and grafted MCM-41 silica spheres with <i>n</i> -octadecyltrihydridosilane.....	106
Figure 5.20. ²⁹ Si NMR spectra of the ungrafted (M2) and grafted MCM-41 silica spheres with <i>n</i> -octadecyltrimethoxysilane.....	107
Figure 5.21. ¹³ C NMR spectra of MCM-41 silica spheres grafted with <i>n</i> -octadecyltrihydridosilane.....	109
Figure 5.22. ¹³ C NMR spectra of MCM-41 silica spheres grafted with <i>n</i> -octadecyltrimethoxysilane.....	110
Figure 5.23. Antisymmetric CH ₂ stretching bands of MCM-41 silica spheres at 293 K, grafted with <i>n</i> -octadecyltrihydridosilane and <i>n</i> -octadecyltrimethoxysilane.....	112
Figure 5.24. Temperature dependence of the antisymmetric CH ₂ stretching band positions for samples M4M and M6M.....	113
Figure 5.25. DRIFT spectra obtained after the exposure of bare TiO ₂ (—) and Ti(Cl) (····) particles to the pyridine+Ar mixture at RT. (A) Spectral region from 1410 to 1645 cm ⁻¹ ; (B) Spectral region from 3500 to 3780 cm ⁻¹	116
Figure 5.26. DRIFT spectra obtained at RT after exposure of the bare TiO ₂ (A) and Ti(Cl) (B) to pyridine+Ar mixture for 5 min (—) and successively to Ar for 1 min (—), 8 min (---) and 15 min, only for TiO ₂ particles (····). Spectral region from 1410 to 1700 cm ⁻¹	118
Figure 5.27. IR spectra for liquid <i>n</i> -octadecyltrihydridosilane (A) and <i>n</i> -octadecyltrihydridosilane grafted on hafnia (B) measured at 293 K.....	119
Figure 5.28. ²⁹ Si CP/MAS NMR spectra of metal oxide substrates grafted with <i>n</i> -octadecyltrichlorosilane (Cl) and <i>n</i> -octadecyltrihydridosilane (H).....	120
Figure 5.29. Reaction of <i>n</i> -octadecyltrichlorosilane (A) and <i>n</i> -octadecyltrihydridosilane (B) with metal oxides (based on grafting density).....	121

Figure 5.30. Antisymmetric and symmetric CH ₂ stretching band spectra between 193 K and 353 K for titaniumdioxide modified with <i>n</i> -octadecyltrihydrosilanes, Ti(H).....	123
Figure 5.31. Temperature dependence of the antisymmetric (above) and symmetric (below) CH ₂ stretching band positions for alkyl chains grafted on four different metal oxide substrates using <i>n</i> -octadecyltrichlorosilanes.....	124
Figure 5.32. Temperature dependence of the antisymmetric (above) and symmetric (below) CH ₂ stretching band positions for alkyl chains grafted on four different metal oxide substrates using <i>n</i> -octadecyltrihydrosilanes.....	126
Figure 5.33. ¹³ C CP/MAS NMR spectra of alkyl chains grafted on four different metal oxide substrates using <i>n</i> -octadecyltrichlorosilanes and <i>n</i> -octadecyltrihydrosilanes.....	127
Figure 5.34. XPS survey spectra of sample 3 before (a) and after (b) the functionalization (3F).....	136
Figure 5.35. ²⁹ Si CP/MAS NMR spectra of C ₁₈ alkyl grafted silica-zirconia mixed oxides using <i>n</i> -octadecyltrichlorosilane.....	137
Figure 5.36. ¹³ C CP/MAS NMR spectra of C ₁₈ alkyl grafted silica-zirconia mixed oxides using <i>n</i> -octadecyltrichlorosilane.....	140
Figure 5.37. Temperature dependence of the symmetric and antisymmetric CH ₂ stretching band spectra of sample 2F.....	142
Figure 5.38. Temperature dependence of the antisymmetric CH ₂ stretching band positions of samples 1F-4F.....	144
Figure 5.39. Number of kink/gtg, double-gauche, and end-gauche conformers per chain (top); Total number of gauche isomers per chain as a function of temperature (bottom) for sample 2F from 193 K to 353 K.....	145
Figure 5.40. SEM micrographs pertaining to samples 1F and 3F.....	147
Figure 5.41. EDX maps carried out at an acceleration voltage of 10kV and relative to a restricted area of sample 2F.....	148
Figure 5.42. EDX maps carried out at an acceleration voltage of 10kV and relative to a restricted area of sample 4F.....	148
Figure 5.43. The antisymmetric CH ₂ stretching band positions of C ₁₈ and C ₃₀ alkyl chains on silica and zirconia compared with C ₁₈ alkyl chains on silica-zirconia mixed oxides at 293 K as a function of surface coverage.....	149

List of Tables

Table 3.1. Conformation-sensitive IR modes used for <i>n</i> -alkyl chain conformational analysis.....	27
Table 4.1. Sample properties of grafted and endcapped MCM-41 silica.....	56
Table 4.2. Textural features of silica and MCM-41 silica spheres.....	58
Table 4.3. Octadecyl grafted MCM-41 silica samples used in this work.....	58
Table 4.4. Characteristics of metal oxides.....	59
Table 4.5. Grafting densities of C ₁₈ alkyl chains on metal oxides.....	60
Table 4.6. Mixed oxide supports used in this work and their textural features.....	61
Table 4.7. Characteristics of C ₁₈ alkyl modified mixed oxides.....	62
Table 5.1. Solvatochromic parameter, π^* , for the solvents used in the present study.....	67
Table 5.2. ²⁹ Si chemical shift values for grafted MCM-41 silica spheres.....	86
Table 5.3. ¹³ C chemical shift values for grafted MCM-41 silica spheres.....	88
Table 5.4. Textural features of octadecyl grafted MCM-41 silica spheres.....	99
Table 5.5. ²⁹ Si chemical shifts for octadecyl grafted MCM-41 silica.....	105
Table 5.6. ¹³ C chemical shifts for octadecyl grafted MCM-41 silica.....	109
Table 5.7. FTIR data of vibrational bands (cm ⁻¹) of liquid and adsorbed pyridine (vs = very strong; s = strong; m = medium; w = weak; v = variable) for comparison of the DRIFT measurements carried out in this study.....	117
Table 5.8. ²⁹ Si single pulse NMR chemical shift values after fitting the experimental spectra for mixed oxides, after humidification and their grafting with C ₁₈ alkyl chains.....	134
Table 5.9. Atomic percentages determined by XPS, before and after functionalization of mixed oxides with C ₁₈ alkyl chains.....	135
Table 5.10. ²⁹ Si chemical shifts for C ₁₈ chains grafted on silica-zirconia mixed oxides.....	138
Table 5.11. ¹³ C chemical shifts for C ₁₈ chains grafted on silica-zirconia mixed oxides.....	141
Table 5.12. Details of the various C ₁₈ alkyl grafted substrates from the present and previous studies.....	150

References

- [1] Y. Kazakevich, H. McNair, Basic Liquid chromatography http://hplc.chem.shu.edu/NEW/HPLC_Book/index.html (1996).
- [2] C.T. Kresge, M.E. Leonowicz, W.J. Roth, J.C. Vartuli, J.S. Beck, *Nature* 359 (1992) 710.
- [3] J.S. Beck, J.C. Vartuli, W.J. Roth, M.E. Leonowicz, C.T. Kresge, K.D. Schmitt, C.T.-W. Chu, D.H. Olson, E.W. Sheppard, S.B. McCullen, J.B. Higgins, J.L. Schlenker, *J. Am. Chem. Soc.* 114 (1992) 10834.
- [4] S. Lim, A. Ranade, G. Du, L.D. Pfefferle, G.L. Haller, *Chem. Mater.* 18 (2006) 5584.
- [5] Q. Huo, J. Feng, F. Schüth, G.D. Stucky, *Chem. Mater.* 9 (1997) 14.
- [6] M. Grün, A.A. Kungunov, S. Schacht, F. Schüth, K.K. Unger, *J. Chromatogr. A* 740 (1996) 1.
- [7] M. Grün, I. Lauer, K.K. Unger, *Adv. Mater.* 9 (1997) 254.
- [8] T. Martin, A. Galarneau, F. DiRenzo, D. Brunel, F. Fajula, S. Heinisch, G. Cretier, J.-L. Rocca, *Chem. Mater.* 16 (2004) 1725.
- [9] T. Martin, A. Galarneau, F. DiRenzo, F. Fajula, D. Plee, *Angew. Chem. Int. Ed.* 41 (2002) 2590.
- [10] K. Kailasam, K. Müller, *J. Chromatogr. A* 1191 (2008) 125.
- [11] K. Kailasam, A. Fels, K. Müller, *Micropor. Mesopor. Mater.* (2008) Article in Press.
- [12] J. Nawrocki, M.P. Rigney, A. McCormick, P.W. Carr, *J. Chromatogr.* 657 (1993) 229.
- [13] M.P. Rigney, E.F. Funkenbusch, P.W. Carr, *J. Chromatogr.* 449 (1990) 291.
- [14] D.A. Hanggi, N.R. Marks, *LC-GC* 11 (1993) 128.
- [15] M. Kawahara, H. Nakamura, T. Kakajima, *J. Chromatogr.* 515 (1990) 149.
- [16] J.J. Pesek, M.T. Matyska, *J. Chromatogr. A* 952 (2002) 1.
- [17] Q.-H. Zhang, Y.-Q. Feng, S.-L. Da, *Anal. Sci.* 15 (1999) 767.
- [18] K. Ohta, *J. Chromatogr. A* 920 (2001) 181.
- [19] C.A. Doyle, J.G. Dorsey, in *Handbook of HPLC*, E. Katz, R. Eksteen, P. Schoenmakers, N. Millers (Eds.), Marcel Dekker, Inc., New York, Chp. 8 (1998) p. 293.
- [20] U.D. Neue, *Encyclopedia of Analytical Chemistry*, Meyers, R. A (ed), Wiley, Chichester, 2000.
- [21] K.K. Unger, *Porous Silica*, Elsevier, Amsterdam, 1979.
- [22] M. Pursch, L.C. Sander, K. Albert, *Anal. Chem.* 68 (1996) 4107.

- [23] C.A. Rimmer, L.C. Sander, S.A. Wise, J.G. Dorsey, *J. Chromatogr. A* 1007 (2003) 11.
- [24] C.A. Doyle, T.J. Vickers, C.K. Mann, J.G. Dorsey, *J. Chromatogr. A* 877 (2000) 25.
- [25] J.E. Pemberton, M. Ho, C.J. Orendorff, M.W. Ducey, *J. Chromatogr. A* 913 (2001) 243.
- [26] S. Singh, J. Wegmann, K. Albert, K. Müller, *J. Phys. Chem. B* 106 (2002) 878.
- [27] C.A. Doyle, T.J. Vickers, C.K. Mann, J.G. Dorsey, *J. Chromatogr. A* 877 (2000) 41.
- [28] L.C. Sander, S.A. Wise, *Adv. Chromatogr.* 25 (1986) 139.
- [29] K.B. Sentell, J.G. Dorsey, *J. Chromatogr.* 461 (1989) 193.
- [30] C.H. Lochmüller, M.L. Hunnicutt, J.F. Mullaney, *J. Phys. Chem.* 89 (1985) 5770.
- [31] R.P.W. Scott, *Silica Gel and Bonded Phases*, John Wiley and Sons, Chichester, England, 1993, p. 1.
- [32] S.R. Cole, J.G. Dorsey, *Biomed. Chromatogr.* 11 (1997) 167.
- [33] A. Vailaya, C. Horvath, *J. Chromatogr. A* 829 (1998) 9.
- [34] L.C. Sander, K.A. Lippa, S.A. Wise, *Anal. Bioanal. Chem.* 382 (2005) 646.
- [35] K.B. Sentell, *J. Chromatogr.* 656 (1993) 231.
- [36] E.F. Vansant, P. VanDerVoort, K.C. Vrancken, *Characterization and Chemical Modification of the Silica Surface*, Elsevier, Amsterdam, 1995.
- [37] Y. Saito, H. Ohta, K. Jinno, *J. Sep. Sci.* 26 (2003) 225.
- [38] J. Nawrocki, C.J. Dunlap, P.W. Carr, J.A. Blackwell, *Biotechnol. Prog.* 10 (1994) 561.
- [39] J.J. Pesek, M.T. Matyska, *Encyclopedia of Chromatography, Cases, J. (Eds.)*, Marcel Dekker, New York, 2001.
- [40] B. Buszewski, M. Jezierska, M. Welnak, D. Berek, *J. High. Resol. Chromatogr.* 21 (1998) 267.
- [41] G.E. Berendsen, L. de Galan, *J. Liq. Chromatogr.* 1 (1978) 561.
- [42] J. Rouquerol, F. Rodríguez-Reinoso, K.S.W. Sing, K.K. Unger, Eds., *Characterization of Porous Solids III*, Elsevier, Amsterdam, 1994.
- [43] S.J. Gregg, K.S.W. Sing, *Adsorption, Surface Area and Porosity*, Second ed., Academic Press, London, 1982.
- [44] F. Rouquerol, J. Rouquerol, K.S.W. Sing, *Adsorption by Powders and Porous Solids*, Academic Press, London, 1999, p. 467.
- [45] S. Lowell, J.E. Shields, *Powder, Surface Area and Porosity*, third ed., Chapman and Hall, London, 1991, p. 250.

- [46] M. Kruk, M. Jaroniec, A. Sayari, *Langmuir* 13 (1997) 6267.
- [47] P. Selvam, S.K. Bhatia, C.G. Sonwane, *Ind. Eng. Chem. Res.* 40 (2001) 3237.
- [48] N. Tanaka, Y. Tokuda, K. Iwaguchi, M. Araki, *J. Chromatogr.* 239 (1982) 761.
- [49] K.B. Sentell, A.N. Henderson, *Anal. Chim. Acta* 246 (1991) 139.
- [50] L.C. Sander, S.A. Wise, *Anal. Chem.* 67 (1995) 3284.
- [51] M. Pursch, L.C. Sander, K. Albert, *Anal. Chem. News & Features* 71 (1999) 733A.
- [52] M. Pursch, D.L. Vanderhart, L.C. Sander, X. Gu, T. Nguyen, S.A. Wise, D.A. Gajewski, *J. Am. Chem. Soc.* 122 (2000) 6997.
- [53] S. Neumann-Singh, J. Villanueva-Garibay, K. Müller, *J. Phys. Chem. B* 108 (2004) 1906.
- [54] M. Pursch, L.C. Sander, H.J. Egelhaaf, M. Raitza, S.A. Wise, D. Oelkrug, K. Albert, *J. Am. Chem. Soc.* 121 (1999) 3201.
- [55] L.C. Sander, J.B. Callis, L.R. Field, *Anal. Chem.* 55 (1983) 1068.
- [56] M.W. Ducey, C.J. Orendorff, J.E. Pemberton, *Anal. Chem.* 74 (2002) 5576.
- [57] S.J. Klätte, T.L. Beck, *J. Phys. Chem.* 97 (1993) 5727.
- [58] I. Yarovsky, M.I. Aguilar, M.T.W. Hearn, *J. Chromatogr. A* 660 (1994) 75.
- [59] S.J. Klätte, T. L. Beck, *J. Phys. Chem.* 99 (1995) 16024.
- [60] I. Yarovsky, M.I. Aguilar, M.T.W. Hearn, *Anal. Chem.* 67 (1995) 2145.
- [61] R.C. Zeigler, G.E. Maciel, *J. Am. Chem. Soc.* 113 (1991) 6349.
- [62] M. Pursch, S. Strohschein, H. Handel, K. Albert, *Anal. Chem.* 68 (1996) 386.
- [63] G. Srinivasan, L.C. Sander, K. Müller, *Anal. Bioanal. Chem.* 384 (2006) 514.
- [64] G. Srinivasan, K. Müller, *J. Chromatogr. A* 1110 (2006) 102.
- [65] G. Srinivasan, M. Pursch, L.C. Sander, K. Müller, *Langmuir* 20 (2004) 1746.
- [66] G. Srinivasan, C. Meyer, N. Welsch, K. Albert, K. Müller, *J. Chromatogr. A* 1113 (2006) 45.
- [67] K. Kailasam, T. Yasmin, K. Albert, K. Müller, Manuscript in preparation.
- [68] G. Srinivasan, S. Neumann-Singh, K. Müller, *J. Chromatogr. A* 1074 (2005) 31.
- [69] G. Srinivasan, A. Kyrlidis, C. McNeff, K. Müller, *J. Chromatogr. A* 1081 (2005) 132.
- [70] K. Kailasam, G. Srinivasan, K. Müller, *J. Chromatogr. A* 1134 (2006) 81.
- [71] K. Kailasam, M.M. Natile, A. Glisenti, K. Müller, Manuscript to be submitted.
- [72] C.H. Lochmuller, A.S. Colborn, M.L. Hunnicutt, J.M. Harris, *J. Am. Chem. Soc.* 106 (1984) 4077.
- [73] C.H. Lochmuller, D.B. Marshall, D.R. Wilder, *Anal. Chim. Acta* 130 (1981) 31.

- [74] C.H. Lochmuller, D.B. Marshall, D.R. Wilder, *Anal. Chem.* 52 (1980) 19.
- [75] C.H. Lochmuller, D.R. Wilder, *Anal. Chim. Acta* 116 (1980) 19.
- [76] R.G. Snyder, *J. Chem. Phys.* 47 (1967) 1316.
- [77] C.A. Doyle, T.J. Vickers, C.K. Mann, J.G. Dorsey, *J. Chromatogr. A* 779 (1997) 91.
- [78] R.C. Zeigler, G.E. Maciel, *J. Phys. Chem.* 95 (1991) 7345.
- [79] D.W. Sindorf, G.E. Maciel, *J. Am. Chem. Soc.* 105 (1983) 1848.
- [80] K. Albert, B. Evers, E. Bayer, *J. Magn. Reson.* 62 (1985) 428.
- [81] M. Gangoda, R.K. Gilpin, J. Figueirinhas, *J. Phys. Chem.* 93 (1989) 4815.
- [82] E.C. Kelusky, C.A. Fyfe, *J. Am. Chem. Soc.* 108 (1986) 1746.
- [83] N. Nagae, US patent number 6, 241, 891 June 5, 2001.
- [84] R.P.W. Scott, C.F. Simpson, *J. Chromatogr.* 197 (1980) 11.
- [85] R.K. Gilpin, M.E. Gangoda, A.E. Krishen, *J. Chromatogr. Sci.* 20 (1982) 345.
- [86] L.A. Cole, J.G. Dorsey, K.A. Dill, *Anal. Chem.* 64 (1992) 1324.
- [87] W.R. Thompson, J.E. Pemberton, *Anal. Chem.* 66 (1994) 3362.
- [88] S.C. Rutan, J.M. Harris, *J. Chromatogr. A* 656 (1993) 197.
- [89] Z. Li, S.C. Rutan, S. Dong, *Anal. Chem.* 68 (1996) 124.
- [90] M.W. Ducey, C.J. Orendorff, J.E. Pemberton, L.C. Sander, *Anal. Chem.* 74 (2002) 5585.
- [91] M.W. Ducey, C.J. Orendorff, J.E. Pemberton, L.C. Sander, *Anal. Chem.* 75 (2003) 3360.
- [92] C. Horvath, W. Melander, I. Molnar, *J. Chromatogr.* 125 (1976) 129.
- [93] B.L. Karger, J.R. Gant, A. Hartkopf, P.H. Weiner, *J. Chromatogr.* 128 (1976) 65.
- [94] A. Vailaya, C. Horvath, *J. Phys. Chem. B* 102 (1998) 701.
- [95] J.A. Marqusee, K.A. Dill, *J. Chem. Phys.* 85 (1986) 434.
- [96] K.A. Dill, *J. Phys. Chem.* 91 (1987) 1980.
- [97] J.G. Dorsey, K.A. Dill, *Chem. Rev.* 89 (1989) 331.
- [98] J. G. Dorsey, W. T. Cooper, *Anal. Chem.*, 66 (1994) 857A.
- [99] D.E. Leyden, Ed. *Silanes, Surfaces, and Interfaces*, Gordon and Breach, New York, 1986.
- [100] E.P. Plueddemann, *Silane coupling agents*, 2nd ed., Plenum: New York, 1991.
- [101] J.J. Pesek, I.E. Leigh, Eds. *Chemically Modified Surfaces*, Royal Society of Chemistry: Cambridge, 1994.
- [102] C.R. Kagan, D.B. Mitzi, C.D. Dimitrakopoulos, *Science* 286 (1999) 945.

- [103] U. Schubert, N. Hüsing, *Synthesis of Inorganic Materials*, Ed., Wiley-VCH, 2000, 343.
- [104] X.S. Zhao, G.Q. (Max) Lu, G.J. Millar, *Ind. Eng. Chem. Res.* 35 (1996) 2075.
- [105] A. Galarneau, J. Iapichella, K. Bonhomme, F. Di Renzo, P. Kooyman, O. Terasaki, F. Fajula, *Adv. Funct. Mater.* 16 (2006) 1657.
- [106] C. Boissière, M. Kümmel, M. Persin, A. Larbot, E. Prouzet, *Adv. Funct. Mater.* 11 (2001) 129.
- [107] K.W. Gallis, J.T. Araujo, K.J. Duff, J.G. Moore, C.C. Landry, *Adv. Mater.* 11 (1999) 1452.
- [108] A. Galarneau, J. Iapichella, D. Brunel, F. Fajula, Z. Bayram-Hahn, K.K. Unger, G. Puy, C. Demesmay, J.-L. Rocca, *J. Sep. Sci.* 29 (2006) 844.
- [109] A. Kurganov, K.K. Unger, T. Issaeva, *J. Chromatogr. A* 753 (1996) 177.
- [110] M. Raimondo, G. Perez, M. Sinibaldi, A. De Stefanis, A.A. Tomlinson, *Chem. Commun.* (1997) 1343.
- [111] C. Thoelen, K. Van de Walle, I.F.J. Vankelecom, P.A. Jacobs, *Chem. Commun.* (1999) 1841.
- [112] C. Boissière, A. Van der Lee, A. El Mansouri, A. Larbot, E. Prouzet, *Chem. Commun.* (1999) 2047.
- [113] Y. Lu, H. Fan, A. Stump, T.L. Ward, T. Rieker, C.J. Brinker, *Nature* 398 (1999) 223.
- [114] J.H. Clark, D.J. Macquarrie, *Chem. Commun.* (1998) 853.
- [115] Y.V. Subba Rao, D.E. De Vos, P.A. Jacobs, *Angew. Chem. Int. Ed. Engl.* 36 (1997) 2661.
- [116] J. Tudor, D. O'Hare, *Chem. Commun.* (1997) 603.
- [117] J. Nawrocki, C. Dunlap, A. McCormick, P.W. Carr, *J. Chromatogr. A* 1028 (2004) 1.
- [118] J. Nawrocki, C. Dunlap, J. Li, J. Zhao, C.V. McNeff, A. McCormick, P.W. Carr, *J. Chromatogr. A* 1028 (2004) 31.
- [119] J.J. Pesek, M.T. Matyska, J. Ramakrishnan, *Chromatographia* 44 (1997) 538.
- [120] A.Y. Fadeev, R. Helmy, S.M. Marcinko, *Langmuir* 18 (2002) 7521.
- [121] A.Y. Fadeev, T.J. McCarthy, *J. Am. Chem. Soc.* 121 (1999) 12184.
- [122] K.V.P.M. Shafi, A. Ulman, X. Yan, N.-L. Yang, M. Himmelhaus, M. Grunze, *Langmuir* 17 (2001) 1726.
- [123] M. Itoh, H. Hattori, K.J. Tanabe, *J. Catal.* 35 (1974) 225.

- [124] H.J.M. Bosman, E.C. Kruissink, J. Vanderspoel, F. Vandenbrink, *J. Catal.* 148 (1994) 660.
- [125] J.B. Miller, E.I. Ko, *J. Catal.* 159 (1996) 58.
- [126] R.G. Simhan, *J. Non-Cryst. Solids* 54 (1983) 335.
- [127] D.A. Neumayer, E. Cartier, *J. Appl. Phys.* 90 (2001) 1801.
- [128] G. Mountjoy, M.A. Holland, P. Gunawidjaja, G.W. Wallidge, D.M. Pickup, R.J. Newport, M.E. Smith, *J. Sol-Gel Sci. Techn.* 26 (2003) 161.
- [129] J.B. Miller, E.I. Ko, *Catal. Today* 35 (1997) 269.
- [130] K.W. Terry, C.G. Lugmair, T.D. Tilley, *J. Am. Chem. Soc.* 119 (1997) 9745.
- [131] L. Armelao, H. Bertagnolli, S. Gross, V. Krishnan, U. Lavrencic-Stangar, K. Müller, B. Orel, G. Srinivasan, E. Tondello, A. Zattin, *J. Mater. Chem.* 15 (2005) 1954.
- [132] L. Armelao, C. Eisenmenger-Sittner, M. Groenewolt, S. Gross, C. Sada, U. Schubert, E. Tondello, A. Zattin, *J. Mater. Chem.* 15 (2005) 1838.
- [133] S. Mascotto, O. Tsetsgee, K. Müller, C. Maccato, B. Smarsly, D. Brandhuber, E. Tondello, S. Gross, *J. Mater. Chem.* 17 (2007) 4387.
- [134] G. Trimmel, S. Gross, G. Kickelbick, U. Schubert, *Appl. Organom. Chem.* 15 (2001) 401.
- [135] A. Stein, B.J. Melde, R.C. Schrodin, *Adv. Mater.* 12 (2000) 1403.
- [136] R. Maoz, J. Sagiv, *J. Colloid Interface Sci.* 100 (1984) 465.
- [137] S.R. Wasserman, G.M. Whitesides, I.M. Tidswell, B.M. Ocko, P.S. Pershan, J.D. Axe, *J. Am. Chem. Soc.* 111 (1989) 5852.
- [138] U. Truedinger, G. Mueller, K.K. Unger, *J. Chromatogr.* 535 (1990) 111.
- [139] C.P. Tripp, M.L. Hair, *Langmuir* 11 (1995) 1215.
- [140] H. Tada, *Langmuir* 11 (1995) 3281.
- [141] J. Iapichella, J.-M. Meneses, I. Beurroies, R. Denoyel, Z. Bayram-Hahn, K.K. Unger, A. Galarneau, *Micropor. Mesopor. Mater.* 102 (2007) 111.
- [142] J.J. Kirkland, J.W. Henderson, *J. Chromatogr. Sci.* 32 (1994) 473.
- [143] M.J. Wirth, H.O. Fatunmbi, *Anal. Chem.* 65 (1993) 822.
- [144] L.C. Sander, S.A. Wise, *Anal. Chem.* 56 (1984) 504.
- [145] J.J. Kirkland, M.A. van Straten, H.A. Claessens, *J. Chromatogr.* 691 (1995) 3.
- [146] K. Kailasam, S. Mascotto, S. Gross, C. Maccato, K. Müller, Manuscript to be submitted.
- [147] T. Welsch, H. Frank, G. Vigh, *J. Chromatogr.* 506 (1990) 97.
- [148] G.B. Cox, *J. Chromatogr. A* 656 (1993) 353.

- [149] N.H.C. Cooke, K. Olsen, *J. Chromatogr. Sci.* 18 (1980) 512.
- [150] A. Pryde, *J. Chromatogr. Sci.* 12 (1974) 486.
- [151] R. Mendelsohn, R.G. Snyder, in K.M. Merz Jr., B. Roux (Eds.), *Biological Membranes*. Birkhäuser, Boston, 1996, p. 145.
- [152] R. Mendelsohn, M.A. Davies, J.W. Brauner, H.F. Schuster, R.A. Dluhy, *Biochemistry* 28 (1989) 8934.
- [153] H. Farida, B.C. James, *J. Am. Chem. Soc.* 93 (1989) 2053.
- [154] R.G. Snyder, H.L. Strauss, C.A. Elliger, *J. Phys. Chem.* 86 (1982) 5145.
- [155] L. Senak, M.A. Davies, R. Mendelsohn, *J. Phys. Chem.* 95 (1991) 2565.
- [156] P.J. Flory, *Statistical Mechanics of Chain Molecules*, Wiley, New York, 1969.
- [157] S. Neumann-Singh, Ph. D Dissertation, Universität Stuttgart, 2003.
- [158] M. Mehring, *Principles of High Resolution NMR in Solids*, Springer-Verlag: Berlin, 2nd ed., 1983.
- [159] A. Abragam, *Principles of Nuclear Magnetism*, Oxford University Press: London, 1961.
- [160] R.R. Ernst, G. Bodenhausen, A. Wokaun, *Principles of Nuclear Magnetic Resonance in One and Two Dimensions*, Clarendon: Oxford, 1987.
- [161] K. Schmidt-Rohr, H.W. Speiss, *Multidimensional solid-state NMR and polymers*, Academic Press: New York, 1994.
- [162] E.R. Andrew, *Progr. NMR. Spectrosc.* 8 (1971) 1.
- [163] E.R. Andrew, W.S. Hinshaw, *Phys. Lett.* 43A (1973) 113.
- [164] A. Pines, M.G. Gibby, J.S. Waugh, *J. Chem. Phys.* 59 (1973) 569.
- [165] S.R. Hartmann, E.L. Hahn, *Phys. Rev.* 128 (1962) 2042.
- [166] G.E. Maciel, D.W. Sindorf, *J. Am. Chem. Soc.* 102 (1980) 7606.
- [167] M. Porsch, R. Brindle, A. Ellwanger, L.C. Sander, C.M. Bell, H. Haendel, K. Albert, *Solid State Nucl. Magn. Res.* 9 (1997) 191.
- [168] D.M. Grant, E.G. Paul, *J. Am. Chem. Soc.* 86 (1964) 2984.
- [169] A.E. Tonelli, *Macromolecules* 11 (1978) 565.
- [170] A.E. Tonelli, *Spectroscopy and Polymer Microstructure, The Conformational Connection*, VCH Publishers, New York, 1989.
- [171] H.P. Lin, C.Y. Mou, *J. Cluster Sci.* 10 (1999) 271.
- [172] S. Brunauer, P.H. Emmet, E. Teller, *J. Am. Chem. Soc.* 60 (1938) 309.
- [173] C.P. Jaroniec, M. Kruk, M. Jaroniec, A. Sayari, *J. Phys. Chem. B* 102 (1998) 5503.
- [174] L. Jelinek, E.sz. Kováts, *Langmuir* 10 (1994) 4225.

- [175] A. Galarneau, D. Desplandier, R. Dutartre, F. Di Renzo, *Micropor. Mesopor. Mater.* 27 (1999) 297.
- [176] E.P. Barrett, L.G. Joyner, P.P. Halenda, *J. Am. Chem. Soc.* 73 (1951) 373.
- [177] P.I. Ravikovitch, S.C. Ó Domhnaill, A.V. Neimark, F. Schüth, K.K. Unger, *Langmuir* 11 (1995) 4765.
- [178] A.V. Neimark, P.I. Ravikovitch, M. Grün, F. Schüth, K.K. Unger, *J. Colloid Interf. Sci.* 207 (1998) 159.
- [179] M. Thommes, in: G.Q. Lu, X.S. Zhao (Eds.), *Nanoporous Materials—Science and Engineering*, vol. 4, Imperial College Press, London, 2004, p. 346.
- [180] H. Knözinger, in: P. Schuster, G. Zundel, C. Sandorfy (Eds.), *The Hydrogen Bond*, vol. 3, North-Holland, Amsterdam, 1976, p. 1263.
- [181] G.A. Parks, *Chem. Rev.* 65 (1965) 177.
- [182] P. Kubelka, F. Munk, *Z. Tech. Phys.* 12 (1931) 593.
- [183] G. Kortum, *Reflectance Spectroscopy*, Springer, New York, 1969.
- [184] D. Briggs, M.P. Seah, *Practical Surface Analysis*, J. Wiley & Sons, 1990.
- [185] J.F. Moulder, W.F. Stickle, P.E. Sobol, K.D. Bomben, *Handbook of X-Ray Photoelectron Spectroscopy*, J. Chastain, Perkin Elemer Corp. Eden Prairie, 1992.
- [186] A. Shirley, *Phys. Rev. B* 5 (1972) 4709.
- [187] NIST XPS Database, X-ray Photoelectron Spectroscopy Database 20, Version 3.0; National Institute of Standards and Technology: Gaithersburg, MD <http://srdata.nist.gov/XPS>
- [188] M.J. Kamlet, J.M. Abboud, M.H. Abraham, R.W. Taft, *J. Org. Chem.* 48 (1983) 2877.
- [189] M.E. Gangoda, R.K. Gilpin, *Langmuir* 6 (1990) 941.
- [190] C.R. Kessel, S. Granick, *Langmuir* 7 (1991) 532.
- [191] B. Pauwels, G. Van Tendeloo, C. Thoelen, W. Van Rhijn, P.A. Jacobs, *Adv. Mater.* 13 (2001) 1317.
- [192] S. Zheng, L. Gao, J. Guo, *Mater. Chem. Phys.* 71 (2001) 174.
- [193] K.S.W. Sing, D.H. Everett, R.A.W. Haul, L. Moscou, R.A. Pierotti, J. Rouquerol, T. Siemieniewska, *Pure Appl. Chem.* 57 (1985) 603.
- [194] T. Kimura, S. Saeki, Y. Sugahara, K. Kuroda, *Langmuir* 15 (1999) 2794.
- [195] H. Engelhardt, P. Orth, *J. Liq. Chromatogr.* 10 (1987) 1999.
- [196] C.-Y. Chen, H.-X. Li, M.E. Davis, *Microporous Mater.* 2 (1993) 17.
- [197] B.A. Grimes, S. Ludtke, K.K. Unger, A.I. Liapis, *J. Chromatogr. A* 979 (2002) 447.

- [198] X. Feng, G.E. Fryxell, L.-Q. Wang, A.Y. Kim, J. Liu, K.M. Kemner, *Science* 276 (1997) 923.
- [199] M.H. Lim, A. Stein, *Chem. Mater.* 11 (1999) 3285.
- [200] F. Meiouet, G. Félix, H. Taibi, H. Hommel, A.P. Legrand, *Chromatographia* 31 (1991) 335.
- [201] R.G. Snyder, M.W. Poore, *Macromolecules* 6 (1973) 708.
- [202] A. Badia, L. Cuccia, L. Demers, F. Morin, R.B. Lennox, *J. Am. Chem. Soc.* 119 (1997) 2682.
- [203] C. Sun, J.C. Berg, *Adv. Colloid Interface Sci.* 105 (2003) 151.
- [204] L. Corrsin, B.J. Fax, R.C. Lord, *J. Chem. Phys.* 21 (1953) 1170.
- [205] E.P. Parry, *J. Catal.* 2 (1963) 371.
- [206] C. Morterra, A. Chiorino, G. Ghiotti, E. Fiescaro, *J. Chem. Soc. Faraday Trans.* 78 (1982) 2649.
- [207] L.H. Little, *Infrared Spectra of Adsorbed Species*, Academic Press: San Diego, CA, 1966.
- [208] L. Ferretto, A. Glisenti, *Chem. Mater.* 15 (2003) 1181.
- [209] R. Helmy, R.W. Wenslow, A.Y. Fadeev, *J. Am. Chem. Soc.* 126 (2004) 7595.
- [210] L. Armelao, S. Gross, K. Müller, G. Pacea, E. Tondello, O. Tsetsgee, A. Zattin, *Chem. Mater.* 18 (2006) 6019.
- [211] J. Sagiv, *J. Am. Chem. Soc.* 102 (1980) 92.
- [212] M.E. McGovern, K.M.R. Kallury, M. Thompson, *Langmuir* 10 (1994) 3607.
- [213] J.B. Brzoska, I.B. Azouz, F. Rondelez, *Langmuir* 10 (1994) 4367.
- [214] R. Wang, J. Guo, G. Baran, S.L. Wunder, *Langmuir* 16 (2000) 568.
- [215] D.L. Allara, A.N. Parikh, F. Rondelez, *Langmuir* 11 (1995) 2357.
- [216] K.I. Hadjiivanov, D.G. Klissurski, *Chem. Soc. Rev.* 25 (1996) 61.
- [217] B.C. Lippens, *Active Alumina*, in: B.G. Linsen (Ed.), *Physical and Chemical Aspects of Adsorbents and Catalysts*, Academic Press, London, 1970.
- [218] J. Nawrocki, P.W. Carr, M.J. Annen, S. Froelicher, *Anal. Chim. Acta* 327 (1996) 261.
- [219] J.A. Rob van Veen, F.T.G. Veltmaat, G. Jonkers, *J. Chem. Soc., Chem. Commun.* 1656 (1985).
- [220] J. Blackwell, P.W. Carr, *J. Chromatogr.* 549 (1991) 43.
- [221] R. Helmy, A.Y. Fadeev, *Langmuir* 18 (2002) 8924.
- [222] I. Yarovsky, M.L. Aguilar, M.T.W. Hearn, *Anal. Chem.* 67 (1995) 2145.

- [223] W.L. Earl, D.L. Vanderhart, *Macromolecules* 12 (1979) 762.
- [224] W. Gao, L. Reven, *Langmuir* 11 (1995) 1860.
- [225] W. Gao, L. Dickinson, C. Grozinger, F.G. Morin, L. Reven, *Langmuir* 12 (1996) 6429.
- [226] A. Badia, W. Gao, S. Singh, L. Demers, L. Cuccia, L. Reven, *Langmuir* 12 (1996) 1262.
- [227] M. Sugi, *J. Mol. Electron.* 1 (1985) 2.
- [228] M. Uchida, T. Tanizaki, T. Oda, T. Kajiyama, *Macromolecules* 24 (1991) 3238.
- [229] P. Tundo, *J. Chem. Soc., Chem. Commun.* 18 (1977) 641.
- [230] M.L. Gee, T.W. Healy, L.R. White, *J. Colloid Interface Sci.* 140 (1990) 450.
- [231] S.M. Levine, S.H. Garofalini, *J. Chem. Phys.* 55 (1976) 9.
- [232] M.M. Natile, A. Galenda, A. Glisenti, S. Mascotto, S. Gross, Manuscript submitted.

Curriculum Vitae

Personal:

Name : Kamalakannan Kailasam
Date of Birth : 17th December 1978
Nationality : Indian

Academic:

- Since October 2004 **Ph.D**
Institute of Physical Chemistry, University of Stuttgart, Germany under the guidance of Prof. Dr. Klaus Müller.
Thesis: Synthesis and Characterization of Mesoporous Silica and Metal Oxide Based Stationary Phase Materials
- 2000 – 2002 **M.Sc. Chemistry**
Bharathidasan University, Tiruchirapalli, Tamilnadu, India.
Thesis: A study on the Transition Metal Complexes of Phthalylsulfathiazole
- 1996 – 1999 **B.Sc. Chemistry**
Bharathidasan University, Tiruchirapalli, Tamilnadu, India.

Work Experience:

- 2000 – 2004 Worked as a Project Assistant in Expertise Centre for Eco-Testing Laboratory (EXCEL) in Central Leather Research Institute (CLRI), Chennai, Tamilnadu, India

Publications:

- (1) **K. Kailasam**, G. Srinivasan, K. Müller, Solvent effects on the conformational order of triacontyl modified silica gels as evaluated by Fourier transform infrared spectroscopy. *Journal of Chromatography A* 2006, 1134, 81-87.
- (2) **K. Kailasam**, K. Müller, Physico-chemical characterization of MCM-41 silica spheres made by the pseudomorphic route and grafted with octadecyl chains. *Journal of Chromatography A* 2008, 1191, 125-135.
- (3) **K. Kailasam**, A. Fels, K. Müller, Octadecyl Grafted MCM-41 Silica Spheres using Trifunctionalsilane Precursors - Preparation and Characterization. *Microporous and Mesoporous Materials* 2009, 117, 136.
- (4) **K. Kailasam**, M.M. Natile, A. Glisenti, K. Müller, FTIR and solid-state NMR studies of octadecyl modified metal oxides from different silane precursors. *Journal of Chromatography A*, Article in Press.
- (5) **K. Kailasam**, S. Gross, S. Mascotto, C. Maccatto, K. Müller, Self-Assembled Monolayers on Silica-Zirconia Mixed Oxide Systems and their Characterization. Manuscript to be submitted.
- (6) **K. Kailasam**, T. Yasmin, K. Albert, K. Müller, Pseudomorphic synthesis of MCM-41 silica spheres and grafting with octadecyl chains – characterization using SAXS, Nitrogen sorption, SEM, FTIR, Solid-state NMR and HPLC techniques. Manuscript in preparation.